The Molecular Underpinnings and Regulation of Amino Acid Pathways in Ewing sarcoma

by

Jennifer A Jiménez

A dissertation submitted in partial fulfillment
of the requirements for the degree of
Doctor of Philosophy
(Cancer Biology)
in the University of Michigan
2022

Doctoral Committee:

Associate Professor David Lombard, Chair
Associate Professor Analisa DiFeo
Professor Elizabeth Lawlor
Associate Professor Costas Lyssiotis
Associate Professor Sriram Venneti

Jennifer A. Jiménez

jejimene@umich.edu

ORCID iD: 0000-0003-3033-1938

Dedication

Dedicated to the cancer patients who inspire us to work our hardest each day. And to my parents, for the many sacrifices that have allowed me to always follow my dreams.

Acknowledgements

I would like to start by thanking my mentor, Beth Lawlor, for your consistent support and for always pushing me to achieve my maximum potential. Your dedication to your students and to the pediatric cancer community at large are such an inspiration. I can't tell you how much I've learned and grown as a scientist and person by working with you, and I will carry all of these lessons with me through life! Many thanks to Costas Lyssiotis and Howard Crawford for taking me in to your labs after the Lawlor lab's move to Seattle. You provided a home for me and a lab family during a time when COVID19 was turning our worlds upside down, and for that, I cannot thank you enough. Costas, your enthusiasm for science is truly unmatched, and I am extremely thankful for your scientific input and mentorship throughout this process. Thank you to my thesis committee members David Lombard, Sriram Venneti, and Analisa DiFeo, for the scientific and personal guidance and for making our meetings so enjoyable.

To the members of the Lawlor and Lyssiotis lab. Most importantly, April Apfelbaum… You have been my lab-mate, my best friend, my twin when mine was hundreds of miles away. I can't thank you enough for being my go-to person for advice in and out of lab, and for the constant laughs and memories! Special thank you to Ally Hawkins for your friendship and constant willingness to help with anything! Thank you to Nicolas Garcia for all of your help with mouse work and for being such a pleasure to work with. To all other Lawlor lab members, thank you for your scientific input and

support through the years. To the members of the Lyssiotis lab, I cannot imagine a more supportive and welcoming lab home, and I am so thankful for the opportunity to work with and learn from each of you. To the students I have had the honor of mentoring. Teaching has brought me some of the greatest joy in graduate school.

To the Cancer Biology Graduate Program, especially Dawn Storball, thank you for making the program run smoothly and for always being available. To the PIBS program, especially Shoba Subramanian and Maggie Gardner, thank you for your guidance and for making the career exploration process less daunting.

I want to end by thanking the most important people in my life. To the lifelong friends I've made at UofM, grad school would not have been the amazing journey it was without the many late nights downtown, the football tailgates, and road trips. To my parents, Jeannette and Raphael, and my brother Daniel, thank you for giving purpose to everything I do and for being my biggest supporters. To my twin sister and best friend from day one, Jessica. I definitely recommend having a twin who's also pursuing a PhD at the same time! Thank you for your constant encouragement. I look up to you in so many ways. Lastly, to my future husband, Zach who has been by my side throughout this entire process. Thank you for celebrating the highs and for consoling me during the lows. It has brought me so much happiness to grow and achieve our goals together.

Financial Acknowledgements

Thank you to the sources of funding that have supported this thesis work, including the UofM Program in Biomedical Sciences (PIBS), Rogel Cancer Center, Rackham Graduate School and Rackham Merit Fellowship, as well as the NIH NRSA Predoctoral Fellowship (F31 CA254079), and NIH Diversity Supplement.

Table of Contents

List of Tables

List of Figures

List of Appendices

List of Abbreviations

αKG: alpha-ketoglutarate
5-mC: 5-methylcytosine
ADI-PEG20: Pegylated arginine deaminase
ALL: Acute lymphocytic leukemia
ASNase: L-asparaginase
ASNS: Asparagine synthetase
ASS1: Argininosuccinate synthetase
ATF4: Activating transcription factor 4
BCAAs: Branched-chain amino acids
BMP: Bone morphogenetic proteins
CHAC1: ChaC Glutathione Specific Gamma-Glutamylcyclotransferase 1
ChIP: Chromatin immunoprecipitation
COMPASS: COMplex of Proteins ASsociated with Set1
DDIT3: DNA damage inducible transcript 3
DHFR: Dihydrofolate reductase
ECM: Extracellular matrix
EMT: Epithelial to mesenchymal transition
ETC: Electron transport chain
FDG–PET: Fluorodeoxyglucose positron emission tomography
FET: FUS/EWSR1/TAF15
GLS: Glutaminase
GSEA: Gene set enrichment analysis
GSH: Reduced glutathione
H3K4: Histone 3, lysine 4
HSC: Hematopoietic stem cell
IGF: Insulin-like growth factor
KMTs: lysine methyltransferases
LC-MS: Liquid chromatography mass spectrometry
LSD1: Lysine-specific histone demethylase 1
MCT: Monocarboxylate transporter
MEN1: Multiple endocrine neoplasia type 1
MLLr: MLL-rearranged
MSC: Mesenchymal stem cell
MSigDB: Molecular Signatures Database
mTORC1: Mammalian target of rapamycin complex 1
NAMPT: Nicotinamide phosphoribosyltransferase
NuRD: Nucleosome remodeling and deacetylase
OE: Over expression
OXPHOS: Oxidative phosphorylation
PcG: Polycomb group

PDGF: Platelet-derived growth factor
PHGDH: Phosphoglycerate dehydrogenase
PSAT1: Phosphoserine aminotransferase 1
PSPH: Phosphoserine phosphatase
qRT-PCR: Quantitative real-time polymerase chain reaction
RANKL: RANK ligand
Redox: Reduction/oxidation
SAM: S-Adenosyl Methionine
SESN2: Sestrin-2
SHMT2: Serine hydroxymethyltransferase 2
SLC1A5: Solute carrier family 1 member 5
SLC7A11: Solute carrier family 7 member 11
SSP: Serine biosynthetic pathway
TCA: Tricarboxylic Acid
TGF-β: Transforming growth factor-beta
THF: Tetrahydrofolate
TME: Tumor microenvironment
TNF: Tumor necrosis factor
TRIB3: Tribbles pseudokinase 3
TrxG: Trithorax group
System x_C-: xCT Cystine/glutamate antiporter

Abstract

Ewing sarcoma is an aggressive pediatric bone and soft tissue tumor, most commonly driven by EWS-FLI1. The standard of care for Ewing sarcoma has not improved in decades, and by far the best predictor of poor prognosis is the presence of metastases at diagnosis. However, regardless of disease presentation, both patients with localized and metastatic disease are treated with maximum doses of chemotherapy. The current treatment protocol has improved the survival rate for patients with localized disease to >70%; however, the outcome for metastatic patients is much less favorable with dismal survival rates of <20%. Furthermore, for survivors of the disease, the intense chemotherapy treatment leaves them with profound toxicities that follow them through life. To this day, the tumor-initiating EWS-FLI1 fusion protein is undruggable, thus it is imperative to better understand the biology of the disease in order to identify new vulnerabilities and develop better-targeted therapies.

The disruption of cellular metabolism by oncogenic drivers is a hallmark of cancer, providing a therapeutic window for targeting dysregulated metabolism in the tumor. EWS-FLI1 rewires the metabolome by mechanisms that are not well understood. Previous work from our lab revealed that the scaffolding protein menin serves an oncogenic role in Ewing sarcoma, partly through regulation of amino acid metabolic pathways. In this thesis, I sought to investigate the molecular mechanisms by which amino acid pathways are dysregulated in Ewing sarcoma and to begin to evaluate

targeting amino acid metabolism as a therapeutic vulnerability. Though transcriptomic analysis and molecular techniques, my work uncovered that EWS-FLI1 and menin both activate the master transcriptional regulator, ATF4. ATF4 functions to maintain cellular homeostasis, in part by upregulating amino acid biosynthetic pathways that support protein synthesis and proliferation, such as the serine biosynthesis pathway (SSP) and asparagine biosynthesis. Hyperactivation of the SSP has been extensively explored as a biomarker in Ewing sarcoma but its importance for driving tumorgenicity is not clear. We also discovered that inhibition of PHGDH partially antagonizes the EWS-FLI1-regulated gene signature, providing a possible explanation for dependence on high-level expression of PHGDH. Additionally, through the use of *in vivo* and *in vitro* models, we found that asparagine synthetase (ASNS) is robustly expressed in Ewing sarcoma and promotes metastatic progression. Mechanistically, this is due, at least in part, to significant changes in the expression of genes related to epithelial-mesenchymal transition (EMT) and extracellular matrix (ECM).

In conclusion, this thesis has elucidated that EWS-FLI1 and menin act to regulate ATF4 activity in Ewing sarcoma, in turn controlling amino acid metabolism pathways that impact metastatic progression. My studies thus highlight disease-driving exploitable metabolic vulnerabilities that may ultimately lead to better-targeted agents to reduce cytotoxic therapy or circumvent its need all together.

Chapter 1 Introduction

Thesis Overview

[1]Ewing sarcoma is a highly aggressive pediatric bone tumor with peak incidence in childhood and adolescence [1]. Standard of care, consisting of high dose chemotherapy, combined with surgery and/or radiation have improved survival rates for patients with localized disease, but the highly cytotoxic treatment regimen has not changed in decades. Further, in the last 30 years there have not been any improvements in the treatment of patients who develop metastatic disease or who relapse after treatment, and their 5-year survival is less than 20% [1]. To this day, the EWS-FLI1 oncogenic fusion is undruggable, thus it is critical to better understand the biology of downstream EWS-FLI1-regulated pathways as well as alternative tumorigenic drivers that may provide targeted therapeutic opportunities. Emerging research in Ewing sarcoma has identified dysregulated metabolism as a consequence of EWS-FLI1 fusion protein expression [2-5] Furthermore, our lab identified an oncogenic role for the scaffolding protein and epigenetic regulator menin and discovered a novel function for menin in the regulation of amino acid metabolic pathways [6, 7]. In this thesis, we begin to dissect the molecular mechanisms by which menin and EWS-FLI1 impact on cellular

[1] Portions of this introduction will be published in *Frontiers in Oncology*, Research Topic: The Multifacets of Tumor Heterogeneity and its Impact on Amino Acid Metabolism. Jennifer A. Jiménez, Elizabeth R. Lawlor, Costas A. Lyssiotis. Amino Acid Metabolism in Primary Bone Sarcomas (*In preparation*).

metabolism and provide evidence that targeting amino acid metabolism and upstream regulators may, in the future, provide a targeted opportunity with clinical potential.

Ewing sarcoma overview

Primary bone cancers encompass approximately 0.2% of all malignant tumors, with osteosarcoma, Ewing sarcoma, and chondrosarcoma representing 90-95% of these diagnoses [8]. Ewing sarcoma is the second most common pediatric bone tumor,

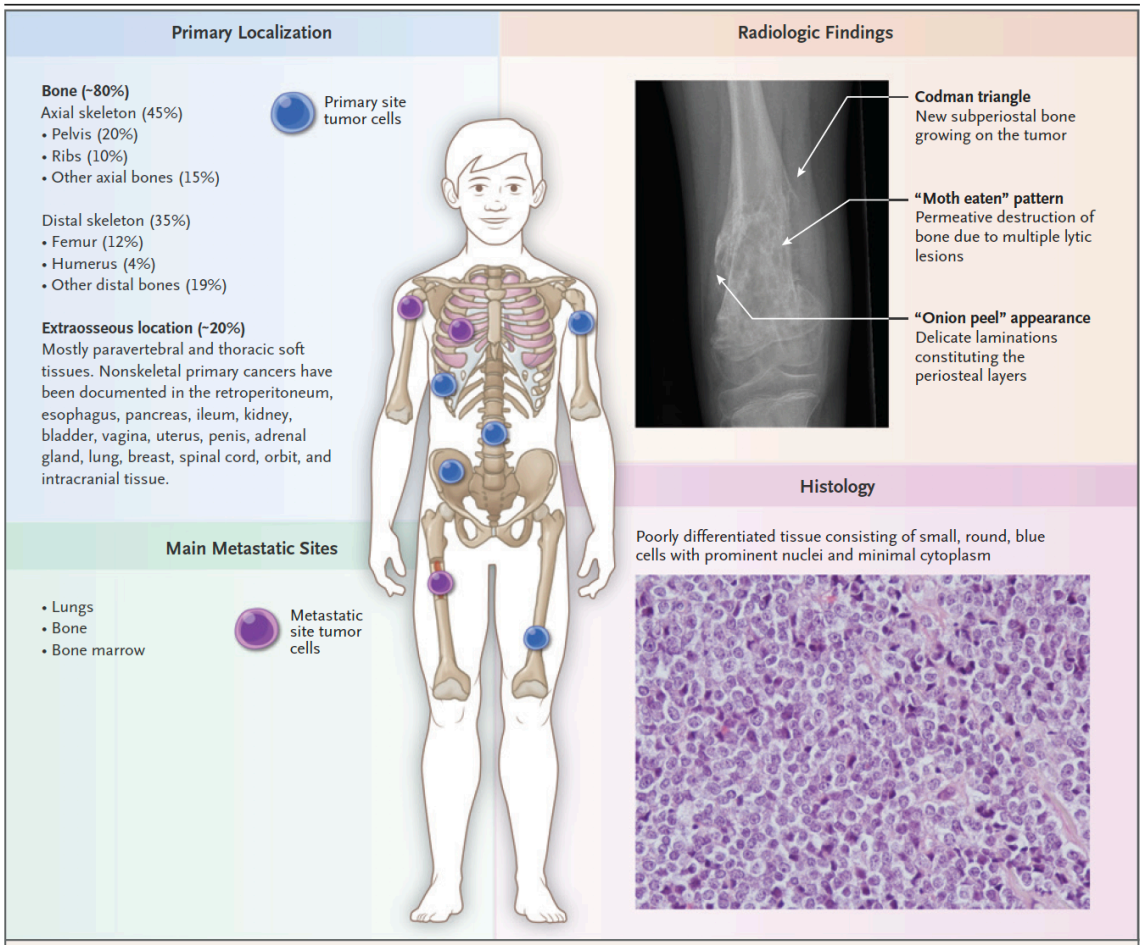

Figure 1-1 Ewing sarcoma clinical presentation

Diagram showing the primary sites where Ewing sarcoma arises (top left), radiographic appearance (top right), most common sites of metastasis (bottom left), and characteristic round small blue cell histology (bottom right). Reproduced with permission from (Riggi, Suva, and Stamenkovic *et al.,* 2021), Copyright Massachusetts Medical Society.

with an incidence of 1 case per 1.5 million in the population, a highest incidence at 15 years of age, and predilection for males. Ewing sarcoma is characterized by a small round blue cell histology of highly undifferentiated cells and can arise both in the bone and in soft tissue sites, most commonly in the pelvis, chest wall, and proximal long bones (femur, humerus, and tibia) of the body (**Figure 1-1**) [45]. Along with histologic examination for small, round, blue cells with prominent nuclei, immunohistochemical indications include strong membrane expression of CD99 (MIC2), a lack of which eliminates a Ewing sarcoma diagnosis. The Ewing sarcoma cell of origin has continually been the topic of debate, with evidence suggesting a mesenchymal stem cell (MSC) of neural crest or mesoderm lineage but no cell of origin has yet been conclusively defined [9].

Current treatment regimens for Ewing sarcoma include chemotherapy consisting of alternating doxorubicin, cyclophosphamide, vincristine, and etoposide, and ifosfamide, to reduce the size of the tumor, followed by local control with surgery and/or radiation, and maintenance chemotherapy [45]. While survival rates for other childhood malignancies, such as leukemia, have improved steadily in recent decades, the five-year survival rate for Ewing sarcoma presenting with metastatic disease at diagnosis has not improved and remains at less than 30%. When metastases do develop, the most common locations are to the bone, bone marrow, and lung, though metastasis to the lymph nodes, liver, and brain has also been observed (**Figure 1-1**) [1, 10]. The presence of metastasis at the time of diagnosis is the most important prognostic indication, as patients with local disease with positive responses to multimodal therapy have a survival rate of more than 70%. However, even for patients with localized

disease, the standard of care for these highly aggressive bone tumors, consisting of high dose chemotherapy, surgery, and radiation, leads to significant long-term toxicities that contribute to diminished quality of life and decreased life expectancy [11].

The EWS-FLI1 chimeric fusion oncoprotein and the epigenome

A conclusive diagnosis of Ewings sarcoma depends on molecular analysis and the presence of an EWS-ETS fusion protein. EWS-ETS fusions result from a reciprocal chromosomal translocation event fusing a FET family member (FUS/EWSR1/TAF15) and a gene encoding a member of the ETS family of transcription factors [26]. The most common translocation is t(11;22) (q24,q12) in 85-90% of cases leading to EWS-FLI1, followed by translocation t(21;22)(q22,q12) leading to the EWS-ERG fusion, occurring in 10-15% of cases [1]. Remaining Ewing sarcomas express rare fusions such as EWS-ETV1, EWS-ETV4, and EWS-FEV, each encompassing <1% of tumors [1]. EWS-FLI1 is the product of a chromosomal translocation fusing the N-terminal domain of EWSR1 to the DNA-binding domain of ETS transcription factor, FLI1. EWSR1 is an RNA binding protein and its N-terminal consists of an intrinsically disordered, low-complexity, prion-like, transactivation domain. The transactivation of EWSR1 is mostly silenced in the wildtype protein but becomes activated after loss of the C-terminal, while the RNA binding domain is lost in the creation of the fusion. Due to its DNA-binding abilities, EWS-FLI1 acts as an aberrant transcription factor that promotes widespread epigenetic and transcriptional reprogramming through its function at enhancers and gene promoters [15-17]. Importantly, while EWS-ETS proteins are considered the tumor-initiating oncogenic event, expression of EWS-FLI1 in most non-transformed primary

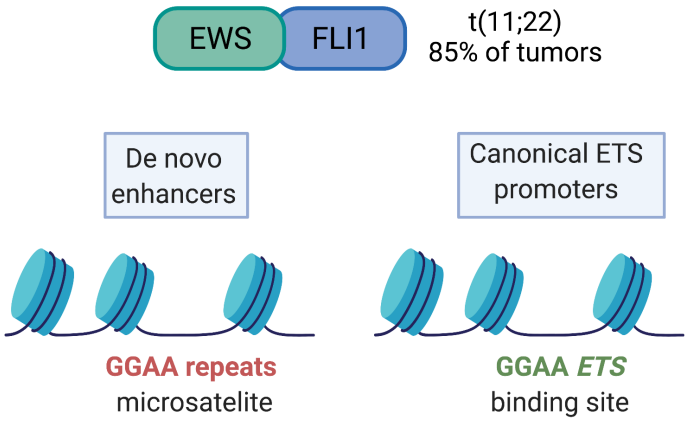

Figure 1-2 EWS-FLI1 and the epigenome

Diagram depicting the two mechanism by which EWS-FLI1 regulates gene expression. EWS-FLI1 can (1) act as a pioneer factor and establish *de novo* enhancers by recruiting the BAF (SWI/SNF) complex to GGAA repeats and aberrantly impact gene expression or (2) bind to canonical ETS GGAA sites at gene promoters. Diagram created with Biorender.com

cells induces senescence and apoptosis [12, 13]. The finding that MSCs are tolerant of EWS-FLI1 expression has thus provided a support for an MSC cell of origin [14, 15].

EWS-FLI1 acts by binding to consensus single GGAA ETS binding sites at promoters, or microsatellite GGAA repeats found throughout the genome (**Figure 1-2**). The binding of EWS-FLI1 to GGAA microsatellites leads to the opening of these regions through the recruitment of the chromatin-remodeling BAF (SWI/SNF) complex and direct interaction with chromatin-modifying machinery such as histone acetyltransferase, p300, and members of histone methyltransferase mixed-lineage leukemia (MLL) complexes, WDR5 and ASH2 [1, 16]. This results in the deposition of histone 3, lysine 27 acetylation (H3K27Ac) and histone 3, lysine 4 methylation (H3K4me1) marks, respectively, both associated with active chromatin. As a result, EWS-FLI1 functions as a pioneer factor to establish enhancers *de novo* from previously silenced regions, and DNA looping thus results in long-range regulatory enhancer interactions with gene promoters of positively regulated EWS-FLI1 target genes, or gene repression through upregulation of transcriptional repressors [16, 17]. Important direct EWS-FLI1 oncogenic target genes that that contribute to pathogenesis include NKX2.2 [18, 19], NR0B1 [20,

21], VRK1 [16] and EZH2 [22]. The role of EWS-FLI1 at wildtype ETS single GGAA repeats at gene promoters is less well characterized. Previous work has suggested that EWS-FLI1 can displace wildtype ETS factors from promoters, resulting in “non-productive” competition that leads to gene repression [16]. Other work has suggested that EWS-FLI1 can interact with the co-repressor complex NuRD (Nucleosome remodeling and deacetylase) and lysine-specific histone demethylase 1 (LSD1) to remove acetyl and methylation groups, respectively, from histones, reducing DNA accessibility [17].

Other than the pathognomonic fusion protein, Ewing sarcomas are otherwise gnomically quiet tumors with few recurrent mutations. Secondary mutations include mutations in STAG*2* in 21% of tumors, *TP53* (7%), and *CDKN2A* (up to 14%) [23-25]. However, some patients only express the EWS-ETS fusion and don’t harbor any additional mutations, supporting that EWS-ETS fusions are the tumor-initiating event and sufficient to promote malignant transformation. While this is an active area of investigation, thus far, efforts to target EWS-FLI1 itself have been largely unsuccessful due to its lack of enzymatic activity and disordered structure. Ongoing studies have aimed at inhibiting EWS-FLI1 activity by interfering with its interaction partners, such as the small molecule YK-4-279, which inhibits the interaction between EWS-FLI1 and RNA-helicase A. YK-4-279 has shown preclinical efficacy but has also displayed limited bioavailability and the acquisition of resistance [26]. Other work is exploring opportunities for gene editing with CRISPR/Cas9 knockout of EWS-FLI1 [27, 28], and recent work has also demonstrated that targeting of E3 ubiquitin ligase, TRIM8, which promotes the degradation of EWS-FLI1, can lead to oncogene overdose and may be a

therapeutically viable strategy to indirectly target EWS-FLI1 [29]. Alternative strategies have focused on agents that reverse the EWS-FLI1 gene signature, such as trabectedin, which showed limited single agent efficacy in phase II trials [30], and LSD1 inhibitors that are currently being evaluated clinically [31].

Menin: a scaffolding protein with diverse functions

Oncogenic fusion proteins, like EWS-FLI1, are able to coopt normal developmental gene expression programs in order to maintain their undifferentiated highly tumorigenic state [32]. Normal development is orchestrated, in part, by the competing actions of multiprotein complexes, namely trithorax group (TrxG) complexes

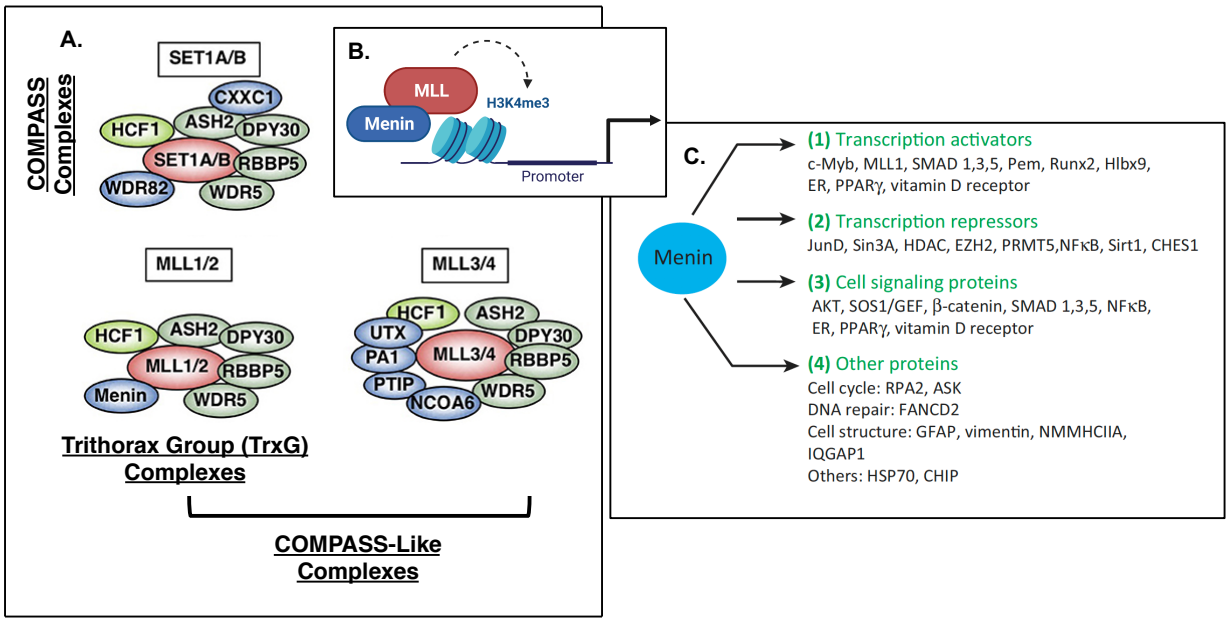

Figure 1-3 Trithorax-dependent and independent functions for menin

A. Diagram depicting the protein subunits of COMPASS and COMPASS-like complexes, which modify chromatin by methylating histone 3, lysine 4 (H3K4). Trithorax group (TrxG) complexes contain the scaffolding protein menin and MLL1 or MLL2 methyltransferases. B. Schematic showing the methyltransferase function of MLL1/2 in depositing the H3K3me3 mark at gene promoters. C. List of diverse functions for menin, in gene regulation, cell signaling, and others. (A) Was adapted from Onodera, Kokubo, Nakayama *et al*., 2018. Creative Commons Attribution License (CC BY). (B) was created with Biorender (C) was taken from Matkar, Thiel, and Hua, 2014. License #5241940177625. Feb 04, 2022.

and polycomb group (PcG) complexes—evolutionarily conserved chromatin modifiers that activate and repress gene transcription, respectively. PcG and TrxG complexes not only play a role during normal development, but have been found to aberrantly function during tumorigenesis as well [33]. Expression of EZH2 and BMI1, two PcG complex proteins, is high and regulated by EWS-FLI1 in Ewing sarcoma, contributing to the tumorigenic phenotype [22, 34-36]. The most well studied targets of PcG and TrxG are *HOX* genes, developmental transcription factors that govern normal development, body patterning, and embryogenesis [37]. Further work from our lab paradoxically showed that, despite high repressive PcG activity, *HOX* gene expression, specifically the posterior *HOXD* (*HOXD10, HOXD11, HOXD13*) genes, is high in Ewing sarcoma, and *HOXD13* contributes to the tumorigenic phenotype [6, 38, 39].

TrxG complexes control gene activation through the action of lysine methyltransferases (KMTs) Set1/MLL, that open chromatin by depositing methylation groups on H3K4 [40]. These complexes are often referred to as COMPASS (COMplex of Proteins ASsociated with Set1), of which there is only one in yeast, 3 in drosophila, and six complexes in vertebrates. These complexes share 4 common subunits, namely WDR5, ASH2, RBBP5, and DPY30, and contain other complex-specific subunits (**Figure 1-3A**). Set1-containing COMPASS complexes in vertebrates execute more global H3K4 di and tri- methylation modifications, while MLL-containing “COMPASS-like” complexes deposit H3K4 di- and tri- methylation marks at development specific genes (**Figure 1-3B**). In mammals, the COMPASS-like complexes contain MLL methyltransferases (MLL1 (*KMT2A*), MLL2 (*KMT2B*), MLL3 (*KMT2C*), or MLL4 (*KMT2D*)). The Drosophila orthologue for COMPASS-like complexes containing MLL1

and MLL2 is referred to as the TrxG complex (**Figure 1-3A**) and from here on will be used interchangeably with human MLL1/2-containing complexes for simplicity. TrxG complexes are required for gene transcription from bivalent loci, such as *HOX* genes, which carry both H3K4me3 active and H3K27me3 PcG repressive marks. MLL1/2-containing TrxG complexes contain 2 additional protein subunits aside from the core 4, namely menin and HCF1.

Menin is a ubiquitously expressed scaffolding protein whose best characterized function is its role as an MLL1/2 binding partner in the context of epigenetic TrxG complexes [41], however, it is appreciated that menin has trithorax-independent non-epigenetic functions as well (**Figure 1-3C)** [41]. Menin is predominately a nuclear protein that is able to bind to DNA in a sequence-independent manner, dictated by its interaction with diverse and context-specific protein binding partners. In this way, menin is able to recruit both transcriptional activators, such as RUNX2 and SMADs, or transcriptional repressors such as JunD [41]. Of note, menin has also been shown to interact with c-MYC at E box sequences and recruit p-TEFb to promote transcriptional elongation of MYC target genes in HT-1080 cells [42]. Menin and MYC were also recently shown to interact in androgen receptor dependent prostate cancer cells, and menin can directly bind to and activate transcription of the *MYC* locus in this context [43]. Lastly, menin has been implicated in cell signaling processes and can regulate transforming-growth-factor beta (TGF-β), and Wnt signaling by directly interacting with SMAD3 and regulating nuclear β-catenin, respectively (**Figure 1-3C**) [41]

Menin in the context of cancer

The scaffolding protein menin was first identified as a bona fide tumor suppressor in the case of multiple endocrine neoplasia type 1 (MEN1) syndrome. Mutations in the *MEN1* gene lead to tumors of endocrine organs such as the pituitary gland, parathyroid, and pancreas [44]. However, menin can have both tumor suppressive and oncogenic functions in cancer, and the most classic example of the latter is in the case of MLL-rearranged (MLLr) leukemias. In MLLr leukemias the *MLL1* gene takes part in a chromosomal translocation with one of several fusion partners, leading to the formation and expression of MLL1 fusion proteins, such as MLL-AF9 and MLL-AF4, that drive leukemogenesis. The MLL1 fusion, menin, LEDGF, wildtype MLL1, and other transcriptional activators like Dot1L and pTEFb bind in complex to activate expression of genes that drive leukemogenesis, such as *HOXA9* and *MEIS1* [45]. The direct interaction between menin and MLL1 fusion proteins is critical for this aberrant gene activation, which led to the development of small molecule inhibitors that disrupt the menin:MLL interaction. These inhibitors have been shown to promote the differentiation of leukemic blasts and to lead to tumor regression [46-48].

The role of menin as an oncogenic driver has also been explored in other tumor types, and pharmacologic menin:MLL inhibitors are being evaluated pre-clinically in solid tumors. Menin has been shown to drive tumorgenicity in prostate cancer, colorectal cancer, sporadic breast cancers, and hepatocellular carcinoma, with oncogenic programs activated by menin:MLL methyltransferase activity [42, 49-51]. In breast cancer specifically, menin can directly interact with the estrogen receptor and bind at enhancers to activate ER target gene expression [51, 52]. In prostate cancer, menin is able to bind to the androgen receptor and recruit MLL to regulate expression of

androgen receptor-dependent genes, and menin inhibition can slow prostate cancer growth *in vivo* [49]. Our work in Ewing sarcoma identified a role for menin in promoting tumorgenicity, with inhibition of either menin or MLL1 significantly reducing Ewing sarcoma growth *in vitro* and *in vivo* [6]. Quite unexpectedly, our unbiased approach employing transcriptomic analysis revealed that the pathways most significantly affected upon menin inhibition related to cellular metabolism, with the serine biosynthesis pathway (SSP) as the most significantly inhibited pathway [7].

Menin as a novel metabolic regulator

Our finding that menin acts as an oncogene to drive metabolic reprogramming had, at the time, not been previously described in other tumor types [7]. It has since been appreciated that this phenomenon may extend to other cancer contexts as well, where menin has been shown to regulate glycolytic and oxidative phosphorylation (OXPHOS) pathways both in breast cancer and colorectal cancer models [42, 50, 53], and more recently has been implicated in an iron-dependent type of programmed cell death termed, ferroptosis [54]. Our finding that menin inhibition drastically impacted cellular metabolism, particularly amino acid biosynthetic pathways [7], motivated us to further understand the importance of cellular metabolism, both in the normal bone, and in the malignant sarcoma context.

Introduction to amino acid metabolism in primary bone sarcomas

Ewing sarcoma and osteosarcoma are predominately cancers of childhood and adolescence. While survival rates for other childhood malignancies, such as leukemia,

have improved steadily in recent decades, the five-year survival rate for Ewing sarcoma and osteosarcoma patients presenting with metastatic disease at diagnosis has not improved and remains, at best, 30% [11]. Furthermore, for patients with localized disease, the standard of care for these highly aggressive bone tumors consists of high dose chemotherapy, surgery, and radiation. This leads to significant long-term toxicities that contribute to decreased life expectancy and diminished quality of life [11].

Normal bone growth and metabolism throughout life are dependent on maintaining a balance between the constant and coincident processes of bone formation and bone resorption. Disruption to this balance in bone remodeling often occurs during normal aging when bone resorption can exceed bone formation, resulting in osteoporosis [55]. In contrast, during adolescence, the time at which Ewing sarcoma and osteosarcoma most commonly arise, rapid growth requires that bone formation, or osteogenesis, exceed the level of bone resorption. The central cellular mediators that carry out the processes of bone building and bone destruction are osteoblasts and osteoclasts, respectively. Normal bone remodeling is a high-energy process that is dependent on cellular metabolic processes, including amino acid pathways. While there is a somewhat limited exploration of amino acid metabolism in normal bone biology and homeostasis, dysregulated metabolism is recognized as a hallmark of cancer [56], where the rewiring of energetic pathways is required for supporting the biosynthetic demands of highly proliferative malignant cells [57]. Early interest in the field of cancer metabolism has focused on glucose metabolism, with more recent work revealing the importance of amino acids in cancer progression [58]. Amino acids play a central role, not only in protein synthesis, but also energy production, nucleotide synthesis, and

maintenance of redox homeostasis [59, 60]. More importantly, advancements have been made in the feasibility of targeting of amino acid metabolic pathways that are rewired in cancer, which may provide a therapeutic vulnerability [59]. This has led to the preclinical and clinical development of therapeutic drugs, such as amino acid degrading enzymes, inhibition of amino acid transporters, and targeting of *de novo* amino acid biosynthetic pathways.

In the following sections, I provide an overview of the amino acid requirements of primary bone malignancies, focused mainly on osteosarcoma and Ewing sarcoma and contrast this with amino acid dependencies in the “normal” bone environment. Lastly, I provide a summary of therapeutically targetable pathways that are currently under study and may, in the future, improve treatment responses and outcomes for patients with primary bone tumors.

Metabolic rewiring in cancer

The observation that cancer cells exhibit a rewiring of metabolic processes can be traced back to the work of Otto Warburg in the 1950s, with his finding that cancer cells preferentially use glycolysis, even in the presence of oxygen [61]. In tumors and proliferative cells, glucose uptake is high. Aerobic glycolysis provides glycolytic intermediates necessary for anabolic reactions that generate building blocks in cells [62]. The uptake and *de novo* synthesis of amino acids is critical for protein synthesis, energy production, as well as the regulation of signaling pathways and maintenance of cellular redox homeostasis. Cancer cells in culture are frequently described as being glucose and glutamine “addicted,” with glucose being the central process for harnessing

energy. Glutamine, the most abundant amino acid in the circulation, is used to fuel the TCA cycle for energy production, and supplies carbon and nitrogen for the generation of biosynthetic precursors such as nucleotides, non-essential amino acids, and fatty acids [63, 64].

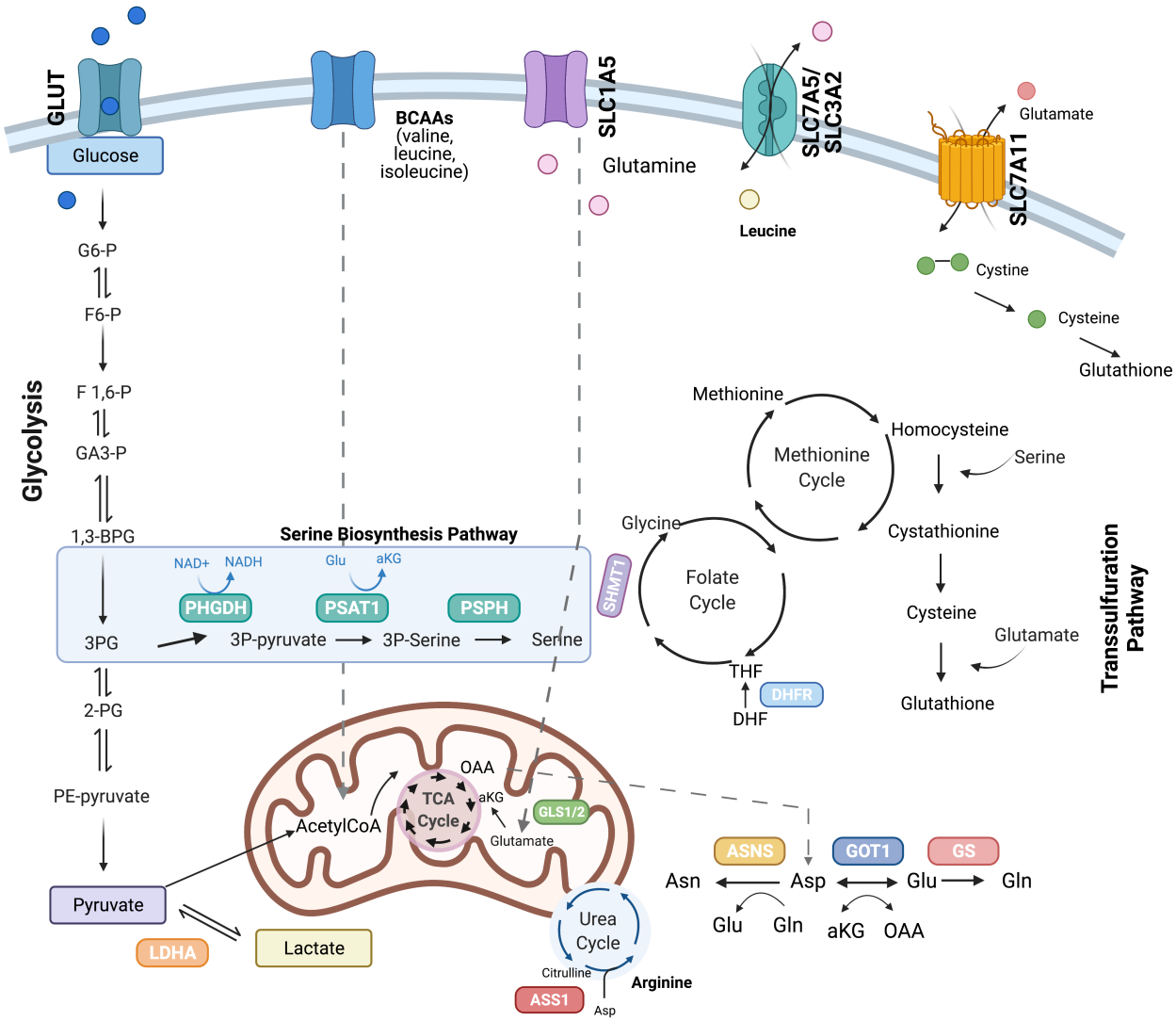

Figure 1-4 Amino acid pathways rewired in cancer

Illustration depicting amino acid pathways linked in an intricate metabolic network. The non-essential amino acid, serine, can be imported or synthesized *de novo* in the serine biosynthesis pathway (SSP), which diverts the 3P-glycerate intermediate of glycolysis. Similarly, cysteine is non-essential and can be synthesized in the transsulfuration pathway Both of these pathways, along with argininosuccinate synthetase 1 (ASS1), and glutamine metabolism have been implicated in sarcoma biology. Figure was created with Biorender.com

Essential amino acids, including the branched chain amino acids (BCAAs) leucine, isoleucine and valine, cannot be synthesized within the cell and instead require import from the extracellular environment. In contrast, non-essential amino acids can be synthesized *de novo*, providing cells with more flexibility when these amino acids become scarce (**Figure 1-4**) [59]. Cancers can become auxotrophic, or dependent on exogenous supply of non-essential amino acids, due to the loss of expression of key enzymes necessary for the synthesis of that amino acid, such as in the case of asparagine, arginine, and glutamine [59, 65, 66]. One of the most successful amino acid targeted therapies to date targets the de novo synthesis of asparagine. It was found in the 1970s that the use of bacterial asparaginase (ASNase) could cure children with pediatric acute lymphoblastic leukemia (ALL) when used as a single agent or as a combination therapy, due to low expression of asparagine synthetase (ASNS), the enzyme that converts aspartate to asparagine in leukemic blasts [67].

Aside from the case of autotrophy for non-essential amino acids, numerous cancers have also been shown to be dependent on other *de novo* amino acid biosynthetic pathways and exhibit upregulated expression of enzymes in these pathways. For example, expression of PHGDH, the rate-limiting enzyme in the serine biosynthetic pathway (SSP), is upregulated in breast cancer and melanoma, due to genomic amplification of the *PHGDH* locus, and the pathway has been shown to be essential for sustaining oncogenic growth [68, 69]. Studies have demonstrated that the effect of inhibition of PHGDH in cancer cells cannot be rescued by extracellular serine, suggesting that other intermediate products of the SSP represent a greater dependency

for these tumors [68]. While research is growing in the area, the investigation of amino acid requirements in primary bone sarcomas has been limited.

Metabolism during normal bone homeostasis

While it is appreciated that the skeleton is a metabolically active organ, and studies investigating the bioenergetic properties of bone can be traced back over 60 years [70-72], until recently, the metabolic dependencies of bone homeostasis had been relatively unexplored. Furthermore, knowledge regarding the amino acid dependencies in normal bone is even more limited. As such, determination and therapeutic exploitation of metabolic vulnerabilities in primary bone tumors, such as Ewing sarcoma and osteosarcoma, has lagged relative that of other tumor types.

Cycle of bone remodeling

The main cell types regulating bone homeostasis are the bone-building osteoblasts and the bone-destroying osteoclasts, which together make up ~5% of cells in the bone. Osteoblasts, and osteocytes originate from common precursor bone marrow mesenchymal stem cells [73], while osteoclasts are multinucleated cells that originate from hematopoietic progenitors in the bone marrow and result from the fusion of myeloid lineage monocytes (osteoclast precursor cells) (**Figure 1-5**). The cycle of bone remodeling consists of two main phases, the formation of bone, whereby osteoblasts function to produce and secrete alpha-1 type-1 collagen and mineralize bone; and bone resorption, where osteoclasts residing in resorption bays digest bone by

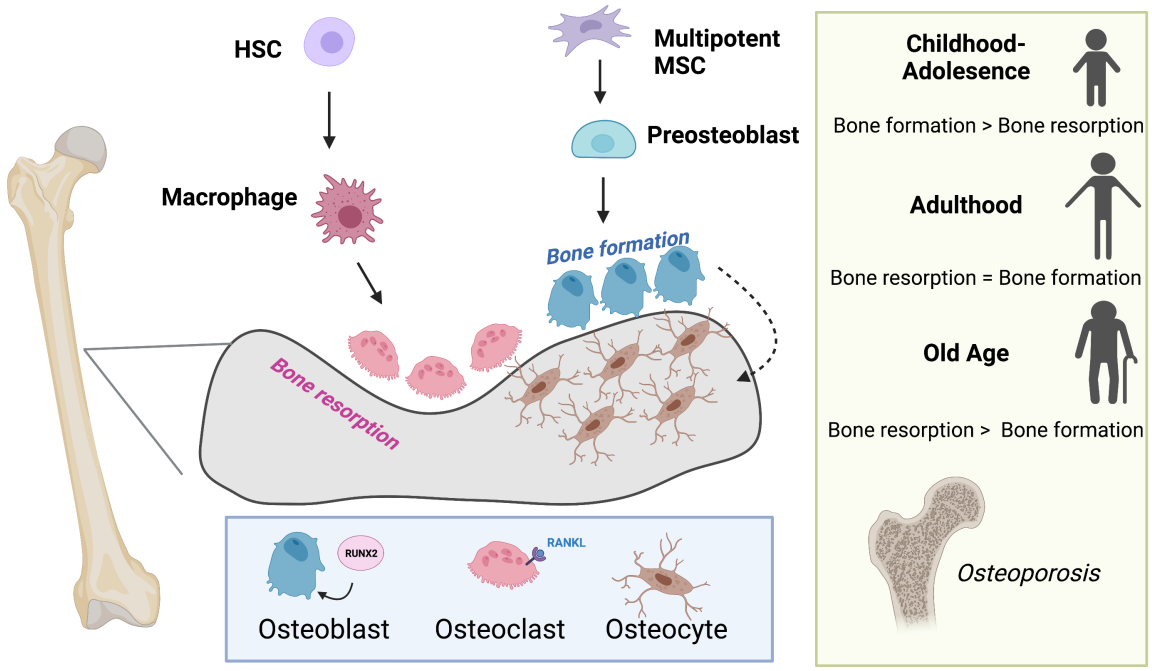

Figure 1-5 Osteoblasts, osteoclasts, and the cycle of bone remodeling

Bone remodeling balances the competing actions of the bone-building osteoblasts, and the osteoclasts that promote bone resorption, which dictates aging. Osteoblasts, and osteocytes originate from common precursor bone marrow mesenchymal stem cells (MSCs), while osteoclasts are multinucleated and originate from hematopoietic stem cells (HSCs) in the bone marrow Successful differentiation of progenitor cells into osteoblasts and osteoclasts requires the transcription factor, RUNX2 and RANK-ligand (RANKL), respectively. Figure was created with Biorender.com.

secreting proteases and acids to promote bone degradation [55]. Osteocytes are terminally differentiated osteoblasts consisting of 90-95% of bone and are the longest living bone cells. They are encased in the matrix of mature bone, and function by secreting matrix proteins and help to regulate osteoblast and osteoclast activity.

The complex signaling and molecular mechanisms that govern bone remodeling have been extensively studied. Successful differentiation of progenitor cells into osteoblasts and osteoclasts is controlled, respectively, by the transcription factor RUNX2 and the cytokine RANK ligand (RANKL), a member of the tumor necrosis factor (TNF) superfamily (**Figure 1-5**) [55]. Osteoblast function is regulated by numerous

autocrine and paracrine signals. In particular, osteoblasts respond to a range of stimuli, including insulin-growth factors (IGF), platelet-derived growth factor (PDGF), TGF-β, and bone morphogenetic proteins (BMP), as well as numerous classical hormones such as parathyroid and thyroid hormones. Similarly, osteoclast function is regulated by hormones including calcitonin, thyroid and parathyroid hormones, IGF-1, and PDGF [55]. Osteoclasts and osteoblasts are the most metabolically active cells in the normal bone environment. Little is known about the bioenergetic properties of osteocytes. Emerging work suggests that osteoblasts and osteoclasts must acquire the proper nutrients and amino acids to sustain their differentiation and execute their proper functions in orchestration of bone remodeling.

ATF4 plays a central role in physiologic bone remodeling

Although studies surrounding the bioenergetics of normal bone homeostasis have been relatively limited, the importance of glucose and glutamine utilization by osteoblasts and osteoclasts has been established. Osteoblasts in particular demonstrate a dependence on aerobic glycolysis that is also observed in cancer cells, and both osteoblasts and osteoclasts have a preferential need for upregulating glycolysis for cell differentiation and function [73]. The reasons for this phenomenon have not been fully elucidated and require further study. One can speculate that this may be a result of a dependency on glycolytic intermediates to fuel necessary biosynthetic reactions, such as *de novo* amino acid synthesis, that further support differentiation and function. It is curious, however, that osteoblasts upregulate expression of activating transcription factor 4 (ATF4), a master transcriptional regulator

of amino acid and stress-response pathways, in the terminal differentiation process [74]. ATF4 has been shown to regulate osteogenic genes and its phosphorylation by RSK2 is needed for differentiation [75]. ATF4 enhances bone formation by activating amino acid import and collagen synthesis, and studies have shown that implementing a high-protein diet in mouse models can overcome the effect of ATF4 loss on skeletal formation [75, 76]. ATF4 expression in osteoblasts has been demonstrated to be regulated at least in part via an mTORC1-GCN2-ATF4 axis [77, 78]. Interestingly, mTORC1 has been shown to play a role in the ATF4-dependent regulation of serine and glycine biosynthesis and downstream collagen production [79], suggesting another downstream pathway that would explain osteoblast dependence on ATF4 signaling.

Primary bone malignancies

Osteosarcoma

Osteosarcomas are the most common primary malignant bone sarcomas, consisting of 40-50% of bone sarcomas [80]. Osteosarcoma is characterized by a bimodal age distribution with peak incidence in children and adolescents, and a median age of 18, as well as a smaller second peak incidence in individuals over 60 years of age. The worldwide incidence of osteosarcoma is 1-3 cases annually per million individuals [81]. Over 75% of osteosarcoma cases occur in the metaphysis of the long bones, most commonly in the distal femur, proximal tibia, and humerus [82]. The current standard of care for osteosarcoma includes a combination of chemotherapy, which may include methotrexate, cisplatin, doxorubicin, ifosfamide, and etoposide, as well as surgery. Osteosarcoma cells are not readily responsive to radiation, so it does not play

a major role in treatment [83]. Due to limited success of new biologically targeted therapies, chemotherapeutic agents have been part of osteosarcoma treatment for decades, and standard of care has largely been unchanged. Commonly occurring genetic lesions or pathway alterations have not been identified in osteosarcoma, though mutations in p53, and Rb have been observed, along with significant cases of aneuploidy [84]. However, to this date, no clear molecular signatures have been identified that have led to successful targeted therapies [82].

Ewing sarcoma

Ewing sarcoma is the second most common pediatric bone tumor, with an incidence of 1 case per 1.5 million in the population and a highest incidence at 15 years of age. Ewing sarcoma can arise both in the bone and in soft tissue sites, most commonly in the pelvis and proximal long bones of the body [1]. Current treatment regimens include chemotherapy consisting of doxorubicin, etoposide, cyclophosphamide, vincristine, and ifosfamide, as well as local control with surgery and/or radiation [1]. Ewing sarcoma is characterized by the presence of EWS-ETS fusion proteins, most commonly EWS-FLI1, which results from a chromosomal t(11;22) translocation [26]. These fusion oncogenes act as the tumor-initiating event leading to malignant transformation. EWS-FLI1 acts as an aberrant transcription factor that promotes widespread epigenetic and transcriptional reprogramming through its function at enhancers and gene promoters [15-17]. Aside from the presence of the EWS-FLI1 fusion protein, Ewing sarcoma tumors are otherwise genomically quiet, with few other

recurrent mutations [32-34]. However, thus far, efforts to target EWS-FLI1 itself have been largely unsuccessful due to its lack of enzymatic activity and disordered structure.

Given the lack of therapeutically targetable mutations in primary bone sarcomas, characterization of metabolic dependencies may identity opportunities for novel therapeutic strategies. To date, investigation of the metabolic properties of sarcomas, in general, has been limited but early studies have begun to provide insights. Studies of sarcoma patients identified that their tumors displayed high rates of glycolytic activity and lactate production [85]. As a result, fluorodeoxyglucose positron emission tomography (FDG–PET) imaging is used clinically as a staging tool for several diverse types of cancers, including osteosarcoma and Ewing sarcoma, where it can be used to identify tumors at the primary site and skeletal and lymph node metastases. This radiographic tool can in some cases also be used to predict patient outcome and follow disease progression [86, 87]. More recently, data have emerged around the rewiring of other metabolic pathways in sarcomas. In the following sections we will summarize our current understanding of amino acid pathways dependencies in osteosarcoma and Ewing sarcoma.

Amino acid dependencies in osteosarcoma and Ewing sarcoma

The serine biosynthetic pathway (SSP) as a key dependency

The most extensively studied amino acid biosynthetic pathway in sarcomas is the SSP. As a non-essential amino acid, serine can be taken up extracellularly or synthesized *de novo*. The SSP utilizes the 3-phosphoglycerate (3-PG) intermediate of glycolysis as the carbon backbone to generate serine de novo via three enzymatic steps

carried out by the enzymes phosphoglycerate dehydrogenase (PHGDH), phosphoserine aminotransferase (PSAT1), and phosphoserine phosphatase (PSPH) (**Figure 1-4**). PHGDH expression is high in both osteosarcoma and Ewing sarcoma [2, 4, 5, 7, 88], and high PHGDH correlates with poor survival in both of these cancers, suggesting a clear dependency of these tumors on the SSP. In addition to its proteinogenic role, serine has numerous additional biological and metabolic functions, thus, the SSP contributes to a much broader metabolic hub. For example, one-carbon units from serine enter the folate cycle, which connects serine synthesis to both the folate and methionine cycles, as well as the transsulfuration pathway (**Figure 1-4**). The sum of metabolites produced by these interconnected networks contribute to de novo purine and pyrimidine synthesis, maintenance of glutathione (GSH) and NADPH pools for redox homeosis, as well as the production of methyl groups to fuel DNA and histone methylation reactions [89]. Preferential use of the SSP thus allows cancer cells to take advantage of the pathway for the generation of biomass and to promote cell growth and division.

Methotrexate is a dihydrofolate reductase (DHFR) inhibitor (**Figure 1-4**) and has been part of the standard of care for osteosarcoma for over 40 years. DHFR is critical enzyme in the folate cycle, downstream of the SSP, which catalyzes the reduction of dihydrofolate to tetrahydrofolate (THF), which is important for DNA synthesis and methylation. Recent mechanistic insights have thus shed light on longstanding empirically determined chemotherapy regimens utilizing methotrexate. In another example targeting these pathways, Rathore *et al.* recently explored the effect of PHGDH inhibition in osteosarcoma cell lines and xenograft models and provided

preclinical evidence for the combination of PHGDH inhibition with inhibition of mTORC1. Using metabolomic and lipidomic profiling, the authors identified the accumulation of fatty acids, BCAAs, S-Adenosy Methionine (SAM), and methionine in osteosarcoma following inhibition of PHGDH using the inhibitor NCT-503 [88]. They were able to show that PHGDH inhibition led to increased expression of SLC7A5 and SLC3A2 transports that drive transport of leucine into the lysosome, leading to mTORC1 activation (**Figure 1-4**). Given this finding, the researchers then demonstrated that combining NCT-503 with non-rapalog mTORC1 inhibitor perhexiline led to tumor reduction in xenograft models [88]. These studies are consistent with prior work, which also demonstrated that mTORC1 regulates osteosarcoma cell proliferation partly via the regulation of serine/glycine metabolism [90].

Numerous studies have focused on defining the role of the SSP in Ewing sarcoma [2, 4, 5, 7]. This work has shown that PHGDH is overexpressed in Ewing sarcoma cell lines and primary patient tumors, and that Ewing sarcoma cells are highly dependent on high activation of the SSP. Furthermore, several groups, including our own have demonstrated that the EWS-FLI1 fusion oncogene regulates expression of key enzymes in the SSP and their metabolic products, including *PHGDH*, *PSAT1*, and *PSPH* expression [2, 4, 5, 91]. In cancers without amplification of the *PHGDH* locus, such as lung cancer, activation of the SSP can be mediated through upregulation of ATF4 [92-95]. As detailed in Chapter 2 of this dissertation, studies from our lab showed that EWS-FLI1 is able to transcriptionally regulate expression of *ATF4* through direct promoter binding, and that ATF4 expression can also be regulated by the scaffolding protein menin, which also has an oncogenic role in Ewing sarcoma (**Figure 1-6**) [6, 91].

However, studies have been inconsistent on the predominate function of the SSP is in supporting Ewing sarcoma tumorgenicity. Some evidence suggests that inhibition of the SSP in Ewing sarcoma affects redox homeostasis and leads to the accumulation of ROS and DNA damage [2]. Other work has implicated PHGDH loss in impacting 2-hydroxyglutarate levels and increasing total histone-3 levels and methylation of histone H3 at lysine (K) 9 and K27, although with varied responses when comparing all of the cell lines evaluated [5]. These studies suggest that the SSP may serve an oncogenic role in Ewing sarcoma via multiple downstream metabolic impacts. In either case, recent work by Issaq and colleagues showed that PHGDH inhibition is a targetable

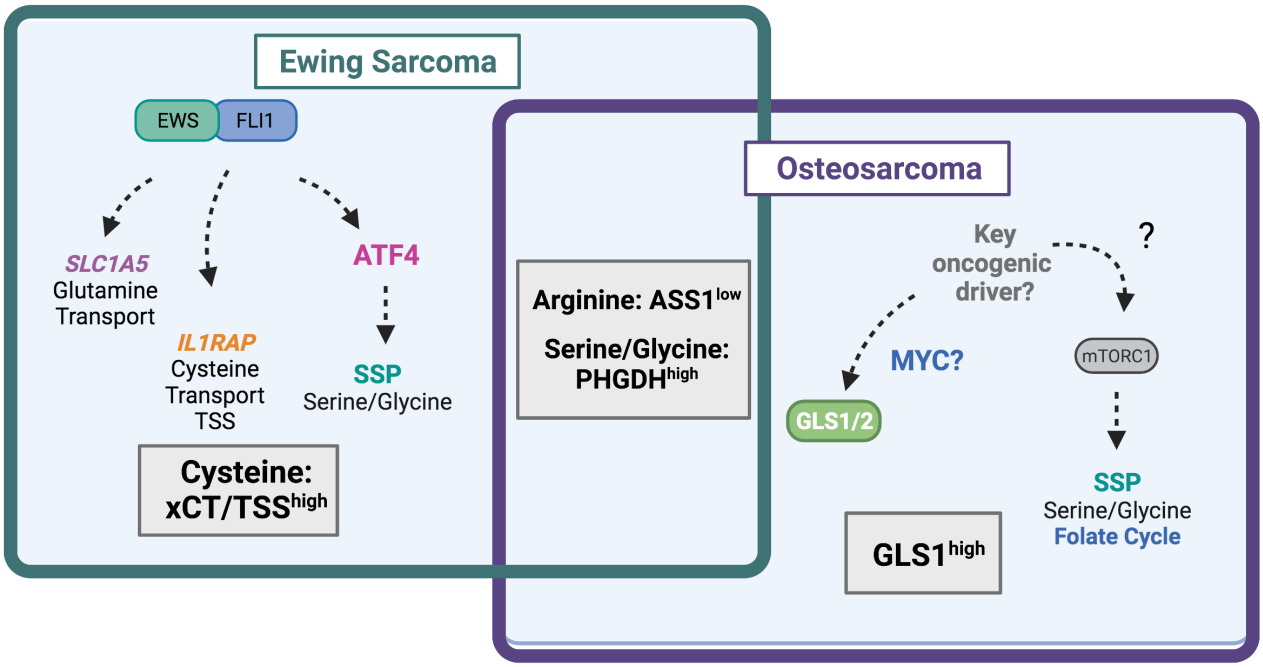

Figure 1-6 Amino acid dependencies in Ewing sarcoma and osteosarcoma

Venn-diagram depicting shared and unique amino acid vulnerabilities in Ewing sarcoma and osteosarcoma. The EWS-FLI1 fusion protein has been shown to directly regulate expression of glutamine transporter *SLC1A5* and *IL1RAP* leading to high glutamine import and cysteine pathway activation, respectively. EWS-FLI1 indirectly regulates the serine biosynthesis pathway (SSP) via ATF4. In osteosarcoma, the SSP also drives tumorgenicity through undefined mechanisms likely involving mTORC1. The mitochondrial enzyme GLS1, which may be under the control of MYC is highly expressed in osteosarcoma and predicts worse survival. Diagram was created with Biorender.com

vulnerability, where combination with inhibition of nicotinamide phosphoribosyltransferase (NAMPT), which blocks synthesis of the PHGDH substrate NAD+, had a synergistic effect *in vitro* and in *in vivo* xenograft models [4].

In primary bone sarcomas, the SSP has received extensive attention, given the high levels of PHGDH that are observed in both osteosarcoma and Ewing sarcoma [2, 4, 5, 7, 88, 90]. While the mechanism of SSP activity in Ewing sarcoma can be attributed to the direct and indirect effects EWS-FLI1 fusion-mediated metabolic reprogramming (Chapter 2), the mechanism by which the SSP is regulated in osteosarcoma is much less clear, likely due to the lack of known oncogenic drivers. Interestingly, wildtype p53 has been shown to reduce PHGDH in melanoma [96]. The majority of osteosarcomas exhibit mutations in p53, suggesting a potential mechanism of SSP regulation [97]. Importantly, PHGDH inhibition has been reported to induce cell death in Ewing sarcoma [5], but not in osteosarcoma where PHGDH inhibition resulted in cytostasis [88]. Whether this represents unique difference between the tumor types or technical experimental variables requires further study. Ewing sarcoma cells exhibit varying sensitivities to serine/glycine withdrawal [7], while all cells show reduced growth with PHGDH loss of function. Additionally, the effectiveness of PHGDH inhibition in osteosarcoma cells does not increase their sensitivity to serine/glycine depletion [88]. This suggests that Ewing sarcoma and osteosarcoma cells may be more dependent on the *de novo* synthesis of serine than the extracellular import of the amino acid.

Glutamine—A conditionally essential amino acid

Glutamine is a non-essential amino acid, as it is able to be synthesized by mammalian cells. Nonetheless, many tumors rely on extracellular glutamine for survival therefore classifying it as a conditionally essential amino acid [64]. Glutamine is the most abundant amino acid in the plasma, at levels between 500 and 750μM. In addition to its proteinogenic functions, glutamine also participates in the synthesis of other non-essential amino acids, as well as acting as an essential carbon and nitrogen donor for the synthesis of nucleotides, GSH, and glycosylation precursors.

Numerous studies have identified a dependence of osteosarcoma and Ewing sarcoma cells on glutamine and glutaminolysis. In cancer cells, the rate-limiting enzyme for glutaminolysis is glutaminase, the mitochondrial enzyme responsible for the conversion of glutamine to glutamate which can exist as one of two isoforms, glutaminase 1 (GLS1) and glutaminase 2 (GLS2). Molecularly, research has shown that MYC induced glutaminolysis occurs specifically in MYC-dependent osteosarcoma cells, but not in osteocytes (**Figure 1-6**) [98]. Work in Ewing sarcoma has demonstrated that EWS-FLI1 positively regulates expression of the glutamine transporter SLC1A5, potentially via the direct binding of the fusion to a regulatory sequence in the *SLC1A5* gene (**Figure 1-6**) [2]. Clinical studies with osteosarcoma patients have shown that GLS1 is highly expressed in osteosarcoma tumor tissue, which predicts poor survival (**Figure 1-6**). The effect of GLS1 inhibition was recently evaluated in osteosarcoma cell lines using metabolic flux analysis and tracing studies. These studies demonstrated that pharmacologic inhibition of GLS1 with CB-839, combined with electron transport chain (ETC) inhibitor metformin, reduced primary tumor growth and metastasis by inhibiting glycolytic and TCA cycle activity [99]. Furthermore, GLS1 expression decreases with

neoadjuvant chemotherapy, suggesting that GLS1 may be predictive of osteosarcoma treatment response [100]. Recent studies have also demonstrated success in therapeutically targeting GLS in cell line and murine models of soft tissue sarcomas [101].

Arginine—A case of auxotrophy in sarcomas

As a non-essential amino acid, arginine can be synthesized *de* novo, by the action of the argininosuccinate synthetase 1 (ASS1) enzyme, which converts citrulline and aspartate to arginine (**Figure 1-4**). Arginine autotrophy can result from the silencing of ASS1 in several tumor types, including sarcomas [102]. In cancers such as lymphomas, bladder cancer, and prostate cancer, diminished ASS1 expression can be due to methylation of the *ASS1* promoter [103]. In the case of sarcomas, a 2016 study found that almost 90% of sarcoma tumors have low ASS1 expression, however, *ASS1* promoter methylation is not observed in sarcomas. Bean *et al.* evaluated 701 bone or soft tissue sarcomas by immunohistochemistry analysis for ASS1 expression and found that the majority of primary bone tumors (87.2%, 34/39) and the majority of primary soft tissue tumors (86.4%, 572/662) had low ASS1 expression. 3 of 10 osteosarcoma tumors evaluated were determined to be ASS1 positive, while 1 of 7 Ewing sarcoma tumors evaluated were ASS1 positive [104]. By characterizing select $ASS1^{Low}$ cell lines, including osteosarcoma and Ewing sarcoma cell lines, the authors further showed that arginine deprivation with pegylated arginine deaminase (ADI-PEG20) led to cytostasis and a dependence on autophagy. Combining ADI-PEG20 with chloroquine, an autophagy inhibitor, led to necroptotic and apoptotic cell death. The authors tested this

synthetic lethal targeting strategy *in vivo* using subcutaneous xenografts in nude mice injected with MNNG/HOS osteosarcoma cells and showed that combining ADI-PEG20 with chloroquine led to the greatest reduction in tumor growth [104]. More recent studies have aimed to investigate the mechanistic basis of arginine dependence in sarcomas. Using a human osteosarcoma cell line model with tetracycline-inducible wildtype p53 expression, Lowman *et al.* were able to demonstrate that glutamine deprivation leads to phosphorylation of p53 at serine residue 15, resulting in the upregulation of arginine transporter *SLC7A3* and an increase in intracellular arginine levels. The authors were able to demonstrate that *SLC7A3* promotes tumor growth by maintaining mTORC1 via arginine influx. Furthermore, they found that ATF4 is also required for regulating SLC7A3 expression upon glutamine starvation [105].

Transsulfuration pathway and cysteine metabolism

Cysteine is another non-essential amino acid, which can be acquired from the extracellular space through several transport mechanisms or synthesized *de novo* in the transsulfuration pathway from serine and methionine (**Figure 1-4**). Cysteine is the rate-limiting substrate for the synthesis of the key antioxidant, GSH, which is critical for the maintenance of cellular redox homeostasis. A drop in GSH can lead to the accumulation of reactive oxygen species (ROS) and/or oxidized membrane phospholipids (lipid ROS). An inability to manage ROS leads to the oxidation of various biomolecules and can culminate in cell death. Thus, cancer cells employ a variety of mechanisms to mitigate ROS burden. As it relates to cysteine, many types of cancers will upregulate SLC7a11 expression, which encodes for xCT, the rate-limiting subunit of the cysteine-glutamate

antiporter system x_C-. In a recent study, application of 3D cultures with Ewing sarcoma cells in proteomic and translatomic screens found that the EWS-FLI1 fusion oncoprotein directly induces expression of system xCT and the transsulfuration pathway, via induction of *IL1RAP* expression, a cell surface IL-1 receptor co-receptor. The researcher found that IL1RAP directly binds system x_C- to increase its activity, and that EWS-FLI1 regulates *IL1RAP* expression through enhancer activation (**Figure 1-6**). IL1RAP was found to be highly expressed in Ewing sarcoma and important for promoting resistance to *anoikis*, detachment-induced cell death, and metastasis [106]. Although little is known about the role of cysteine and GSH metabolism in osteosarcoma, it has been demonstrated that osteosarcoma cell are dependent on methionine, suggesting that they may display a similar dependence on cysteine levels [107].

Bone microenvironment and metastasis

Metabolism in the bone tumor microenvironment

Bone consists of cells derived from MSCs, and tumors that arise in bone are considered sarcomas [108]. However, the precise cell of origin for both osteosarcoma and Ewing sarcoma is still unclear and highly debated [9, 80]. Stem and/or progenitor cells, particularly MSCs of mesoderm or neural crest origin have been proposed as the cell of origin for Ewing sarcoma [9], and recent data suggest that osteosarcoma cells can arise at multiple stages of bone development, from MSCs as well as osteoblasts and osteoclasts [80]. The timing of genetic and signaling events during development which govern transformation are not well known. Furthermore, how dysregulated

metabolism contributes to oncogenesis within cells undergoing transformation in the primary bone is not known. Moreover, how metabolic crosstalk with other cells in the tumor microenvironment (TME) contributes to transformation and tumorgenicity also warrants further exploration.

The function of non-malignant cells in mesenchymal tumors has been less studied when compared to epithelial cancers of adulthood [109]. Additionally, a distinguishing feature of sarcomas is that the distinction between malignant and stromal cells can be unclear, due to the mesenchymal origin of the tumor cells themselves [109]. Primary bone sarcomas grow in specialized and complex bone microenvironment that are highly vascularized and contain osteoclasts, osteoblasts, osteocytes, stromal cells (MSCs, fibroblasts), vascular cells (endothelial cells and pericytes), immune cells (macrophages, lymphocytes), and a mineralized extracellular matrix (ECM) [83]. This is fertile soil for tumor cells to hijack growth promoting pathways such as cytokines, chemokines, and growth factors in the bone microenvironment [83]. Remodeling and resorption of bone is a key feature of primary bone malignancies like osteosarcoma and Ewing sarcoma, leading to a highly osteolytic bone environment that provides space for growth of the tumor [109-111]. How metabolic crosstalk maintains this osteolytic environment is not well known.

MSCs have been shown to favorably impact osteosarcoma progression and contribute to osteolysis [112, 113]. Several studies have centered around the role of lactate in promoting an acidic microenvironment. Lactate released by both cancer cells and cells in the TME plays a prominent role in tumor progression, by increasing angiogenesis, motility and the migration of cancer cells [114]. Studies in osteosarcoma

models have demonstrated that lactate derived from MSCs feeds osteosarcoma [115]. MSCs are induced by adjacent osteosarcoma cells to undergo Warburg metabolism and increase lactate secretion and expression of the monocarboxylate transporter 4 (MCT4) lactate exporter. Lactate from MSCs feeds osteosarcoma and osteosarcoma cells import lactate via monocarboxylate transporter 1 (MCT1). This indirectly increases mitochondrial biogenesis and promotes the migration of osteosarcoma cells [115]. The mechanisms linking lactate metabolism to mitochondrial biogenesis and cell migration remain exciting avenues for further exploration.

Insights into the metabolic functions of the bone TME can also be gleaned from cancers that metastasize to the bone, such as breast cancer, prostate cancer, and multiple myeloma [116]. For example, Pollari *et al.* show that serine from breast cancer cells in the metastatic bone microenvironment contributes to the formation of bone resorbing human osteoclasts and may contribute to osteolysis [117]. Additionally, similar to studies in osteosarcoma, bone metastatic cancer cells have also been shown to release lactate via MCT4, which is taken up by MCT1 in osteoclasts to fuel oxidative phosphorylation and collagen resorption [118]. Interestingly, studies in multiple myeloma have shown that multiple myeloma cells prevent the differentiation of bone marrow stromal cells into osteoblasts in part by depleting glutamine. Finally, osteoblast differentiation increased expression of *ASNS* and asparagine could rescue osteoblast differentiation after glutamine depletion [119]. This examination of amino acid cross talk in the primary tumor of osteosarcoma an Ewing sarcoma is clearly lacking and further exploring this complex interaction with tumor-supporting cells in the bone

microenvironment will be central to determining the effectiveness of metabolic therapies and predicting potential resistance mechanisms in sarcomas.

Primary versus metastatic metabolism

The ability to starve cancer cells through dietary restriction and/or the use of targeted therapies has garnered extensive attention recently [120]. However, it is clear that the cancer context in which these therapies are evaluated is key to determining their therapeutic potential, and that the metabolic dependencies of the primary tumor differ from those of metastatic lesions. For instance, in breast cancer models, researchers have demonstrated that lung and brain metastases are more sensitive to targeting of serine biosynthesis than the primary tumor site, in part due to serine biosynthesis-dependent activation of mTORC1 [121-124]. In the brain, the low availability of serine and glycine makes brain metastases more sensitive to inhibition of PHGDH [122]. A deep understanding of metabolic dependencies in the tumor niche in bone for osteosarcoma and Ewing sarcoma compared to common sites of metastasis, such as the lung, is lacking and warrant further study.

Studies have begun to look at metabolic differences associated with metastasis in bone sarcomas. Using metabolic profiling and metabolic flux analysis in high and low metastatic cell lines, recent work has suggested that metastatic osteosarcoma cells activate pathways such as arginine, GSH, and fatty acid metabolism [125-127]. Additionally, GLS1 has recently been shown to play a role in promoting metastasis in osteosarcoma [99]. These studies have been more limited in Ewing sarcoma, though recent work, as previously described, has implicated cysteine metabolism downstream

of IL1RAP in promoting metastasis [106]. This work would benefit greatly from additional models for spontaneous metastasis, as the current models do not readily metastasize before mice succumb to primary tumor burden [128].

Therapeutic applications targeting amino acid metabolism in sarcomas

The current standard of care for sarcoma, consisting of surgery, chemotherapy and radiation has improved the life expectancy for patients, but survival has since plateaued without meaningful improvements in 30 years. Therefore, new therapies as well as diagnostic and prognostic tools are needed. As it relates to metabolism, there are new therapies under clinical evaluation for sarcomas. As previously discussed, preclinical studies showed that ~90% of sarcomas have low expression of *ASS1* making these cells more dependent on extracellular sources of arginine [104]. Further studies showed that treatment of $ASS1^{Low}$ sarcoma cell lines with PEGylated arginine deiminase (ADI-PEG20) sensitized cells to cell death induced by the chemotherapeutic agents, gemcitabine and docetaxel, leading to a still active Phase II clinical trial starting in May 2018 of ADI-PEG 20 in combination with gemcitabine and docetaxel for the treatment of bone and soft tissue sarcoma, including osteosarcoma, Ewing sarcoma, and small cell lung cancer (NCT03449901) [104, 129]. However, there are challenges in the clinical use of ADI-PEG20, due to acquired resistance to ADI-PEG20 by upregulation of ASS1 [104] or rewiring of other metabolic pathways, such an increased dependence on glutamine anaplerosis and the serine biosynthetic pathway upon arginine starvation [130]. Targeting these compensatory pathways with addition of a

GLS inhibitor or PHGDH inhibitor has been found to result in synthetic lethality in several models, including leiomyosarcoma [130].

Telaglenastat (CB-839) is a potent orally bioavailable GLS inhibitor that has exhibited anti-tumor activity in breast cancer and lymphoma [131, 132]. Current clinical trials are evaluating its efficacy in hematologic and solid cancers [133]. A recent metabolomics study tested the effect of GLS inhibition with CB-839 in undifferentiated pleomorphic sarcoma (UPS) and soft tissue sarcomas and found that GLS inhibition causes cell death [101]. These findings are promising for the translation of CB-839 to the clinic, especially for patients with osteosarcoma that exhibit high GLS1 activity [99, 100]. However, the use of GLS inhibitors needs to be carefully evaluated, given that in some contexts GLS dependency may be a phenomenon of cancer cells *in vitro* and tumors acquire compensatory mechanisms when GLS is inhibited *in vivo* [134, 135]. Given the dependency of numerous cancers on the SSP and PHGDH expression, PHGDH inhibition is a promising therapeutic vulnerability. Several small molecule enzymatic inhibitors against PHGDH are under preclinical development [123, 136, 137], however, none are yet ready for clinical examination [138].

Metabolomics technology has allowed for the profiling of cancer-associated metabolites, which could provide insight into tumor specific biomarkers. A recent 2020 study evaluated changes in amino acid levels between 23 sarcoma patients and 30 healthy control subjects using liquid chromatography-tandem mass spectrometry (LC-MS/MS). The researchers identified 4 amino acids or amino acid derivatives (glutamine, sarcosine, homoproline and citrulline) which decreased and 3 (carnosine, lysine, and glutamic acid) which increased in sarcoma patients [139]. Thus, this and future work in

this area will provide a potentially promising lead requiring further evaluation in larger cohorts of patients in order to determine the utility of metabolic profiling in patients. Though these patient-centered studies are very preliminary, the hope is that the identification of bone sarcoma-specific metabolic biomarkers will allow this technology to be used in the future for the diagnosis and monitoring of sarcoma patients.

Concluding remarks on amino acid metabolism in primary bone sarcomas

Many questions remain to be addressed when investigating metabolic dependencies in the bone tumor niche. Given the metabolic requirements during bone differentiation, the effect of amino acid therapies on normal developmental processes is something that should be thoughtfully considered for pediatric patients. Furthermore, differential amino acid requirements between the primary bone tumor and metastatic sites are not known and presents another open area of investigation with clinical implications. Based on precedent with metabolic therapies, and dynamic compensatory mechanisms, it is likely that targeting co-vulnerabilities will serve as the most viable option for patients, warranting further investigation into combination treatments that incorporate amino acid therapy.

Summary and Thesis Aims

Oncogenes reprogram cellular metabolism to sustain rapid growth and proliferation, and this rewiring is required for transformation and cell survival [140]. Ewing sarcoma is an aggressive pediatric bone and soft tissue tumor that is most

commonly driven by the pathognomonic EWS-FLI1 fusion oncogene. EWS-FLI1 is a transcription factor that promotes widespread epigenetic reprogramming and altered transcription but, to this day, is undruggable [15-17]. The functions of EWS-FLI1 on transcriptional dysregulation have been well characterized, but the metabolic consequences of this rewiring and how Ewing sarcoma cells manage the cellular demands imposed by this oncogenic stress are not well understood. Our laboratory also previously reported that the scaffolding protein menin is overexpressed by and promotes Ewing sarcoma cell tumorgenicity, partly by modulating cellular metabolism and amino acid biosynthetic pathways [18, 19]. We thus hypothesized that the oncogenic activities of EWS-FLI1 and menin may be mechanistically linked through their regulation of metabolic rewiring and that downstream pathways may thus contribute to maintenance of a highly tumorigenic state. In this thesis, we addressed this hypothesis through the following three aims.

Aim 1: Define the molecular mechanism(s) by which the epigenetic scaffolding protein, menin and EWS-FLI1 regulate cellular metabolism, including serine biosynthesis pathway (SSP) activation in Ewing sarcoma.

Aim 2: Identify pathways downstream of menin/EWS-FLI1-regulated metabolism that contribute to the tumorigenic phenotype and may be exploited therapeutically.

Aim 3: Determine why Ewing sarcomas are dependent on high-level expression of PHGDH and serine biosynthesis (SSP) pathway activation.

References

1. Riggi, N., M.L. Suva, and I. Stamenkovic, *Ewing's Sarcoma.* N Engl J Med, 2021. **384**(2): p. 154-164.
2. Sen, N., et al., *EWS-FLI1 reprograms the metabolism of Ewing sarcoma cells via positive regulation of glutamine import and serine-glycine biosynthesis.* Mol Carcinog, 2018.
3. Yeung, C., et al., *Targeting Glycolysis through Inhibition of Lactate Dehydrogenase Impairs Tumor Growth in Preclinical Models of Ewing Sarcoma.* Cancer Res, 2019. **79**(19): p. 5060-5073.
4. Issaq, S.H., et al., *EWS-FLI1-regulated serine synthesis and exogenous serine are necessary for Ewing sarcoma cellular proliferation and tumor growth.* Mol Cancer Ther, 2020.
5. Tanner, J.M., et al., *EWS/FLI is a Master Regulator of Metabolic Reprogramming in Ewing Sarcoma.* Mol Cancer Res, 2017. **15**(11): p. 1517-1530.
6. Svoboda, L.K., et al., *Tumorigenicity of Ewing sarcoma is critically dependent on the trithorax proteins MLL1 and menin.* Oncotarget, 2017. **8**(1): p. 458-471.
7. Svoboda, L.K., et al., *Menin regulates the serine biosynthetic pathway in Ewing sarcoma.* J Pathol, 2018. **245**(3): p. 324-336.
8. Palmerini, E., A. Righi, and E.L. Staals, *Rare Primary Malignant Bone Sarcomas.* Cancers (Basel), 2020. **12**(11).
9. Lin, P.P., Y. Wang, and G. Lozano, *Mesenchymal Stem Cells and the Origin of Ewing's Sarcoma.* Sarcoma, 2011. **2011**.
10. Balamuth, N.J. and R.B. Womer, *Ewing's sarcoma.* Lancet Oncol, 2010. **11**(2): p. 184-92.
11. Molina, E.R., et al., *Modeling the Tumor Microenvironment and Pathogenic Signaling in Bone Sarcoma.* Tissue Eng Part B Rev, 2020. **26**(3): p. 249-271.
12. Deneen, B. and C.T. Denny, *Loss of p16 pathways stabilizes EWS/FLI1 expression and complements EWS/FLI1 mediated transformation.* Oncogene, 2001. **20**(46): p. 6731-41.
13. Lessnick, S.L., C.S. Dacwag, and T.R. Golub, *The Ewing's sarcoma oncoprotein EWS/FLI induces a p53-dependent growth arrest in primary human fibroblasts.* Cancer Cell, 2002. **1**(4): p. 393-401.
14. Riggi, N., et al., *Development of Ewing's sarcoma from primary bone marrow-derived mesenchymal progenitor cells.* Cancer Res, 2005. **65**(24): p. 11459-68.
15. Castillero-Trejo, Y., et al., *Expression of the EWS/FLI-1 oncogene in murine primary bone-derived cells Results in EWS/FLI-1-dependent, ewing sarcoma-like tumors.* Cancer Res, 2005. **65**(19): p. 8698-705.
16. Riggi, N., et al., *EWS-FLI1 utilizes divergent chromatin remodeling mechanisms to directly activate or repress enhancer elements in Ewing sarcoma.* Cancer Cell, 2014. **26**(5): p. 668-681.
17. Sankar, S., et al., *Mechanism and relevance of EWS/FLI-mediated transcriptional repression in Ewing sarcoma.* Oncogene, 2013. **32**(42): p. 5089-100.
18. Owen, L.A., A.A. Kowalewski, and S.L. Lessnick, *EWS/FLI mediates transcriptional repression via NKX2.2 during oncogenic transformation in Ewing's sarcoma.* PLoS One, 2008. **3**(4): p. e1965.

19. Smith, R., et al., *Expression profiling of EWS/FLI identifies NKX2.2 as a critical target gene in Ewing's sarcoma.* Cancer Cell, 2006. **9**(5): p. 405-16.
20. Kinsey, M., et al., *EWS/FLI and its downstream target NR0B1 interact directly to modulate transcription and oncogenesis in Ewing's sarcoma.* Cancer Res, 2009. **69**(23): p. 9047-55.
21. Kinsey, M., R. Smith, and S.L. Lessnick, *NR0B1 is required for the oncogenic phenotype mediated by EWS/FLI in Ewing's sarcoma.* Mol Cancer Res, 2006. **4**(11): p. 851-9.
22. Richter, G.H., et al., *EZH2 is a mediator of EWS/FLI1 driven tumor growth and metastasis blocking endothelial and neuro-ectodermal differentiation.* Proc Natl Acad Sci U S A, 2009. **106**(13): p. 5324-9.
23. Brohl, A.S., et al., *The genomic landscape of the Ewing Sarcoma family of tumors reveals recurrent STAG2 mutation.* PLoS Genet, 2014. **10**(7): p. e1004475.
24. Crompton, B.D., et al., *The genomic landscape of pediatric Ewing sarcoma.* Cancer Discov, 2014. **4**(11): p. 1326-41.
25. Tirode, F., et al., *Genomic landscape of Ewing sarcoma defines an aggressive subtype with co-association of STAG2 and TP53 mutations.* Cancer Discov, 2014. **4**(11): p. 1342-53.
26. Lamhamedi-Cherradi, S.E., et al., *An Oral Formulation of YK-4-279: Preclinical Efficacy and Acquired Resistance Patterns in Ewing Sarcoma.* Mol Cancer Ther, 2015. **14**(7): p. 1591-604.
27. Martinez-Lage, M., et al., *In vivo CRISPR/Cas9 targeting of fusion oncogenes for selective elimination of cancer cells.* Nat Commun, 2020. **11**(1): p. 5060.
28. Cervera, S.T., et al., *Therapeutic Potential of EWSR1-FLI1 Inactivation by CRISPR/Cas9 in Ewing Sarcoma.* Cancers (Basel), 2021. **13**(15).
29. Seong, B.K.A., et al., *TRIM8 modulates the EWS/FLI oncoprotein to promote survival in Ewing sarcoma.* Cancer Cell, 2021. **39**(9): p. 1262-1278 e7.
30. Baruchel, S., et al., *A phase 2 trial of trabectedin in children with recurrent rhabdomyosarcoma, Ewing sarcoma and non-rhabdomyosarcoma soft tissue sarcomas: a report from the Children's Oncology Group.* Eur J Cancer, 2012. **48**(4): p. 579-85.
31. Pishas, K.I., et al., *Therapeutic Targeting of KDM1A/LSD1 in Ewing Sarcoma with SP-2509 Engages the Endoplasmic Reticulum Stress Response.* Mol Cancer Ther, 2018. **17**(9): p. 1902-1916.
32. Lawlor, E.R. and C.J. Thiele, *Epigenetic changes in pediatric solid tumors: promising new targets.* Clin Cancer Res, 2012. **18**(10): p. 2768-79.
33. Mills, A.A., *Throwing the cancer switch: reciprocal roles of polycomb and trithorax proteins.* Nat Rev Cancer, 2010. **10**(10): p. 669-82.
34. Riggi, N., et al., *EWS-FLI-1 expression triggers a Ewing's sarcoma initiation program in primary human mesenchymal stem cells.* Cancer Res, 2008. **68**(7): p. 2176-85.
35. von Levetzow, C., et al., *Modeling initiation of Ewing sarcoma in human neural crest cells.* PLoS One, 2011. **6**(4): p. e19305.
36. Douglas, D., et al., *BMI-1 promotes ewing sarcoma tumorigenicity independent of CDKN2A repression.* Cancer Res, 2008. **68**(16): p. 6507-15.

37. Hanson, R.D., et al., *Mammalian Trithorax and polycomb-group homologues are antagonistic regulators of homeotic development.* Proc Natl Acad Sci U S A, 1999. **96**(25): p. 14372-7.
38. Svoboda, L.K., et al., *Overexpression of HOX genes is prevalent in Ewing sarcoma and is associated with altered epigenetic regulation of developmental transcription programs.* Epigenetics, 2014. **9**(12): p. 1613-25.
39. von Heyking, K., et al., *The posterior HOXD locus: Its contribution to phenotype and malignancy of Ewing sarcoma.* Oncotarget, 2016. **7**(27): p. 41767-41780.
40. Ford, D.J. and A.K. Dingwall, *The cancer COMPASS: navigating the functions of MLL complexes in cancer.* Cancer Genet, 2015. **208**(5): p. 178-91.
41. Matkar, S., A. Thiel, and X. Hua, *Menin: a scaffold protein that controls gene expression and cell signaling.* Trends Biochem Sci, 2013. **38**(8): p. 394-402.
42. Wu, G., et al., *Menin enhances c-Myc-mediated transcription to promote cancer progression.* Nat Commun, 2017. **8**: p. 15278.
43. Luo, Y., et al., *The scaffold protein menin is essential for activating the MYC locus and MYC-mediated androgen receptor transcription in androgen receptor-dependent prostate cancer cells.* Cancer Commun (Lond), 2021. **41**(12): p. 1427-1430.
44. Lemmens, I., et al., *Identification of the multiple endocrine neoplasia type 1 (MEN1) gene. The European Consortium on MEN1.* Hum Mol Genet, 1997. **6**(7): p. 1177-83.
45. Krivtsov, A.V. and S.A. Armstrong, *MLL translocations, histone modifications and leukaemia stem-cell development.* Nat Rev Cancer, 2007. **7**(11): p. 823-33.
46. Borkin, D., et al., *Pharmacologic inhibition of the Menin-MLL interaction blocks progression of MLL leukemia in vivo.* Cancer Cell, 2015. **27**(4): p. 589-602.
47. Klossowski, S., et al., *Menin inhibitor MI-3454 induces remission in MLL1-rearranged and NPM1-mutated models of leukemia.* J Clin Invest, 2020. **130**(2): p. 981-997.
48. Krivtsov, A.V., et al., *A Menin-MLL Inhibitor Induces Specific Chromatin Changes and Eradicates Disease in Models of MLL-Rearranged Leukemia.* Cancer Cell, 2019. **36**(6): p. 660-673 e11.
49. Malik, R., et al., *Targeting the MLL complex in castration-resistant prostate cancer.* Nat Med, 2015. **21**(4): p. 344-52.
50. Katona, B.W., et al., *Combined Menin and EGFR Inhibitors Synergize to Suppress Colorectal Cancer via EGFR-Independent and Calcium-Mediated Repression of SKP2 Transcription.* Cancer Res, 2019. **79**(9): p. 2195-2207.
51. Dreijerink, K.M.A., et al., *Enhancer-Mediated Oncogenic Function of the Menin Tumor Suppressor in Breast Cancer.* Cell Rep, 2017. **18**(10): p. 2359-2372.
52. Dreijerink, K.M., et al., *Menin links estrogen receptor activation to histone H3K4 trimethylation.* Cancer Res, 2006. **66**(9): p. 4929-35.
53. Chou, C.W., et al., *Menin and Menin-Associated Proteins Coregulate Cancer Energy Metabolism.* Cancers (Basel), 2020. **12**(9).
54. Kato, I., T. Kasukabe, and S. Kumakura, *MeninMLL inhibitors induce ferroptosis and enhance the antiproliferative activity of auranofin in several types of cancer cells.* Int J Oncol, 2020. **57**(4): p. 1057-1071.

55. Hadjidakis, D.J. and Androulakis, II, *Bone remodeling.* Ann N Y Acad Sci, 2006. **1092**: p. 385-96.
56. Warburg, O., F. Wind, and E. Negelein, *The Metabolism of Tumors in the Body.* J Gen Physiol, 1927. **8**(6): p. 519-30.
57. Faubert, B., A. Solmonson, and R.J. DeBerardinis, *Metabolic reprogramming and cancer progression.* Science, 2020. **368**(6487).
58. Lieu, E.L., et al., *Amino acids in cancer.* Exp Mol Med, 2020. **52**(1): p. 15-30.
59. Vettore, L., R.L. Westbrook, and D.A. Tennant, *New aspects of amino acid metabolism in cancer.* Br J Cancer, 2020. **122**(2): p. 150-156.
60. Choi, B.H. and J.L. Coloff, *The Diverse Functions of Non-Essential Amino Acids in Cancer.* Cancers (Basel), 2019. **11**(5).
61. Koppenol, W.H., P.L. Bounds, and C.V. Dang, *Otto Warburg's contributions to current concepts of cancer metabolism.* Nat Rev Cancer, 2011. **11**(5): p. 325-37.
62. Whitburn, J. and C.M. Edwards, *Metabolism in the Tumour-Bone Microenvironment.* Curr Osteoporos Rep, 2021.
63. Liberti, M.V. and J.W. Locasale, *The Warburg Effect: How Does it Benefit Cancer Cells?* Trends Biochem Sci, 2016. **41**(3): p. 211-218.
64. Wise, D.R. and C.B. Thompson, *Glutamine addiction: a new therapeutic target in cancer.* Trends Biochem Sci, 2010. **35**(8): p. 427-33.
65. Feun, L., et al., *Arginine deprivation as a targeted therapy for cancer.* Curr Pharm Des, 2008. **14**(11): p. 1049-57.
66. Lomelino, C.L., et al., *Asparagine synthetase: Function, structure, and role in disease.* J Biol Chem, 2017. **292**(49): p. 19952-19958.
67. Clavell, L.A., et al., *Four-agent induction and intensive asparaginase therapy for treatment of childhood acute lymphoblastic leukemia.* N Engl J Med, 1986. **315**(11): p. 657-63.
68. Possemato, R., et al., *Functional genomics reveal that the serine synthesis pathway is essential in breast cancer.* Nature, 2011. **476**(7360): p. 346-50.
69. Locasale, J.W., et al., *Phosphoglycerate dehydrogenase diverts glycolytic flux and contributes to oncogenesis.* Nat Genet, 2011. **43**(9): p. 869-74.
70. Borle, A.B., N. Nichols, and G. Nichols, Jr., *Metabolic studies of bone in vitro. I. Normal bone.* J Biol Chem, 1960. **235**: p. 1206-10.
71. Peck, W.A., S.J. Birge, Jr., and S.A. Fedak, *Bone Cells: Biochemical and Biological Studies after Enzymatic Isolation.* Science, 1964. **146**(3650): p. 1476-7.
72. Cohn, D.V. and B.K. Forscher, *Aerobic metabolism of glucose by bone.* J Biol Chem, 1962. **237**: p. 615-8.
73. Motyl, K.J., et al., *Energy Metabolism of Bone.* Toxicol Pathol, 2017. **45**(7): p. 887-893.
74. Karner, C.M. and F. Long, *Glucose metabolism in bone.* Bone, 2018. **115**: p. 2-7.
75. Chan, W.C.W., et al., *Regulation and Role of Transcription Factors in Osteogenesis.* Int J Mol Sci, 2021. **22**(11).
76. Elefteriou, F., et al., *ATF4 mediation of NF1 functions in osteoblast reveals a nutritional basis for congenital skeletal dysplasiae.* Cell Metab, 2006. **4**(6): p. 441-51.

77. Hu, G., et al., *The Amino Acid Sensor Eif2ak4/GCN2 Is Required for Proliferation of Osteoblast Progenitors in Mice.* J Bone Miner Res, 2020. **35**(10): p. 2004-2014.
78. Karner, C.M., et al., *Increased glutamine catabolism mediates bone anabolism in response to WNT signaling.* J Clin Invest, 2015. **125**(2): p. 551-62.
79. Selvarajah, B., et al., *mTORC1 amplifies the ATF4-dependent de novo serine-glycine pathway to supply glycine during TGF-beta1-induced collagen biosynthesis.* Sci Signal, 2019. **12**(582).
80. Rathore, R. and B.A. Van Tine, *Pathogenesis and Current Treatment of Osteosarcoma: Perspectives for Future Therapies.* J Clin Med, 2021. **10**(6).
81. Kansara, M., et al., *Translational biology of osteosarcoma.* Nat Rev Cancer, 2014. **14**(11): p. 722-35.
82. Isakoff, M.S., et al., *Osteosarcoma: Current Treatment and a Collaborative Pathway to Success.* J Clin Oncol, 2015. **33**(27): p. 3029-35.
83. Corre, I., et al., *The Osteosarcoma Microenvironment: A Complex But Targetable Ecosystem.* Cells, 2020. **9**(4).
84. Martin, J.W., J.A. Squire, and M. Zielenska, *The genetics of osteosarcoma.* Sarcoma, 2012. **2012**: p. 627254.
85. Shaw, J.H., D.M. Humberstone, and R.R. Wolfe, *Energy and protein metabolism in sarcoma patients.* Ann Surg, 1988. **207**(3): p. 283-9.
86. Hawkins, D.S., et al., *Evaluation of chemotherapy response in pediatric bone sarcomas by [F-18]-fluorodeoxy-D-glucose positron emission tomography.* Cancer, 2002. **94**(12): p. 3277-84.
87. Harrison, D.J., M.T. Parisi, and B.L. Shulkin, *The Role of (18)F-FDG-PET/CT in Pediatric Sarcoma.* Semin Nucl Med, 2017. **47**(3): p. 229-241.
88. Rathore, R., et al., *Metabolic compensation activates pro-survival mTORC1 signaling upon 3-phosphoglycerate dehydrogenase inhibition in osteosarcoma.* Cell Rep, 2021. **34**(4): p. 108678.
89. Amelio, I., et al., *Serine and glycine metabolism in cancer.* Trends Biochem Sci, 2014. **39**(4): p. 191-8.
90. Wang, D.W., et al., *A novel mechanism of mTORC1-mediated serine/glycine metabolism in osteosarcoma development.* Cell Signal, 2017. **29**: p. 107-114.
91. Jimenez, J.A., et al., *EWS-FLI1 and Menin Converge to Regulate ATF4 Activity in Ewing Sarcoma.* Mol Cancer Res, 2021. **19**(7): p. 1182-1195.
92. DeNicola, G.M., et al., *NRF2 regulates serine biosynthesis in non-small cell lung cancer.* Nat Genet, 2015. **47**(12): p. 1475-81.
93. Reina-Campos, M., et al., *Increased Serine and One-Carbon Pathway Metabolism by PKClambda/iota Deficiency Promotes Neuroendocrine Prostate Cancer.* Cancer Cell, 2019. **35**(3): p. 385-400 e9.
94. Ding, J., et al., *The histone H3 methyltransferase G9A epigenetically activates the serine-glycine synthesis pathway to sustain cancer cell survival and proliferation.* Cell Metab, 2013. **18**(6): p. 896-907.
95. Xia, Y., et al., *Metabolic Reprogramming by MYCN Confers Dependence on the Serine-Glycine-One-Carbon Biosynthetic Pathway.* Cancer Res, 2019. **79**(15): p. 3837-3850.

96. Ou, Y., et al., *p53 Protein-mediated regulation of phosphoglycerate dehydrogenase (PHGDH) is crucial for the apoptotic response upon serine starvation.* J Biol Chem, 2015. **290**(1): p. 457-66.
97. Chen, X., et al., *Recurrent somatic structural variations contribute to tumorigenesis in pediatric osteosarcoma.* Cell Rep, 2014. **7**(1): p. 104-12.
98. Anso, E., et al., *Metabolic changes in cancer cells upon suppression of MYC.* Cancer Metab, 2013. **1**(1): p. 7.
99. Ren, L., et al., *Glutaminase-1 (GLS1) inhibition limits metastatic progression in osteosarcoma.* Cancer Metab, 2020. **8**: p. 4.
100. Zhang, S.P., et al., *Significance of neoadjuvant chemotherapy (NACT) in limb salvage treatment of osteosarcoma and its effect on GLS1 expression.* Eur Rev Med Pharmacol Sci, 2018. **22**(19): p. 6538-6544.
101. Lee, P., et al., *Targeting glutamine metabolism slows soft tissue sarcoma growth.* Nat Commun, 2020. **11**(1): p. 498.
102. Dillon, B.J., et al., *Incidence and distribution of argininosuccinate synthetase deficiency in human cancers: a method for identifying cancers sensitive to arginine deprivation.* Cancer, 2004. **100**(4): p. 826-33.
103. Delage, B., et al., *Promoter methylation of argininosuccinate synthetase-1 sensitises lymphomas to arginine deiminase treatment, autophagy and caspase-dependent apoptosis.* Cell Death Dis, 2012. **3**: p. e342.
104. Bean, G.R., et al., *A metabolic synthetic lethal strategy with arginine deprivation and chloroquine leads to cell death in ASS1-deficient sarcomas.* Cell Death Dis, 2016. **7**(10): p. e2406.
105. Lowman, X.H., et al., *p53 Promotes Cancer Cell Adaptation to Glutamine Deprivation by Upregulating Slc7a3 to Increase Arginine Uptake.* Cell Rep, 2019. **26**(11): p. 3051-3060 e4.
106. Zhang, H.F., et al., *Proteomic screens for suppressors of anoikis identify IL1RAP as a promising surface target in Ewing sarcoma.* Cancer Discov, 2021.
107. Mecham, J.O., et al., *The metabolic defect of methionine dependence occurs frequently in human tumor cell lines.* Biochem Biophys Res Commun, 1983. **117**(2): p. 429-34.
108. Dorfman, H.D. and B. Czerniak, *Bone cancers.* Cancer, 1995. **75**(1 Suppl): p. 203-10.
109. Ehnman, M., et al., *The Tumor Microenvironment of Pediatric Sarcoma: Mesenchymal Mechanisms Regulating Cell Migration and Metastasis.* Curr Oncol Rep, 2019. **21**(10): p. 90.
110. Norregaard, K.S., et al., *Osteosarcoma and Metastasis Associated Bone Degradation-A Tale of Osteoclast and Malignant Cell Cooperativity.* Int J Mol Sci, 2021. **22**(13).
111. Redini, F. and D. Heymann, *Bone Tumor Environment as a Potential Therapeutic Target in Ewing Sarcoma.* Front Oncol, 2015. **5**: p. 279.
112. Avnet, S., et al., *Cancer-associated mesenchymal stroma fosters the stemness of osteosarcoma cells in response to intratumoral acidosis via NF-kappaB activation.* Int J Cancer, 2017. **140**(6): p. 1331-1345.

113. Cortini, M., et al., *Tumor-Activated Mesenchymal Stromal Cells Promote Osteosarcoma Stemness and Migratory Potential via IL-6 Secretion.* PLoS One, 2016. **11**(11): p. e0166500.
114. Taddei, M.L., et al., *Lactate in Sarcoma Microenvironment: Much More than just a Waste Product.* Cells, 2020. **9**(2).
115. Bonuccelli, G., et al., *Role of mesenchymal stem cells in osteosarcoma and metabolic reprogramming of tumor cells.* Oncotarget, 2014. **5**(17): p. 7575-88.
116. Weilbaecher, K.N., T.A. Guise, and L.K. McCauley, *Cancer to bone: a fatal attraction.* Nat Rev Cancer, 2011. **11**(6): p. 411-25.
117. Pollari, S., et al., *Enhanced serine production by bone metastatic breast cancer cells stimulates osteoclastogenesis.* Breast Cancer Res Treat, 2011. **125**(2): p. 421-30.
118. Lemma, S., et al., *MDA-MB-231 breast cancer cells fuel osteoclast metabolism and activity: A new rationale for the pathogenesis of osteolytic bone metastases.* Biochim Biophys Acta Mol Basis Dis, 2017. **1863**(12): p. 3254-3264.
119. Chiu, M., et al., *Myeloma Cells Deplete Bone Marrow Glutamine and Inhibit Osteoblast Differentiation Limiting Asparagine Availability.* Cancers (Basel), 2020. **12**(11).
120. Butler, M., L.T. van der Meer, and F.N. van Leeuwen, *Amino Acid Depletion Therapies: Starving Cancer Cells to Death.* Trends Endocrinol Metab, 2021. **32**(6): p. 367-381.
121. Rinaldi, G., et al., *In Vivo Evidence for Serine Biosynthesis-Defined Sensitivity of Lung Metastasis, but Not of Primary Breast Tumors, to mTORC1 Inhibition.* Mol Cell, 2021. **81**(2): p. 386-397 e7.
122. Ngo, B., et al., *Limited Environmental Serine and Glycine Confer Brain Metastasis Sensitivity to PHGDH Inhibition.* Cancer Discov, 2020. **10**(9): p. 1352-1373.
123. Pacold, M.E., et al., *A PHGDH inhibitor reveals coordination of serine synthesis and one-carbon unit fate.* Nat Chem Biol, 2016. **12**(6): p. 452-8.
124. Sullivan, M.R., et al., *Increased Serine Synthesis Provides an Advantage for Tumors Arising in Tissues Where Serine Levels Are Limiting.* Cell Metab, 2019. **29**(6): p. 1410-1421 e4.
125. Fritsche-Guenther, R., et al., *Progression-Dependent Altered Metabolism in Osteosarcoma Resulting in Different Nutrient Source Dependencies.* Cancers (Basel), 2020. **12**(6).
126. Ren, L., et al., *Metabolomics uncovers a link between inositol metabolism and osteosarcoma metastasis.* Oncotarget, 2017. **8**(24): p. 38541-38553.
127. Dean, D.C., et al., *From genomics to metabolomics: emerging metastatic biomarkers in osteosarcoma.* Cancer Metastasis Rev, 2018. **37**(4): p. 719-731.
128. Imle, R., F.K.F. Kommoss, and A. Banito, *Preclinical In Vivo Modeling of Pediatric Sarcoma-Promises and Limitations.* J Clin Med, 2021. **10**(8).
129. Prudner, B.C., et al., *Arginine Starvation and Docetaxel Induce c-Myc-Driven hENT1 Surface Expression to Overcome Gemcitabine Resistance in ASS1-Negative Tumors.* Clin Cancer Res, 2019. **25**(16): p. 5122-5134.

130. Kremer, J.C., et al., *Arginine Deprivation Inhibits the Warburg Effect and Upregulates Glutamine Anaplerosis and Serine Biosynthesis in ASS1-Deficient Cancers.* Cell Rep, 2017. **18**(4): p. 991-1004.
131. Jacque, N., et al., *Targeting glutaminolysis has antileukemic activity in acute myeloid leukemia and synergizes with BCL-2 inhibition.* Blood, 2015. **126**(11): p. 1346-56.
132. Gross, M.I., et al., *Antitumor activity of the glutaminase inhibitor CB-839 in triple-negative breast cancer.* Mol Cancer Ther, 2014. **13**(4): p. 890-901.
133. Song, M., et al., *Recent Development of Small Molecule Glutaminase Inhibitors.* Curr Top Med Chem, 2018. **18**(6): p. 432-443.
134. Davidson, S.M., et al., *Environment Impacts the Metabolic Dependencies of Ras-Driven Non-Small Cell Lung Cancer.* Cell Metab, 2016. **23**(3): p. 517-28.
135. Biancur, D.E., et al., *Compensatory metabolic networks in pancreatic cancers upon perturbation of glutamine metabolism.* Nat Commun, 2017. **8**: p. 15965.
136. Mullarky, E., et al., *Identification of a small molecule inhibitor of 3-phosphoglycerate dehydrogenase to target serine biosynthesis in cancers.* Proc Natl Acad Sci U S A, 2016. **113**(7): p. 1778-83.
137. Wang, Q., et al., *Rational Design of Selective Allosteric Inhibitors of PHGDH and Serine Synthesis with Anti-tumor Activity.* Cell Chem Biol, 2017. **24**(1): p. 55-65.
138. McNamee, M.J., D. Michod, and M.V. Niklison-Chirou, *Can small molecular inhibitors that stop de novo serine synthesis be used in cancer treatment?* Cell Death Discov, 2021. **7**(1): p. 87.
139. Jia, B., et al., *The free amino acid profiles and metabolic biomarkers of predicting the chemotherapeutic response in advanced sarcoma patients.* Clin Transl Oncol, 2020. **22**(12): p. 2213-2221.
140. Nagarajan, A., P. Malvi, and N. Wajapeyee, *Oncogene-directed alterations in cancer cell metabolism.* Trends Cancer, 2016. **2**(7): p. 365-377.

Chapter 2 EWS-FLI1 and Menin Converge to Regulate ATF4 Activity in Ewing sarcoma

Summary

[2]Ewing sarcomas are driven by EWS-ETS fusions, most commonly EWS-FLI1, which promote widespread metabolic reprogramming, including activation of serine biosynthesis. We previously reported that serine biosynthesis is also activated in Ewing sarcoma by the scaffolding protein menin through as yet undefined mechanisms. Here, we investigated whether EWS-FLI1 and/or menin orchestrate serine biosynthesis via modulation of ATF4, a stress-response gene that acts as a master transcriptional regulator of serine biosynthesis in other tumors. Our results show that in Ewing sarcoma, ATF4 levels are high and that ATF4 modulates transcription of core serine synthesis pathway (SSP) genes. Inhibition of either EWS-FLI1 or menin leads to loss of ATF4, and this is associated with diminished expression of SSP transcripts and proteins. We identified and validated an EWS-FLI1 binding site at the *ATF4* promoter,

---

[2] This research was originally published in *Molecular Cancer Research*. Jennifer A. Jiménez, April A. Apfelbaum, Allegra G. Hawkins, Laurie K. Svoboda, Abhijay Kumar, Ramon Ocadiz Ruiz, Alessandra X. Garcia, Elena Haarer, Zeribe C. Nwosu, Joshua Bradin, Trupta Purohit, Dong Chen, Tomasz Cierpicki, Jolanta Grembecka, Costas A. Lyssiotis, and Elizabeth R. Lawlor. EWS-FLI1 and Menin Converge to Regulate ATF4 Activity in Ewing sarcoma. Mol Cancer Res. 2021;19(7):1182-1195.

indicating that the fusion can directly activate ATF4 transcription. In contrast, our results suggest that menin-dependent regulation of ATF4 is mediated by transcriptional and post-transcriptional mechanisms. Importantly, our data also reveal that the downregulation of SSP genes that occurs in the context of EWS-FLI1 or menin loss is indicative of broader inhibition of ATF4-dependent transcription. Moreover, we find that menin inhibition similarly leads to loss of ATF4 and the ATF4-dependent transcriptional signature in MLL-rearranged B-cell acute lymphoblastic leukemia, extending our findings to another cancer in which menin serves an oncogenic role. *Implications*: These studies provide new insights into metabolic reprogramming in Ewing sarcoma and also uncover a previously undescribed role for menin in the regulation of ATF4.

Introduction

Ewing sarcoma is an aggressive bone and soft tissue tumor and the second most common pediatric bone tumor. Despite maximally intensive therapy, Ewing sarcoma remains lethal for a third of patients, and survival rates for patients with metastatic or relapsed disease are dismal [1-3]. Furthermore, the current standard of care leaves patients with profound and devastating long-term toxicities [4-6]. Ewing sarcoma is defined by the presence of EWS-ETS fusion proteins, most commonly EWS-FLI1, which results from a t(11;22) chromosomal translocation, fusing the N-terminal domain of EWSR1 to the DNA-binding domain of FLI1 [2]. This tumor-initiating event leads to malignant transformation of the cell of origin, which is presumed to be a stem or progenitor cell of mesoderm or neural crest lineage [7]. EWS-FLI1 initiates and maintains tumorigenicity through diverse functions that converge on disruption of normal

transcriptional regulation and splicing [8-11]. In particular, EWS-ETS proteins promote widespread epigenetic and transcriptional reprogramming by binding and creating *de novo* enhancers at GGAA microsatellites in intergenic regions and by direct promoter binding [8-10]. Significantly, aside from the presence of the pathognomonic gene fusions, Ewing sarcoma tumors are genomically quiet, with few other recurrent mutations [12-14]. Thus, the molecular mechanisms underlying tumor initiation and progression are inherently linked to the function of EWS-ETS proteins.

Metabolic reprogramming is essential for tumor cell survival under conditions of stress, including both cell intrinsic (e.g., genotoxic, proliferative, protein folding) and extrinsic (e.g., hypoxia, nutrient deprivation, growth constraint) stressors. In recent years it has become apparent that tumor cells orchestrate complex and interconnected enzymatic programs to retain metabolic homeostasis under conditions of stress, including the regulation of amino acid biosynthesis pathways [15]. Serine is a non-essential amino acid that, in addition to its proteinogenic role, is used for the maintenance of redox, epigenetic, and proliferative homeostasis. Significantly, many cancers display enhanced activation of and dependence on the serine synthesis pathway (SSP) for tumor survival and propagation [16]. Recent studies from our group and others have reported that Ewing sarcomas are highly dependent on SSP activity, and that 3-phosphoglycerate dehydrogenase (*PHGDH*), the rate-limiting enzyme in the pathway, is highly overexpressed by Ewing sarcoma cell lines and patient tumors [17-20]. Knockdown of EWS-FLI1 leads to loss of SSP gene expression and pathway activation, revealing that the fusion contributes directly or indirectly to SSP activation [17, 19, 20]. In addition, we reported that the scaffolding protein and trithorax complex

protein menin also maintains SSP activity in Ewing sarcoma cells, and that this is mediated in part through epigenetic activation of *PHGDH* [18]. Nevertheless, the precise molecular mechanisms that control hyperactivation of the SSP in Ewing sarcoma remain to be elucidated.

In melanoma and breast cancers, the SSP is often activated as a result of amplification of the *PHGDH* locus [21, 22]. In contrast, in non-small cell lung cancer and other solid tumors that lack *PHGDH* amplification, activation of the SSP has been attributed to activating transcription factor 4 (ATF4), a master transcriptional regulator of amino acid metabolism and stress responses [15, 16, 23-27]. ATF4 orchestrates a distinct gene expression program that allows cancer cells to adapt to an increased demand for metabolites and macromolecules, supporting growth and survival in harsh environments [15]. In the current work, we investigated whether ATF4 contributes to SSP activation in Ewing sarcoma and whether EWS-FLI1- and/or menin-mediated effects on this metabolic pathway involve ATF4. Our findings provide evidence that ATF4 does indeed act as a central node in SSP modulation in Ewing sarcoma, acting downstream of both EWS-FLI1 and menin. Importantly, we also find that the effects of menin on the ATF4-SSP response are not limited to Ewing sarcoma but are also evident in mixed lineage leukemia (MLL)-rearranged (MLLr) leukemia cells. These results provide novel insights into the molecular mechanisms by which cellular metabolism is rewired in Ewing sarcoma. In addition, they reveal a previously undescribed connection between menin and ATF4.

Results

ATF4 regulates serine biosynthesis pathway expression in Ewing sarcoma

To determine the molecular mechanism by which the SSP is activated in Ewing sarcoma, we first investigated ATF4, given that it regulates the pathway in other cancers [16, 23-27]. Gene expression studies of tumor biopsies show that *ATF4* transcript expression is highly variable in Ewing sarcoma tumors *in vivo* (**Figure 2-1A**). Our studies of Ewing sarcoma cell lines *in vitro* revealed similarly variable expression of *ATF4* mRNA and protein, but levels were generally higher in Ewing than non-Ewing cells under ambient conditions (**Figure 2-1B**). Given its status as a highly dynamic and stress-induced transcription factor, this variability in expression is not unexpected [28]. Knockdown of ATF4 in Ewing sarcoma cells led to reduced cell proliferation, as determined by direct cell counting (**Figure 2-1C**) and real-time proliferation assays (**Supplementary Fig. S2-1A**), indicating that, in standard culture conditions, ATF4 supports the proliferative state. The SSP generates serine *de novo* by diverting the 3-phosphogycerate intermediate from glycolysis via three enzymatic steps requiring the enzymes PHGDH, phosphoserine aminotransferase (PSAT1), and phosphoserine phosphatase (PSPH) [29]. Loss of ATF4 was accompanied by marked and reproducible downregulated expression of all three core SSP transcripts (**Figure 2-1D**) and proteins (**Figure 2-1E**). Chromatin immunoprecipitation qPCR (ChIP-qPCR) studies confirmed that ATF4 binding is enriched at the *PHGDH* and *PSAT1* promoters, supporting direct transcriptional regulation of these genes by ATF4 (**Figure 2-1F**). Of note, we were unable to successfully design primers capturing the *PSPH* promoter region due to high

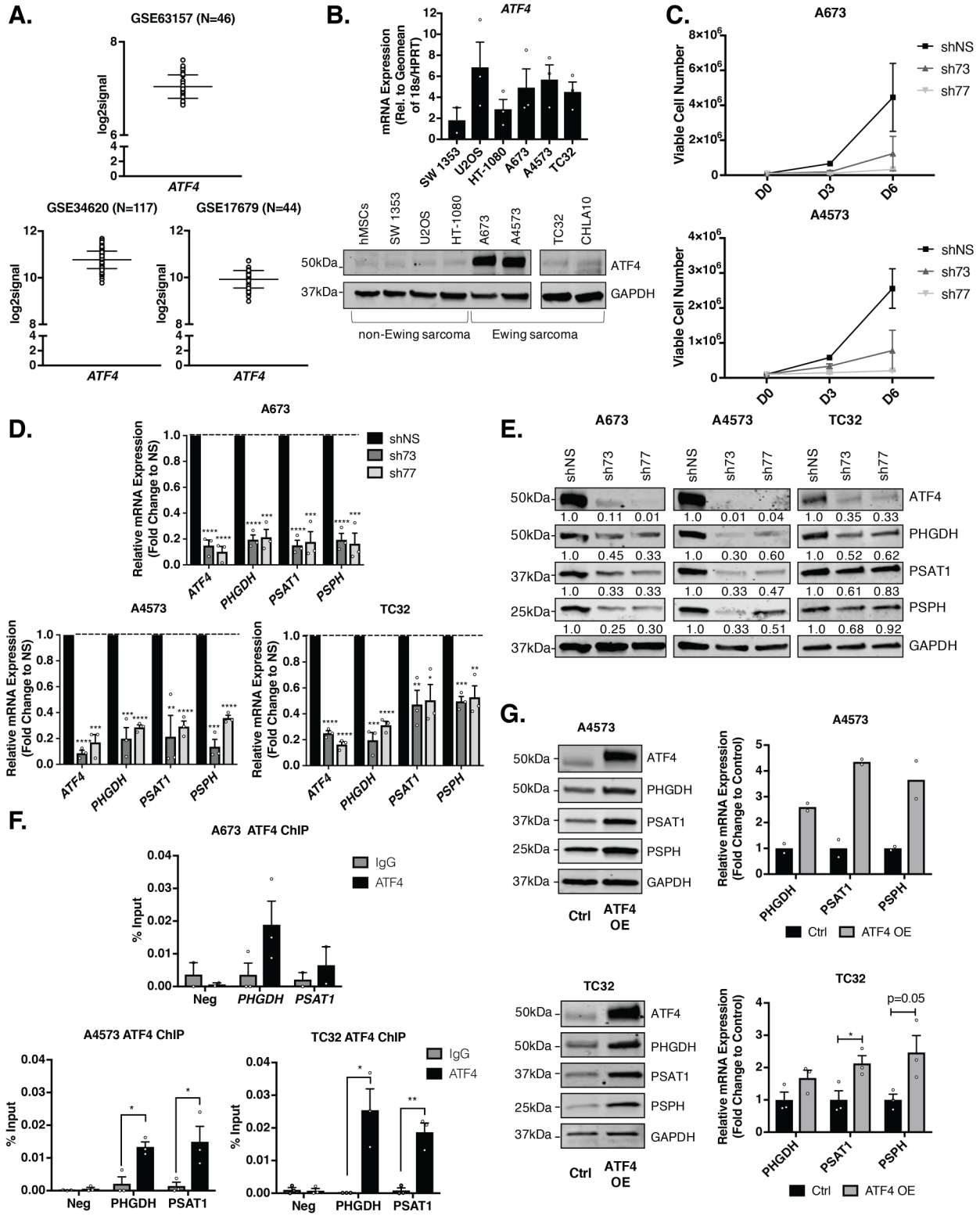

Figure 2-1 ATF4 modulates serine biosynthesis pathway genes in Ewing sarcoma.

sequence homology with other regions in the genome, which we believe has precluded

A, ATF4 gene expression in patient tumors from three independently published Ewing sarcoma datasets [48-50]. B, ATF4 mRNA and protein levels in Ewing sarcoma cell lines and non-Ewing mesenchymal cell lines (N=3). C, Trypan blue exclusion proliferation assay after shRNA knockdown of ATF4 (N=2). D, qRT-PCR and E, representative western blot of SSP (PHGDH, PSAT1, and PSPH) mRNA and protein (A673 & A4573- 30 µg, TC32- 50 µg) in Ewing sarcoma cell lines after 96 hours of shATF4 knockdown (N=3). F, Chromatin immunoprecipitation qRT-PCR (ChIP-qPCR) for ATF4 at PHGDH and PSAT1 gene promoters. Negative control is a promoter region in chr2 without ATF4 binding (N=3). G, Representative western blots and qRT-PCR for SSP expression in ATF4 overexpressing (OE) Ewing sarcoma cells (A4573- 30 µg, TC32- 50 µg) (N=2, N=3). Error bars represent SEM from independent biological replicates. * $p<0.05$; ** $p<0.01$; *** $p<0.001$; **** $p<0.0001$; Two-tailed t-test.

other groups from similarly investigating ATF4 binding at this region [23, 24]. Having shown that loss of ATF4 resulted in loss of SSP gene expression, we next transduced cells with a mouse *Atf4* cDNA overexpression construct (ATF4 OE) and discovered that forced over-expression of the protein resulted in a further increase in SSP genes and proteins (**Figure 2-1G**). These results demonstrate that in Ewing sarcoma, like other cancers, ATF4 directly regulates expression of core SSP genes.

EWS-FLI1 directly binds to the ATF4 gene promoter

Although a role for EWS-FLI1 in regulation of the SSP has been described previously [17, 19, 20], and direct EWS-FLI1 binding to regulatory regions of all SSP genes has been reported [17], the mechanistic basis of fusion-mediated SSP activation is controversial and has yet to be fully elucidated. To begin to decipher whether EWS-FLI1 may function to regulate the SSP, at least in part via ATF4, we stably knocked down EWS-FLI1 using FLI1-targeted lentiviral shRNA in three Ewing sarcoma cell lines (A673, A4573, TC32). Ewing sarcomas do not express wildtype FLI1, permitting targeted knockdown of the fusion. Our results confirmed the published data, demonstrating that loss of EWS-FLI1 leads to downregulation of SSP gene and protein

expression (**Figure 2-2A-B**) [17, 19, 20]. In addition, following EWS-FLI1 knockdown, cells show a concomitant and time-dependent loss of ATF4 and ATF4 target gene expression (**Figure 2-2C-D**). These findings were corroborated in a fourth Ewing sarcoma cell line, CHLA10 (**Supplementary Fig. S2-2A**). In all cell lines, loss of ATF4 protein was coincident with loss of gene expression, suggesting that EWS-FLI1 may regulate ATF4 transcription. To address whether EWS-FLI1 might directly bind and activate the *ATF4* locus, we interrogated public ChIP-seq data for potential EWS-FLI1 binding sites in the *ATF4* promoter and more distal GGAA microsatellites that may act as *de novo* enhancers [30]. This analysis revealed a strong EWS-FLI1 binding peak in the *ATF4* promoter region, a region that was also defined by this group to be among a core set of EWS-FLI1 binding sites (**Fig. 2-2E**) [8]. Consistent with gene activation, the *ATF4* promoter was also enriched with H3K4me3 and H3K27Ac marks (**Figure 2-2E**). In contrast, enrichment of EWS-FLI1 was not consistently evident at the *PHGDH* promoter or the other SSP gene promoters, despite the presence of the active chromatin-associated histone modifications (**Figure 2-2E and Supplementary Fig. S2-2B**) [8, 31]. Preferential binding of EWS-FLI1 to the *ATF4* promoter and the absence of binding at the *PHGDH* promoter was validated by ChIP-qPCR in A673 cells in comparison to the EWS-FLI1-negative U2OS osteosarcoma cell line (**Figure 2-2F**). Together these data demonstrate that EWS-FLI1 positively modulates expression of *ATF4* mRNA transcription, and that this modulation is likely to, at least in part, mediate fusion-dependent regulation of the SSP in Ewing sarcoma.

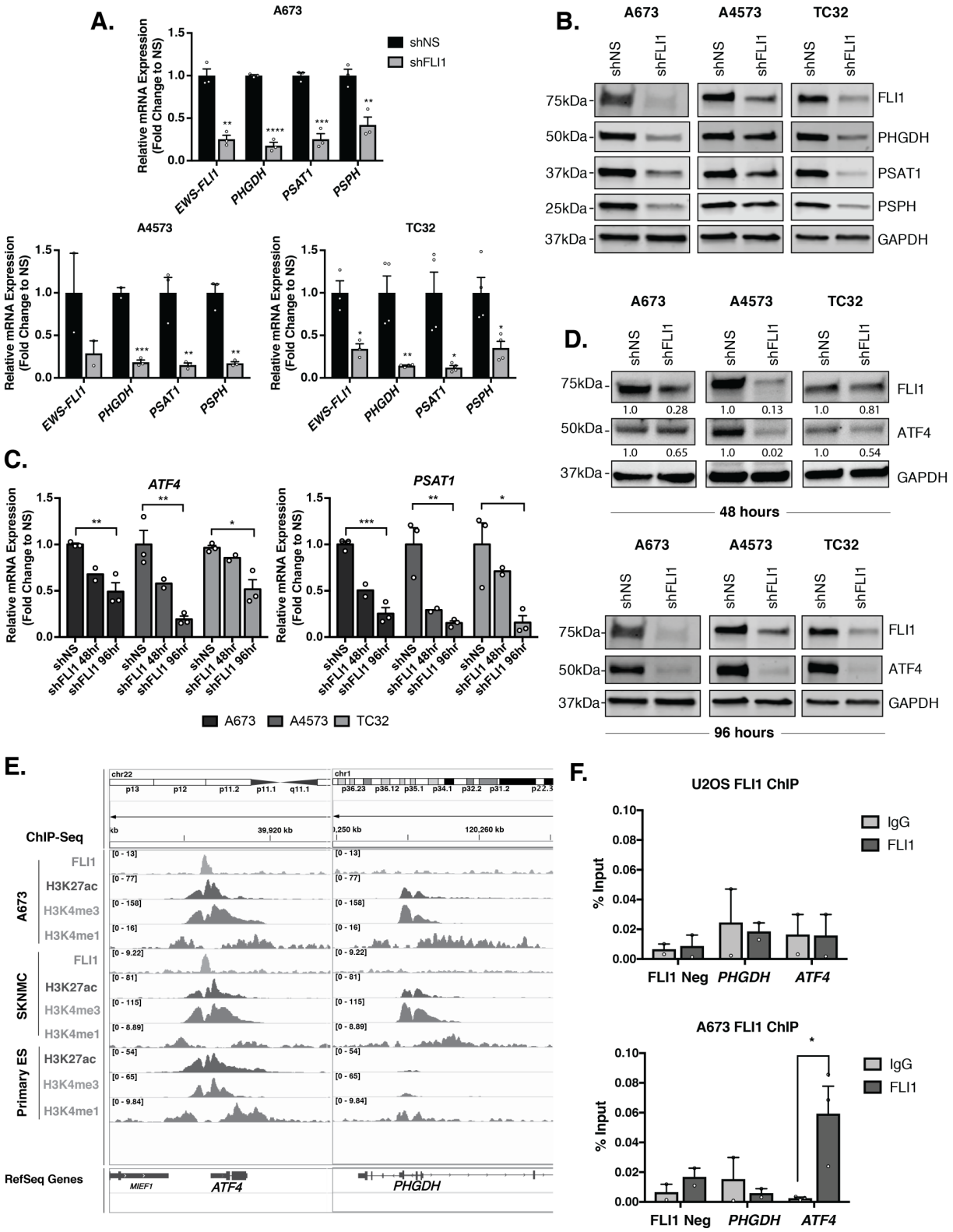

Figure 2-2 EWS-FLI1 directly binds to and activates ATF4.

A, qRT-PCR and B, representative western blot (30 μg) for FLI1 (EWS-FLI1), and SSP (PHGDH, PSAT1, and PSPH) mRNA and protein levels after 96 hours of EWS-FLI1 knockdown (N=3, N=4). C, qRT-PCR for ATF4 and PSAT1 mRNA at 48 (N=2) and 96 (N=3) hours post-shFLI1 knockdown in A673, A4573, and TC32 cells. D, Representative western blot (30 μg) for FLI1 (EWS-FLI1) and ATF4 protein levels after 48 and 96 hours of FLI1 (EWS-FLI1) knockdown (N=3). Western blots depicted for FLI1 and GAPDH are the same as those presented in panel B and are reproduced here for ease of comparison. E, Integrative Genomics Viewer (IGV) screenshot of publicly available ChIP-seq tracks for FLI1 (EWS-FLI1), H3K27Ac, and H3K4me3 at the ATF4 and PHGDH gene promoters in Ewing sarcoma cell lines and primary tumors [8]. F, ChIP-qPCR for FLI1 (EWS-FLI1) at the PHGDH and ATF4 gene promoters (N=3). Negative control is a region in chr2 without EWS-FLI1 binding. Error bars represent SEM from independent biological replicates. * $p<0.05$; ** $p<0.01$; *** $p<0.001$; **** $p<0.0001$; Two-tailed t-test.

Menin inhibition leads to loss of ATF4 and associated downregulation of the SSP

Menin is a ubiquitously expressed scaffolding protein whose best characterized function is its role as an MLL binding partner in the context of epigenetic trithorax complexes [32]. Disruption of menin: MLL interactions in MLLr leukemias leads to tumor regression, and menin inhibition has also been shown to slow the growth of some solid tumors, including prostate cancer and Ewing sarcoma [33-35]. Our previously published work demonstrated that pharmacologic and genetic menin loss-of-function in Ewing sarcoma leads to downregulation of SSP gene expression and activity [18]. We first compared menin protein expression in a panel of EWS-FLI1 fusion-positive Ewing sarcoma cell lines and other malignant and non-malignant mesenchymal cells: human mesenchymal stem cells (hMSCs), immortalized fibroblasts (293FT), chondrosarcoma (SW 1353), osteosarcoma (U2OS), and fibrosarcoma (HT-1080). As we previously published, menin expression is higher in Ewing sarcoma cell lines than in non-malignant human mesenchymal stem cells (hMSCs) [34]. Levels of menin are also high in immortalized fibroblasts (293FT) and U2OS cells but are low in soft tissue sarcoma cell

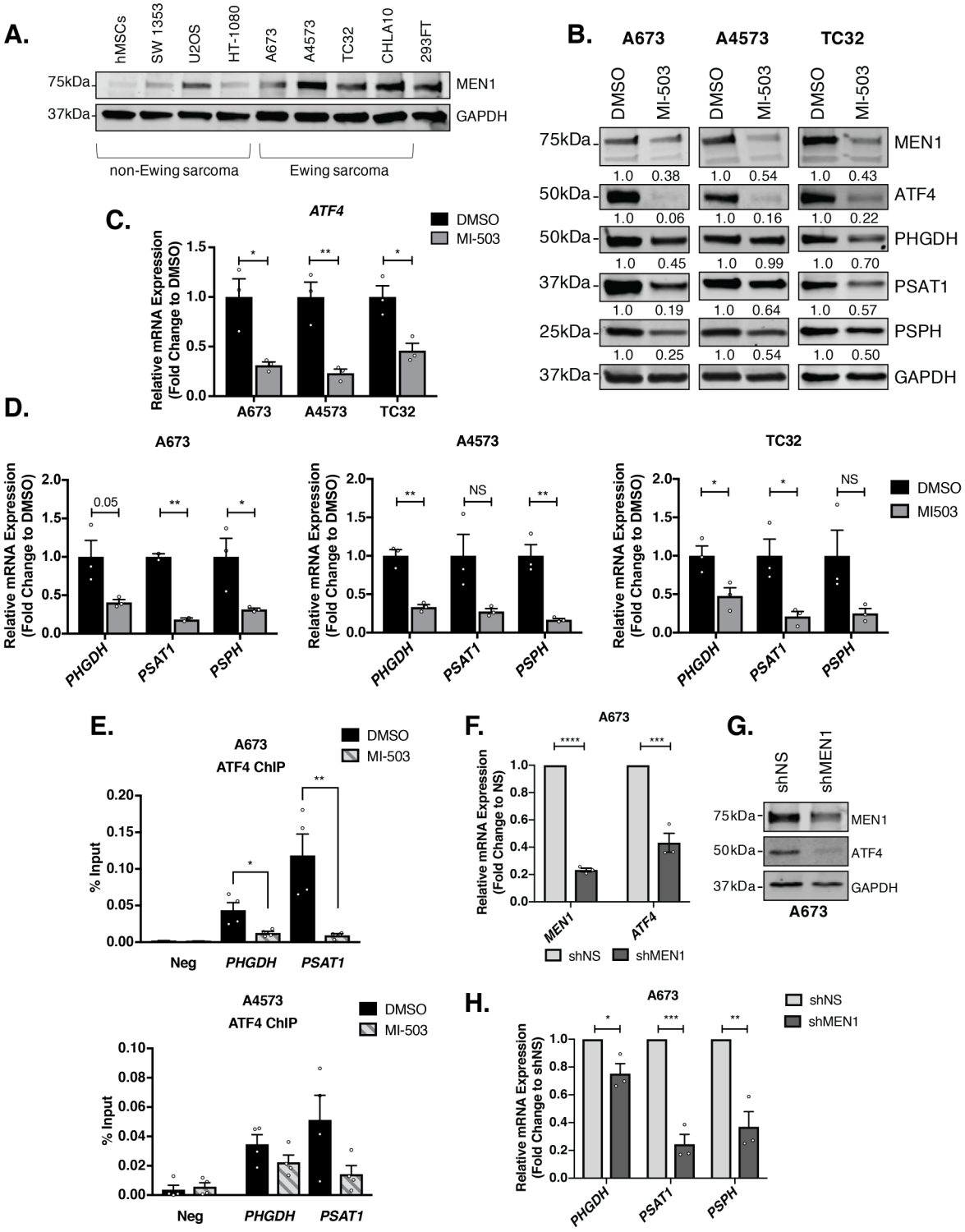

Figure 2-3 Menin inhibition leads to loss of ATF4 in Ewing sarcoma.

A, Representative western blot (50 µg) of MEN1 in a panel of Ewing sarcoma and non-Ewing sarcoma cell lines. B, Representative western blot (A673 & A4573- 30 µg, TC32- 50 µg) for ATF4 and SSP (PHGDH, PSAT1, and PSPH) protein after 96 hours of treatment with 3 µM

lines (HT-1080, SW 1353) (**Figure 2-3A**). To determine whether menin inhibition

MI-503 or DMSO control (N=3). C, qRT-PCR for ATF4 and D, SSP (PHGDH, PSAT1, and PSPH) mRNA in three Ewing sarcoma cell lines after 96 hours of treatment with 3 μM MI-503 or DMSO (N=3). E, ChIP-qPCR for ATF4 at PHGDH and PSAT1 gene promoters after 96 hours of 3 μM MI-503 treatment compared to DMSO control (N=4). F, qRT-PCR for MEN1 and ATF4 mRNA after 72 hours of doxycycline (dox)-inducible MEN1 knockdown (N=3). G, Representative western blot (30 μg) of MEN1 and ATF4 in A673 dox-inducible shNS or shMEN1 cells after 72 hours treatment with dox. H, qRT-PCR for SSP mRNA after MEN1 knockdown (N=3). Error bars represent SEM from independent biological replicates. * p<0.05; **p<0.01; *** p<0.001; **** p<0.0001; Two-tailed t-test.

influences ATF4 expression, we exposed cells to the menin inhibitor MI-503, as previously described [18, 34]. Consistent with our published data [34], treatment with MI-503 suppressed cell growth, albeit to a lesser degree than ATF4 knockdown (**Supplementary Fig. S2-1A-B**). In addition, MI-503 induced a time-dependent reduction in menin protein (**Figure 2-3B, Supplementary Fig. S2-3A-B**), with no change in menin mRNA (**Supplementary Fig. S2-3D**) [34]. Given the consistent and reproducible loss of menin protein at 96 hours, we next assessed levels of ATF4 and SSP genes at this timepoint. As shown, menin loss was accompanied by a dramatic reduction in *ATF4* mRNA and protein, and by reduction in SSP gene and protein expression, as previously reported (**Figure 2-3B-D**) [18]. Moreover, ChIP-qPCR studies confirm that ATF4 enrichment at the *PHGDH* and *PSAT1* promoters is diminished following menin inhibition (**Figure 2-3E**). Thus, inhibition of menin leads to loss of ATF4, loss of ATF4-binding at SSP gene promoters, and diminished SSP gene transcription. Importantly, levels of EWS-FLI1 were unaffected (**Supplementary Fig. S2-3A-B**), revealing that menin inhibition does not inhibit ATF4 via downregulation of the fusion protein.

In our experience, stable knockdown of menin in Ewing sarcoma cell lines is difficult to achieve [34]. Therefore, to validate MI-503 studies, we generated cells harboring a

doxycycline-inducible shRNA to permit acute silencing of the gene. In comparison to MI-503 treatment, shRNA knockdown of menin led to a much less pronounced effect on cell proliferation (**Supplementary Fig. S2-1C**); however, even with a modest knockdown of menin, Ewing sarcoma cells displayed loss of ATF4 mRNA and protein (**Figure 2-3F-G**) and downregulation of SSP gene expression (**Figure 2-3H**). Together, these data support the hypothesis that menin, either directly or indirectly, contributes to maintenance of ATF4 expression in Ewing sarcoma cells.

To address whether menin may function to regulate ATF4 through its role in the epigenetic trithorax complexes, we measured H3K4me3 levels in Ewing sarcoma cell lines treated with MI-503. No reduction in global H3K4me3 was observed in inhibitor-treated cells after 96 hours, despite marked reduction in ATF4 at this time point (**Figure 2-4A**). Importantly, targeted ChIP-qPCR studies of the *ATF4* gene promoter confirmed that local H3K4me3 enrichment was also unaffected by MI-503 (**Figure 2-4B**). Menin's interaction with either MLL1 or MLL2 (KMT2A or KMT2B) methyltransferases is required for the deposition of H3K4me3 by trithorax complexes at gene promoters [32]. We previously reported that knockdown of MLL1 does not have a significant impact on expression of *PHGDH*, *PSAT1*, and *PSPH* [18]. To examine whether the impact of menin inhibition on ATF4 and SSP gene expression could be mediated by interaction with MLL2 rather than MLL1, we knocked down *KMT2B* by shRNA. As shown, knockdown of MLL2 also had no significant impact on *ATF4* or SSP gene expression

(**Figure 2-4C**). Thus, these data suggest that acute inhibition of menin may lead to

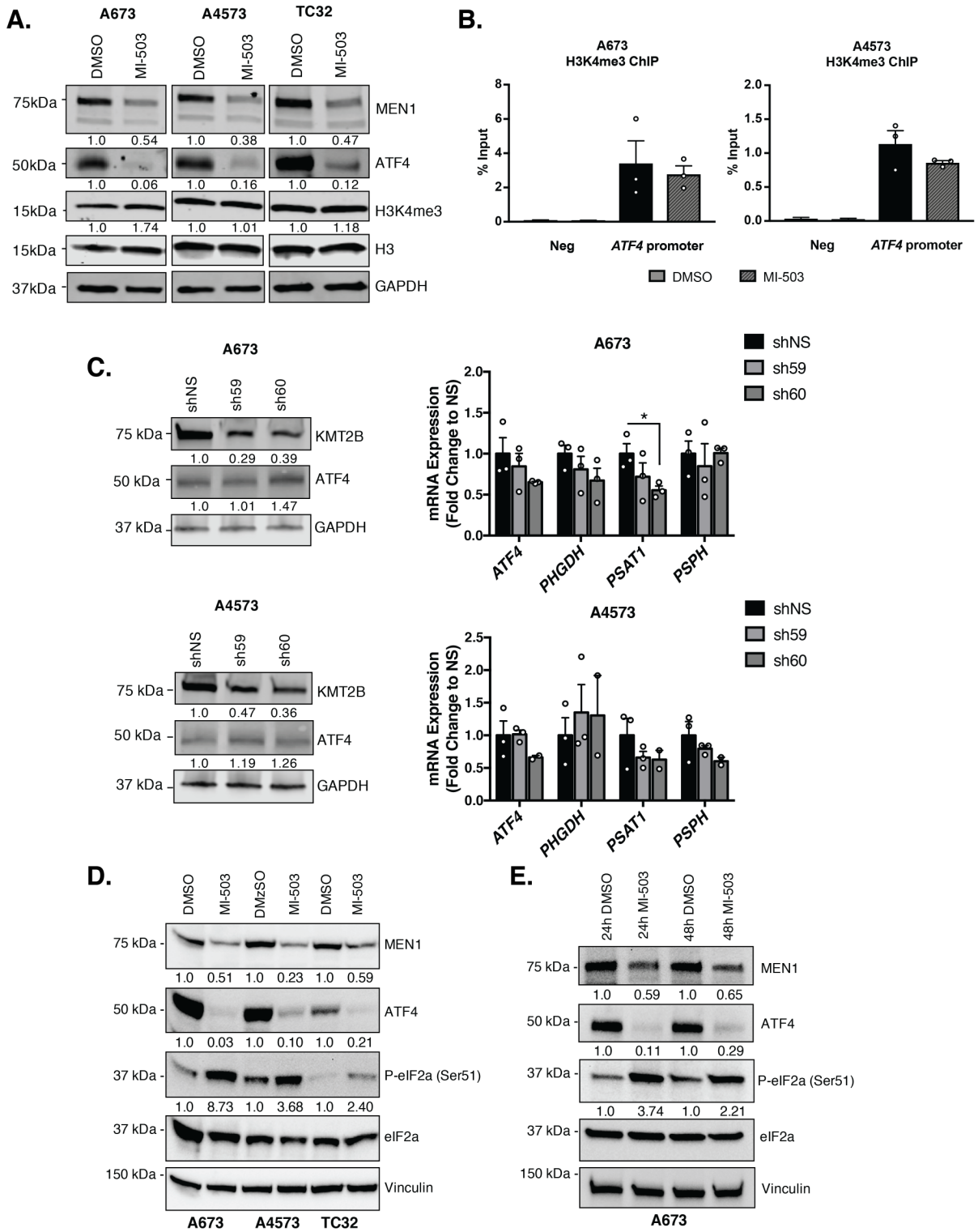

Figure 2-4 Menin inhibition downregulates ATF4 expression in an H3K4me3-independent manner.

A, Representative western blot (A673 & A4573- 30 µg, TC32- 50 µg) of MEN1, ATF4, H3K4me3 and total H3 levels after 96 hours of treatment with 3 µM MI-503 or DMSO control. B, ChIP-qPCR for H3K4me3 enrichment at the ATF4 gene promoter after 96 hours of MI-503 treatment compared to DMSO control. Negative control is a gene desert region in chr2 without H3K4me3 enrichment (N=3). C, Representative western blot of MLL2 (KMT2B), MEN1, and ATF4 protein after knockdown of MLL2, and qRT-PCR for ATF4 and SSP (PHGDH, PSAT1, PSPH) mRNA after KMT2B knockdown (N=3). D, Representative western blot for MEN1, ATF4, phosphorylated-eIF2a (Ser51) and total eIF2a after 96 hours of 3 µM MI-503 treatment in A673, A4573, and TC32 cells (N=3). E, Representative western blot for P-eIF2a (Ser51) and total eIF2a after 24 and 48 hours of 3 µM MI-503 treatment in A673 cells (N=2). Error bars represent SEM from independent biological replicates. * $p<0.05$; Two-tailed t-test.

downregulation of ATF4 by trithorax complex-independent mechanisms.

To begin to address potential alternate mechanisms of ATF4 regulation by menin, we performed a timecourse study. As shown, our findings revealed that, although transcript and protein levels were both reduced by MI-503 in A673 cells, ATF4 protein was very rapidly downregulated despite more modest effects on transcript expression (**Supplementary Fig. S2-3A-C**). Reductions in ATF4 protein were accompanied by reduction in ATF4 target gene, *PSAT1* (**Supplementary Fig. S2-3C**). The striking and early loss of ATF4 protein in A673 cells led us hypothesize that, in addition to its effects on gene transcription, inhibition of menin might also influence post-transcriptional regulation of ATF4. ATF4 protein levels are tightly regulated by multiple post-transcriptional mechanisms, the most well characterized of which is the integrated stress response (ISR). In response to diverse cell stressors, including endoplasmic reticulum stress, amino acid deprivation, and others, stress-sensing kinases activate the ISR by inducing phosphorylation of eukaryotic initiation factor 2-alpha (eIF2a) at serine 51 [15]. In response to increased P-eIF2a, cells shut down global protein translation and selectively upregulate translation of ATF4. Therefore, we exposed cells to MI-503 and measured P-eIF2a (Ser51). As shown, and in direct contrast to our expectations, MI-503 treated cells showed a reproducible increase in P-eIF2a (Ser51), coincident with

loss of ATF4 protein at timepoints as early as 24 hours (**Figure 2-4D-E**). Thus, acute inhibition of menin in Ewing sarcoma cells leads to activation of the ISR, but the expected increase in ATF4 protein is blocked. Ongoing studies are investigating the mechanism underlying this block and whether the paradoxical loss of ATF4 protein downstream of ISR activation is a direct consequence of menin inhibition or an indirect effect mediated by feedback pathways.

EWS-FLI1 and menin loss induce broad downregulation of ATF4-dependent gene expression

The marked and reproducible reduction of ATF4 expression in the context of both EWS-FLI1 and menin inhibition led us to hypothesize that broader ATF4-dependent transcriptional programs beyond just the SSP might be impacted by modulation of either or both of these proteins. In particular, we wondered about expression of adaptive genes that are activated downstream of ATF4 in the context of stress responses such as the unfolded protein response, amino acid response, and the oxidative stress response [15]. To address this, we interrogated previously published RNA-seq data that were generated from Ewing sarcoma cells following either EWS-FLI1 knockdown or menin inhibition [8, 17, 18, 36]. As shown, EWS-FLI1 knockdown in A673 cells [36] led to downregulation of *ATF4, PHGDH, PSAT1,* and *PSPH*, as well as other known ATF4-modulated stress response genes such as *ASNS*, *TRIB3*, *NARS1*, and *MTHFD2* (**Figure 2-5A**). This expression profile was at least partially restored upon rescue with an RNAi-resistant EWS-FLI1 cDNA, confirming the role of the fusion in transcriptional

regulation of both ATF4 and multiple of its downstream targets. Consistent with this finding, two additional

and independent RNA-seq studies [8, 17] corroborate the finding that loss of EWS-FLI1 leads to diminished expression of an ATF4 gene signature (**Supplementary Fig. S2-4A-B**). We validated these sequencing-based studies using qRT-PCR, confirming

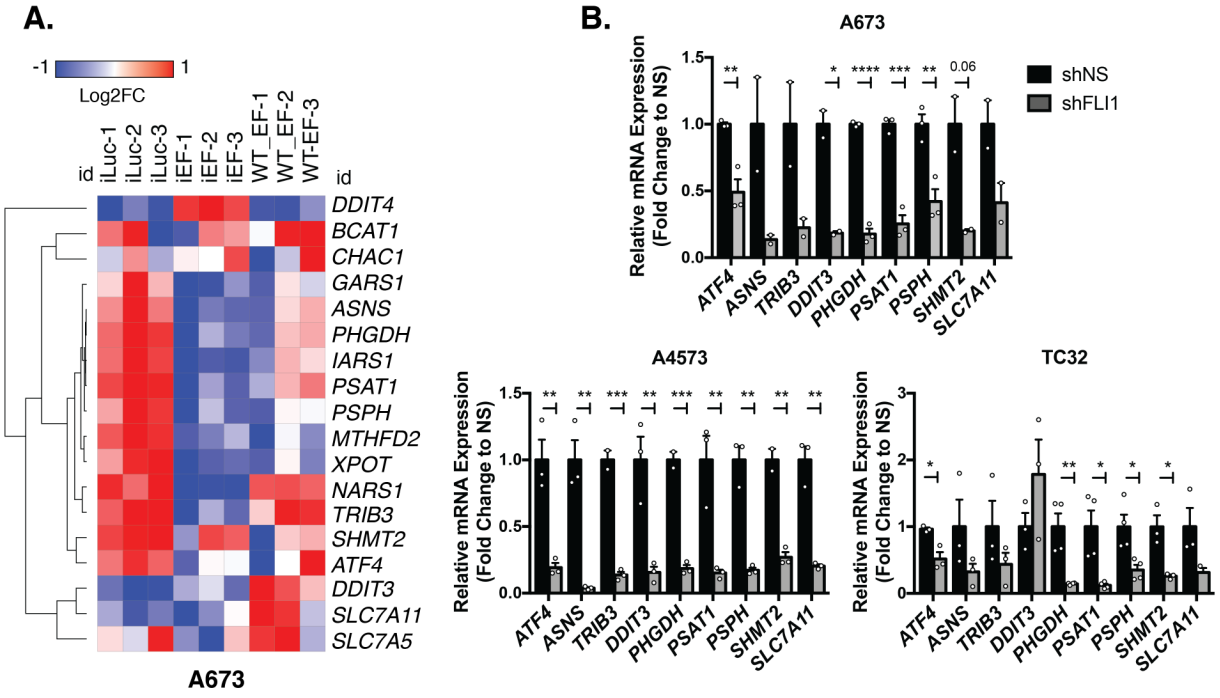

Figure 2-5 EWS-FLI1 inhibition in Ewing sarcoma broadly inhibits an ATF4-dependent gene expression program.

A, Heatmap of Log2Fold Change in expression from publicly available RNA-seq data of shRNA knockdown of EWS-FLI1 (iEF), luciferase-targeting control (iLuc), and wildtype EWS-FLI1 cDNA (WT-EF) rescue in A673 cells [36]. B, qRT-PCR validation of ATF4 and select ATF4 target genes after 96 hours of FLI1 (EWS-FLI1) knockdown (N=3, N=4). Error bars represent SEM from independent biological replicates. * p<0.05; ** p<0.01; *** p<0.001; **** p<0.0001; Two-tailed t-test.

that acute knockdown of EWS-FLI1 leads to profound and reproducible downregulation of *ATF4* as well as multiple ATF4-regulated stress response genes (**Figure 2-5B**).

Next, we analyzed previously published nascent RNA-seq data from MI-503-treated

Ewing sarcoma cell lines [18]. These data show that numerous ATF4 target genes, including *TRIB3*, *SESN2*, *ASNS*, *CHAC1*, and *SLC7A11* were reproducibly downregulated in the context of acute menin inhibition (**Figure 2-6A-B**). Furthermore, bioinformatic analysis of transcription factor binding sites in promoters of significantly downregulated genes revealed ATF4 binding sites to be most highly and significantly over- represented (**Figure 2-6C**). These unbiased genomic studies were validated by qRT-PCR analysis of independently treated Ewing sarcoma cells (**Figure 2-6D**).

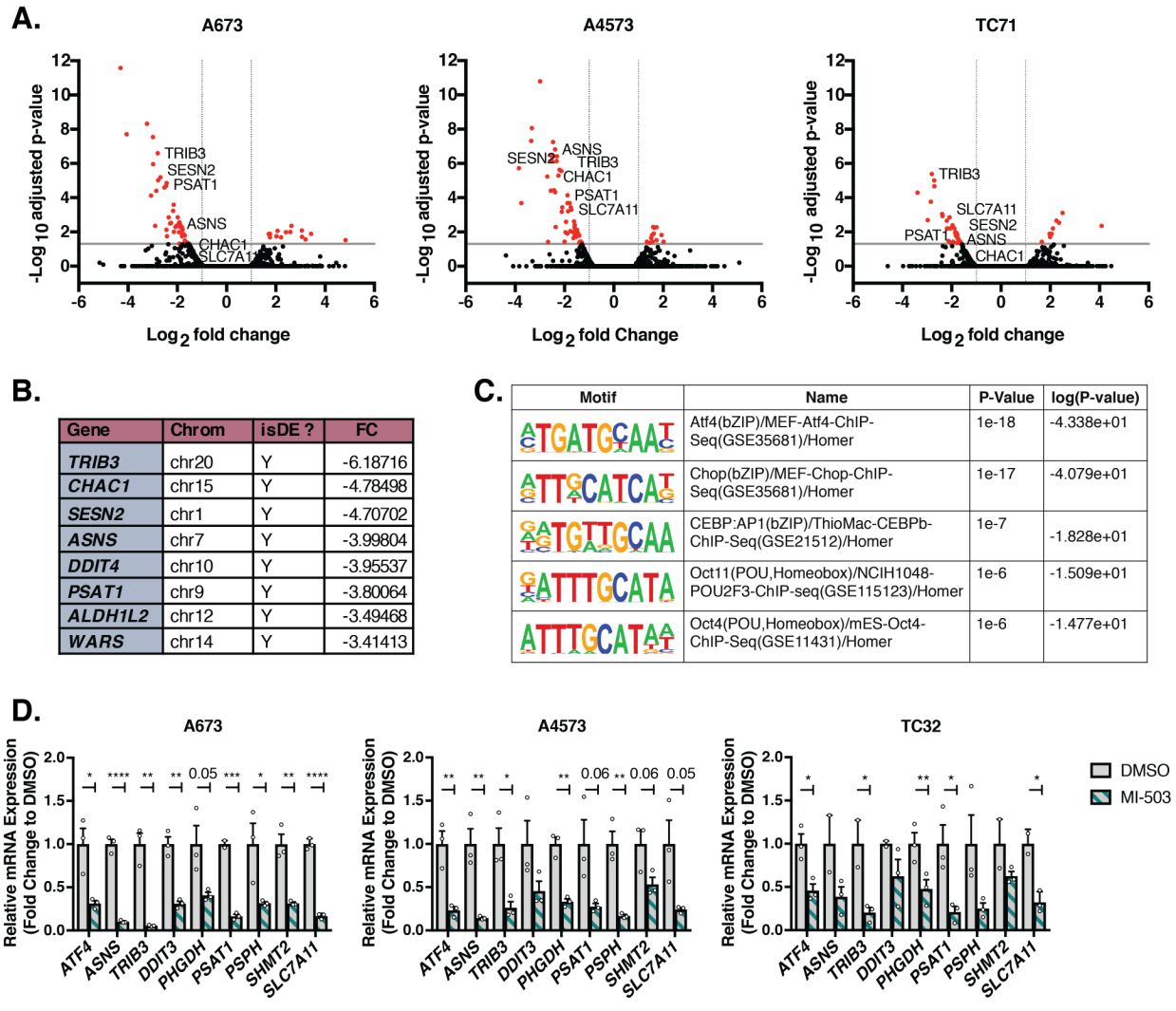

Gene	Chrom	isDE ?	FC
TRIB3	chr20	Y	-6.18716
CHAC1	chr15	Y	-4.78498
SESN2	chr1	Y	-4.70702
ASNS	chr7	Y	-3.99804
DDIT4	chr10	Y	-3.95537
PSAT1	chr9	Y	-3.80064
ALDH1L2	chr12	Y	-3.49468
WARS	chr14	Y	-3.41413

Motif	Name	P-Value	log(P-value)
	Atf4(bZIP)/MEF-Atf4-ChIP-Seq(GSE35681)/Homer	1e-18	-4.338e+01
	Chop(bZIP)/MEF-Chop-ChIP-Seq(GSE35681)/Homer	1e-17	-4.079e+01
	CEBP:AP1(bZIP)/ThioMac-CEBPb-ChIP-Seq(GSE21512)/Homer	1e-7	-1.828e+01
	Oct11(POU,Homeobox)/NCIH1048-POU2F3-ChIP-seq(GSE115123)/Homer	1e-6	-1.509e+01
	Oct4(POU,Homeobox)/mES-Oct4-ChIP-Seq(GSE11431)/Homer	1e-6	-1.477e+01

Figure 2-6 Menin inhibition identifies an ATF4-dependent gene expression signature.

A, Volcano plot of global changes in mRNA levels from previously published RNA-seq of MI-503-treated A673, A4573, and TC71 Ewing sarcoma cells [18]. Cells were treated with 3 μM vehicle (MI-NC) or MI-503 for 72 hours and analyzed by bromouridine sequencing (Bru-seq). Genes marked in red show <-2-fold change in gene expression and adjusted $p<0.05$. B, Top downregulated genes from combined Bru-seq data of all three cell lines after 3 μM MI-503 treatment for 72 hours [18]. C, Top transcription factor motifs identified using the HOMER software by motif analysis of promoters of genes downregulated in (A) from three independent cell lines (A673, A4573. TC71). D, qRT-PCR of ATF4 and select ATF4 target genes after 96 hours of treatment with 3 μM MI-503 or DMSO control (N=3). Error bars represent SEM from independent biological replicates. * $p<0.05$; ** $p<0.01$; *** $p<0.001$; **** $p<0.0001$; Two-tailed t-test.

All together, these data lead us to conclude that both EWS-FLI1 and menin regulate ATF4 expression and activity in Ewing sarcoma cells, and that acute inhibition of either protein leads to a loss of the ATF4-dependent stress response gene signature.

Menin inhibition impacts ATF4 and its target genes in MLLr leukemia

To our knowledge, menin has not previously been implicated in regulation of ATF4 or the ATF4-mediated, stress-associated transcriptional signature. Menin is broadly recognized to function as a tumor suppressor gene, largely as a consequence of its role in familial cancers in preventing endocrine tumor development. However, it also plays an essential pro-tumorigenic role in the context of MLLr leukemia [32]. Indeed, the tumorigenicity of MLLr leukemias is profoundly dependent on menin, given its function as an obligate binding partner for oncogenic MLL-fusion proteins, and menin inhibition is currently being evaluated as a tumor-specific, biologically targeted therapy in these diseases [37, 38]. To address whether menin influences ATF4 and its target genes in MLLr leukemia cells, we exposed two MLLr leukemia cell lines – MV4;11, a B-cell acute lymphoblastic leukemia (ALL) cell line, and MOLM13, an acute myeloid leukemia (AML) cell line – to MI-3454, a next-generation and more potent pharmacologic inhibitor of

menin through its interference with menin: MLL-fusion protein interactions [38]. Remarkably, and consistent with menin inhibition in Ewing sarcoma cells, *ATF4* and ATF4 target gene expression were significantly reduced in MV4;11 cells at nanomolar drug concentrations that inhibit leukemogenesis (**Figure 2-7A**). By comparison, although some effect was also apparent in MOLM13 cells, the impact was much less

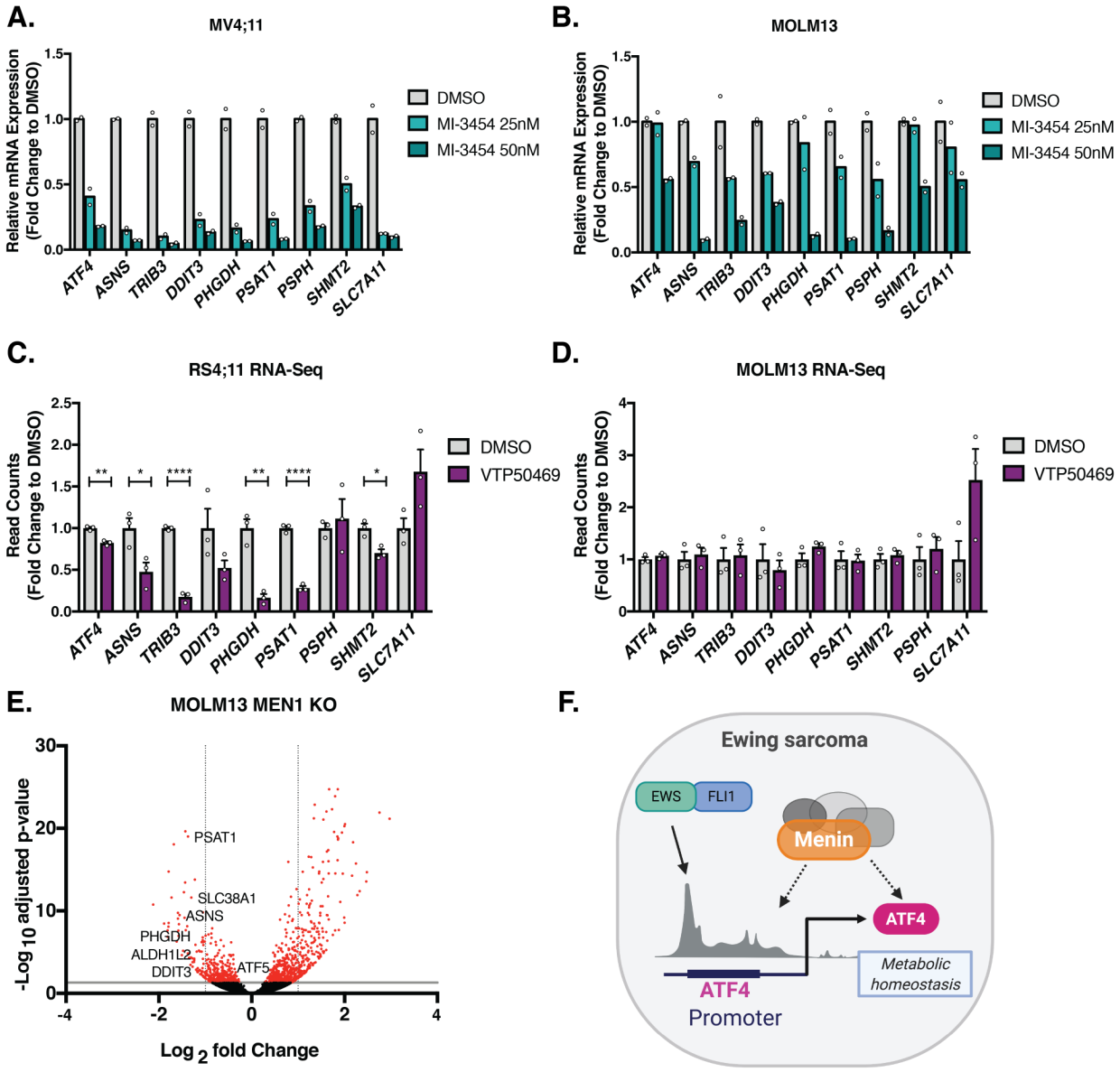

Figure 2-7 Menin inhibition downregulates ATF4 activity in MLLr leukemia cell lines.

A, qRT-PCR of MV4:11 and B, MOLM13 AML cell lines after 7 days of treatment with 25 and 50 nM MI-3454, a next-generation menin inhibitor, or DMSO control (N=2). C, Histogram of publicly available RNA-seq in RS4;11, and D, MOLM13 cell lines after 7 days of treatment with 330 nM VTP50469 (N=3) [37]. E, Volcano plot of publicly available RNA-seq data from MOLM13 cells following 6 days of MEN1 knockout [37]. Upregulated genes with adjusted p > 30 are excluded. Genes marked in red show <-2-fold change in gene expression and p <0.05. F, Working model in which the EWS-FLI1 oncogene in Ewing sarcoma and high menin expression converge on regulation of ATF4. Error bars represent SEM from independent biological replicates. * p<0.05; ** p<0.01; *** p<0.001; **** p<0.0001; Two-tailed t-test.

pronounced and was mainly evident only at the higher dose of inhibitor (**Figure 2-7B**). To complement these results, we interrogated publicly available RNA-Seq data from MLLr cells that were exposed to a different, independently developed menin: MLL inhibitor, VTP50469 [37]. VTP50469-treated B-cell ALL cells (RS4;11) showed a modest reduction in expression of *ATF4* and its target genes (**Figure 2-7C**). In contrast, VTP50469 induced no demonstrable effect on the ATF4 transcriptional signature in MOLM13 cells (**Figure 2-7D**). Intriguingly, however, CRISPR/Cas9-mediated knockout of menin in MOLM13 cells [37] was associated with a significant downregulation of several ATF4 target genes, including *PSAT1*, *PHGDH*, *ASNS*, and *DDIT3* (**Figure 2-7E**). Thus, these data suggest that menin may also contribute to regulation of ATF4 and its stress-response transcriptional signature in MLLr leukemia.

Discussion

Hyperactivation of the SSP has been identified as a central metabolic dependency in multiple different solid tumors [16], and we and others have demonstrated this pathway to be of key biologic and translational relevance to Ewing sarcoma [17-20]. The mechanisms of SSP activation differ in different tumor types and both EWS-FLI1 and menin have been implicated in the context of Ewing sarcoma [17-20]. In tumors that

lack genomic amplification of the *PHGDH* locus, hyperactivation of the SSP is most often under the control of master transcriptional regulators, in particular ATF4 [15]. ATF4 is a ubiquitously expressed stress response gene whose function is critically important for maintenance of metabolic homeostasis in both normal and cancer cells, especially under conditions where cells are subjected to the stress of limited resources, such as glucose, amino acids, and oxygen [15]. Although metabolic reprogramming is evident in Ewing sarcoma, ATF4 has not previously been implicated in mediating this process in these tumors [17-19, 39, 40]. Our current findings provide evidence that ATF4 directly binds to and maintains SSP gene expression in Ewing sarcoma and lend support for the hypothesis that ATF4 acts downstream of both EWS-FLI1 and menin in their respective regulation of the SSP (**Figure 2-7F**). Moreover, our data show that, in addition to their impact on the SSP, maintenance of ATF4 by EWS-FLI1 and menin contributes to expression of a broader ATF4-dependent transcriptional program. To our knowledge, a link between ATF4 and either EWS-FLI1 or menin has not been previously described. Although prior work suggested that EWS-FLI1 does not regulate ATF4 [17, 19], our studies demonstrate direct binding of the *ATF4* promoter by the fusion, confirming previously published ChIP-seq data [8, 31]. In addition, we find that knockdown of the fusion leads to diminished expression of *ATF4* mRNA, which is also consistent with some prior studies [8, 17, 36]. Notably, we and others have observed that, although EWS-FLI1 knockdown universally leads to reduced ATF4 expression in Ewing sarcoma cells, the extent of loss is highly influenced by the cell line, time, cell culture media, and other technical and biologic variables. We speculate that this variability explains the contradictory findings of prior published studies and is indicative

of the dynamic and multi-faceted nature of ATF4 regulation and of its central role in maintaining cell homeostasis. In support of this, we observed that knockdown of ATF4 is deleterious to Ewing sarcoma cell growth, and that cells with forced over-expression of murine ATF4 (m*Atf4)* rapidly down-regulate transcription of endogenous *ATF4* in order to maintain homeostatic levels of the protein (data not shown). In addition, we observed that *ATF4* mRNA expression is exquisitely sensitive to changes in the microenvironment that would result in cell stress, including changes in pH, confluence, and nutrient availability. Thus, we conclude that, although EWS-FLI1 directly binds and activates the *ATF4* promoter, other transcription factors that contribute to ATF4 regulation under conditions of cell stress, such as NRF2 [15, 23] or MYC [41], may rapidly compensate for reductions in mRNA that are associated with loss of the fusion.

Although EWS-FLI1 and other related EWS-ETS fusions are unique to Ewing sarcoma, menin is a ubiquitously expressed scaffolding protein that has context-dependent roles in both tumor suppression and tumor promotion. In MLLr leukemia, inhibition of menin leads to downregulation of tumor-promoting oncogenes, such as HOXA9 and MEIS1, that are under the control of MLL fusions, and this is accompanied by differentiation of leukemic blasts and tumor involution [35]. In Ewing sarcoma, our prior work showed that menin contributes to tumorigenicity through mechanisms that are not clearly linked to cellular differentiation and are instead associated with cell metabolism, in particular maintenance of the SSP [18, 34]. In the current work, we have discovered that the mechanism of menin-mediated regulation of SSP gene expression is, at least in part, mediated by ATF4. In addition, the loss of ATF4 and SSP gene expression that results from menin inhibition is accompanied by reduced expression of

multiple stress-response genes that are under the transcriptional control of ATF4. Significantly, analysis of menin inhibitor-treated MLLr leukemia cells revealed a similar loss of ATF4 and ATF4 target gene expression. These findings suggest that the contribution of menin to regulation of ATF4 is not unique to Ewing sarcoma.

Menin's functions in normal and cancer cell biology are diverse and dependent on its highly cell type- and context-dependent protein interaction partners [32]. Although the exact molecular mechanisms of menin action in ATF4 regulation remain to be fully elucidated, our studies suggest that they are independent of its interactions with MLL proteins in the trithorax complexes. Enrichment of H3K4me3 at the *ATF4* gene promoter remains robust at a time point when MI-503 has induced profound loss of ATF4 protein expression. In addition, acute knockdown of MLL1 or MLL2 (KMT2A or KMT2B) does not reproduce the effect of menin inhibition [18]. Indeed, although the *ATF4* transcript is reproducibly reduced by menin inhibition, we observed that loss of ATF4 protein is often more immediate and more pronounced. This suggests that menin may also contribute to post-transcriptional regulation ATF4. This novel hypothesis is supported by our observation that MI-503 leads to activation of the ISR, a key regulator of ATF4 protein translation. However, in direct contrast to expectations, activation of the ISR by MI-503 is associated with loss rather than gain of ATF4 protein. The reasons for this disconnect remain unclear and we are now investigating how menin inhibition blocks ATF4 upregulation in the context of ISR activation. Of note, it has been shown that mTORC1 can regulate *ATF4* mRNA stability and ATF4 translation [42], an ISR-independent mechanism for ATF4 regulation that we are also exploring.

Menin inhibitors are now being tested in early phase clinical trials for MLLr leukemia (registered at www.clinicaltrials.gov as #NCT04067336 and #NCT04065399). Their efficacy as anti-leukemic agents are linked to their induction of blast cell differentiation and death, downstream of menin: MLL inhibition. Significantly, however, there is now emerging evidence from several groups, including with our own, that menin inhibitors may have additional effects on cell metabolism. Specifically, menin inhibitors have recently been shown to alter the cellular energetics and glycolysis of breast cancer cells, as well as to induce ferroptosis, an iron-dependent form of oxidative stress-induced cell death in ovarian and other carcinoma cells [43, 44]. Intriguingly, the demonstration of effects of menin inhibition on ferroptosis were uniquely observed with MI-503 and its related compounds and not reproduced with the VTP-50469 compound [44]. This suggests that the biologic impact of menin inhibitors on cell metabolism and cell death may be distinct. This is noteworthy for Ewing sarcoma, where VTP-50469 was recently shown to have no impact on tumor cell viability *in vitro* or tumorigenicity *in vivo* [45]. We speculate that differential effects of MI-503 on cell metabolism, possibly via selective inhibition of ATF4 and induction of oxidative stress, may explain the differences in the response of Ewing sarcoma cells to different menin inhibitors. A direct comparison between different modes of menin inhibition, pharmacologic and genetic, and a deep mechanistic evaluation of the effect of each of these approaches on menin and its interaction partners is now required to fully resolve why, how, and in which cellular contexts, menin inhibition influences cellular metabolism.

In summary, through an in-depth analysis of published sequencing data and new mechanistic studies, we provide the first evidence that EWS-FLI1 and menin converge

to maintain SSP gene expression through activation of ATF4. In addition, our data show that this regulation of ATF4 has downstream effects on expression of multiple ATF4 target genes that are important for maintenance of cellular homeostasis under conditions of stress. Finally, we show that menin-mediated regulation of this ATF4-dependent transcriptional program may also be functionally important in MLLr leukemias.

Materials and Methods

Cell Lines

Ewing sarcoma cell lines were obtained from the Children's Oncology Group (COG) cell bank (cogcell.org). U2OS, HT-1080, SW 1353, and HEK 293FT cells were obtained directly from ATCC. Human marrow stromal cells (hMSCs) were kindly provided by Dr. Kurt Hankenson at the University of Michigan. Cells were not cultured past 20 passages. A673, A4573, and TC32 cells were cultured in RPMI 1640 (Corning). CHLA10 cells were cultured in IMDM media (Gibco), supplemented with 1X Insulin-Transferrin-Selenium (Gibco) and 20% fetal bovine serum. 293FT, HT-1080, and SW 1353 cell lines were cultured in DMEM medium, high glucose (Gibco). DMEM media for SW 1353 cells was supplemented with 1% antibiotic-antimycotic (Gibco) without additional glutamine. U2OS cells were cultured in McCoy's 5A medium (Gibco). hMSCs were cultured in MEM Alpha medium (Gibco) supplemented with 1% antibiotic-antimycotic (Gibco) and 20% fetal bovine serum. All media were supplemented with 10% fetal bovine serum (FBS—Atlas Biologicals) and 1% L-glutamine (Life Technologies), unless otherwise noted, and grown at 37°C, 5% CO_2. Identities were

confirmed by short tandem repeat (STR) profiling. All cell lines were routinely tested for mycoplasma contamination as described previously **[18]**.

Chemical Synthesis of Menin-MLL Inhibitors and Treatments

MI-503 and MI-3454 were prepared using the synthetic procedures previously reported [35, 38]. RNA from MI-3454-treated RS4;11 and MOLM13 leukemia cell lines was provided by Dr. Jolanta Grembecka's laboratory at the University of Michigan. Cells were treated as previously published, with 25 or 50 nM MI-3454 for 7 days [38]. For MI-503 treatment studies, cells were plated in 100 mm dishes, media was changed the following day and supplemented with 3 μM MI-503 (IC_{50}) or DMSO control, and cells were collected after 96 hours. For Ewing sarcoma cell lines, cells were plated at the following densities: 0.75 X 10^6 (A673), 0.25 X10^6 (A4573), and 3.25 X 10^6 (TC32) cells/100 mm dish.

Generation of Cell Lines Expressing shRNA, or Over-expressing ATF4

For the following plasmids: pLKO.1 shNS (non-silencing control), shATF4, shFLI1, and shKMT2B (Sigma-Aldrich MISSION shRNA library); pLenti CMV/Puro empty and m*Atf4* (Addgene); and TRIPZ Inducible Lentiviral shNS and shMEN1 (Dharmacon); concentrated (10X) lentivirus production was carried out by the University of Michigan Vector Core facility or prepared in the laboratory following standard procedures [46]. In brief, plasmids were co-transfected with pCD/NL-BH*DDD (Addgene) and pMD2.G (Addgene) plasmids into 293FT packaging cells using PEI. 24 hours post-transfection, sodium butyrate was added to plates for 6 hours. Viral supernatant was collected 48 hours after transfection and filtered through 40 μM filters. Ewing sarcoma cell lines were

plated in complete media in 100 mm dishes. Viral supernatant was added to the media at 1X concentration and removed after 24-hour incubation. Cells were selected by supplementing the media with 1.5 μg/mL puromycin (Gibco) for 48 hours before collection. TRIPZ inducible shNS and shMEN1 cells were grown in tetracycline (tet)-free FBS-containing media (Takara Bio). Viral supernatant was added to cells in serum-free media, and media was supplemented with 5 mL complete tet-free media 6-8 hours post-transduction. Media was replaced with puromycin-selective media 48 hours post-transduction. Cells underwent two rounds of transduction with inducible shNS and shMEN lentivirus to maximize efficiency. Doxycycline was added to cells at 1 μg/mL and replenished every 24 hours, and shRNA expression was monitored by expression of RFP. See Appendix II for shRNA sequences and plasmid information. The m*Atf4* plasmid was kindly provided by Dr. Lewis Cantley's laboratory at Weill Cornell Medicine. m*Atf4* has sufficient sequence homology to h*ATF4* and has been used previously in other human cancer studies [23].

Proliferation Assays

For Trypan blue exclusion proliferation assays, shATF4 knockdown and shNon-silencing (shNS) control cells were seeded at 100,000 cells per dish in 60 mm dishes after puromycin selection. Floating and adherent cells were collected at day 3 and day 6 after plating, and viable cells were quantified using a Countess Automated Cell Counter (Invitrogen). Real-time cell analysis (RTCA) of cell proliferation was monitored using the xCELLigence DP system (Agilent). Before cell seeding, E-plates were coated with 0.2% gelatin and equilibrated for 1 hour at 37°C, 5% CO_2 with 100 μL of media per well. 5 x

10^3 (A673), or 3 x 10^3 (A4573) cells were plated per well to a final volume of 200 µL, and the plate was equilibrated for 30 minutes.

Western Blotting

Cells were detached with trypsin-EDTA (0.05%) (Gibco), washed with PBS (Gibco), and lysed in RIPA buffer (Thermo Fisher) supplemented with protease inhibitor cocktail and phosphatase inhibitor cocktail tablets (Roche). Cleared supernatants were subjected to protein quantification by *DC* (detergent compatible) protein assay (Bio-Rad). Western blot was performed using the Bio-Rad Mini-PROTEAN Tetra System. Proteins were resolved by SDS-PAGE (4-15%), transferred to 0.45 µM nitrocellulose membranes, and blocked in 1:1 TBS Odyssey Blocking Buffer (LI-COR) and 1X TBST for 1 hour at room temperature. Membranes were incubated rotating overnight at 4°C with primary antibody. See Appendix II for list of antibodies and dilutions. Membranes were then washed 4 times for 5 minutes each in TBST and probed with secondary antibody IRDye 680RD Goat anti-Mouse IgG 1:15,000, IRDye 800CW Goat anti-Rabbit IgG 1:10,000 (LI-COR), or donkey anti-Rabbit IgG peroxidase-linked secondary (Cytiva) 1:10,000. Quantification was performed using LI-COR Image Studio software or Bio-rad Image Lab Software.

Quantitative Real-Time PCR

Total RNA was extracted from cells at the same time as protein collection using *Quick*-RNA MiniPrep Kit (Zymo Research), and RNA was subjected to reverse transcription using iSCRIPT cDNA Synthesis Kit (Bio-Rad) following the manufacturer's protocol. Quantitative real-time PCR (qRT-PCR) was performed using fluorescent universal

SYBR-Green Supermix (Bio-Rad) for designed primers or TaqMan Fast Universal PCR Master Mix (Applied Biosystems) with TaqMan probes. Analysis was performed in triplicate using the Light-Cycler 480 System (Roche) and average Cp values were normalized relative to the geometric mean of two housekeeping genes (18s and HPRT, or 18s and EEF1A1 for SYBR; 18s and B2M for TaqMan Assay). Primer sequences and TaqMan probes are provided in Supplementary Table S1.

Chromatin Immunoprecipitation (ChIP) Quantitative PCR

Chromatin immunoprecipitation (ChIP) to assess enrichment for ATF4, H3K4me3, and EWS-FLI1 was performed using the Zymo-Spin ChIP kit (Zymo Research) with Protein G-Dynabeads (Life Technologies) following the manufacturer's protocol. Briefly, 5 million cells were harvested for ChIP (1 million cells per 1 mL ChIP reaction). Cells were formaldehyde fixed and chromatin was fragmented using the Biorupter Pico Sonicator (Diagenode) (30s on/30s off for 30 cycles). Chromatin was incubated with the following antibodies: 0.34 µg/IP anti-ATF4 (ATF-4 (D4B8) Rabbit mAb, Cell Signaling 11815), 0.5 µg/IP anti-H3K4me3 ChIP-seq grade (Diagenode C15410003-50), 5 µg/IP anti-FLI1 ChIP Grade (abcam ab15289), 5 µg/IP Rabbit IgG polyclonal isotype control (Abcam ab37415), overnight on a rotator at 4°C. Antibody-chromatin complexes were incubated with Protein G-Dynabeads for 2 hours. Washes, elution, reverse crosslinking, and proteinase K digestion were carried out per manufacturer's protocol. DNA was eluted in 20 µL, and ChIP-qPCR was performed as described above. Primer sequences for the *ATF4* and SSP gene promoters, and negative control regions are detailed in Supplementary Table S1.

Motif Analysis

Bromouridine sequencing (Bru-Seq) of MI-503-treated Ewing sarcoma cell lines was performed previously [18]. Transcripts with absolute fold change greater than 2.0 and mean RPKM > 0.5 were categorized as differentially expressed. Promoter regions of downregulated genes (fold change < -2.0), were analyzed for enriched motifs using the findMotifs.pl function from the HOMER analysis suite. Genes were searched within 2 Kb of their transcription start site for motifs of 8, 10, or 12 nucleotides in length to identify enriched motifs in gene promoters [47].

Microarrays, RNA-Seq, and ChIP-Seq Datasets

The mRNA expression of *ATF4* in Ewing sarcoma patient tumors was determined using three previously published microarray datasets: GSE63157 [48], GSE34620 [49], and GSE17679 [50]. RNA-sequencing data for EWS-FLI1 knockdown are from three independent studies, publicly available at GSE122535 [36], GSE103843 [17], and GSE61950 [8]. To determine the differentially expressed genes between the experimental groups, read counts were analyzed with *DESeq2* package (v 1.22.2) in R. Heatmap for GSE122535 [36] was generated using normalized expression values from *DESeq2* and the Morpheus matrix visualization and analysis software (Morpheus, https://software.broadinstitute.org/morpheus). Bromouridine sequencing (nascent RNA-seq) of MI-503-treated Ewing sarcoma cells was re-analyzed from previously reported data [18]. RNA-sequencing for VTP-50469 treatment in RS4;11 and MOLM13 cell lines and CRISPR-mediated menin knockout in MOLM13 cells are publicly available at GSE127506 and GSE137813, respectively [37]. The ChIP-seq datasets we acquired for FLI1, H3K27Ac, and H3K4me3 are publicly available at NCBI Gene Expression

Omnibus (GEO) under the GEO accession: GSE61953 [8], and NCBI Sequencing Read Archive (SRA) under the accession number SRA096176 and accessible at: http://www.medical-epigenomics.org/papers/tomazou2015/ [31]. Data was visualized using the Integrative Genomics Viewer (IGV) or UCSC Genome Browser platforms, respectively, at each region of interest.

Statistical Analysis

All data is plotted using Prism (GraphPad) and bar plots represent the mean ± SEM. Prism was used to perform two-tailed, unpaired t-test analysis. $P < 0.05$ was considered statistically significant. For volcano plots of RNA-seq data, differential expression values greater than 2-fold or less than -2-fold and adjusted $P < 0.05$ were considered significant, and cutoffs are indicated on plot.

Acknowledgements

We would like to thank members of the Lawlor, Lyssiotis, Grembecka and Cierpicki labs for intellectual input, as well as the University of Michigan Rogel Cancer Center Vector and Sequencing Cores. We gratefully acknowledge Dr. Lewis Cantley for the *Atf4* expression plasmid. Illustration was created with BioRender.com. Support for this work was provided by the following sources: National Institute of Health: F31 CA254079 (JJ), R01 CA218116 (ERL), T32 CA009676 (AA), K00 CA234810 (AGH); R01 CA200660 (JG); R37CA237421, R01CA248160, R01CA244931 (CAL); and P50 CAP30CA046592 to the Rogel Cancer Center. The authors also gratefully acknowledge additional funding support from the Rogel Cancer Center (collaborative research grant to ERL and CAL;

CaRSIP summer internship to AG & EH), and the U-M Department of Pediatrics Charles Woodson Collaborative Research Award and Russell G. Adderley endowment.

References

1. Balamuth, N.J. and R.B. Womer, *Ewing's sarcoma.* Lancet Oncol, 2010. **11**(2): p. 184-92.
2. Lawlor, E.R. and P.H. Sorensen, *Twenty Years on: What Do We Really Know about Ewing Sarcoma and What Is the Path Forward?* Crit Rev Oncog, 2015. **20**(3-4): p. 155-71.
3. Womer, R.B., et al., *Randomized controlled trial of interval-compressed chemotherapy for the treatment of localized Ewing sarcoma: a report from the Children's Oncology Group.* J Clin Oncol, 2012. **30**(33): p. 4148-54.
4. Armstrong, G.T., et al., *Aging and risk of severe, disabling, life-threatening, and fatal events in the childhood cancer survivor study.* J Clin Oncol, 2014. **32**(12): p. 1218-27.
5. Ginsberg, J.P., et al., *Long-term survivors of childhood Ewing sarcoma: report from the childhood cancer survivor study.* J Natl Cancer Inst, 2010. **102**(16): p. 1272-83.
6. Youn, P., et al., *Long-term cause-specific mortality in survivors of adolescent and young adult bone and soft tissue sarcoma: a population-based study of 28,844 patients.* Cancer, 2014. **120**(15): p. 2334-42.
7. Lin, P.P., Y. Wang, and G. Lozano, *Mesenchymal Stem Cells and the Origin of Ewing's Sarcoma.* Sarcoma, 2011. **2011**.
8. Riggi, N., et al., *EWS-FLI1 utilizes divergent chromatin remodeling mechanisms to directly activate or repress enhancer elements in Ewing sarcoma.* Cancer Cell, 2014. **26**(5): p. 668-681.
9. Tomazou, E.M., et al., *Epigenome mapping reveals distinct modes of gene regulation and widespread enhancer reprogramming by the oncogenic fusion protein EWS-FLI1.* Cell Rep, 2015. **10**(7): p. 1082-95.
10. Boulay, G., et al., *Cancer-Specific Retargeting of BAF Complexes by a Prion-like Domain.* Cell, 2017. **171**(1): p. 163-178 e19.
11. Selvanathan, S.P., et al., *Oncogenic fusion protein EWS-FLI1 is a network hub that regulates alternative splicing.* Proc Natl Acad Sci U S A, 2015. **112**(11): p. E1307-16.
12. Brohl, A.S., et al., *The genomic landscape of the Ewing Sarcoma family of tumors reveals recurrent STAG2 mutation.* PLoS Genet, 2014. **10**(7): p. e1004475.
13. Crompton, B.D., et al., *The genomic landscape of pediatric Ewing sarcoma.* Cancer Discov, 2014. **4**(11): p. 1326-41.
14. Tirode, F., et al., *Genomic landscape of Ewing sarcoma defines an aggressive subtype with co-association of STAG2 and TP53 mutations.* Cancer Discov, 2014. **4**(11): p. 1342-53.
15. Wortel, I.M.N., et al., *Surviving Stress: Modulation of ATF4-Mediated Stress Responses in Normal and Malignant Cells.* Trends Endocrinol Metab, 2017. **28**(11): p. 794-806.
16. Mattaini, K.R., M.R. Sullivan, and M.G. Vander Heiden, *The importance of serine metabolism in cancer.* J Cell Biol, 2016. **214**(3): p. 249-57.

17. Sen, N., et al., *EWS-FLI1 reprograms the metabolism of Ewing sarcoma cells via positive regulation of glutamine import and serine-glycine biosynthesis.* Mol Carcinog, 2018.
18. Svoboda, L.K., et al., *Menin regulates the serine biosynthetic pathway in Ewing sarcoma.* J Pathol, 2018. **245**(3): p. 324-336.
19. Tanner, J.M., et al., *EWS/FLI is a Master Regulator of Metabolic Reprogramming in Ewing Sarcoma.* Mol Cancer Res, 2017. **15**(11): p. 1517-1530.
20. Issaq, S.H., et al., *EWS-FLI1-regulated serine synthesis and exogenous serine are necessary for Ewing sarcoma cellular proliferation and tumor growth.* Mol Cancer Ther, 2020.
21. Locasale, J.W., et al., *Phosphoglycerate dehydrogenase diverts glycolytic flux and contributes to oncogenesis.* Nat Genet, 2011. **43**(9): p. 869-74.
22. Possemato, R., et al., *Functional genomics reveal that the serine synthesis pathway is essential in breast cancer.* Nature, 2011. **476**(7360): p. 346-50.
23. DeNicola, G.M., et al., *NRF2 regulates serine biosynthesis in non-small cell lung cancer.* Nat Genet, 2015. **47**(12): p. 1475-81.
24. Zhao, E., et al., *KDM4C and ATF4 Cooperate in Transcriptional Control of Amino Acid Metabolism.* Cell Rep, 2016. **14**(3): p. 506-519.
25. Ding, J., et al., *The histone H3 methyltransferase G9A epigenetically activates the serine-glycine synthesis pathway to sustain cancer cell survival and proliferation.* Cell Metab, 2013. **18**(6): p. 896-907.
26. Reina-Campos, M., et al., *Increased Serine and One-Carbon Pathway Metabolism by PKClambda/iota Deficiency Promotes Neuroendocrine Prostate Cancer.* Cancer Cell, 2019. **35**(3): p. 385-400 e9.
27. Xia, Y., et al., *Metabolic Reprogramming by MYCN Confers Dependence on the Serine-Glycine-One-Carbon Biosynthetic Pathway.* Cancer Res, 2019. **79**(15): p. 3837-3850.
28. Dey, S., et al., *Both transcriptional regulation and translational control of ATF4 are central to the integrated stress response.* J Biol Chem, 2010. **285**(43): p. 33165-74.
29. Yang, M. and K.H. Vousden, *Serine and one-carbon metabolism in cancer.* Nat Rev Cancer, 2016. **16**(10): p. 650-62.
30. Grunewald, T.G.P., et al., *Ewing sarcoma.* Nat Rev Dis Primers, 2018. **4**(1): p. 5.
31. Bilke, S., et al., *Oncogenic ETS fusions deregulate E2F3 target genes in Ewing sarcoma and prostate cancer.* Genome Res, 2013. **23**(11): p. 1797-809.
32. Matkar, S., A. Thiel, and X. Hua, *Menin: a scaffold protein that controls gene expression and cell signaling.* Trends Biochem Sci, 2013. **38**(8): p. 394-402.
33. Malik, R., et al., *Targeting the MLL complex in castration-resistant prostate cancer.* Nat Med, 2015. **21**(4): p. 344-52.
34. Svoboda, L.K., et al., *Tumorigenicity of Ewing sarcoma is critically dependent on the trithorax proteins MLL1 and menin.* Oncotarget, 2017. **8**(1): p. 458-471.
35. Borkin, D., et al., *Pharmacologic inhibition of the Menin-MLL interaction blocks progression of MLL leukemia in vivo.* Cancer Cell, 2015. **27**(4): p. 589-602.
36. Theisen, E.R., et al., *Transcriptomic analysis functionally maps the intrinsically disordered domain of EWS/FLI and reveals novel transcriptional dependencies for oncogenesis.* Genes Cancer, 2019. **10**(1-2): p. 21-38.

37. Krivtsov, A.V., et al., *A Menin-MLL Inhibitor Induces Specific Chromatin Changes and Eradicates Disease in Models of MLL-Rearranged Leukemia.* Cancer Cell, 2019. **36**(6): p. 660-673 e11.
38. Klossowski, S., et al., *Menin inhibitor MI-3454 induces remission in MLL1-rearranged and NPM1-mutated models of leukemia.* J Clin Invest, 2020. **130**(2): p. 981-997.
39. Issaq, S.H., et al., *Glutamine synthetase is necessary for sarcoma adaptation to glutamine deprivation and tumor growth.* Oncogenesis, 2019. **8**(3): p. 20.
40. Yeung, C., et al., *Targeting Glycolysis through Inhibition of Lactate Dehydrogenase Impairs Tumor Growth in Preclinical Models of Ewing Sarcoma.* Cancer Res, 2019. **79**(19): p. 5060-5073.
41. Mo, H., et al., *ATF4 regulated by MYC has an important function in anoikis resistance in human osteosarcoma cells.* Mol Med Rep, 2018. **17**(3): p. 3658-3666.
42. Park, Y., et al., *mTORC1 Balances Cellular Amino Acid Supply with Demand for Protein Synthesis through Post-transcriptional Control of ATF4.* Cell Rep, 2017. **19**(6): p. 1083-1090.
43. Chou, C.W., et al., *Menin and Menin-Associated Proteins Coregulate Cancer Energy Metabolism.* Cancers (Basel), 2020. **12**(9).
44. Kato, I., T. Kasukabe, and S. Kumakura, *MeninMLL inhibitors induce ferroptosis and enhance the antiproliferative activity of auranofin in several types of cancer cells.* Int J Oncol, 2020. **57**(4): p. 1057-1071.
45. Kurmasheva, R.T., et al., *Evaluation of VTP-50469, a menin-MLL1 inhibitor, against Ewing sarcoma xenograft models by the pediatric preclinical testing consortium.* Pediatr Blood Cancer, 2020. **67**(7): p. e28284.
46. von Levetzow, C., et al., *Modeling initiation of Ewing sarcoma in human neural crest cells.* PLoS One, 2011. **6**(4): p. e19305.
47. Heinz, S., et al., *Simple combinations of lineage-determining transcription factors prime cis-regulatory elements required for macrophage and B cell identities.* Mol Cell, 2010. **38**(4): p. 576-89.
48. Volchenboum, S.L., et al., *Gene Expression Profiling of Ewing Sarcoma Tumors Reveals the Prognostic Importance of Tumor-Stromal Interactions: A Report from the Children's Oncology Group.* J Pathol Clin Res, 2015. **1**(2): p. 83-94.
49. Postel-Vinay, S., et al., *Common variants near TARDBP and EGR2 are associated with susceptibility to Ewing sarcoma.* Nat Genet, 2012. **44**(3): p. 323-7.
50. Savola, S., et al., *High Expression of Complement Component 5 (C5) at Tumor Site Associates with Superior Survival in Ewing's Sarcoma Family of Tumour Patients.* ISRN Oncol, 2011. **2011**: p. 168712.

Chapter 3 EWS-FLI1 Regulates ASNS and Metastatic Potential in Ewing sarcoma

Summary

In our Chapter 2 studies, we found that in Ewing sarcoma, EWS-FLI1 and the scaffolding protein menin regulate the serine biosynthesis pathway via converging regulation of the master transcriptional regulator, ATF4. As a downstream effector of the integrated stress response, ATF4 promotes the transcription of metabolic genes that increase the import and synthesis of amino acids. Our studies in Chapter 3, began with the goal of investigating metabolic targets downstream of this EWS-FLI1-menin-ATF4 axis in order to identify therapeutic vulnerabilities that may synergize with EWS-FLI1 loss of function.

Our data revealed that expression of ASNS (asparagine synthetase), the rate-limiting enzyme responsible for the *de novo* synthesis of asparagine, is reduced with EWS-FLI1 loss. Interestingly, using shRNA-mediated knockdown and pharmacologic inhibition of EWS-FLI1 with doxorubicin, we show that loss of EWS-FLI1 function does not synergize with depletion of asparagine to reduce cell viability *in vitro*. We further characterized the effect of loss of ASNS expression *in vivo* using shRNA knockdown and found that, while ASNS expression is not required for primary tumor growth using subcutaneous tumor models, ASNS is required for metastatic dissemination and engraftment, as indicated by tail-vein metastasis models. Interestingly, dietary asparagine restriction did not phenocopy the effect of ASNS loss of function on reducing metastatic tumor burden, and both control and EWS-FLI1 knockdown cells behaved

similarly *in vivo* regardless of dietary asparagine levels. Intriguingly, transcriptomic analysis of ASNS loss-of-function by RNA-seq *in vitro* demonstrates that the loss of ASNS leads to widespread up modulation of epithelial mesenchymal transition (EMT) and extracellular matrix (ECM)-modifying genes, such as matrix metalloproteinases (MMPs) and collagens. Our results thus suggest that ASNS may play a key role in regulating the metastatic ability of Ewing sarcoma cells, which we hypothesize to, at least in part, result from impacts on epithelial and mesenchymal gene programs.

Introduction

The rewiring of cellular metabolism has been recognized as a hallmark of cancer since over a century ago [1]. Malignant cells hijack biosynthetic pathways in order to support the increased demand for macromolecules needed to sustain high levels of proliferation [2]. Many enzymatic pathways are selectively upregulated in the tumor, providing a therapeutic window and tumor-specific vulnerabilities that may be exploited in metabolically-targeted therapies [3]. Previously published work in Ewing sarcoma using zebrafish has uncovered a model of cell heterogeneity where low EWS-FLI1-expressing cells, EWS-FLI1 “Low”, are thought to exhibit more mesenchymal features, more cell-matrix interactions, and more invasive properties; while cells expressing high levels of EWS-FLI1, EWS-FLI1 “High” cells have more cell-cell interactions and are more proliferative [4]. However, the distinct metabolic dependencies of these populations of cells is not well understood. In the case of pediatric cancers like Ewing sarcoma, where the standard of care consists of maximum-tolerated doses of cytotoxic chemotherapy, and for which the treatment regimen has not improved in decades, the

potential to use metabolic therapies in combination with or in place of highly genotoxic agents to specifically target cells with high propensity for metastasis, is a an especially attractive approach.

Non-essential amino acids can be synthesized *de novo*, providing cells with more flexibility when these amino acids are in short supply [5]. When cells are unable to synthesize these non-essential amino acids, they can become auxotrophic, or dependent on their exogenous availability. This phenomenon explains the success of one of the first metabolic therapies and cornerstone of treatment for acute lymphoblastic leukemia (ALL) with the use of the asparagine-degrading enzyme, L-asparaginase (ASNase). In the 1970s, it was found that bacterial ASNase was curative for children with pediatric ALL [6], later discovered to be due to low expression of asparagine synthetase (ASNS), the enzyme that converts aspartate to asparagine in leukemic blasts [7]. Evidence in solid tumors also demonstrates that high ASNS correlates with tumor growth and predicts poor prognosis, and high ASNS expression has been shown to promote metastasis in breast cancer models [8]. However, besides being critical for protein synthesis, the role that asparagine plays in promoting tumor growth is not well understood, and recent studies have implicated functions in mTORC1 signaling, amino acid exchange, and redox [9-11]. The investigation of amino acid requirements in pediatric sarcomas, such as Ewing sarcoma, has been limited, and, to our knowledge the biological function of asparagine in maintaining tumorgenicity has yet to be explored in Ewing sarcoma.

We and others have demonstrated that Ewing sarcomas are critically dependent on high-level activation of the serine biosynthetic pathway (SSP) [12-15]. Furthermore,

our recent work showed that the SSP is one of a number of key amino acid pathways regulated downstream of the EWS-FLI1 fusion protein via transcriptional regulation of the master transcription factor ATF4 [16]. We demonstrated that EWS-FLI1 directly binds and activates *ATF4* in Ewing sarcoma cells and that this transcriptional axis regulates amino acid and stress response gene signatures. Our studies identified ASNS, as one of a number of target genes within the ATF4-dependent gene signature. In the current study, we investigated the role of ASNS and its amino acid product, asparagine, in regulating tumor-promoting phenotypes in Ewing sarcoma using *in vitro* and *in vivo* models. We also examined whether EWS-FLI1 “Low” cells are differentially sensitive to asparagine depletion. LC/MS-based metabolomic and protein expression analysis, demonstrate that inhibition of the EWS-FLI1 fusion protein through both genetic and pharmacologic means leads to loss of ASNS protein expression and decreased levels of asparagine. In contrast to our expectations, EWS-FLI1-inhibited cells did not show diminished survival or growth in response to ASNase treatment or asparagine withdrawal. Rather, our studies instead uncovered a role for ASNS in regulating metastatic dissemination in Ewing sarcoma. Moreover, the reduced metastatic potential was uniquely seen in the context of ASNS loss of function but not with dietary asparagine restriction. Preliminary data suggest that ASNS loss may impact epithelial mesenchymal transition (EMT) and extracellular matrix (ECM) transcriptional programs, which may explain consequent changes in cell state that impact metastatic phenotypes.

Results

ASNS is highly expressed in Ewing sarcoma

Our previously published data demonstrated that knockdown of the oncogenic fusion protein EWS-FLI1 in Ewing sarcoma led to downregulation of an ATF4-regulated gene expression program, including transcript expression of asparagine synthetase

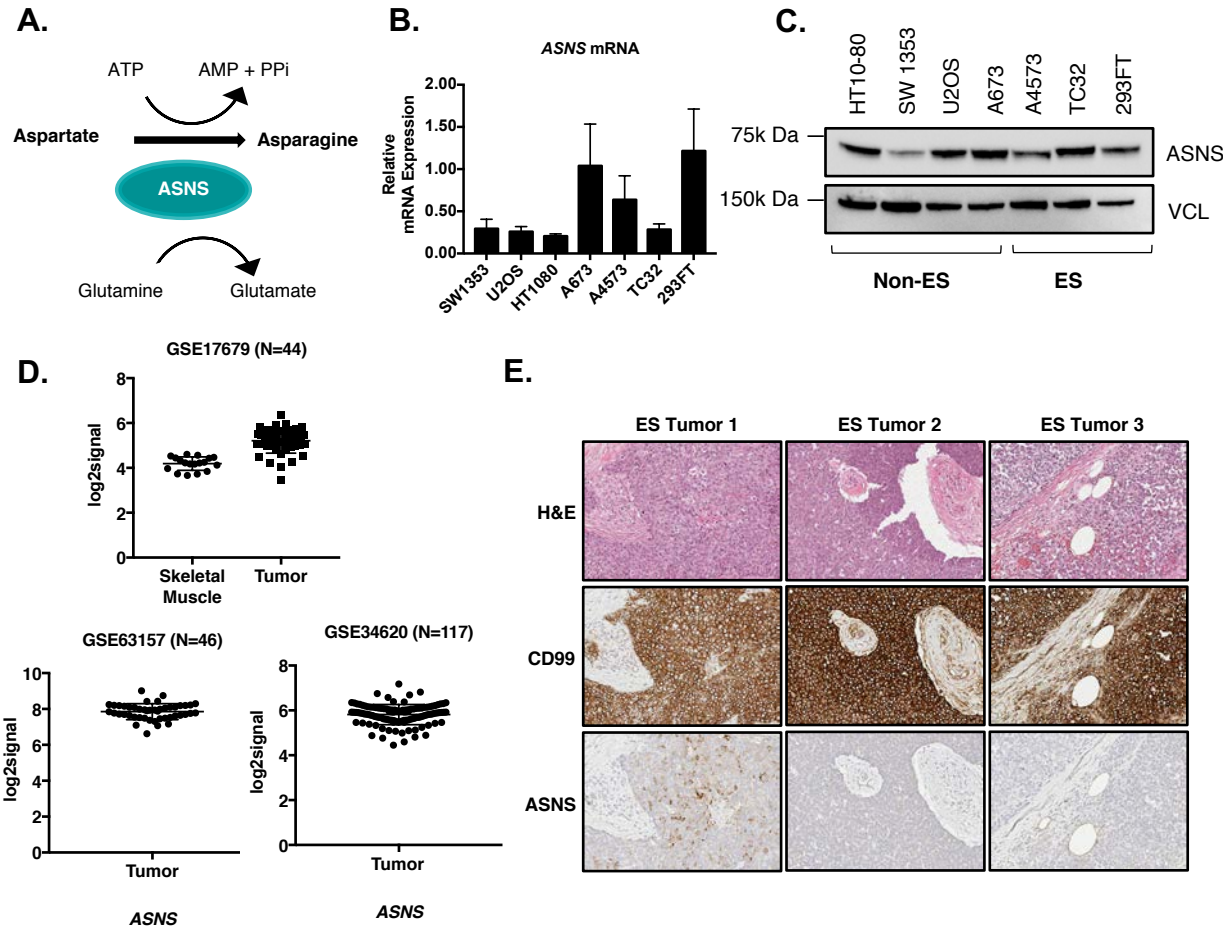

Figure 3-1 ASNS is expressed in Ewing sarcoma

A. Diagram depicting enzymatic activity of ASNS, the rate-limiting enzyme that generates asparagine from aspartate and glutamine. B. qRT-PCR of ASNS expression in a panel of Ewing (ES) and non-Ewing (Non-ES) mesenchymal cell lines. C. Western blot of ASNS expression from cell line panel in (A). D. *ASNS* gene expression in patient tumors from three independently published Ewing sarcoma datasets (Volchenboum *et al.*, 2015; Postel-Vinay *et al*, 2012; Savola *et al.,* 2011) E. H&E staining and immunohistochemistry for ASNS and CD99 in Ewing sarcoma tissue blocks from tumor resections.

(*ASNS*) [16]. The enzyme ASNS is responsible for synthesizing asparagine *de novo* from glutamine and aspartate (**Figure 3-1A**). The success in the clinical use of ASNase for pediatric leukemias owes to the uniquely low levels of ASNS expression in these cancers. Consequently, leukemic blasts are unable to readily synthesize asparagine *de novo* and are hypersensitive to the extracellular depletion of the amino acid source [7]. Given the therapeutic targetability of this pathway, and the clinical use of ASNase in pediatric patients, we sought to further characterize the relevance of ASNS to Ewing sarcoma biology. We thus first aimed to determine baseline levels of ASNS in Ewing sarcoma. Our data show that ASNS mRNA and protein are heterogenous in Ewing sarcoma cell lines and found at levels comparable to other mesenchymal cell lines and 239FT HEK cells (**Figure 3-1B-C).** Additionally, gene expression studies of tumor biopsies also show that *ASNS* mRNA is high in Ewing sarcoma tumors (**Figure 3-1D**). We next performed immunohistochemistry to evaluate ASNS protein in Ewing sarcoma tissue blocks of tumor resections from three adult patients and also found heterogeneity in ASNS expression between tumor samples and within the tumor, with certain areas of CD99+ tumor staining more strongly for ASNS (Ewing sarcoma (ES) Tumor #1) (**Figure 3-1E**).

EWS-FLI1 loss reduces ASNS and asparagine abundance

We next sought to determine whether *ASNS* expression is regulated by the EWS-FLI1 fusion. To test this, we stably knocked down EWS-FLI1 using FLI1-targeted lentiviral shRNA in four Ewing sarcoma cell lines (A673, A4573, TC32, CHLA10), and assessed ASNS transcript and protein levels 96 hours post transduction. Knockdown of

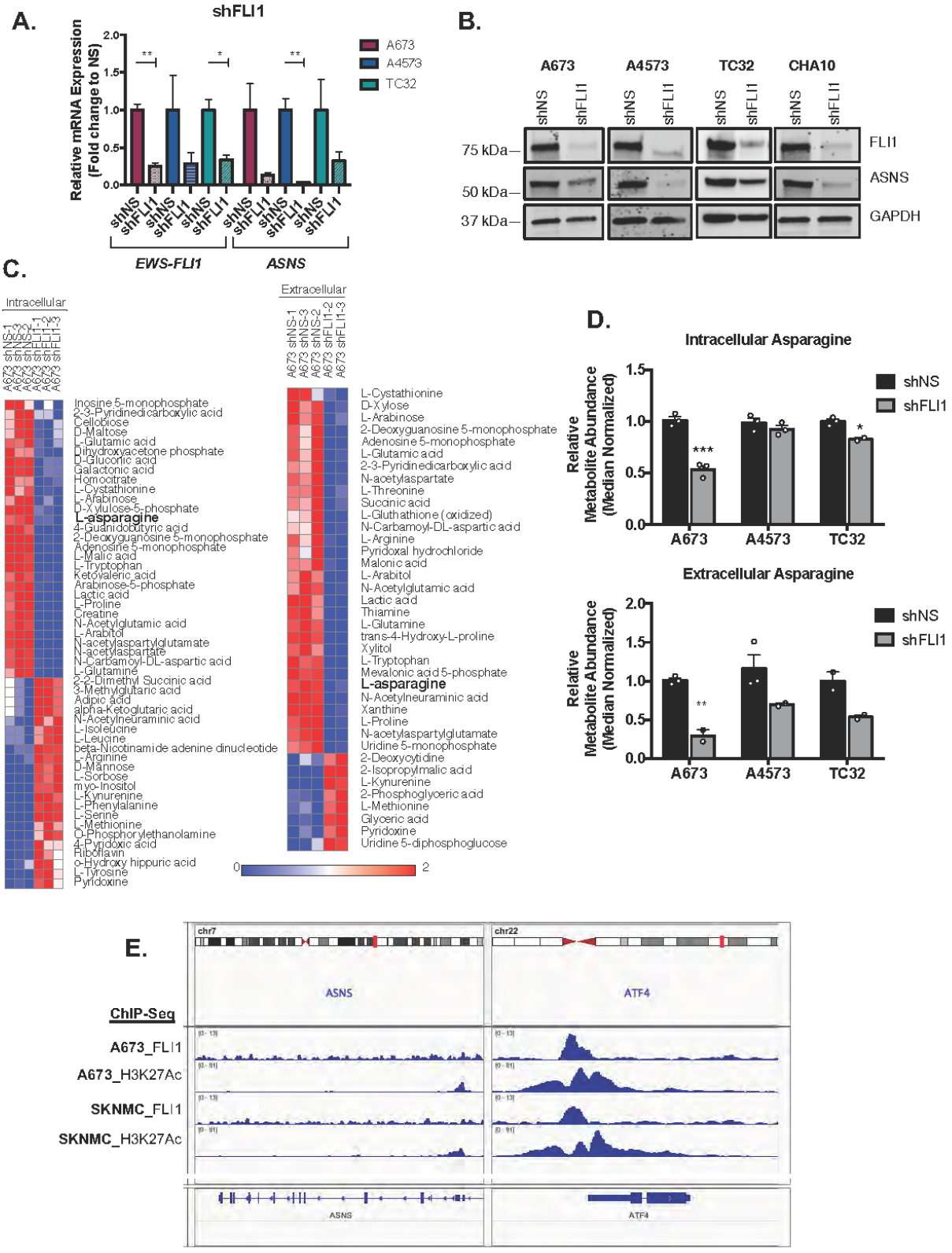

Figure 3-2: EWS-FLI1 knockdown reduces ASNS expression and asparagine abundance

EWS-FLI1 led to robust reductions in ASNS mRNA and protein across all cell lines

A. qRT-PCR for *EWS-FLI1* and *ASNS* transcripts after 96 hours of EWS-FLI1 knockdown B. Western blot of FLI1 (EWS-FLI1) and ASNS protein after 96 hours of shFLI1 knockdown. C. Heatmap representing significantly changed intracellular metabolites ($p<0.05$) from LC/MS metabolomics 96 hours after shRNA EWS-FLI1 knockdown. D. Relative abundance of intracellular and extracellular asparagine between shNS control and shFLI1. E. IGV screenshot of Chromatin immunoprecipitation (ChIP)-sequencing tracks from publicly available FLI1 (EWS-FLI1) and H3K27Ac ChIP in A673 and SKNMC Ewing sarcoma cell line (Riggi et al. 2014).

evaluated (**Figure 3-2A-B**). Having demonstrated significant reductions in ASNS protein with EWS-FLI1 knockdown, we hypothesized that loss of ASNS would result in reduced asparagine synthesis and, consequently, lower asparagine abundance intracellularly. To evaluate this, we profiled three Ewing sarcoma cell lines for both intracellular and extracellular metabolites by liquid chromatography-coupled tandem mass spectrometry (LC/MS)-based metabolomics 96 hours after stable transduction with shFLI1. Indeed, asparagine abundance was significantly reduced intracellularly in A673 and TC32 cells (**Figure 3-2C-D, Figure 3-3A**) and extracellular asparagine levels also trended toward reduction with EWS-FLI1 knockdown (**Figure 3-2C-D, Figure 3-3B**). To explore whether EWS-FLI1 may regulate *ASNS* expression via direct promoter binding in addition to its regulation via ATF4, as we previously reported [16], we interrogated published ChIP-sequencing data for EWS-FLI1 binding sites at regulatory regions around the *ASNS* gene. We found no enrichment for EWS-FLI1 at *ASNS* regulatory regions or evidence for GGAA microsatellite repeats (**Figure 3-2E**) [17], in stark contrast to our previously published EWS-FLI1 binding site at the *ATF4* promoter [16]. Together, these results support the mechanism that EWS-FLI1, via ATF4 regulation, impacts ASNS and ASNS-dependent pools of asparagine.

ASNS is required for Ewing sarcoma cell growth in vitro in the absence of asparagine

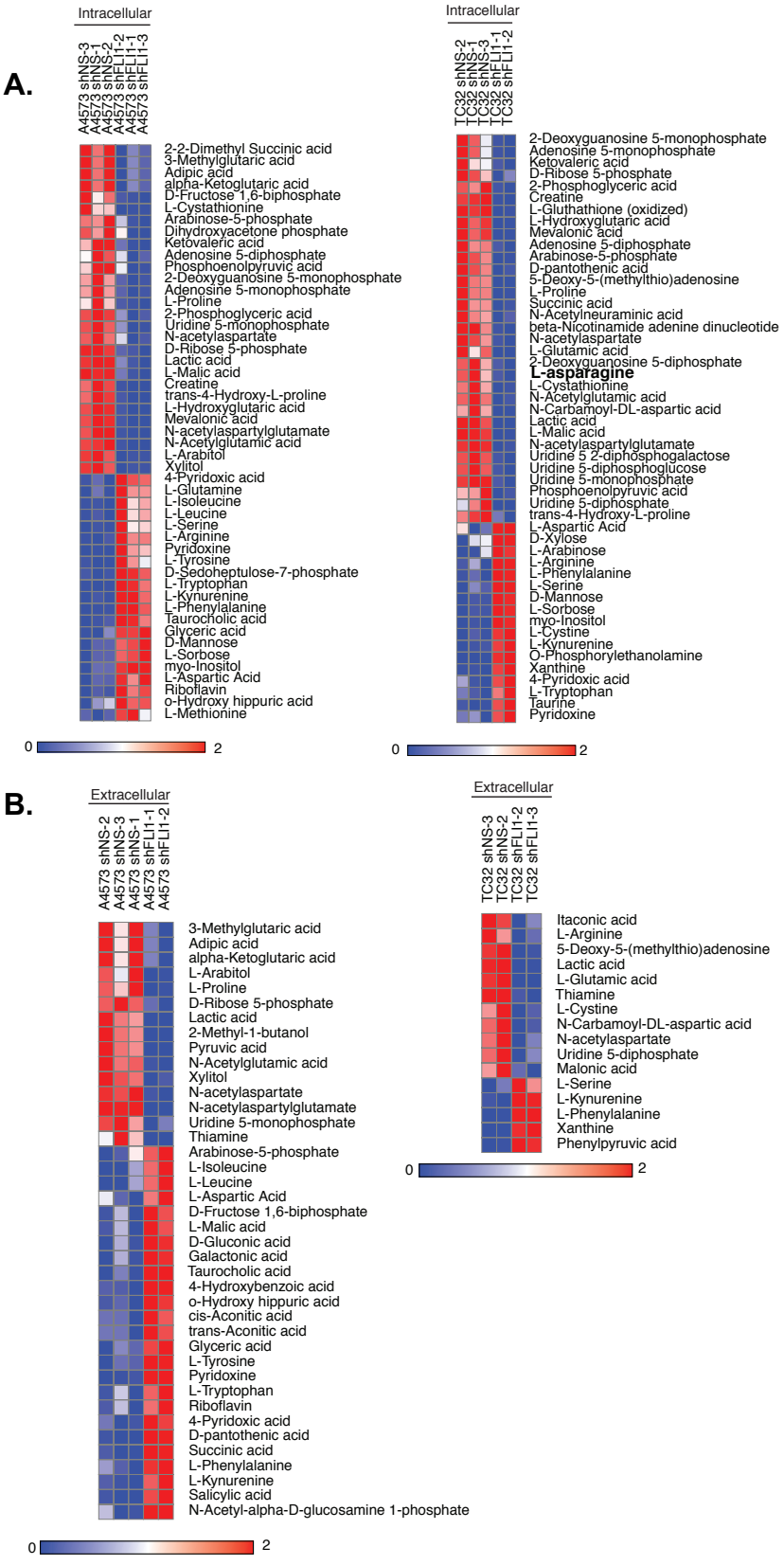

Figure 3-3: shFLI1 LC/MS metabolomics in A4573 and TC32 cells

A. Heatmap representing significantly changed intracellular and B. extracellular metabolites ($p<0.05$) from LC/MS metabolomics 96 hours after shRNA EWS-FLI1 knockdown.

To determine whether asparagine and ASNS function to impact Ewing sarcoma cell viability and tumorigenic phenotypes, we began by evaluating the growth of Ewing sarcoma call lines upon asparagine withdrawal. Our analysis of real-time proliferation of three Ewing sarcoma cell lines (A673, A4573, TC32), revealed that, when cultured in DMEM deficient in asparagine, the growth of Ewing sarcoma cells was not differentially affected by

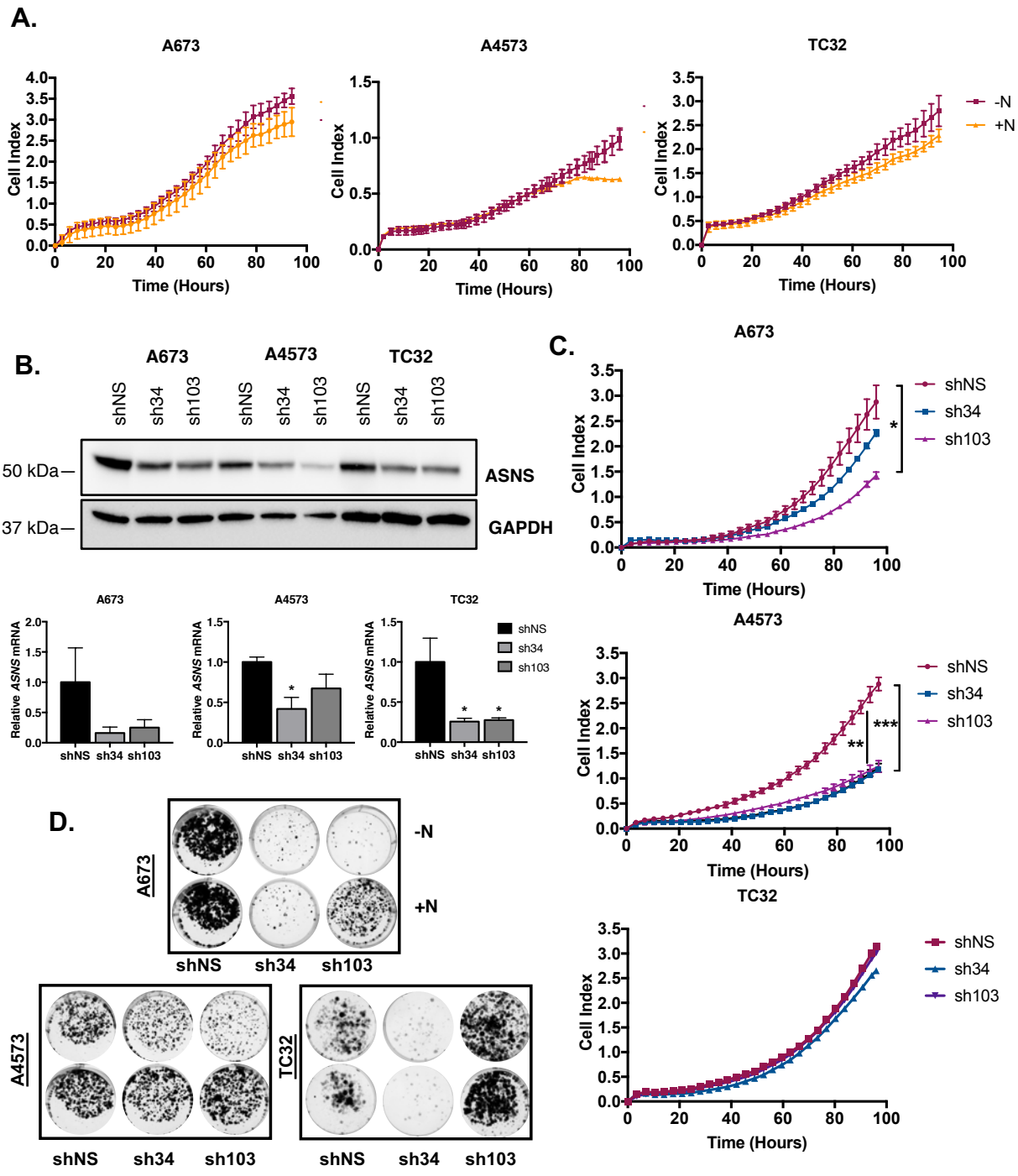

Figure 3-4: ASNS is required for ewing sarcoma cell growth in the absence of extracellular asparagine

A. Real time proliferation of Ewing sarcoma cells in the presence or absence of 1mM asparagine. B. Western blot depicting ASNS protein reduction with shRNA-mediatied ASNS knockdown. C. Real-time xCelligence proliferation assay of ASNS knockdown and control cells in media lacking asparagine. D. Clonogenic assay of A673, A4573, and TC32 cells with ASNS knockdown cultured in media with 1mM asparagine (+N) or lacking asparagine (-N). Error bars represent SEM from independent biological replicates. * p<0.05; ** p<0.01; *** p<0.001; **** p<0.0001; Two-tailed t-test.

the presence or absence of asparagine re-supplementation (**Figure 3-4A**). We next used two shRNA constructs to knock down ASNS (**Figure 3-4B**) and again evaluated the effects on proliferation after removing asparagine from the media. Loss of ASNS led to significantly reduced cell proliferation in two of the three cell lines tested (A673 and A4573) (**Figure 3-4C**). We next assess cell survival and the ability of cells to form colonies after ASNS loss by clonogenic assay and found that ASNS knockdown led to marked reduction in colony forming ability in A673 cells, with more subtle reductions in A4573 (**Figure 3-4D**). Interestingly, supplementation of the media with 1mM asparagine could rescue the decrease in colony formation to varying degrees across cell lines and constructs (**Figure 3-4D**). Thus, while the response is varied with shRNA-mediated knockdown, loss of ASNS expression leads to reduced cell viability and colony-forming ability, particularly under asparagine-low conditions. Our studies therefore suggest that Ewing sarcoma cells are not auxotrophic for asparagine at baseline and display sensitivity to asparagine loss only when ASNS expression is reduced genetically.

EWS-FLI1 "Low" cells do not show selective growth inhibition with asparagine loss

Our data reproducibly showed that knockdown of EWS-FLI1 led to decreased levels of ASNS and a diminished abundance of asparagine (**Figure 3-2**). Therefore, we wondered whether these EWS-FLI1 "Low" cells may exhibit greater sensitivity to the FDA-approved, clinically available drug, L-asparaginase (ASNase) or extracellular asparagine withdrawal. To begin to address this question, we first treated Ewing sarcoma cells with increasing doses of ASNase *in vitro* and compared their viability to

two leukemia cell lines (MOLM13 and MV4;11) treated with the same doses (**Figure 3-5A**). Our results show that Ewing sarcoma cells are relatively resistant to ASNase, when compared to the highly sensitive ALL cell line, MV4;11. Ewing sarcoma cells maintained some viability, even at the highest doses of ASNase (**Figure 3-5A**). We next knocked down EWS-FLI1 with shRNA and evaluated the sensitivity of EWS-FLI1 knockdown cells to depletion of asparagine from the media. Our results show that the viability of EWS-FLI1 knockdown cells is not further reduced by asparagine withdrawal

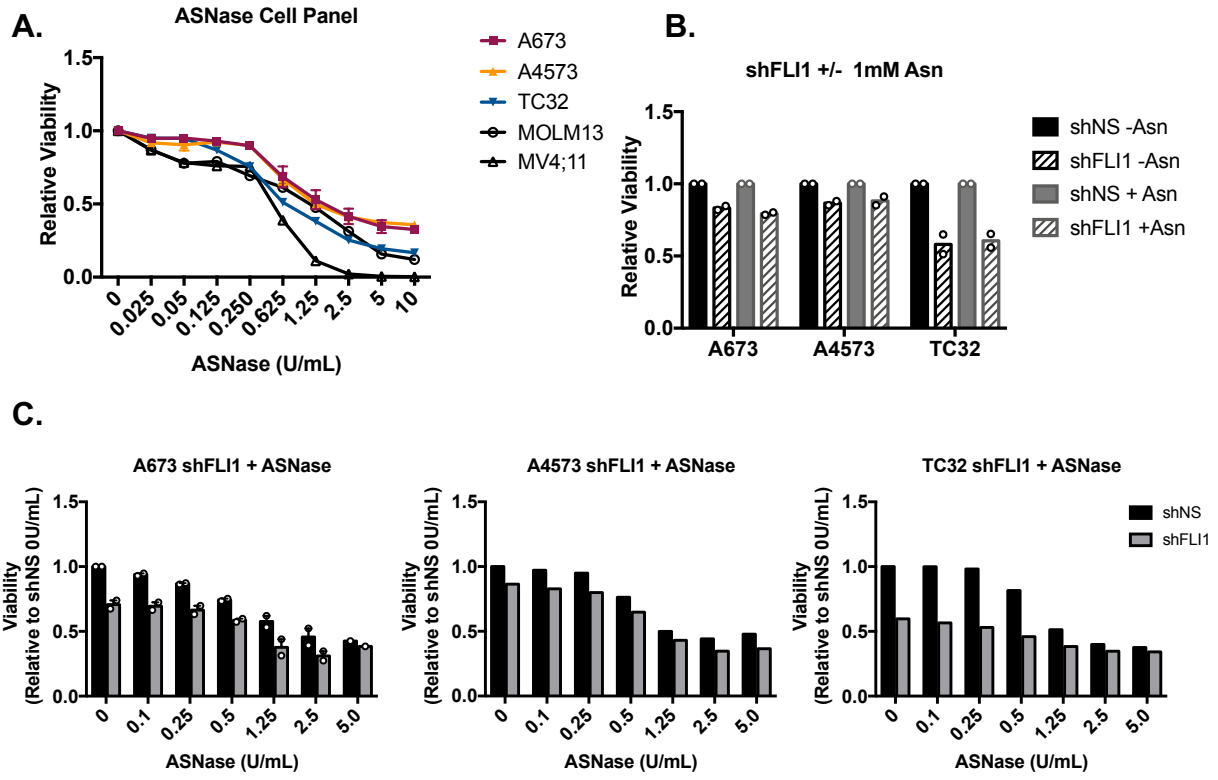

Figure 3-5: EWS-FLI1 "Low" cells are not sensitized to asparagine withdrawal

A. Dose-response curve of Ewings cell lines (A673, A4573, and TC32), B-cell acute lymphoblastic leukemia cells (MV4;11) and acute myeloid leukemia cells (AML) treated with increasing concentrations of L-asparaginase (ASNase) for 72 hours. B. Viability assay for A673, A4573, and TC32 control (shNS) and shFLI1 cells cultured in media with 1mM asparagine (+N) or no asparagine (-N). C. Viability assay of FLI1 (EWS-FLI1) knockdown A673 cells treated with ASNase for 72 hours. Error bars represent SEM from independent biological replicates. * $p<0.05$; ** $p<0.01$; *** $p<0.001$; **** $p<0.0001$; Two-tailed t-test.

(**Figure 3-5B**). Similarly, treatment of EWS-FLI1 knockdown cells with ASNase did not further inhibit the growth of EWS-FLI1 “Low” cells (**Figure 3-5C**). Therefore, these data suggest that the growth of EWS-FLI1 “Low” cells is not selectively inhibited under conditions of asparagine depletion.

Doxorubicin treatment downregulates ASNS but does not synergize with asparagine loss

The chemotherapeutic agent, doxorubicin, is part of the backbone of current Ewing sarcoma therapy [18]. Previous work demonstrated that doxorubicin antagonizes the EWS-FLI1-induced gene expression signature and leads to reduced levels of EWS-FLI1 protein [19]. To complement our genetic approach for targeting the EWS-FLI1 fusion, we sought to determine whether pharmacologic targeting of EWS-FLI1 activity with doxorubicin also leads to reductions in ASNS expression, consequently exposing a potential vulnerability to asparagine withdrawal. Evaluation of publicly available gene expression data from A673 Ewing sarcoma cells treated with EC_{50} and 2X EC_{50} doses of doxorubicin for 1, 3, and 6 days demonstrated that treatment with doxorubicin led to a dose and time-dependent reduction in *ASNS* transcript, with a greater than 50% reduction in transcript after 6 days of treatment (**Figure 3-6A**). To validate these findings, we measured ASNS and EWS-FLI1 protein levels in two independent cell lines following exposure to increasing concentrations of doxorubicin. After 72 hours we observed a dose- dependent decrease in ASNS protein (**Figure 3-6B)** in both cell lines.

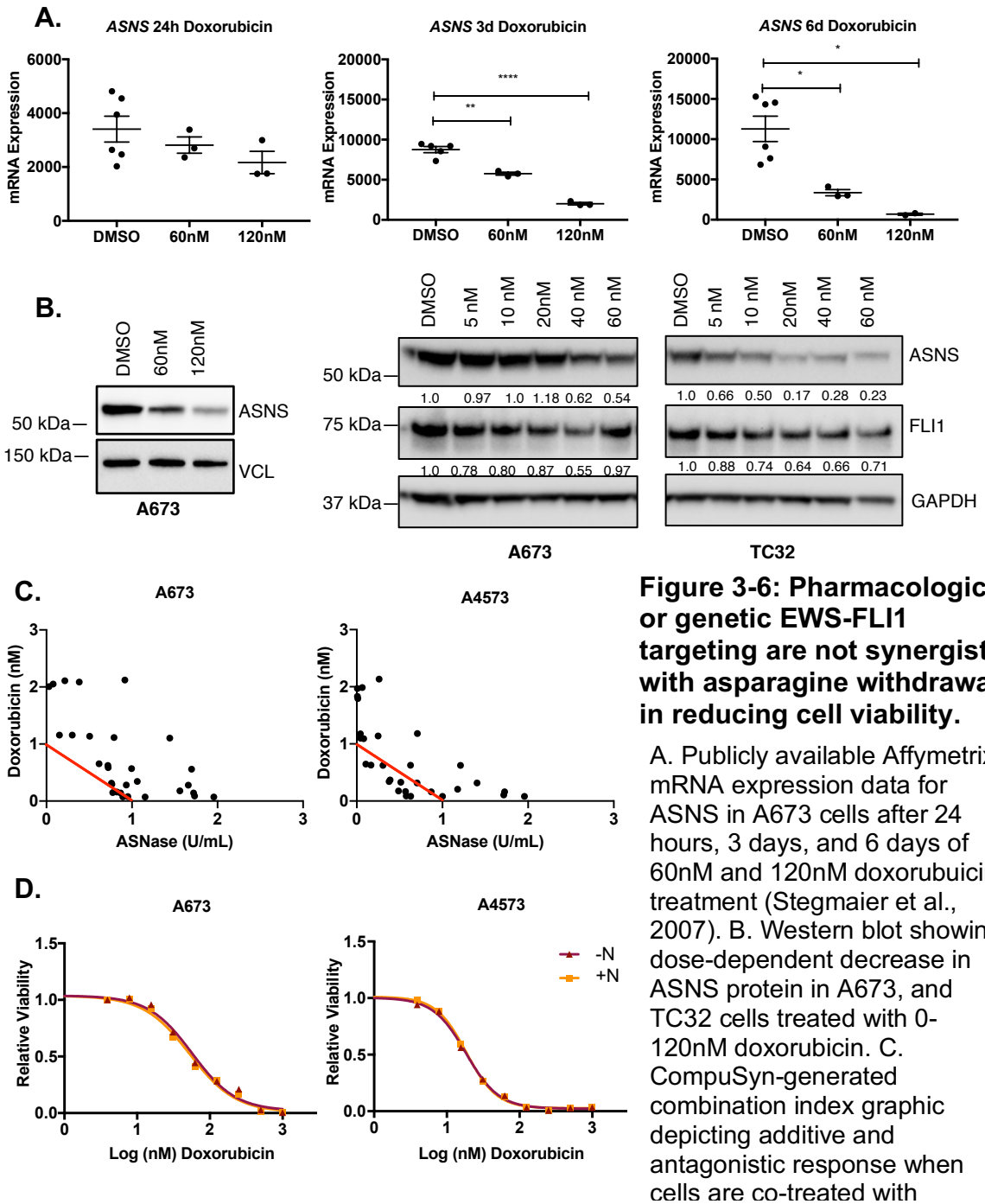

Figure 3-6: Pharmacologic or genetic EWS-FLI1 targeting are not synergistic with asparagine withdrawal in reducing cell viability.

A. Publicly available Affymetrix mRNA expression data for ASNS in A673 cells after 24 hours, 3 days, and 6 days of 60nM and 120nM doxorubuicin treatment (Stegmaier et al., 2007). B. Western blot showing dose-dependent decrease in ASNS protein in A673, and TC32 cells treated with 0-120nM doxorubicin. C. CompuSyn-generated combination index graphic depicting additive and antagonistic response when cells are co-treated with ASNase and doxorubicin for 72 hours. D. Dose response curve for doxorubicin treatment in media with 1mM asparagine (+N) or no asparagine (-N). Error bars represent SEM from independent biological replicates. * p<0.05; ** p<0.01; *** p<0.001; **** p<0.0001; Two-tailed t-test.

However, although a trend is seen in both cell lines (**Figure 3-6B**), we did not observe a striking loss of EWS-FLI1 protein as previously reported [19].

The reproducible loss of ASNS expression induced by doxorubicin exposure led us to explore whether this may provide a therapeutically viable synergistic combination with the use of ASNase. Given that Ewing sarcoma cells are sensitive to asparagine loss when ASNS expression is low (**Figure 3-4C-D**), we hypothesized that doxorubicin would synergistically inhibit the growth of Ewing sarcoma cells when combined with ASNase exposure. To test if doxorubicin would sensitize Ewing cells to ASNase, we next performed a combination study by co-treating two Ewing sarcoma cell lines with titrating doses of both drugs. In contrast to our expectations, we found that the combination index for the two agents fell around 1 or greater than 1 on average, indicating, at best additive, and mainly antagonistic interactions at most doses (**Figure 3-6C**). Consistent with an absence of synergy between asparagine loss and doxorubicin, sensitivity of Ewing sarcoma cells to doxorubicin was unchanged in asparagine-depleted media (**Figure 3-6D**). These results further support that despite the effects of both pharmacologic and genetic EWS-FLI1-targeting methods to reduce ASNS levels, the presumed reduction in ASNS-regulated *de novo* asparagine synthesis does not expose a sensitization to the extracellular depletion of asparagine. All together, these findings using multiple complementary methods demonstrate that the viability and proliferation of EWS-FLI1-low Ewing sarcoma cells are not differentially sensitive to asparagine depletion *in vitro*.

ASNS is required for metastatic colonization in Ewing sarcoma

Intrigued by our finding that EWS-FLI1 inhibition did not provide sensitization to the elimination of extracellular asparagine pools, despite demonstrating robust

reductions in ASNS levels, we were motivated to investigate whether ASNS may serve a different function in regulating Ewing sarcoma tumorigenic phenotypes distinct from cell proliferation. Providing precedent for the premise that ASNS may serve alternate oncogenic functions, recent work in breast cancer using *in vivo* mouse models determined that ASNS and asparagine availability are important regulators of a pro-metastatic phenotype [20]. To examine whether ASNS is required for metastatic spread and colonization, we injected A673 shASNS and control cells into the tail vein of NOD/SCID mice and monitored engraftment with bioluminescence imaging bi-weekly. A673 cells have been well characterized and documented to predominantly metastasize to the liver [21]. Knockdown of ASNS led to a delay in engraftment of cells into the liver and starkly reduced signal in the liver by day 22 (**Figure 3-7A**). At takedown on day 28 after injection, the total number and size of metastatic tumor nodules in the liver was dramatically reduced with knockdown compared to the shNS control (**Figure 3-7B**). Protein extraction from these tumors and western blot analysis showed that ASNS expression was variable across mice, but, on average, ASNS protein levels were reduced in tumors from mice injected with shASNS cells (**Figure 3-7C**).

Asparagine availability has been shown to impact migratory and invasive phenotypes in other cancer contexts [20, 22-24]. In order to determine whether asparagine impacts on cell migration in Ewing sarcoma, we performed transwell migration assays in asparagine replete and depleted conditions, demonstrating than asparagine availability indeed increases the migratory potential of Ewing sarcoma cells *in vitro* (**Figure 3-7D**). A key feature of metastatic cells is the ability for anchorage independent growth and surviving anoikis, detachment-induced cell death [25]. We next

employed a soft agar colony forming assay to evaluate the ability of ASNS knockdown cells to survive in the absence of cell-attachment and found that loss of ASNS

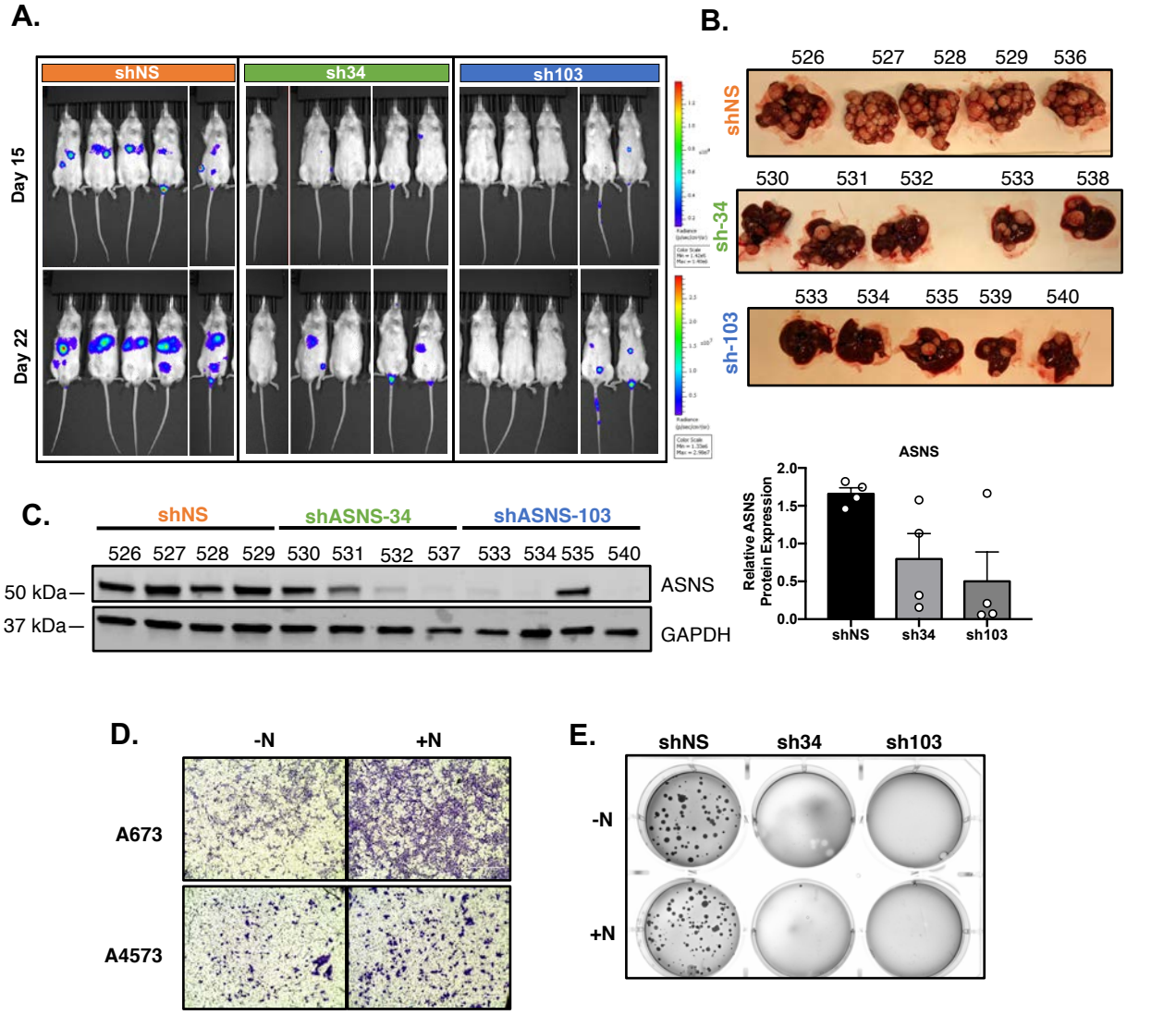

Figure 3-7: ASNS is required for metastatic colonization

A. IVIS bioluminescence images 15 and 22 days after injection of A673 fLuc-GFP control (shNS) and ASNS knockdown (sh34, sh103) cells injected by tail vein into NOD/SCID mice. B. Mouse livers at takedown from control and ASNS-knockdown conditions from experiment in (A). C. Western blot analysis and quantitation for ASNS generated from tumor nodules extracted from (B). D. Transwell migration assay of A673 and A4573 cells cultured for 24 hours in the presence or absence of 1mM asparagine (-N/+N). E. Soft agar colony formation assay of A673 ASNS knockdown and shNS control cells cultured in the presence or absence of 1mM asparagine (-N/+N). Error bars represent SEM from independent biological replicates. * $p<0.05$; ** $p<0.01$; *** $p<0.001$; **** $p<0.0001$; Two-tailed t-test.

completely abolished the ability of A673 cells to form colonies upon ASNS knockdown in the presence and absence of extracellular asparagine (**Figure 3-7E**). These results support that loss of ASNS may impact metastatic progression through impacts on migration and anoikis resistance phenotypes.

Findings in other models have shown that, while metastatic progression is dependent on asparagine, local tumor growth is unaffected by disruption of asparagine supply [20, 26]. Consistent with these prior studies, knockdown of ASNS did not significantly reduce subcutaneous tumor growth, although sh103 had a modest growth-inhibitory effect (**Figure 3-8A-B**). Similar to the tail vein metastatic model, shASNS subcutaneous tumors largely maintained ASNS knockdown when assessed at

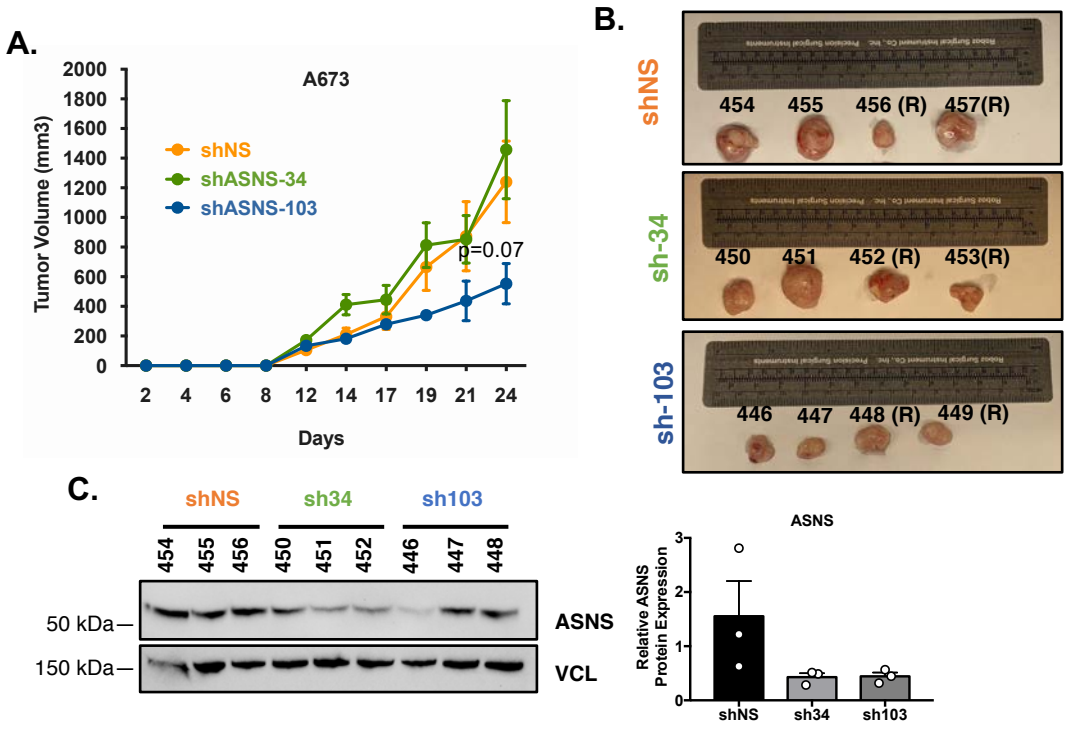

Figure 3-8: ASNS is dispensable for local tumor growth

A. Comparison of subcutaneous tumor growth for 24 days from mice injected with shNS or shASNS cells in the flank. B. Images comparing flank tumor sizes from (A) at endpoint. C. Western blot analysis and quantitation for ASNS expression in subcutaneous tumor lysates from (B) at endpoint. Error bars represent SEM from independent biological replicates. * p<0.05; ** p<0.01; *** p<0.001; **** p<0.0001; Two-tailed t-test.

takedown day 26 (**Figure 3-8C**). In sum, these results suggest that ASNS promotes metastasis *in vivo* but is not required for tumor growth at the primary site or at locations of tumor engraftment once colonization has been established.

ASNS regulates epithelial mesenchymal transition (EMT) signatures in Ewing sarcoma

To begin to explore the mechanism by which ASNS regulates metastatic phenotypes, we performed unbiased RNA-sequencing on A673 Ewing sarcoma cells with stable knockdown of ASNS *in vitro* using the same experimental set up as for our *in vivo* tail vein experiment (**Figure 3-7A**). Interestingly, our results revealed a more pronounced effect of ASNS loss on the upregulation of transcripts, with many fewer genes that were significantly downregulated (**Figure 3-9A**). We observed robust and highly significant transcriptomic changes that were shared between the two shRNA constructs targeting ASNS, with 26 downregulated, and 237 upregulated genes that changed more than 2-fold in expression (**Figure 3-9A**). Further analysis of KEGG and HALLMARK pathways using the Molecular Signatures Database revealed enrichment in focal adhesion, extracellular matrix (ECM), and epithelial mesenchymal transition gene sets in the significantly upregulated transcripts, while downregulated targets were enriched for metabolic processes such as fatty acid biosynthesis and cholesterol homeostasis (**Figure 3-9A**). Of note, upregulated transcripts included several genes implicated in ECM and ECM degradation processes, such as (*MMP3*, *MMP10*, *TGFBI*, *COL1A2*, and *TNC*).

In breast cancer models, the promotion of an invasive metastatic phenotype regulated by asparagine abundance has been demonstrated to be associated with

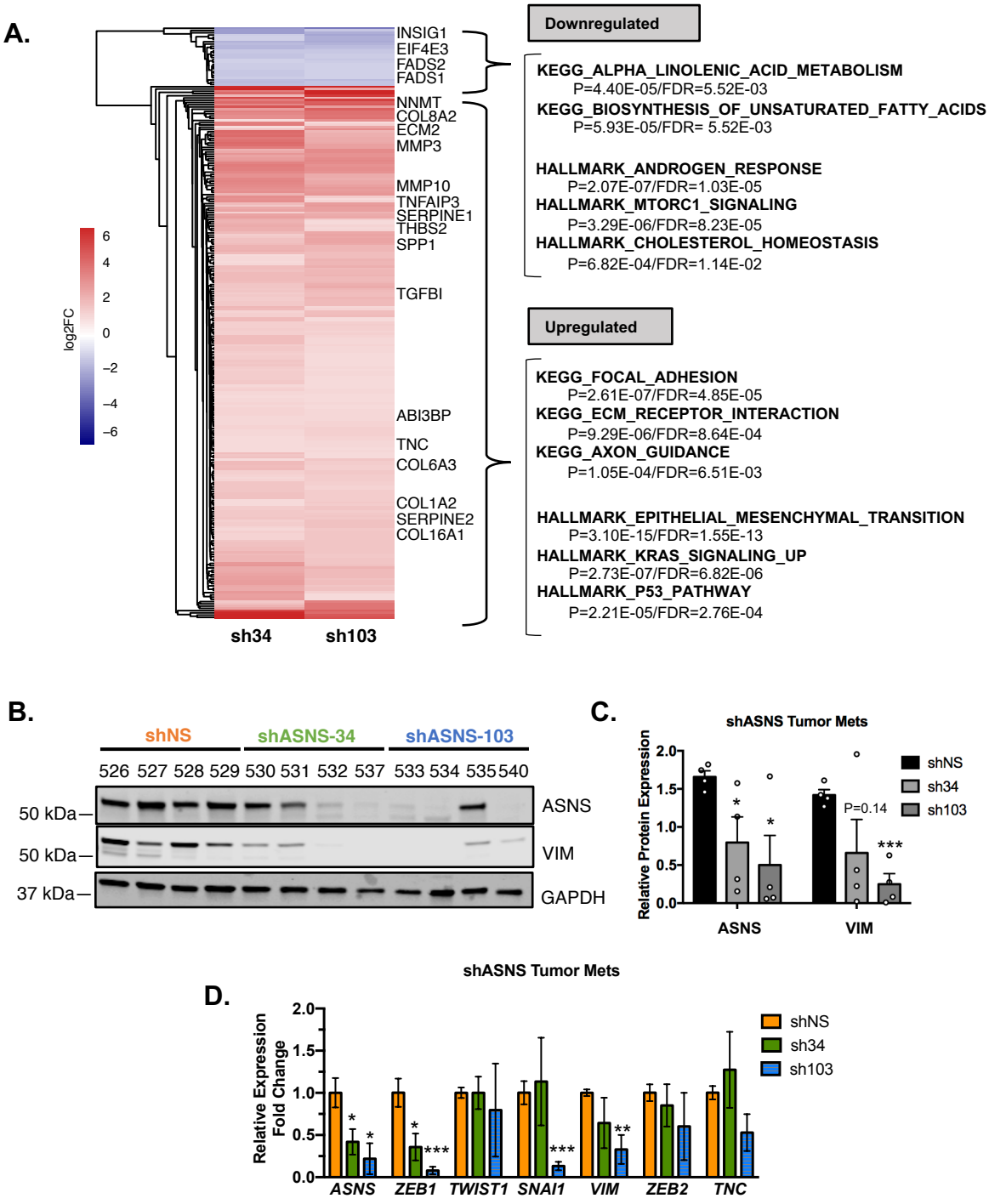

Figure 3-9: ASNS loss impacts epithelial mesenchymal transition and extracellular matrix gene expression signatures

A. Hierarchical clustering heatmap of differentially expressed transcripts (pAdjusted <0.05, -1<log2FoldChange>1) between shNS control and shASNS A673 cells depeleted of asparagine for 24 hours. MSig Database analysis for top KEGG and HALLMARK pathways represented in shared upregulated and downregulated genes between sh34 and sh103. B. Western blot analysis and C. quantitation for vimentin expression from tumor met lysates generated in (Fig 3-5C). D. qRT PCR analysis for epithelial mesenchymal transition (EMT) marker expression in RNA extracted from met tumors in (Fig 3-5B). Error bars represent SEM from independent biological replicates. * p<0.05; ** p<0.01; *** p<0.001; **** p<0.0001; Two-tailed t-test.

transcriptional and protein level changes in asparagine-rich proteins important for EMT, such as TWIST1 and vimentin, and downregulation of epithelial programs, including expression of *CDH1* (E-cadherin) [20]. We sought to examine whether our *in vitro* transcriptomic data was also reflected *in vivo* by changes in EMT-associated proteins with shASNS knockdown. In fact, we found that protein expression of the mesenchymal marker, vimentin, was significantly reduced in metastatic liver tumors that developed from mice injected with shASNS knockdown cells by tail vein (**Figure 3-9B-C**). When comparing tumors from each experimental condition, quantitative real-time PCR (qRT-PCR) analysis revealed trending decreases in vimentin transcript, and significant downregulation of select other EMT markers (ZEB1, and *SNAI1*), although variable effects on other EMT-markers, ZEB2, TNC, and TWIST1 were observed (**Figure 3-9D**). In sum, these finding suggest that *in vitro*, loss of ASNS expression leads to widespread upregulation in programs relating to EMT and ECM integrity, while metastatic nodules that are able to colonize and grow *in vivo* from ASNS knockdown cells, exhibit variable but decreased expression of select EMT-related transcripts. Thus, we hypothesize that ASNS-dependent regulation of cell state may explain the reduced metastatic tumor formation with ASNS loss *in vivo.*

Dietary asparagine restriction does not impact in vivo metastasis

Cellular asparagine levels can also be modified by changing the asparagine content in the diet. Therefore, we took a complementary approach to ASNS loss of function and tested the effect of limiting dietary asparagine on metastatic potential in vivo. NOD/SCID mice were placed on 4% or 0% L-asparagine content chow diet, injected with stably transduced control (shNS) or EWS-FLI1 knockdown (shFLI1) cells by tail vein, and monitored for tumor growth by bioluminescence imaging (**Figure 3-10A-B**). This experiment aimed to test several hypotheses. First, as the key oncogenic driver in Ewing sarcoma, we expected that loss of EWS-FLI1 would result in reduced tumor growth. Second, if asparagine is indeed the key mediator in regulating metastasis, we predicted that limiting asparagine abundance through dietary restriction would phenocopy the effect of ASNS loss on inhibiting metastatic dissemination even under EWS-FLI1 control conditions. Third, our finding that EWS-FLI1 impacts asparagine levels via ASNS led us to hypothesize that EWS-FLI1 knockdown cells would be further sensitized to asparagine loss in vivo and exhibit the greatest reduction in metastatic growth. As expected, loss of EWS-FLI1 expression led to dramatically and significantly reduced metastatic growth detected by bioluminescence at 24 days post injection (**Figure 3-10B**). Interestingly, bioluminescence imaging at 1-day post injection revealed infiltrating cells in the lungs of mice injected with shFLI1 cells in both the 0% asparagine and 4% asparagine groups, an effect that was not observed in the shNS mice (**Figure 3-10B**). Control group mice were all taken down when the first mouse reached endpoint (day 27) and shFLI1 mice were maintained until reaching endpoint

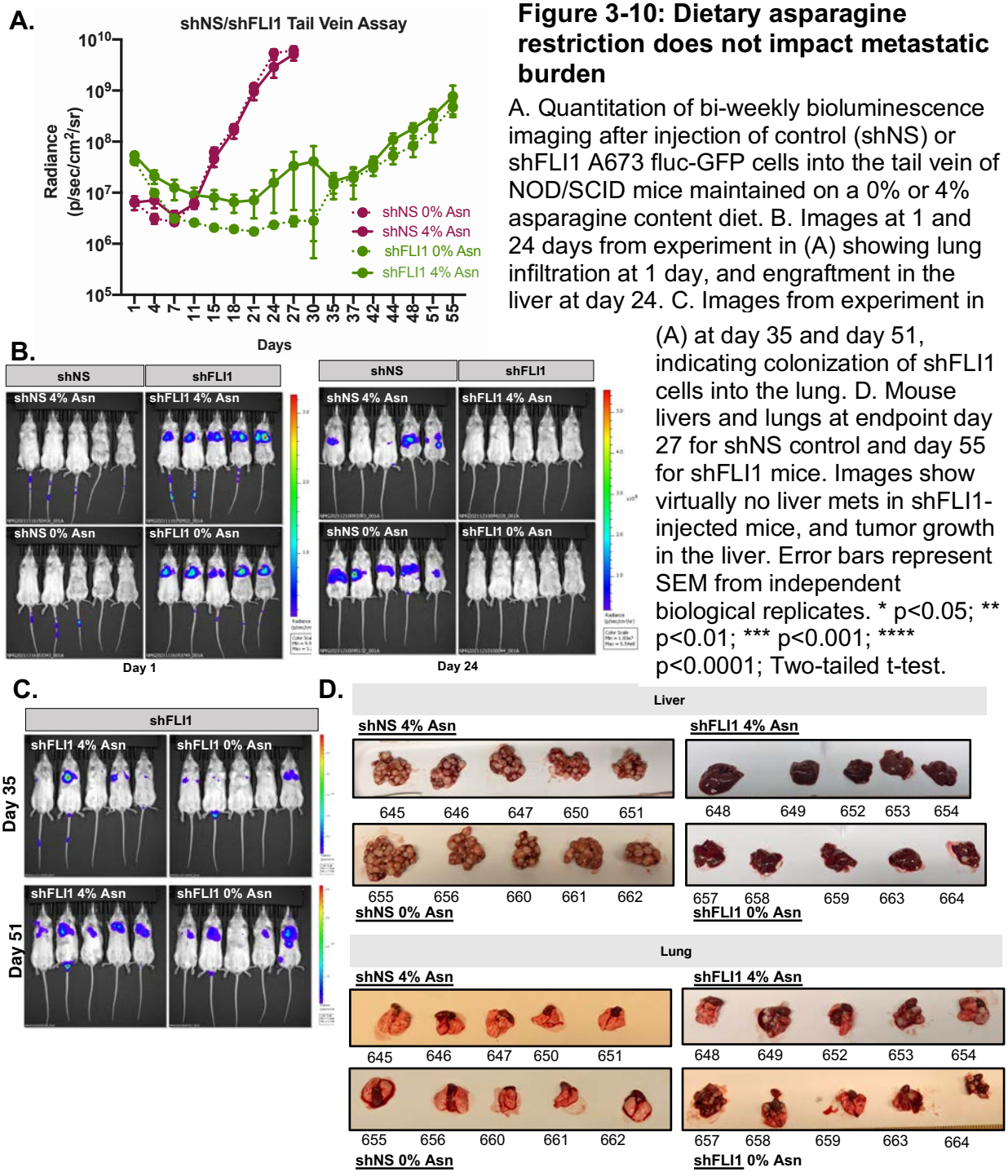

Figure 3-10: Dietary asparagine restriction does not impact metastatic burden

A. Quantitation of bi-weekly bioluminescence imaging after injection of control (shNS) or shFLI1 A673 fluc-GFP cells into the tail vein of NOD/SCID mice maintained on a 0% or 4% asparagine content diet. B. Images at 1 and 24 days from experiment in (A) showing lung infiltration at 1 day, and engraftment in the liver at day 24. C. Images from experiment in (A) at day 35 and day 51, indicating colonization of shFLI1 cells into the lung. D. Mouse livers and lungs at endpoint day 27 for shNS control and day 55 for shFLI1 mice. Images show virtually no liver mets in shFLI1-injected mice, and tumor growth in the liver. Error bars represent SEM from independent biological replicates. * $p<0.05$; ** $p<0.01$; *** $p<0.001$; **** $p<0.0001$; Two-tailed t-test.

(day 55). Mice injected with shFLI1 cells on both diets exhibited a delay in cell engraftment, with signal first appearing in the lung and not the liver at ~day 35 (**Figure 3-10C**). At endpoint, organs were harvested and assed for tumor growth, revealing a

clear separation between control cells engrafting and growing in the liver, and shFLI1 cells engrafting in the lung (**Figure 3-10D**). Our data indicate that EWS-FLI1 knockdown itself impacts the location and rate of metastatic growth, but dietary asparagine restriction does not affect the course of metastatic colonization or growth in either control or EWS-FLI1 knockdown conditions.

Discussion

Each step of tumorigenesis and metastasis requires exquisitely finetuned regulation of metabolic pathways, and oncogenic activation promotes metabolic rewiring in order to support the high bioenergetic demands of cancer progression [3]. Ewing sarcoma is a highly aggressive pediatric bone and soft tissue for which the standard of care has not improved in decades [18]. While many cancers are able to grow at the primary site for numerous years before metastasizing, other cancers, like Ewing sarcoma, can be metastatic at diagnosis when the primary tumor remains small, for reasons that are not well understood [27]. The 5-year survival rate for metastatic or relapsed Ewing sarcoma patients is less than 20%, and 10% for patients with bone metastasis [18, 28, 29]. Therefore, there is a huge unmet need to better understand metastatic regulators in Ewing sarcoma and develop better targeted therapies.

Pathognomonic EWS-ETS fusion proteins, the most common of which is EWS-FLI1, promote Ewing sarcoma tumorigenesis by inducing widespread transcriptional and epigenetic reprogramming [17, 30, 31], however, the metabolic consequences of EWS-FLI1 expression hadn't been explored until relatively recently [13]. Findings by our group and others have demonstrated that EWS-FLI1 broadly impacts the cellular

metabolome, particularly by impacting amino acid biosynthetic pathways, such as the serine biosynthesis pathway [12-15]. Our most recent work elucidated an EWS-FLI1-ATF4 axis by which EWS-FLI1, in cooperation with the scaffold protein menin, promotes metabolic homeostasis by direct promoter binding and transcriptional regulation of the stress-induced master regulator, activating transcription factor 4 (ATF4) [16]. These studies identified asparagine synthetase (*ASNS*) the rate-limiting enzymatic regulator for *de novo* asparagine synthesis, among the target genes downstream of ATF4, which we further pursued in this chapter.

The success of bacterial L-asparaginase (ASNase) to treat patients with acute lymphoblastic leukemia (ALL) [6, 32] owes to the unique promoter silencing of *ASNS* expression, rendering these cancers auxotrophic for extracellular asparagine [7]. To this date, ASNase has not been approved for use in the treatment of solid tumors, largely owing to dose-limiting toxicities [32]. However, numerous studies have identified ASNS as a biomarker that predict poor prognosis in solid tumors, and ASNS is amplified in glioma [11, 20, 22-24, 26]. Our current findings provide evidence that ASNS is expressed in Ewing sarcoma and is regulated by the oncogenic fusion, EWS-FLI1. Through LC/MS-based metabolomics profiling, we further find that loss of EWS-FLI1 leads to diminished cellular pools of both intracellular and extracellular asparagine. Importantly, these data are in agreement with previously published metabolic profiling of EWS-FLI1 knockdown cells, which showed significant reductions in intracellular asparagine [13]. The absence of EWS-FLI1 binding at the *ASNS* promoter or regulatory regions surrounding the *ASNS* gene suggest that this regulation happens as a consequence downstream of reductions in the ASNS transcriptional regulator, ATF4,

which we have published to be regulated by EWS-FLI1 [16]. Notably, we observed that ASNS transcript and protein expression is highly heterogenous, both in culture and in primary tumor tissue, likely owing to its dynamic regulation, in part by ATF4, in response to conditions of limiting nutrients, oxygen, etc.

To our knowledge, this is the first study that has implicated ASNS as an important metabolic driver in Ewing sarcoma. Our findings show that ASNS maintains Ewing sarcoma cell viability in the absence of extracellular asparagine, and that loss of ASNS leads to reduced colony formation. We thus speculated that inhibition of EWS-FLI1 might sensitize Ewing sarcoma cells to depletion of asparagine. In contrast to our expectations, we found that treatment of EWS-FLI1 knockdown cells with ASNase or exposure to asparagine depletion did not selectively reduce the viability of EWS-FLI1 “Low” cells. Through complementary methods to inhibit EWS-FLI1 with doxorubicin, we found that doxorubicin exposure decreased ASNS levels in dose-dependent manner. We therefore predicted that combined treatment with ASNase or asparagine withdrawal would provide a therapeutically viable combination strategy to potentially reduce doxorubicin dosage by combining with ASNase. In contrast, we did not observe synergy between ASNase and either asparagine loss of treatment with ASNase *in vitro*. We hypothesize that, due to intricate mechanisms regulating ASNS, EWS-FLI1-inhibited cells are likely able to metabolically rewire upon more long-term asparagine limitation in order to maintain ASNS at levels high enough, and upregulate concordant pathways, in order to reach homeostasis and prevent cell death.

Notably, in our investigation of ASNS functions *in vivo*, we found that ASNS loss led to reduced metastatic tumor burden. In contrast, we find that ASNS is dispensable

for primary tumor growth, consistent with published work in breast cancer and melanoma [20, 26, 33]. Although ASNS loss-of-function leads to a stark reduction in time to metastatic engraftment and total metastatic tumor burden, the function that ASNS plays in allowing cells to survive the metastatic process is still unclear. Intriguingly, our results demonstrate that while asparagine availability regulates cell migration *in vitro*, depletion of asparagine by dietary restriction does not reproduce the impact of ASNS knockdown on reducing metastasis *in vivo*. This suggests that asparagine itself may not be the important factor in promoting metastasis, but rather there may be other metabolic influences at play when the enzymatic conversion of aspartate to asparagine is inhibited, and/or non-canonical non-enzymatic functions for ASNS. For instance, reductions in ASNS would presumably lead to a buildup of aspartate and glutamine, both of which serve functions in cancer progression [34-36]. Further studies using ASNase *in vivo* and/or complementary approaches to target ASNS, such as through CRISPR/Cas9, or direct pharmacologic inhibitors of the ASNS enzyme are needed to more deeply address this question [37, 38].

Our unbiased exploration of transcriptomic changes impacted by ASNS knockdown *in vitro* suggest that loss of ASNS leads to upregulation in pro-EMT and extracellular matrix modifying pathways. This finding is intriguing, given prior work implicating ASNS and asparagine in the regulation of metastasis via generation of asparagine-rich EMT factors [20], and our previously published work describing pro-metastatic subpopulations of ECM secreting cells [39, 40]. Additionally, we observe a disconnect between transcriptional changes *in vitro* and transcriptional and protein expression changes for EMT markers *in vivo*, suggesting that ASNS knockdown cells

that are able to colonize and grow a tumor are distinct from ASNS knockdown cells that have not encountered an *in vivo* environment. Ewing sarcomas are classified as mesenchymal tumors, with a presumed mesenchymal stem cell cell of origin, and are thus unable to undergo classical epithelial mesenchymal transition characteristic of carcinomas [41]. Emerging work exploring the developmental origins of Ewing sarcoma has proposed that Ewing sarcomas exist on a developmental continuum between neural ectodermal and mesoderm states, and that this interim undifferentiated state contributes to tumorigenic potential [42]. We thus speculate that ASNS may function to maintain the aggressive undifferentiated phenotype, and that loss of ASNS may push cells to a more differentiated state that is less metastatic. Alternatively, it is possible that ASNS loss is in some way impacting the translation of proteins important for EMT via mTORC1 regulation, as previously described [10], and that the upregulated EMT, ECM transcriptome *in vitro* represents upregulation in expression to compensate for protein level reductions. Importantly, these data also suggest that while doxorubicin was not found to be synergistic with ASNase in inhibiting the growth of Ewing sarcoma cells, doxorubicin's effect on ASNS may impact on the mesenchymal cell state. These hypotheses and exploration of possible non-canonical roles for ASNS warrant further investigation.

Two previous studies have examined ASNS and asparagine as a vulnerability in other sarcoma models, and some work suggests that ASNS is important for resisting redox stress [43, 44]. The blood has some of the highest levels of oxidants in the body, and metastatic cells that survive this stress undergo metabolic adaptations that confer oxidative stress resistance [45]**.** One study employing RNA-seq on asparagine-depleted

sarcoma cells found that ribosome, tRNA biosynthesis, and oxidative phosphorylation were upregulated when ASNS knockdown cells were depleted of asparagine [43]. Although it is possible that ASNS may play a role in maintaining redox homeostasis in Ewing sarcoma, as published in other contexts [11, 43], our data lead us to believe that ASNS may also, in part, function in regulating cell state through the regulation of EMT and ECM modifying factors.

In summary, through in-depth analysis using metabolomic, transcriptomic, and *in vivo* mouse tumor models, we provide new evidence that ASNS is an important regulator of Ewing sarcoma metastasis, and that EWS-FLI1 directly impacts ASNS expression and asparagine abundance. Additionally, expression analysis of ASNS knockdown cells *in vitro* revealed stark impacts of EMT and ECM processes which may be important implicated in regulating cell state and metastatic potential.

Materials and Methods

Cell Lines

Ewing sarcoma cell lines were obtained from the Children's Oncology Group (COG) cell bank (cogcell.org). U2OS, HT-1080, SW 1353, and HEK 293FT cells were obtained directly from ATCC. MOLM13 and MV4;11 cells were obtained from collaborators at the University of Michigan. Cells were not cultured past 20 passages. A673, A4573, and TC32 cells were cultured in RPMI 1640 (Corning) and 293FT, HT-1080, U2OS, and SW 1353 cell lines were cultured in DMEM medium, high glucose (Gibco), unless otherwise stated. CHLA10 cells were cultured in IMDM media (Gibco), supplemented with 1X Insulin-Transferrin-Selenium (Gibco) and 20% fetal bovine serum. MOLM13 and

MV4;11 cells were cultured in suspension flasks in RPMI media with 10% heat inactivated FBS. All media were supplemented with 10% fetal bovine serum (FBS—Atlas Biologicals) and 1% L-glutamine (Life Technologies), unless otherwise noted, and grown at 37°C, 5% CO_2. For asparagine add back studies, DMEM with 10% dialyzed FBS (HyClone) was used, supplemented with L-asparagine (Sigma) at indicated concentration. Identities were confirmed by short tandem repeat (STR) profiling. All cell lines were routinely tested for mycoplasma contamination as described previously [14].

Chemical Inhibitors and Treatments

Doxorubicin (Tocris Bioscience) was dissolved in DMSO and single-agent dose-response curve was determined by serial drug dilution and viability assay by Cell Titer Glo 2.0 (Promega). PEGylated asparaginase (ASNase) was diluted as indicated (U/mL) and viability was assessed by Cell Titer Glo 2.0 (Promega) assay after treatment.

Generation of Cell Lines Expressing shRNA

For the following plasmids: pLKO.1 shNS (non-silencing control), and shFLI1 (Sigma-Aldrich MISSION shRNA library), concentrated (10X) lentivirus production was carried out by the University of Michigan Vector Core facility or prepared in the laboratory following standard procedures [46]. For shASNS (Sigma-Aldrich MISSION shRNA library) and its corresponding shNS control, plasmids were co-transfected with pLP/VSVG (Invitrogen, Life Technologies) and psPax2 (Addgene) plasmids into 293FT packaging cells using Lipofectamine 2000. 24 hours post-transfection, media was replaced. Viral supernatant was collected 72 hours after transfection, spun down for 15 minutes at 4000 rpm, and the clarified supernatant was concentrated with Lenti-X-

concentrator (Takara). Ewing sarcoma cell lines were plated in complete media in 100 mm dishes. Viral supernatant was added to the media at 1X concentration and removed after 24-hour incubation. Cells were selected by supplementing the media with 1.5 µg/mL puromycin (Gibco) for 48 hours before collection. See Appendix II for shRNA sequences and plasmid information.

LC/MS Metabolomics

Isolating polar metabolites

Cells were seeded to aim for 70% confluence on the day of metabolite extraction. Cells were cultured in 2 mL of growth media per well of a 6 well plate and incubated for 48 hours. For intracellular metabolite extraction, cells were then incubated in 1 mL/well of ice-cold 80% methanol on dry ice for 10 minutes. Following the incubation, the wells were scraped with a pipet tip and transferred to a 1.5 mL tube on dry ice. To analyze extracellular metabolomes, 0.8 mL of ice-cold 100% methanol was added to 0.2 mL of media, mixed well, and incubated on dry ice for 10 minutes. Samples were clarified by centrifugation at 16,000 rpm for 10 minutes at 4°C, and metabolite supernatant was transferred to a fresh 1.5 mL tube. Metabolite levels of fractions were normalized to the protein content of a parallel sample, and all samples were lyophilized via speed vac after clarification by centrifugation. Dried metabolite pellets from cells or media were re-suspended in 50:50 HPLC grade MeOH:H2O mixture for metabolomics analysis.

The data were pre-processed with Agilent MassHunter Workstation Quantitative Analysis Software (B0900). The pre-processed data were then processed further for quality control. Each sample was normalized to the total intensity of all metabolites and

each metabolite abundance level was then normalized to the median of all abundance levels for comparisons, statistical analyses, and visualizations. The statistical significance test was done by a two-tailed t-test with a significance threshold level of 0.05, unless otherwise noted.

Heatmaps were generated and data clustered using Morpheus Matrix Visualization and analysis tool (https://software.broadinstitute.org/morpheus).

Tumor Immunohistochemistry

The University of Michigan Institutional Review Board provided a waiver of informed consent (HUM00067293) to obtain deidentified formalin-fixed, paraffin-embedded tissue blocks. Immunohistochemical staining was performed on the DAKO Autostainer (DAKO, Carpinteria, CA) using DAKO Envision+ and diaminobenzadine (DAB) as the chromogen. De-paraffinized tissue sections were labeled with ASNS (Santa Cruz, sc-365809, mouse monoclonal antibody) at 1:100 dilution for 60 minutes at ambient temperature. Microwave citric acid epitope retrieval was using 10 mM Tris HCl/1 mM EDTA pH9 was performed prior to staining, and FLEX polymer HRP was used for detection. Appropriate negative (no primary antibody) and positive controls were stained in parallel to ascertain antibody specificity.

Proliferation Assays

xCelligence

Real-time cell analysis (RTCA) of cell proliferation was monitored using the xCELLigence DP system (Agilent). Before cell seeding, E-plates were coated with 0.2%

gelatin and equilibrated for 1 hour at 37°C, 5% CO_2 with 100 µL of media per well. 5 × 10^3 (A673), or 3 × 10^3 (A4573) cells were plated per well to a final volume of 200 µL, and the plate was equilibrated for 30 minutes.

Cell Titer Glo 2.0

Cells were seeded in 96-well white wall, white bottom plates (Corning) at 5,000 cells/well (A673), 3,000 cells/well (A4573), and 10,000 cells/well (TC32) in 50 or 100uL of media. The following day, 50uL or 100uL of media containing the treatment was added, and cells were incubated for 72 hours. At endpoint, the plate was equilibrated to room temperature for 30 minutes, and Cell Titer Glo 2.0 reagent (Promega G9243) was added at 20uL per 100uL of media in the plate. Plates were rocked, protected from light, on orbital shaker for 20 minutes, and luminescence was measured for 500ms using a SpectraMax M3 Microplate reader (Molecular Devices).

Clonogenic Assays

Colony formation was assessed by plating stably transduced cells as a single-cell suspension of 3X10^3 cells per well of a 6-well plate in 2mLs of media. Media was replaced every 3 days and cells were fixed and stained after 2-3 weeks in culture. Cells were fixed using a 100% methanol, stained with 0.5% crystal violet, washed with distilled H_2O.

Soft Agar Colony Formation Assay

Colony formation was assessed by plating a single-cell suspension of 1×10^4 cells per well of 6-well plates in 0.35% agarose on a layer of 0.5% agarose. Media was changed

to 0.5mL fresh DMEM with or without 1mM asparagine ever 3 days. Colonies were stained with a solution of 0.005% crystal violet, 10% ethanol ~3 weeks later.

Transwell Migration Assays

A total of $1X10^5$cells (A673) or 0.6 $X10^5$ cells (A4573) were added to 24-well transwell inserts containing 0.8-mm pores (Corning) in 100uL of media. 600uL of appropriate media was added to the well chamber, and migration was assessed for cells migrating through the membrane. For A673 cells, cells were allowed to migrate from serum-complete media in the insert to with serum-free media in the bottom chamber, and for A4573 cells, cells were allowed to migrate from serum-free media in the insert to with serum-complete media in the bottom chamber. For asparagine supplementation studies, cells were cultured for 24 hours in DMEM with or without 1mM asparagine (Sigma Aldrich) in media containing dialyzed FBS (Hyclone), cells were then plated in transwells and incubated for another 24 hours before staining. Cells were fixed using a 100% methanol, membranes were stained with 0.5% crystal violet, and inserts were washed with distilled H_2O.

In vivo Tumor Assays

For subcutaneous tumor assays, 2.5 X 10^5 stably transduced control (shNS) or ASNS knockdown (shASNS) cells were resuspended in PBS, diluted 1:1 in Matrigel, and injected subcutaneously into NOD/SCID mice (strain 005557 from Jackson Laboratory). Each mouse received an injection of either shNS or shASNS on the right flank, and tumor formation and growth was measured by calipers every other day. All mice were euthanized at end point when the tumor of one animal reach 2cm in any direction. For

metastatic assays, 0.5 X 10^6 or 1 X 10^6 fLuc-GFP labeled cells were injected via tail vein. Imaging was carried out weekly with the Xenogen IVIS bioluminescence system (Perkin Elmer), and tumor burden quantified using Living Image software (Perkin Elmer). Mice were monitored until one animal reached the end point described in our IACUC protocol (~4 weeks), at which point all mice were euthanized. Tumor formation and location was confirmed by dissection. For L-asparagine-adjusted diets, mice were given an asparagine deficient diet (0% asparagine- Envigo Cat# TD.160365), or an asparagine-rich diet (4% asparagine- Envigo Cat# TD.160366), and mice were placed on this diet starting one week prior to initiation of the study. All diets were isonitrogenous and contained similar calorie densities

Western Blotting

Cells were detached with trypsin-EDTA (0.05%) (Gibco), washed with PBS (Gibco), and lysed in RIPA buffer (Thermo Fisher) supplemented with protease inhibitor cocktail and phosphatase inhibitor cocktail tablets (Roche). Cleared supernatants were subjected to protein quantification by Pierce BCA assay Protein Assay Kit (Thermo Fisher). Western blot was performed using the Mini Gel Tank (Life Technologies). Proteins were resolved by SDS-PAGE using 4–12% Bis-Tris gels, transferred to 0.45 µM PVDF membranes after methanol activation, and blocked in 5% milk dissolved in 1X TBST for 1 hour at room temperature. Membranes were incubated rotating overnight at 4°C with primary antibody. See Appendix II for list of antibodies and dilutions. Membranes were then washed 4 times for 5 minutes each in 1X TBST and probed with secondary antibody anti-Mouse IgG HRP-linked antibody 1:10,000 (Cell Signaling Technologies), or anti-Rabbit IgG HRP-linked antibody 1:10,000 (Cell Signaling Technologies). Proteins were

detected with Clarity ECL substrate (Bio-Rad), and quantification was performed using Bio-rad Image Lab Software.

Quantitative Real-Time PCR

Total RNA was extracted from cells at the same time as protein collection using RNeasy Mini Kit (Qiagen), and RNA was subjected to reverse transcription using iSCRIPT cDNA Synthesis Kit (Bio-Rad) following the manufacturer's protocol. Quantitative real-time PCR (qRT-PCR) was performed using Fast SYBR-Green Master Mix (Applied Biosystems) for designed primers (Invitrogen). Analysis was performed in triplicate using the QuantStudio Real-Time PCR System, 384-well format (Applied Biosystems) and average Cp values were normalized relative to the geometric mean of two housekeeping genes (18s and EEF1A1) See Appendix II for primer sequences.

Publicly Available Microarray Datasets and ChIP Sequencing

The mRNA expression of *ASNS* in Ewing sarcoma patient tumors was determined using three previously published microarray datasets: GSE63157 [47] GSE34620 [48] and GSE17679 [49]. Expression data for A673 cells treated with Doxorubicin at two doses (EC_{50} and $2xEC_{50}$) at three time points (24 hours, 3 days, and 5 days), available at GSE6930 [19] was used to determine the effect of Doxorubicin on *ASNS* expression. The ChIP-seq datasets we acquired for FLI1 and H3K27Ac are publicly available at NCBI Gene Expression Omnibus (GEO) under the GEO accession: GSE61953 [17].

RNA Sequencing

RNA-sequencing was performed in A673 cells following ASNS knockdown. Libraries were prepared by *Novogene* and sequenced using an Illumina HiSeq 2500 for 50-bp

single-end reads. Adapter trimming of paired-end fastq files was performed using Trim Galore (Babraham Institute). Trimmed reads were then aligned to GRCh38 using STAR aligner [50] with `--quantMode GeneCounts` to count the number of reads per gene while mapping. Differential expression analysis was performed using the default parameters from the DESeq2 package [51].

Statistical Analysis

All data is plotted using Prism (GraphPad) and bar plots represent the mean ± SEM. Prism was used to perform two-tailed, unpaired t-test analysis. $P < 0.05$ was considered statistically significant. For volcano plots of RNA-seq data, differential expression values greater than 2-fold or less than −2-fold and adjusted $P < 0.05$ were considered significant, and cutoffs are indicated on plot. For combination studies, the combination index (CI) was used to determine the degree of drug interaction using CompuSyn software.

References

1. Warburg, O., F. Wind, and E. Negelein, *The Metabolism of Tumors in the Body.* J Gen Physiol, 1927. **8**(6): p. 519-30.
2. Faubert, B., A. Solmonson, and R.J. DeBerardinis, *Metabolic reprogramming and cancer progression.* Science, 2020. **368**(6487).
3. Martinez-Reyes, I. and N.S. Chandel, *Cancer metabolism: looking forward.* Nat Rev Cancer, 2021. **21**(10): p. 669-680.
4. Franzetti, G.A., et al., *Cell-to-cell heterogeneity of EWSR1-FLI1 activity determines proliferation/migration choices in Ewing sarcoma cells.* Oncogene, 2017. **36**(25): p. 3505-3514.
5. Vettore, L., R.L. Westbrook, and D.A. Tennant, *New aspects of amino acid metabolism in cancer.* Br J Cancer, 2020. **122**(2): p. 150-156.
6. Clavell, L.A., et al., *Four-agent induction and intensive asparaginase therapy for treatment of childhood acute lymphoblastic leukemia.* N Engl J Med, 1986. **315**(11): p. 657-63.
7. Jiang, J., et al., *Promoter demethylation of the asparagine synthetase gene is required for ATF4-dependent adaptation to asparagine depletion.* J Biol Chem, 2019. **294**(49): p. 18674-18684.
8. Chiu, M., et al., *Asparagine Synthetase in Cancer: Beyond Acute Lymphoblastic Leukemia.* Front Oncol, 2019. **9**: p. 1480.
9. Krall, A.S., et al., *Asparagine couples mitochondrial respiration to ATF4 activity and tumor growth.* Cell Metab, 2021. **33**(5): p. 1013-1026 e6.
10. Krall, A.S., et al., *Asparagine promotes cancer cell proliferation through use as an amino acid exchange factor.* Nat Commun, 2016. **7**: p. 11457.
11. Thomas, T.M., et al., *Elevated Asparagine Biosynthesis Drives Brain Tumor Stem Cell Metabolic Plasticity and Resistance to Oxidative Stress.* Mol Cancer Res, 2021. **19**(8): p. 1375-1388.
12. Sen, N., et al., *EWS-FLI1 reprograms the metabolism of Ewing sarcoma cells via positive regulation of glutamine import and serine-glycine biosynthesis.* Mol Carcinog, 2018.
13. Tanner, J.M., et al., *EWS/FLI is a Master Regulator of Metabolic Reprogramming in Ewing Sarcoma.* Mol Cancer Res, 2017. **15**(11): p. 1517-1530.
14. Svoboda, L.K., et al., *Menin regulates the serine biosynthetic pathway in Ewing sarcoma.* J Pathol, 2018. **245**(3): p. 324-336.
15. Issaq, S.H., et al., *EWS-FLI1-regulated serine synthesis and exogenous serine are necessary for Ewing sarcoma cellular proliferation and tumor growth.* Mol Cancer Ther, 2020.
16. Jimenez, J.A., et al., *EWS-FLI1 and Menin Converge to Regulate ATF4 Activity in Ewing Sarcoma.* Mol Cancer Res, 2021. **19**(7): p. 1182-1195.
17. Riggi, N., et al., *EWS-FLI1 utilizes divergent chromatin remodeling mechanisms to directly activate or repress enhancer elements in Ewing sarcoma.* Cancer Cell, 2014. **26**(5): p. 668-681.
18. Riggi, N., M.L. Suva, and I. Stamenkovic, *Ewing's Sarcoma.* N Engl J Med, 2021. **384**(2): p. 154-164.

19. Stegmaier, K., et al., *Signature-based small molecule screening identifies cytosine arabinoside as an EWS/FLI modulator in Ewing sarcoma.* PLoS Med, 2007. **4**(4): p. e122.
20. Knott, S.R.V., et al., *Asparagine bioavailability governs metastasis in a model of breast cancer.* Nature, 2018. **554**(7692): p. 378-381.
21. O'Neill, A.F., et al., *Targeted imaging of Ewing sarcoma in preclinical models using a 64Cu-labeled anti-CD99 antibody.* Clin Cancer Res, 2014. **20**(3): p. 678-87.
22. Lin, H.H., et al., *Autophagic reliance promotes metabolic reprogramming in oncogenic KRAS-driven tumorigenesis.* Autophagy, 2018. **14**(9): p. 1481-1498.
23. Du, F., et al., *SOX12 promotes colorectal cancer cell proliferation and metastasis by regulating asparagine synthesis.* Cell Death Dis, 2019. **10**(3): p. 239.
24. Zhang, J., et al., *Asparagine plays a critical role in regulating cellular adaptation to glutamine depletion.* Mol Cell, 2014. **56**(2): p. 205-218.
25. Guadamillas, M.C., A. Cerezo, and M.A. Del Pozo, *Overcoming anoikis--pathways to anchorage-independent growth in cancer.* J Cell Sci, 2011. **124**(Pt 19): p. 3189-97.
26. Apfel, V., et al., *Therapeutic Assessment of Targeting ASNS Combined with l-Asparaginase Treatment in Solid Tumors and Investigation of Resistance Mechanisms.* ACS Pharmacol Transl Sci, 2021. **4**(1): p. 327-337.
27. Pantel, K., C. Alix-Panabieres, and S. Riethdorf, *Cancer micrometastases.* Nat Rev Clin Oncol, 2009. **6**(6): p. 339-51.
28. Balamuth, N.J. and R.B. Womer, *Ewing's sarcoma.* Lancet Oncol, 2010. **11**(2): p. 184-92.
29. Gaspar, N., et al., *Ewing Sarcoma: Current Management and Future Approaches Through Collaboration.* J Clin Oncol, 2015. **33**(27): p. 3036-46.
30. Tomazou, E.M., et al., *Epigenome mapping reveals distinct modes of gene regulation and widespread enhancer reprogramming by the oncogenic fusion protein EWS-FLI1.* Cell Rep, 2015. **10**(7): p. 1082-95.
31. Boulay, G., et al., *Cancer-Specific Retargeting of BAF Complexes by a Prion-like Domain.* Cell, 2017. **171**(1): p. 163-178 e19.
32. Koprivnikar, J., J. McCloskey, and S. Faderl, *Safety, efficacy, and clinical utility of asparaginase in the treatment of adult patients with acute lymphoblastic leukemia.* Onco Targets Ther, 2017. **10**: p. 1413-1422.
33. Pathria, G., et al., *Translational reprogramming marks adaptation to asparagine restriction in cancer.* Nat Cell Biol, 2019. **21**(12): p. 1590-1603.
34. Sullivan, L.B., et al., *Aspartate is an endogenous metabolic limitation for tumour growth.* Nat Cell Biol, 2018. **20**(7): p. 782-788.
35. Garcia-Bermudez, J., et al., *Aspartate is a limiting metabolite for cancer cell proliferation under hypoxia and in tumours.* Nat Cell Biol, 2018. **20**(7): p. 775-781.
36. Lieu, E.L., et al., *Amino acids in cancer.* Exp Mol Med, 2020. **52**(1): p. 15-30.
37. Gutierrez, J.A., et al., *An inhibitor of human asparagine synthetase suppresses proliferation of an L-asparaginase-resistant leukemia cell line.* Chem Biol, 2006. **13**(12): p. 1339-47.

38. Koroniak, L., et al., *Synthesis and characterization of an N-acylsulfonamide inhibitor of human asparagine synthetase.* Org Lett, 2003. **5**(12): p. 2033-6.
39. Hawkins, A.G., et al., *Wnt/beta-catenin-activated Ewing sarcoma cells promote the angiogenic switch.* JCI Insight, 2020. **5**(13).
40. Pedersen, E.A., et al., *Activation of Wnt/beta-Catenin in Ewing Sarcoma Cells Antagonizes EWS/ETS Function and Promotes Phenotypic Transition to More Metastatic Cell States.* Cancer Res, 2016. **76**(17): p. 5040-53.
41. Lin, P.P., Y. Wang, and G. Lozano, *Mesenchymal Stem Cells and the Origin of Ewing's Sarcoma.* Sarcoma, 2011. **2011**.
42. Miller, H.E., et al., *Reconstruction of Ewing Sarcoma Developmental Context from Mass-Scale Transcriptomics Reveals Characteristics of EWSR1-FLI1 Permissibility.* Cancers (Basel), 2020. **12**(4).
43. Bauer, C., et al., *Lack of Electron Acceptors Contributes to Redox Stress and Growth Arrest in Asparagine-Starved Sarcoma Cells.* Cancers (Basel), 2021. **13**(3).
44. Hettmer, S., et al., *Functional genomic screening reveals asparagine dependence as a metabolic vulnerability in sarcoma.* Elife, 2015. **4**.
45. Drapela, S. and A.P. Gomes, *Metabolic requirements of the metastatic cascade.* Curr Opin Syst Biol, 2021. **28**.
46. von Levetzow, C., et al., *Modeling initiation of Ewing sarcoma in human neural crest cells.* PLoS One, 2011. **6**(4): p. e19305.
47. Volchenboum, S.L., et al., *Gene Expression Profiling of Ewing Sarcoma Tumors Reveals the Prognostic Importance of Tumor-Stromal Interactions: A Report from the Children's Oncology Group.* J Pathol Clin Res, 2015. **1**(2): p. 83-94.
48. Postel-Vinay, S., et al., *Common variants near TARDBP and EGR2 are associated with susceptibility to Ewing sarcoma.* Nat Genet, 2012. **44**(3): p. 323-7.
49. Savola, S., et al., *High Expression of Complement Component 5 (C5) at Tumor Site Associates with Superior Survival in Ewing's Sarcoma Family of Tumour Patients.* ISRN Oncol, 2011. **2011**: p. 168712.
50. Dobin, A., et al., *STAR: ultrafast universal RNA-seq aligner.* Bioinformatics, 2013. **29**(1): p. 15-21.
51. Love, M.I., W. Huber, and S. Anders, *Moderated estimation of fold change and dispersion for RNA-seq data with DESeq2.* Genome Biol, 2014. **15**(12): p. 550.

Chapter 4 Functions for PHGDH in Ewing sarcoma

Summary

In Chapter 2, we showed that EWS-FLI1 and the scaffolding protein menin regulate the serine biosynthesis pathway (SSP) via converging regulation of the master transcriptional regulator, ATF4. As a downstream effector of the integrated stress response, ATF4 promotes the transcription of metabolic genes that increase the import and synthesis of amino acids.

Several studies, from our group and others, have focused on the importance of the SSP in Ewing sarcoma, and results have demonstrated that continued high-level expression of PHGDH, the rate-limiting enzyme in the SSP, is critical for Ewing sarcoma proliferation *in vitro* and *in vivo*. The SSP is part of several interconnected metabolic pathways, whose metabolic products play key functions in redox balance, epigenetic maintenance, and nucleotide synthesis, among others. However, the precise output of the SSP that is chiefly responsible for the dependence of Ewing sarcoma cells on the pathway is not yet known. In the current study, we employed unbiased transcriptomic analysis of PHGDH-inhibited cells, as well as single amino acid add back experiments with SSP-generated metabolites (αKG, GSH, nucleosides) to begin to gain insight into Ewing sarcoma-specific vulnerabilities regulated by flux through the SSP. Our preliminary findings suggest that neither αKG nor antioxidant homeostasis though GSH synthesis dictate the proliferative defect in Ewing sarcoma cells upon PHGDH inhibition. Further, our RNA-seq analysis demonstrated that NCT-503 and PHGDH knockdown

largely impact the transcriptome though independent mechanism but showed a common overlap in the antagonism of an EWS-FLI1-regulated gene expression program. Further studies will focus on the molecular mechanism by which PHGDH inhibition may impact EWS-FLI1 stability and/or function, as well as systematically address the effects of genetic and pharmacologic inhibition of PHGDH on the metabolome.

Introduction

Metabolic pathways are central for the generation of metabolites and macromolecules that support proliferation, such as nucleotides, antioxidants, amino acids, and proteins, and flux through these pathways is altered with oncogenic stress as well as changes in the tumor microenvironment [1]. Importantly, models of breast cancer, melanoma, and most recently now in Ewing sarcoma have shown that the ability of solid cancers to grow and metastasize may depend on metabolic changes that allow cells to resist amino acid deficiency and oxidative stress [2-4]. Several studies have particularly investigated the importance of the *de novo* serine biosynthesis pathway (SSP) as a biomarker and tumorigenic driver in Ewing sarcoma [5-8]. Expression of PHGDH, the rate-limiting enzyme in the SSP, as well as other SSP enzymes is high in Ewing sarcoma, and predicts poor survival in patients [5, 6]. Furthermore, *in vitro* and *in vivo* models have shown that Ewing sarcomas are critically sensitive to genetic loss and small-molecule inhibition of PHGDH activity [5-8].

As a major metabolic hub, the SSP diverts the glycolytic intermediate 3-phosphogycerate (3PG) to contribute to the *de novo* synthesis of serine via three

enzymatic steps requiring the enzymes, PHGDH, PSAT1, and PSPH [9]. Additionally, direction of 1 carbon units into the folate and methionine cycles leads to the generation of metabolites such as glutathione (GSH), important for redox balance, and S-Adenosyl Methionine (SAM) and alpha-ketoglutarate (αKG), both important for histone and DNA methylation homeostasis [9]. In other cancer contexts, such as in melanoma and breast cancer, hyperactivation of the SSP is attributed to amplification of the *PHGDH* locus [10, 11]. In contrast, in non-small cell lung cancer and other solid tumors that lack *PHGDH* amplification, activation of the SSP is under the control of activating transcription factor 4 (ATF4), a master transcriptional regulator of amino acid metabolism and stress responses [12-18]. Amplifications in *PHGDH* are not observed in Ewing sarcoma, and as detailed in Chapter 2 of this dissertation research, the EWS-FLI1 fusion protein regulates the SSP via direct transcriptional regulation of *ATF4* by EWS-FLI1 and through a menin-ATF4 containing axis [19]. While it is known that PHGDH expression is high in Ewing sarcoma, and that Ewing sarcomas depend on both an exogenous and *de novo* serine supply for *in vivo* tumor growth, the precise metabolic output of the SSP or fate of serine that is responsible for the critical dependence on serine metabolism is still unclear.

In the current study, we sought to begin to systematically evaluate metabolic outputs downstream of PHGDH and their contribution to Ewing sarcoma cell survival. Through early exploratory add back experiments, we show that neither nucleoside addition nor supplementation with αKG are able to rescue the growth inhibition induced by the pharmacologic PHGDH inhibitor, NCT-503. Additionally, preliminary findings suggest that GSH metabolism may also not be the key output of *de novo* serine

biosynthesis. While early data indicates that co-treatment with SAM and NCT-503 may partially rescue growth inhibition, this in combination with previous data from our lab showing little effect on histone methylation with SSP pathway inhibition indicate that the SSP-dependent mechanisms regulating Ewing sarcoma growth and survival are quite complex. Our unbiased approach using RNA-sequencing to assess the effect of both pharmacologic and genetic inhibition of the SSP on the transcriptome revealed that downstream transcriptional targets of PHGDH are inversely related with EWS-FLI1-regulated targets. These data suggest a novel mechanism by which PHGDH may contribute to the regulation of EWS-FLI1 fusion protein levels and/or activity. Further work in this study will elucidate the precise molecular mechanisms linking flux through the SSP to EWS-FLI1 biology, possibility revealing novel targets that could be exploited therapeutically.

Results

Rescuing PHGDH loss of function with SSP metabolites

In order to begin to address which metabolic output of the serine biosynthesis pathway (SSP) (**Figure 4-1A**) may be most important for maintaining Ewing sarcoma cell viability, we took advantage of the small molecule inhibitor, NCT-503, which non-competitively inhibits PHGDH, the rate-limiting enzyme in the SSP [20]. NCT-503 has been shown to inhibit Ewing sarcoma cell proliferation in a dose-dependent manner *in vitro*, and to modestly, but significantly reduce tumor growth in *in vivo* subcutaneous tumor models as a single agent [6, 8, 21]. Studies have suggested that, in Ewing sarcoma, PHGDH is implicated in the generation of the oncometabolite 2-

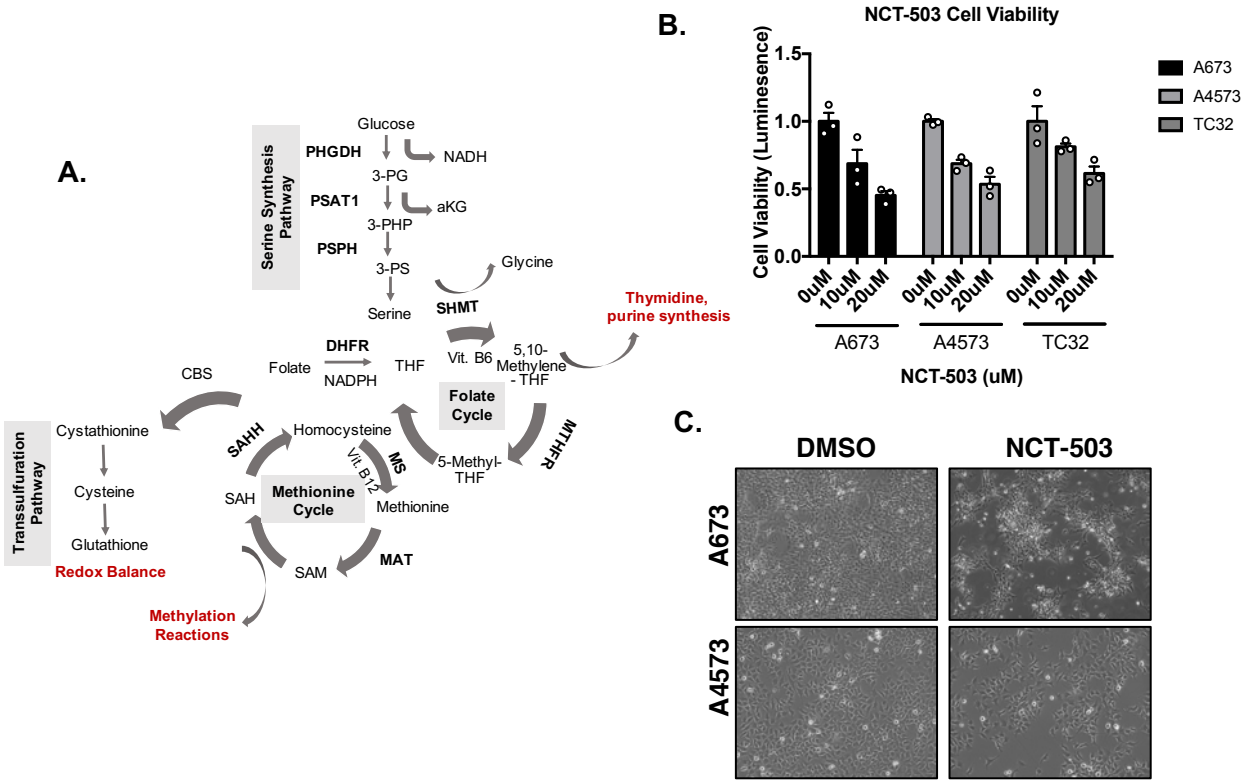

Figure 4-1 NCT-503 treatment inhibits cell growth in Ewing sarcoma

A. Cell viability after 72 hours of treatment with 10 or 20μM NCT-503 in three Ewing sarcoma cell lines (N=3). B. Diagram depicting the serine biosynthesis pathway (SSP) and its network with the folate and methionine cycles. Enzymes are denoted in bold. C. Brightfield images of A673 and A4573 cells treated with 20μM NCT-503 for 72 hours.

hydoxyglutarate and the regulation of histone methylation [6, 22]. Other work suggests that inhibition of serine biosynthesis leads to redox stress and DNA damage via decreases in NADPH and GSH [5]. However, this work has not been able to demonstrate a full or even partial rescue of cell viability with any SSP-derived metabolic product. We first determined that treatment with 10 and 20μM NCT-503 led to 30 and 50% reduction in cell viability, respectively, in line with previous findings (**Figure 4-1B**) [8]. After 72 hours of treatment, we observed significantly halted cell proliferation (**Figure 4-1C).** Next, we asked whether addition of alpha-ketoglutarate (αKG) may rescue the growth inhibitory effects of NCT-503. αKG is an anaplerotic intermediate of

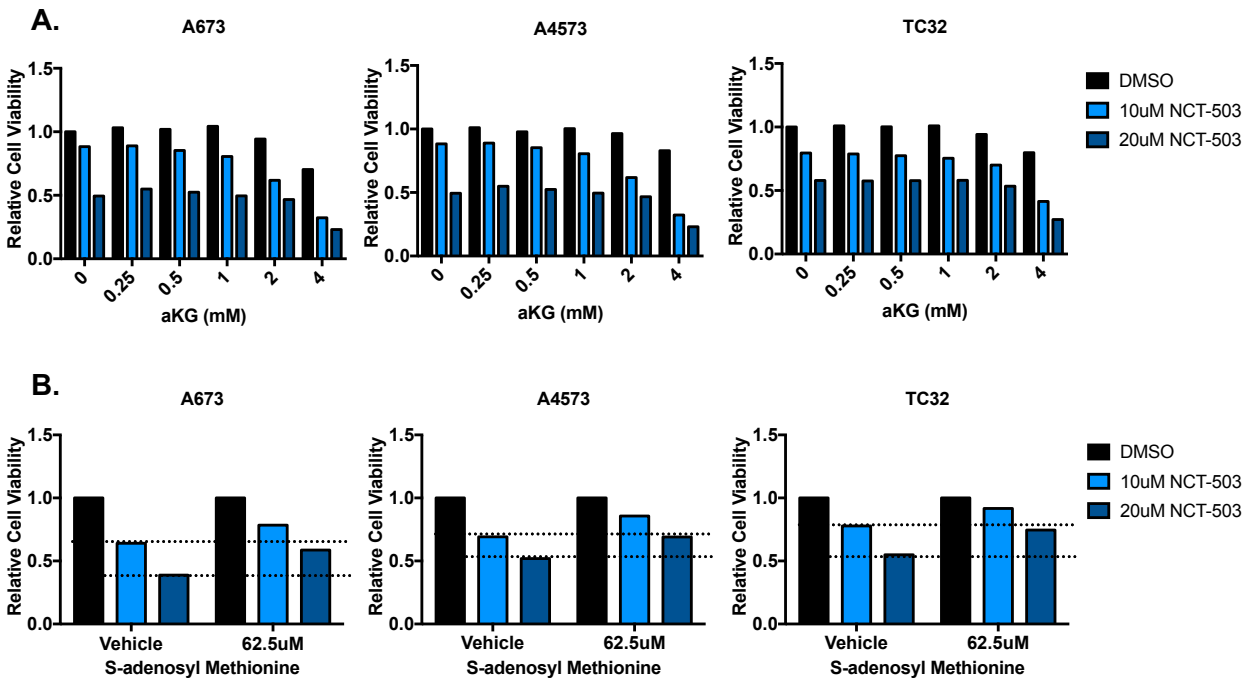

Figure 4-2 S-Adenosyl Methionine but not aKG supplementation may partially rescue the effects of NCT-503

A. Cell viability after 72 hours of co-treatment with 10 or 20μM NCT-503 and cell-permeable a-ketoglutarate (N=1). B. Cell viability after 72 hours of co-treatment with 10 or 20μM NCT-503 and S-Adenosyl Methionine (N=1).

the transamination of glutamate to 3-phosphohydroxypyruvate (3-PHP) by PSAT1 (**Figure 4-1A**), which fuels about 50% of the tricarboxylic acid (TCA) cycle and regulates histone methylation [11]. Prior studies have demonstrated that silencing of both EWS-FLI1 and PHGDH leads to decreased levels of αKG [5]. In our hands, treatment with up to 4mM αKG did not show any rescue of cell viability after 72 hours of co-treatment with NCT-503. (**Figure 4-2A**), suggesting that inhibition of αKG-regulated pathways may not be the predominant mediator of Ewing sarcoma cell viability promoted by PHGDH enzymatic function.

Aside from the generation of serine itself, serine functions as the primary carbon donor for the methionine and mitochondrial folate cycles downstream and provides one-carbon units to generate methionine from homocysteine, and further produce S-

Adenosyl Methionine (SAM) from methionine (**Figure 4-1A**) [9, 23]. SAM acts as a methyl donor for histone and DNA methylation reactions. Given our result that αKG alone was not able to rescue the growth inhibitory effects of NCT-503, we next sought to determine whether treatment with SAM may rescue PHGDH inhibition. We similarly treated cells with 10 and 20μM NCT-503 in media supplemented with 0-500μM SAM and showed that, at doses of SAM that did not impact cell viability, co-treatment with NCT-503 and SAM led to a partial yet subtle rescue of cell viability (**Figure 4-2B**). Although very preliminary, this may suggest that maintenance of methylation via methyl groups provided from SAM may at least in part explain the dependency of Ewing sarcoma cells on continued flux through the SSP. In contrast, however, work from our group using ModSpec mass spectrometry analysis to look at more than 80 different histone modifications showed no reproducible changes in histone modifications (mono- di- and tir- methylation, and acetylation) with genetic PHGDH knockdown (Data not shown), indicating that loss of the enzyme itself does not significantly impact the histone methylation landscape.

NCT-503 treatment rescues erastin-induced ferroptotic growth inhibition

Recent work has convincingly demonstrated that the maintenance of cysteine and GSH pools is critical for redox homeostasis and Ewing sarcoma cell survival both *in vitro* and *in vivo* [4]. Particularly, the generation of antioxidants is important for surviving anoikis, or detachment induced cell death associated with the metastatic cascade [4]. Given the prior work clearly demonstrating significant reductions in GSH levels with PHGDH loss of function, we quite logically reasoned that maintaining GSH levels may

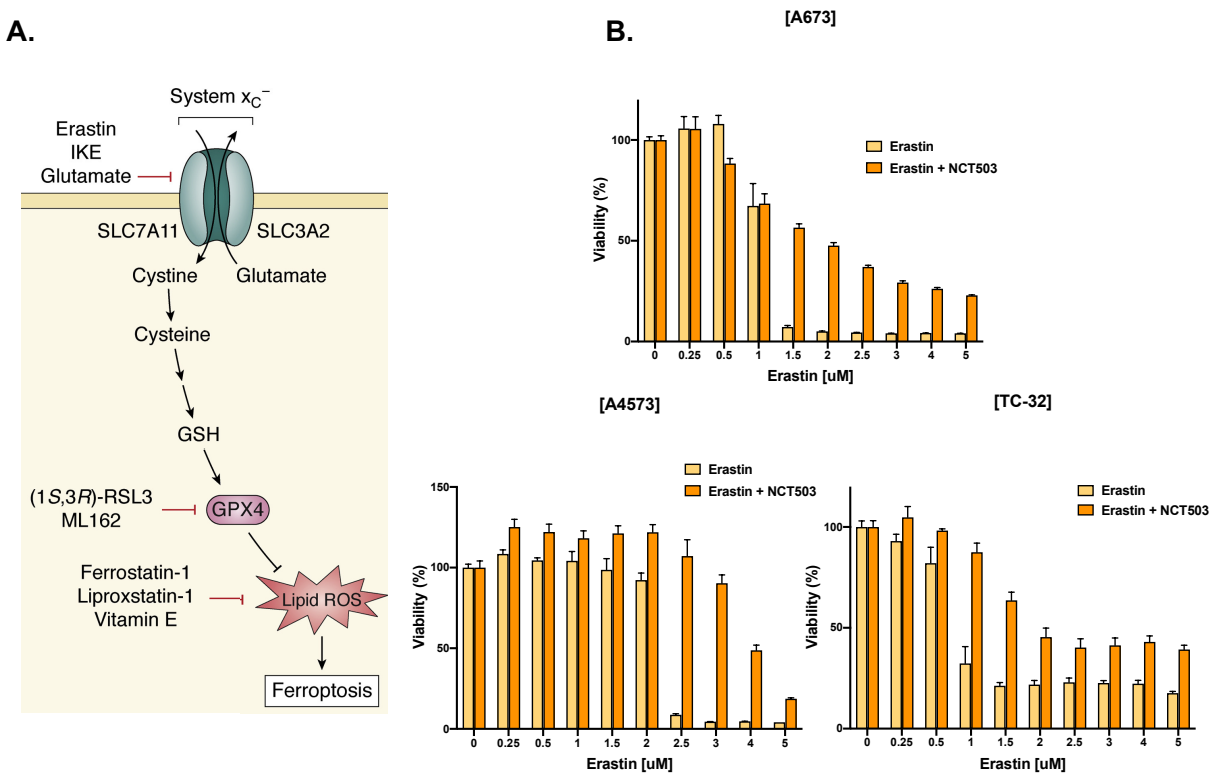

Figure 4-3 Pharmacological inhibition of PHGDH with NCT-503 rescues erastin-induced ferroptosis

A. Diagram depicting system xc- anti-porter and the fate of imported cystine in protecting against ferroptosis. B. Cell viability after 72 hours of co-treatment with 10μM NCT-503 and 0-5μM erastin. Error bars are from technical replicates (N=1). Data were generated by Mohammed Ahmed, PhD. A is taken from Mbah and Lyssiotis, 2022. Creative Commons Attribution License: CC BY 4.0

be central to the function of the SSP in Ewing sarcoma [5]. GSH depletion results in the buildup of reactive oxygen species (ROS); as well as oxidized membrane phospholipids, termed lipid ROS; and ferroptosis, an iron-dependent form of cell death [24]. GSH generation can come from the *de novo* synthesis of glycine as a product of the SSP, or from cysteine, which cells can acquire from import via system x_C- or through its synthesis in the transsulfuration pathway (**Figure 4-3A**) [24]. We thus hypothesized that treatment with erastin, a system x_C- inhibitor and ferroptosis-inducer (**Figure 4-3A**), would lead to synergistic effects when combined with NCT-503 and promote enhanced

cell death. To our surprise, co-treatment of cells with increasing concentrations of erastin and 10μM NCT-503 led to a partial rescue of cell viability (**Figure 4-3B**). Therefore, and in contrast to previous work, this suggests that NCT-503 does not push cells to have increased oxidative stress that can sensitize cells to ferroptosis inducers.

Rescuing growth inhibition from PHGDH loss of function with nucleosides

As previously mentioned, serine is the primary carbon donor for the mitochondrial folate cycle, by donating its side chain carbon to folate and thus generating glycine and methylene tetrahydrofolate (mTHF). The synthesis of folate and glycine pools as byproducts of the SSP promotes the generation of purines and thus contribute to nucleotide synthesis (**Figure 4-1A**). Folate cannot cross the mitochondrial membrane without cleavage to formate, and formate contains a single carbon atom that reacts directly with tetrahydrofolate (THF), generating formyl-THF that acts as a one-carbon donor for purine synthesis. Glycine gets incorporated into the purine backbone [25]. Work in several cancer cell line models has shown that nucleotides or nucleosides alone can rescue the growth inhibitory effects of PHGDH inhibition [20, 26], while other studies have shown that formate and glycine are able to rescue PHGDH loss of function [27, 28]. To examine whether nucleosides are able to rescue growth in the context of PHGDH inhibition in Ewing sarcoma, we treated cells with 10μM NCT-503 in media supplemented with or without nucleosides and assessed growth in real time for 4 days. Our results demonstrated that addition of nucleosides did not improve the growth of NCT-503-treated cells (**Figure 4-4A**). Next, we took a genetic approach to knock down PHGDH expression using lentiviral shRNA transduction (**Figure 4-4B**), which also leads

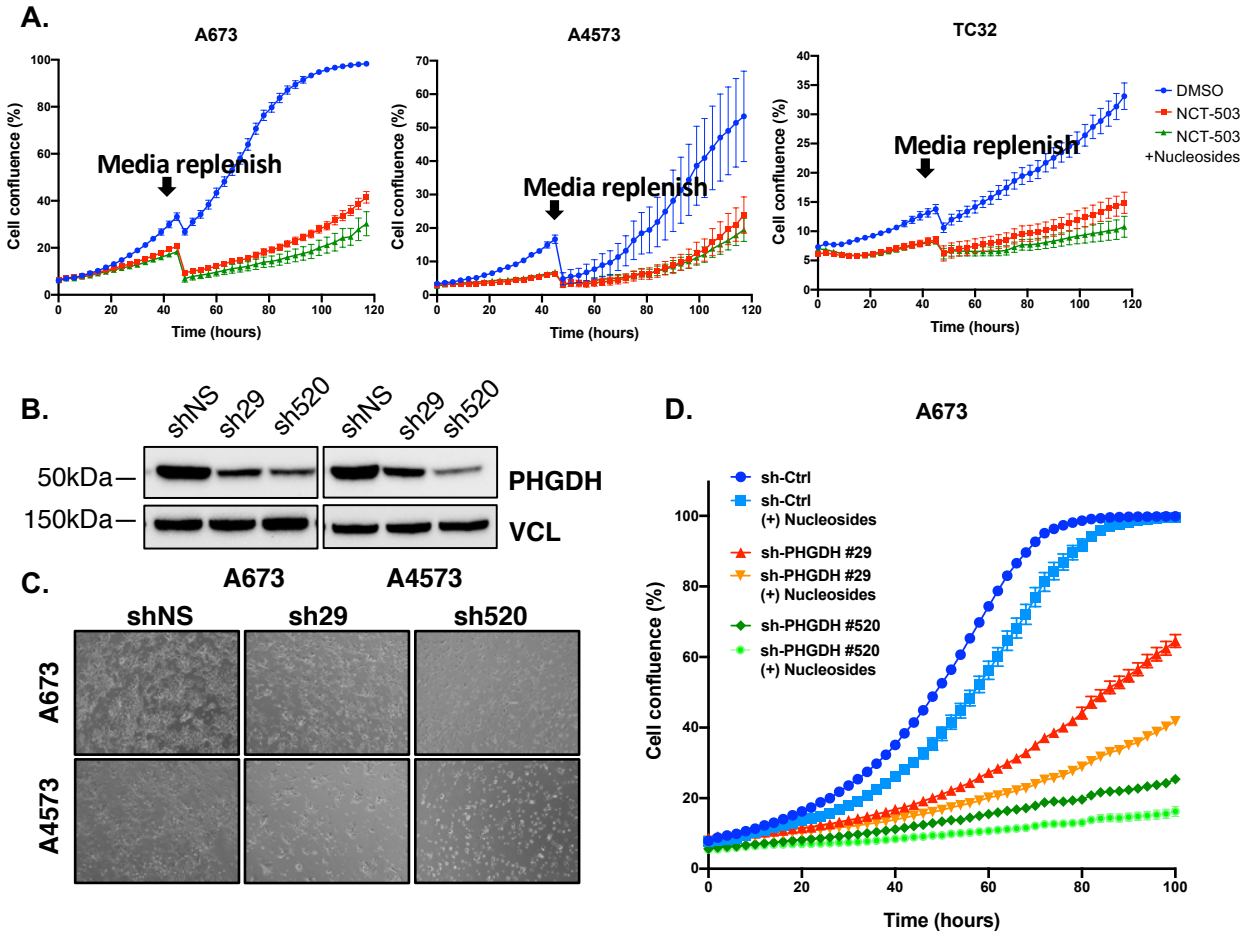

Figure 4-4 Nucleosides do not rescue growth inhibition from genetic or pharmacologic inhibition of PHGDH

A. Incucyte Live Cell Analysis of cell proliferation with 10μM NCT-503 treatment +/- 50uL/mL nucleoside supplementation in the media (N=1). B. Representative western blot for PHGDH protein 96 hours after lentiviral transduction with shNS or shPHGDH (sh29, sh520) (N=3). C. Brightfield images of A673 and A4573 cells after 7d of shPHGDH knockdown (sh29, sh520) compared to shNS control. D. IncuCyte cell proliferation analysis of shPHGDH or control cells +/- 50uL/mL nucleoside supplementation (N=1). Data in A and the right panel of B were generated by Mohamed Ahmed, PhD.

to dramatically reduced cell growth (**Figure 4-4C-D**). Similar to our finding with NCT-503, nucleotide supplementation was not able to rescue the growth of cells with genetic knockdown of PHGDH (**Figure 4-4D**).

RNA-sequencing of NCT-503 treatment and shPHGDH knockdown

The substantial dependence of Ewing sarcoma cells on PHGDH expression and lack of significant rescue of proliferation by systematic add back studies led us to take an unbiased approach at evaluating gene programs and pathways affected by PHGDH inhibition. To our knowledge there is one study that has performed RNA-seq on PHGDH knockdown endothelial cells [29], and one additional study that used a NanoString Metabolism Gene panel to determine the effect of NCT-503 treatment in osteosarcoma cells [30], therefore, the global effects of PHGDH inhibition on the transcriptome in PHGDH-dependent cancer cells has largely been unexplored. To address this open area, we treated A673 and A4573 Ewing sarcoma cells with 20μM (IC_{50}) concentration of NCT-503 for 72 hours (**Figure 4-5A**) and extracted RNA from these cells for RNA-sequencing. In parallel, we performed RNA-sequencing on A673 and A4573 with PHGDH knockdown using two short hairpins targeting PHGDH (sh29, sh520) and one non-targeting control sequence (shNS), at 96 hours post-transduction (**Figure 4-5A**). Volcano plot depiction of transcriptomic changes with shPHGDH knockdown showed more significantly upregulated transcripts than significantly downregulated with fold changes greater than 2. In contrast, for NCT-503 treatment, comparison of significantly up and downregulated genes was about the same, with 176 transcripts significantly upregulated more than 2-fold, and 190 transcripts significantly downregulated more than 2-fold.

While we and others have published that there is heterogeneity between Ewing sarcoma cell lines in their response to serine and glycine withdrawal [5, 7, 8] both pharmacologic and genetic inhibition of PHGDH leads to dramatically reduced cell viability. This supports that additional metabolic precursors provided from flux through

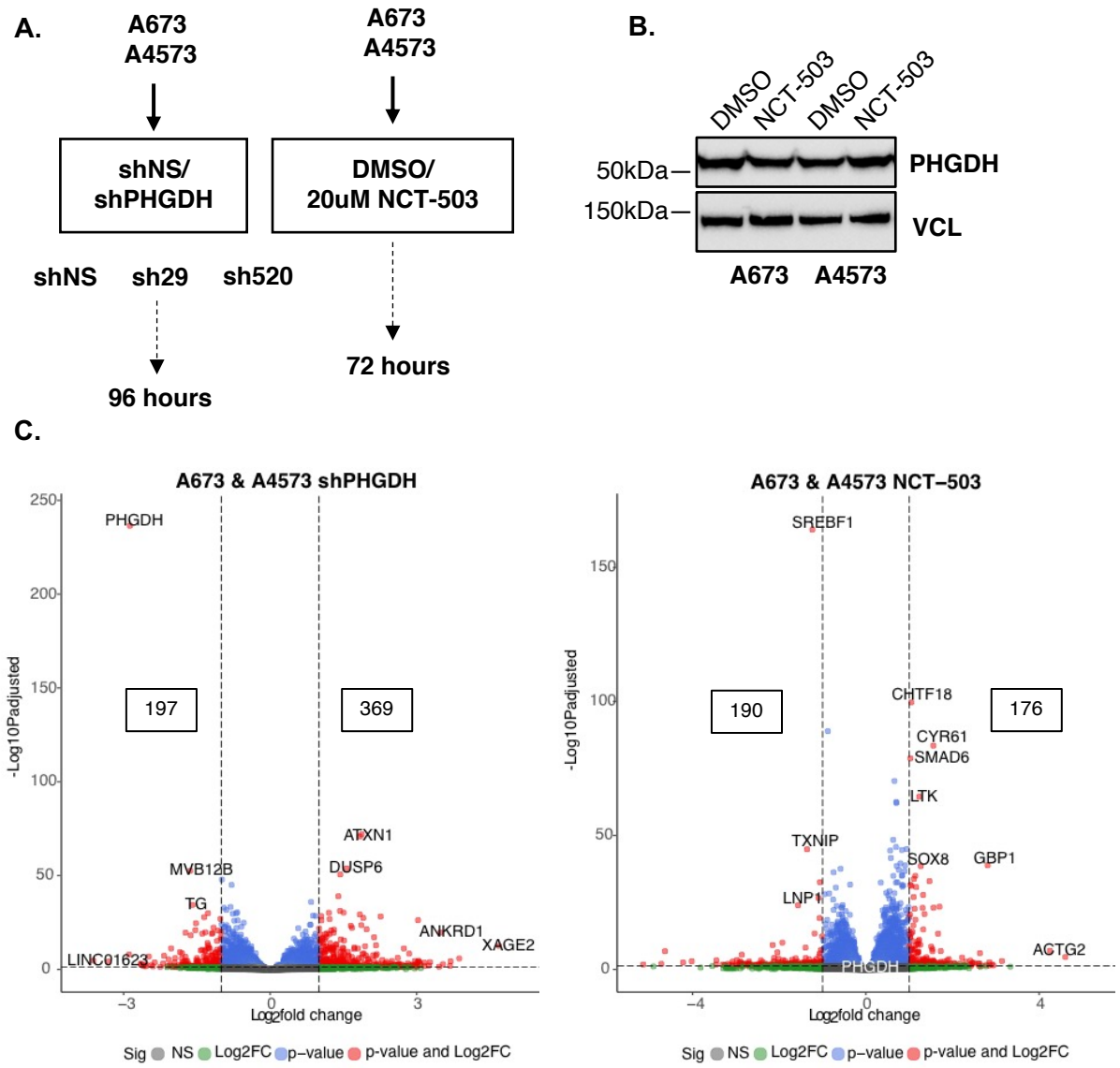

Figure 4-5 RNA-seq of genetic and Pharmacologic PHGDH inhibition

A. Schematic for RNA-seq sample treatments, A673 and A4573 cells were treated with 20μM NCT-503 or DMSO or lentivirally transduced with shNS or shPHGDH (sh29, sh520) vectors and collected after 72 and 96 hours, respectively (N=3). B Representative western blot for PHGDH protein after 72 hours of treatment with 20μM NCT-503 (N=3) C. Volcano plot depicting shared transcriptional changes in A673 and A4573 cells comparing sh29 and sh520 versus shNS (left) and NCT-503 treatment vs DMSO control (N=3).

de novo serine biosynthesis may provide a survival advantage over the import of serine and glycine alone. To evaluate potential pathways that are common to the effects of NCT-503 and PHGDH knockdown, we performed pathway enrichment analysis using

the Molecular Signatures (MSig) Database on the overlap in downregulated and

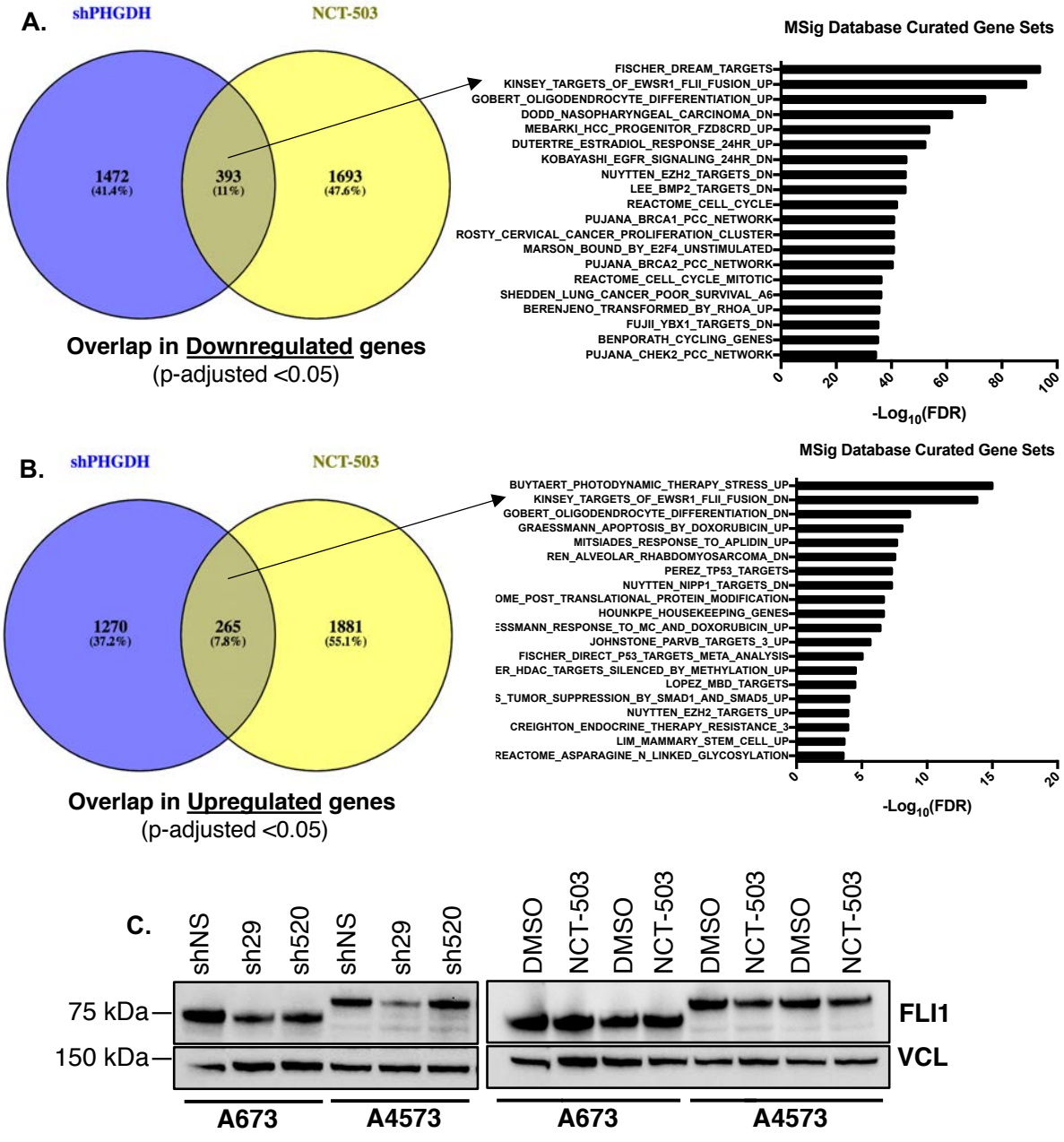

Figure 4-6 Transcriptional targets of PHGDH show inverse relationship with EWS-FLI1 targets

A. Overlap in significantly upregulated transcripts (p-adjusted <0.05) between shPHGDH and NCT-503 treatment conditions (Left) Molecular Signatures (MSig) Database overrepresentation analysis of enriched gene sets in downregulated genes. B. Overlap in significantly downregulated transcripts (p-adjusted<0.05) between shPHGDH and NCT-503 (Left) MSig Database overrepresentation analysis of enriched gene set containing upregulated genes.

upregulated transcripts with shPHGDH and NCT-503. 393 transcripts were significantly (p-adjusted <0.05) downregulated in both shPHGDH and NCT-503 conditions, while 265 genes were significantly upregulated and shared between shPHGDH and NCT-503. To interrogate which pathways may be represented in these shared genes, we examined the MSig Database for top curated gene sets for both conditions. Quite interestingly, overrepresentation analysis identified “Targets of EWS-FLI1 Up”, those genes upregulated by EWS-FLI1, among transcripts that were repressed by PHGDH inhibition (**Figure 4-6A**), and “Targets of EWS-FLI1 Down,” those genes downregulated by EWS-FLI1, among transcripts that were upregulated with PHGDH inhibition (**Figure**

KINSEY_TARGETS_OF_EWSR1_FLII_FUSION_UP [1290]		
AURKA	HELLS	JOSD1
BUB1	SMC2	RAB28
RRM2	TTF2	GLE1
MCM10	CDCA2	OXCT1
MCM2	MSH6	GOT1
CDC45	NUCKS1	GON7
MCM7	BLM	DNAAF5
ATAD2	GTSE1	ANKH
TPX2	PLK1	PLS1
LMNB1	MCM5	NANP
PRIM1	ASF1B	GDAP1
KIF4A	ESPL1	PPP5C
CDC6	WDR76	WWOX
GINS1	DDIAS	TAFA5
MELK	CDCA8	MACROH2A2
NCAPG	SPC25	XRN2
KIF11	C1orf112	FRMD5
MKI67	E2F2	ZNF232
DNA2	DNMT1	NUDT12
CDCA7	E2F7	ZNF850
UHRF1	ZWINT	**SCNN1G**
MCM8	CHAF1A	STEAP1
KNL1	KIF14	RBM12
DEPDC1B	NUP155	PRPS2
PRR11	BRIP1	SDHAF3
SMC4	MPHOSPH9	OMA1
CCNB1	PAICS	PPP2R1B
ECT2	RMI2	LARP4
CCNF	NEIL3	KRR1
OIP5	NUP205	NUDT5
CDC25C	ORC2	VKORC1L1
NUF2	NUP160	FH
NSD2	C18orf54	HADH
LIN9	RHNO1	FAR1
KIF20B	PKP4	PPIF
SGO2	C19orf48	HMGN5
KIF18A	TFDP1	ISOC1
MCM4	C9orf40	OSBPL3
NCAPH	STIP1	UCK2
RACGAP1	SSRP1	ORC5
MCM6	USP39	TUBGCP4
MCM3	PLSCR1	METTL8
TIMM21	TRMT61B	

KINSEY_TARGETS_OF_EWSR1_FLII_FUSION_DN [336]
HDAC5
UBE2H
DOK4
GOLGA2
RHOB
AP5Z1
TSPYL2
CCS
KLF2
ORAI2
IER5L
NLRP1
CST3
INAFM2
FSTL1
MXRA8
MVP
MMP24OS
ZNF423
IGDCC4
RBMS3
FRMD6
VGLL4
ATOH8

Table 4-1 List of KINSEY Targets of EWS-FLI1 Fusion Up and EWS-FLI1 Fusion Down Significantly Changed with PHGDH Inhibition

List of genes within the KINSEY Targets of EWSR1 FLI1 Fusion Up (Left) or EWSR1 Fusion Down (Right) that were significantly (pAdjusted <0.05) downregulated (Left) or upregulated (Right) and shared between shPHGDH and NCT-503.

4-6B). Analysis of genes within the Kinsey EWS-FLI1 Up and Down gene sets revealed many more EWS-FLI1 upregulated genes downregulated with PHGDH inhibition (128) than EWS-FLI1-inhibited genes that were upregulated with PHGDH inhibition (24) (**Table 4-1**). This suggests that PHGDH inhibition, both genetic and pharmacologic, may lead to partial inhibition of an EWS-FLI1-regulated gene expression program. We therefore questioned whether inhibition of PHGDH may affect EWS-FLI1 protein levels. However, western blot analysis showed variable effects on EWS-FLI1 levels with both

Gene Set Name	# Genes in Gene Set (K)	# Genes in Overlap (k)	k/K	p-value	FDR q-value
REACTOME_CELL_CYCLE	691	66	0.0955	2.14E-45	6.38E-42
REACTOME_CELL_CYCLE_MITOTIC	559	56	0.1002	1.30E-39	1.93E-36
REACTOME_CELL_CYCLE_CHECKPOINTS	292	38	0.1301	2.50E-31	2.48E-28
REACTOME_G2_M_CHECKPOINTS	168	23	0.1369	6.40E-20	4.77E-17
REACTOME_M_PHASE	415	32	0.0771	1.63E-19	9.73E-17
WP_CELL_CYCLE	122	20	0.1639	4.35E-19	2.16E-16
KEGG_CELL_CYCLE	125	20	0.16	7.19E-19	3.06E-16
REACTOME_MITOTIC_G1_PHASE_AND_G1_S_TRANSITION	149	21	0.1409	1.44E-18	5.38E-16
REACTOME_ACTIVATION_OF_THE_PRE_REPLICATIVE_COMPLEX	33	13	0.3939	2.21E-18	7.31E-16
REACTOME_ACTIVATION_OF_ATR_IN_RESPONSE_TO_REPLICATION_STRESS	37	13	0.3514	1.32E-17	3.95E-15

Gene Set Name	# Genes in Gene Set (K)	# Genes in Overlap (k)	k/K	p-value	FDR q-value
HALLMARK_E2F_TARGETS	200	35	0.175	1.52E-33	7.58E-32
HALLMARK_G2M_CHECKPOINT	200	34	0.17	3.62E-32	9.04E-31
HALLMARK_MITOTIC_SPINDLE	199	20	0.1005	7.67E-15	1.28E-13
HALLMARK_MTORC1_SIGNALING	200	16	0.08	1.23E-10	1.23E-09
HALLMARK_MYC_TARGETS_V1	200	16	0.08	1.23E-10	1.23E-09
HALLMARK_OXIDATIVE_PHOSPHORYLATION	200	12	0.06	6.02E-07	5.01E-06
HALLMARK_BILE_ACID_METABOLISM	112	7	0.0625	1.06E-04	7.58E-04
HALLMARK_MYC_TARGETS_V2	58	5	0.0862	2.35E-04	1.47E-03
HALLMARK_SPERMATOGENESIS	135	7	0.0519	3.36E-04	1.87E-03
HALLMARK_FATTY_ACID_METABOLISM	158	7	0.0443	8.59E-04	4.29E-03

Table 4-2 MSig Database gene set enrichment analysis for significantly downregulated genes with PHGDH inhibition.

Top overlapping gene sets for 393 significantly (P-adjusted <0.05) downregulated genes from RNA-Seq shared by both shPHGDH conditions and NCT-503 treatment in both A673 and A4573 cells.

NCT-503 and shRNA knockdown of PHGDH (**Figure 4-6C**), perhaps indicating more indirect regulatory mechanisms.

Aside from a clearly enriched EWS-FLI1 signature, MSig database analysis of Canonical Pathways identified a somewhat unsurprising overrepresentation of cell cycle genes sets for the commonly downregulated genes in NCT-503 and shPHGDH conditions, suggesting that both treatments lead to a general inhibition of cell proliferation (**Table 4-2**). However, further analysis of Hallmark Gene sets identified

Gene Set Name	# Genes in Gene Set (K)	# Genes in Overlap (k)	k/K	p-value	FDR q-value
REACTOME_POST_TRANSLATIONAL_PROTEIN_MODIFICATION	1434	33	0.023	3.08E-10	9.17E-07
REACTOME_ASPARAGINE_N_LINKED_GLYCOSYLATION	305	12	0.0393	8.24E-07	1.23E-03
REACTOME_RETROGRADE_TRANSPORT_AT_THE_TRANS_GOLGI_NETWORK	49	5	0.102	1.62E-05	1.27E-02
REACTOME_MEMBRANE_TRAFFICKING	629	15	0.0238	1.71E-05	1.27E-02
REACTOME_NERVOUS_SYSTEM_DEVELOPMENT	580	14	0.0241	2.86E-05	1.71E-02
WP_TGFBETA_RECEPTOR_SIGNALING	58	5	0.0862	3.72E-05	1.85E-02
WP_TGFBETA_RECEPTOR_SIGNALING_IN_SKELETAL_DYSPLASIAS	62	5	0.0806	5.14E-05	2.07E-02
REACTOME_SYNTHESIS_OF_SUBSTRATES_IN_N_GLYCAN_BIOSYTHESIS	63	5	0.0794	5.56E-05	2.07E-02
REACTOME_VESICLE_MEDIATED_TRANSPORT	724	15	0.0207	8.39E-05	2.61E-02
REACTOME_TP53_REGULATES_TRANSCRIPTION_OF_GENES_INVOLVED_IN_G1_CELL_CYCLE_ARREST	14	3	0.2143	9.15E-05	2.61E-02

Gene Set Name	# Genes in Gene Set (K)	# Genes in Overlap (k)	k/K	p-value	FDR q-value
HALLMARK_P53_PATHWAY	200	8	0.04	5.10E-05	2.55E-03
HALLMARK_PROTEIN_SECRETION	96	5	0.0521	4.07E-04	6.50E-03
HALLMARK_TGF_BETA_SIGNALING	54	4	0.0741	4.15E-04	6.50E-03
HALLMARK_PEROXISOME	104	5	0.0481	5.87E-04	6.50E-03
HALLMARK_APOPTOSIS	161	6	0.0373	6.50E-04	6.50E-03
HALLMARK_EPITHELIAL_MESENCHYMAL_TRANSITION	200	6	0.03	1.98E-03	1.10E-02
HALLMARK_HEME_METABOLISM	200	6	0.03	1.98E-03	1.10E-02
HALLMARK_MYOGENESIS	200	6	0.03	1.98E-03	1.10E-02
HALLMARK_TNFA_SIGNALING_VIA_NFKB	200	6	0.03	1.98E-03	1.10E-02
HALLMARK_UV_RESPONSE_UP	158	5	0.0316	3.71E-03	1.86E-02

Table 4-3 MSig Database gene set enrichment analysis for significantly upregulated genes with PHGDH inhibition.

Top overlapping gene sets for 265 significantly (P-adjusted <0.05) upregulated genes from RNA-Seq shared by both shPHGDH conditions and NCT-503 treatment in both A673 and A4573 cells.

enrichment for mTORC1, Fatty Acid, and Oxidative Phosphorylation pathways, signifying possible metabolic impact of inhibiting SSP flux (**Table 4-2**). On the other hand, pathways upregulated with PHGDH inhibition revealed gene sets for post-translational protein modification, protein secretion, TGF-β signaling, and epithelial to mesenchymal transition (**Table 4-3**). In summary, our transcriptomic analysis revealed novel metabolic and non-metabolic pathways that may help explain Ewing sarcoma susceptibility to PHGDH inhibition.

Discussion

Several studies, from our group and others, have focused on the importance of the serine biosynthesis pathway (SSP) in Ewing sarcoma, and results have demonstrated that high expression of PHGDH, the rate-limiting enzyme in the SSP, as well as other key enzymes in the pathway, predicts poor patient outcome. PHGDH is critical for maintaining Ewing sarcoma cell proliferation both *in vitro* and *in vivo,* but the precise output of the SSP, which lies at the core of a major interconnected metabolic hub, that could explain the dependency of Ewing sarcoma cells on the pathway has not yet been fully elucidated [5-8]. Further, it is clear from other studies that have failed to rescue PHGDH loss with extracellular serine, that the *de novo* synthesis of serine functions distinctly from simply importing extracellular serine [11]. Additionally, recent studies have also described non-canonical functions for PHGDH, independent of its enzymatic role in the SSP, further expanding its potential role in sustaining oncogenic cell growth [31] .

Our previously published work using LC/MS-based metabolomics demonstrated that flux through the SSP is high in Ewing sarcoma and regulated, in part, by menin [7]. Further, work by other groups has implicated roles for serine metabolism in protecting against redox stress, as well as altering the histone methylation landscape in Ewing sarcoma [5, 6]. However, our data has not led us to conclusively demonstrate that any one SSP-regulated metabolic output can explain the very acute dependence of Ewing sarcomas on high level maintenance of PHGDH protein and enzymatic activity. This is not surprising given prior work showing variable results upon single metabolite add backs to rescue PHGDH inhibition. Previous findings have demonstrated that NCT-503 treatment leads to G1/S cell cycle arrest and that only nucleosides or nucleoside precursor supplementation, such as formate and glycine, lead to a partial rescue of cell viability [20, 26-28]. Further, treatment with NCT-503 in Ewing sarcoma cells leads to reduced formate levels [5]. Therefore, while our lack of rescue with nucleosides upon NCT-503 treatment is puzzling, this may be due to technical difference in treatment duration and concentration, or the need to supplement with formate and glycine as nucleoside precursors. Furthermore, other paradigm-shifting work has suggested that, in contrast, ribose and cell-permeable αKG are sufficient to reverse the proliferative defects of PHGDH inhibition which alters nucleotide synthesis independent of flux through the SSP [26]. Of note, our initial studies have focused on single metabolite add-back experiments with NCT-503 treatment and have not addressed the effect of adding back multiple metabolites in combination, which may give insight into conditions that rescue the inhibition of proliferation. These studies would also need to be fully expanded to include genetic knockdown or knockout targeting of PHGDH in parallel with

pharmacologic inhibition. Additional experiments using LC/MS metabolomics and tracing would help further support our findings and determine the most significant impacts with pharmacologic and genetic loss.

Although additional experiments are needed to truly tease out the precise mechanism(s), this ongoing work combined with previous findings from our lab would contribute to the hypothesis that neither sustaining redox balance nor histone methylation are at the center of PHGDH's enzymatic function to sustain growth specifically in Ewing sarcoma. One intriguing result from our preliminary data is that S-Adenosyl Methionine (SAM) may partially rescue the inhibitory effect of NCT-503. However, previous ModSpec analysis from our group has demonstrated no reproducible effect on histone modifications with PHGDH inhibition (Data not shown). This raises the interesting hypothesis that perhaps we need to evaluate the role of SAM in serving as a methyl donor for DNA methylation distinctly from histone methylation. Importantly, Ewing sarcoma's exhibit distinct DNA methylation signatures, with both specifically hyper and hypo-methylated regions, and that this pattern correlates with developmental cell state, suggestive of a potential cell of origin [32]. Previous work measuring 5-methylcytosine (5-mC) levels as a readout for global DNA methylation in a single cell line after PHGDH knockdown suggested that loss of PHGDH does not impact 5-mC [6]. Thus, whether DNA methylation lies downstream of flux through the SSP to maintain Ewing sarcoma tumorgenicity is something that has not been extensively studied and requires more investigation.

Our unbiased RNA-sequencing studies comparing NCT-503 and shRNA-mediated knockdown of PHGDH show that NCT-503 inhibition and knockdown of

PHGDH impact the transcriptome through largely independent mechanisms. Importantly, inhibition with NCT-503 did not impact PHGDH protein levels, as has been previously published [5], allowing us to test the effect of inhibiting PHGDH enzymatic activity and protein levels independently. Thus, it is likely that loss of the PHGDH protein with shRNA leads to distinct effects compared to disruption of PHGDH's enzymatic function alone. Further, the unique effects of NCT-503 and PHGDH knockdown may allude to potential off-target impacts of NCT-503 that warrant further study. Interestingly, our Gene Set Enrichment Analysis (GSEA) using the Molecular Signatures Database to interrogate curated datasets support that PHGDH inhibition may partially antagonize the EWS-FLI1 regulated gene signature. The overlap in downregulated and upregulated pathways upon PHGDH inhibition revealed an inverse relationship with EWS-FLI1 targets. Furthermore, the effects on EWS-FLI1 protein with PHGDH inhibition were variable, but suggest possible impacts on EWS-FLI1 expression, that could explain the repression of and EWS-FLI1-regulated gene signature. Future work will be focused on examining the precise mechanism for this antagonism. For instance, EWS-FLI1 protein levels have be regulated by O-GlcNAcylation, and glutaminase inhibition has been shown to reduce O-GlcNAcylation [33]. Whether similar mechanisms link serine metabolism to EWS-FLI1 stability requires further exploration.

Of note, our analysis of canonical pathways revealed that genes downregulated by both NCT-503 and PHGDH knockdown largely encompass genes relating to cell cycle. Our ongoing efforts will be focused on identifying potential upstream regulators of the cell cycle program, regulated by EWS-FLI1 or other, that may explain the

vulnerability of Ewing sarcoma cells to PHGDH loss. Of note pathways downregulated by NCT-503 and PHGDH knockdown included genes relating to mTORC1 signaling, which regulates mRNA translation. Work in pancreatic cancer cells has shown that PHGDH is able to regulate translation initiation by interacting with eIF4A1 and eIF4E [31]. Therefore, these findings may shed light on non-canonical functions for PHGDH, such as its role in translation and protein synthesis, which remains to be explored. Curiously, pathways upregulated with PHGDH inhibition include TGF-β signaling and extracellular matrix (ECM) and epithelial mesenchymal transition (EMT) related pathways. Work linking serine metabolism to ECM composition has shown that TGF-β signaling can regulate the SSP and generate glycine which is required for synthesis of a collagen-rich ECM [34, 35]. We hypothesize that it is possible that altered glycine synthesis is leading to reductions in ECM and cytoskeletal organization that thus induces transcriptional upregulation changes in these pathways.

Lastly, we made the unexpected observation that NCT-503 treatment was able to rescue cells from ferroptosis, contrary to our expectations. This suggests that NCT-503 treatment somehow upregulates antioxidants that protect against ferroptotic death. One target of interest that we identified as it relates to redox homeostasis upon NCT-503 treatment is TXNIP (thioredoxin-interacting protein), which has been shown to be positively regulated by EWS-FLI1 and to induce oxidative stress in Ewing sarcoma [36]. Thioredoxin is a major regulator of cellular redox signaling, and TXNIP inhibits the antioxidant function of thioredoxin, leading to ROS accumulation and cell stress. Interestingly, our results show that NCT-503 treatment leads to significant downregulation of TXNIP expression, suggesting a potential increase in thioredoxin

function and protection from oxidative stress induced by NCT-503. This may provide insight into GSH-independent compensatory pathways that may preclude our ability to recue PHGDH inhibition with antioxidants.

In sum, through systematic metabolite add back studies and unbiased transcriptomic analysis, our study sheds new light on Ewing sarcoma-specific mechanisms for hyperactivation of the SSP. We provide novel evidence that PHGDH inhibition leads to a possible antagonized EWS-FLI1 gene expression signature and propose that PHGDH-dependent effects on maintaining viability may be independent of PHGDH's role in maintaining redox balance and histone modification.

Materials and Methods

Cell Lines

Ewing sarcoma cell lines were obtained from the Children's Oncology Group (COG) cell bank (cogcell.org). Cells were not cultured past 20 passages. A673, A4573, and TC32 cells were cultured in RPMI 1640 (Corning). CHLA10 cells were cultured in IMDM media (Gibco), supplemented with 1X Insulin-Transferrin-Selenium (Gibco) and 20% fetal bovine serum. All media were supplemented with 10% fetal bovine serum (FBS—Atlas Biologicals) and 1% L-glutamine (Life Technologies), unless otherwise noted, and grown at 37°C, 5% CO_2. Identities were confirmed by short tandem repeat (STR) profiling. All cell lines were routinely tested for mycoplasma contamination as described previously [7].

Chemical Inhibitors and Treatments

NCT-503 (Cayman Chemical) was dissolved in DMSO and single-agent dose-response curve was determined by serial drug dilution and viability assay by Cell Titer Glo 2.0 (Promega). S-(5′-Adenosyl)-L-methionine chloride dihydrochloride (Sigma, A7007-5MG) was dissolved in sterile ddH_2O, Dimethyl 2-oxoglutarate (cell-permeable a-ketoglutarate, 349631-5G) (Sigma) solution was added to media directly, and errastin (Millipore Sigma, E7781-1MG) was dissolved in DMSO.

Generation of Cell Lines Expressing shRNA

For the following plasmids: pLKO.1 shNS (non-silencing control), and shPHGDH (Sigma-Aldrich MISSION shRNA library) plasmids were co-transfected with pLP/VSVG (Invitrogen, Life Technologies) and psPax2 (Addgene) plasmids into 293FT packaging cells using Lipofectamine 2000. 24 hours post-transfection, media was replaced. Viral supernatant was collected 72 hours after transfection, spun down for 15 minutes at 4000 rpm, and the clarified supernatant was concentrated with Lenti-X-concentrator (Takara). Ewing sarcoma cell lines were plated in complete media in 60 mm dishes. Viral supernatant was added to the media at 1X concentration and removed after 24-hour incubation. Cells were selected by supplementing the media with 1.5 μg/mL puromycin (Gibco) for 48 hours before collection. See Appendix II for shRNA sequences and plasmid information.

Proliferation Assays

IncuCyte Live Cell Imaging

Cells were seeded at 3,000 (A673 and A4573), or 5,000 (TC32) cells/well in 96 well plates and proliferation was evaluated in real time for 72 hours using the IncuCyte Live

Cell Analysis instrument. For nucleoside supplementation studies, EmbryoMax Nucleosides (100X) (Millipore Sigma) were diluted at 50uL per mL (150μM cytidine, 150μM guanosine, 150μM uridine, 150μM adenosine, 60μM thymidine) in RPMI media, and media was replenished every 48 hours.

Cell Titer Glo 2.0 & MTT Assay

Cells were seeded in 96-well white wall, white bottom plates (Corning) at 5,000 cells/well (A673), 3,000 cells/well (A4573), and 10,000 cells/well (TC32) in 50 or 100uL of media. The following day, 50uL or 100uL of media containing the treatment was added, and cells were incubated for 72 hours. At endpoint, the plate was equilibrated to room temperature for 30 minutes, and Cell Titer Glo 2.0 reagent (Promega G9243) was added at 20uL per 100uL of media in the plate. Plates were rocked, protected from light, on orbital shaker for 20 minutes, and luminescence was measured for 500ms using a SpectraMax M3 Microplate reader (Molecular Devices). For erastin NCT-503 combination experiments, viability was assessed after 72 hours with MTT assay (Sigma).

Western Blotting

Cells were detached with trypsin-EDTA (0.05%) (Gibco), washed with PBS (Gibco), and lysed in RIPA buffer (Thermo Fisher) supplemented with protease inhibitor cocktail and phosphatase inhibitor cocktail tablets (Roche). Cleared supernatants were subjected to protein quantification by Pierce BCA assay Protein Assay Kit (Thermo Fisher). Western blot was performed using the Mini Gel Tank (Life Technologies). Proteins were resolved by SDS-PAGE using 4–12% Bis-Tris gels, transferred to 0.45 μM PVDF membranes after methanol activation, and blocked in 5% milk dissolved in 1X TBST for 1 hour at

room temperature. Membranes were incubated rotating overnight at 4°C with primary antibody. See Appendix II for list of antibodies and dilutions. Membranes were then washed 4 times for 5 minutes each in 1X TBST and probed with secondary antibody anti-Mouse IgG HRP-linked antibody 1:10,000 (Cell Signaling Technologies), or anti-Rabbit IgG HRP-linked antibody 1:10,000 (Cell Signaling Technologies). Proteins were detected with Clarity ECL substrate (Bio-Rad), and quantification was performed using Bio-rad Image Lab Software.

RNA Sequencing

RNA-sequencing was performed in A673 and A4573 cells following treatment with NCT-503 or after PHGDH knockdown. Libraries were prepared by *Novogene* and sequenced using an Illumina HiSeq 2500 for 50-bp single-end reads. Adapter trimming of paired-end fastq files was performed using Trim Galore (Babraham Institute). Trimmed reads were then aligned to GRCh38 using STAR aligner [37] with `--quantMode GeneCounts` to count the number of reads per gene while mapping. Differential expression analysis was performed using the default parameters from the DESeq2 package [38].

Statistical Analysis

All data is plotted using Prism (GraphPad) and bar plots represent the mean ± SEM. Prism was used to perform two-tailed, unpaired t-test analysis. $P < 0.05$ was considered statistically significant. For volcano plots of RNA-seq data, differential expression values greater than 2-fold or less than −2-fold and adjusted $P < 0.05$ were considered significant, unless otherwise specified, and cutoffs are indicated on plot.

References

1. Luengo, A., D.Y. Gui, and M.G. Vander Heiden, *Targeting Metabolism for Cancer Therapy.* Cell Chem Biol, 2017. **24**(9): p. 1161-1180.
2. Piskounova, E., et al., *Oxidative stress inhibits distant metastasis by human melanoma cells.* Nature, 2015. **527**(7577): p. 186-91.
3. Knott, S.R.V., et al., *Asparagine bioavailability governs metastasis in a model of breast cancer.* Nature, 2018. **554**(7692): p. 378-381.
4. Zhang, H.F., et al., *Proteomic screens for suppressors of anoikis identify IL1RAP as a promising surface target in Ewing sarcoma.* Cancer Discov, 2021.
5. Sen, N., et al., *EWS-FLI1 reprograms the metabolism of Ewing sarcoma cells via positive regulation of glutamine import and serine-glycine biosynthesis.* Mol Carcinog, 2018.
6. Tanner, J.M., et al., *EWS/FLI is a Master Regulator of Metabolic Reprogramming in Ewing Sarcoma.* Mol Cancer Res, 2017. **15**(11): p. 1517-1530.
7. Svoboda, L.K., et al., *Menin regulates the serine biosynthetic pathway in Ewing sarcoma.* J Pathol, 2018. **245**(3): p. 324-336.
8. Issaq, S.H., et al., *EWS-FLI1-regulated serine synthesis and exogenous serine are necessary for Ewing sarcoma cellular proliferation and tumor growth.* Mol Cancer Ther, 2020.
9. Amelio, I., et al., *Serine and glycine metabolism in cancer.* Trends Biochem Sci, 2014. **39**(4): p. 191-8.
10. Locasale, J.W., et al., *Phosphoglycerate dehydrogenase diverts glycolytic flux and contributes to oncogenesis.* Nat Genet, 2011. **43**(9): p. 869-74.
11. Possemato, R., et al., *Functional genomics reveal that the serine synthesis pathway is essential in breast cancer.* Nature, 2011. **476**(7360): p. 346-50.
12. Wortel, I.M.N., et al., *Surviving Stress: Modulation of ATF4-Mediated Stress Responses in Normal and Malignant Cells.* Trends Endocrinol Metab, 2017. **28**(11): p. 794-806.
13. Mattaini, K.R., M.R. Sullivan, and M.G. Vander Heiden, *The importance of serine metabolism in cancer.* J Cell Biol, 2016. **214**(3): p. 249-57.
14. DeNicola, G.M., et al., *NRF2 regulates serine biosynthesis in non-small cell lung cancer.* Nat Genet, 2015. **47**(12): p. 1475-81.
15. Zhao, E., et al., *KDM4C and ATF4 Cooperate in Transcriptional Control of Amino Acid Metabolism.* Cell Rep, 2016. **14**(3): p. 506-519.
16. Ding, J., et al., *The histone H3 methyltransferase G9A epigenetically activates the serine-glycine synthesis pathway to sustain cancer cell survival and proliferation.* Cell Metab, 2013. **18**(6): p. 896-907.
17. Reina-Campos, M., et al., *Increased Serine and One-Carbon Pathway Metabolism by PKClambda/iota Deficiency Promotes Neuroendocrine Prostate Cancer.* Cancer Cell, 2019. **35**(3): p. 385-400 e9.
18. Xia, Y., et al., *Metabolic Reprogramming by MYCN Confers Dependence on the Serine-Glycine-One-Carbon Biosynthetic Pathway.* Cancer Res, 2019. **79**(15): p. 3837-3850.
19. Jimenez, J.A., et al., *EWS-FLI1 and Menin Converge to Regulate ATF4 Activity in Ewing Sarcoma.* Mol Cancer Res, 2021. **19**(7): p. 1182-1195.

20. Pacold, M.E., et al., *A PHGDH inhibitor reveals coordination of serine synthesis and one-carbon unit fate.* Nat Chem Biol, 2016. **12**(6): p. 452-8.
21. Seo, J., et al., *Atf4 regulates obesity, glucose homeostasis, and energy expenditure.* Diabetes, 2009. **58**(11): p. 2565-73.
22. Fan, J., et al., *Human phosphoglycerate dehydrogenase produces the oncometabolite D-2-hydroxyglutarate.* ACS Chem Biol, 2015. **10**(2): p. 510-6.
23. Zeng, J.D., et al., *Serine and one-carbon metabolism, a bridge that links mTOR signaling and DNA methylation in cancer.* Pharmacol Res, 2019. **149**: p. 104352.
24. Mbah, N.E. and C.A. Lyssiotis, *Metabolic regulation of ferroptosis in the tumor microenvironment.* J Biol Chem, 2022: p. 101617.
25. Tibbetts, A.S. and D.R. Appling, *Compartmentalization of Mammalian folate-mediated one-carbon metabolism.* Annu Rev Nutr, 2010. **30**: p. 57-81.
26. Reid, M.A., et al., *Serine synthesis through PHGDH coordinates nucleotide levels by maintaining central carbon metabolism.* Nat Commun, 2018. **9**(1): p. 5442.
27. Tajan, M., et al., *Serine synthesis pathway inhibition cooperates with dietary serine and glycine limitation for cancer therapy.* Nat Commun, 2021. **12**(1): p. 366.
28. Labuschagne, C.F., et al., *Serine, but not glycine, supports one-carbon metabolism and proliferation of cancer cells.* Cell Rep, 2014. **7**(4): p. 1248-58.
29. Vandekeere, S., et al., *Serine Synthesis via PHGDH Is Essential for Heme Production in Endothelial Cells.* Cell Metab, 2018. **28**(4): p. 573-587 e13.
30. Rathore, R., et al., *Metabolic compensation activates pro-survival mTORC1 signaling upon 3-phosphoglycerate dehydrogenase inhibition in osteosarcoma.* Cell Rep, 2021. **34**(4): p. 108678.
31. Ma, X., et al., *Phosphoglycerate dehydrogenase promotes pancreatic cancer development by interacting with eIF4A1 and eIF4E.* J Exp Clin Cancer Res, 2019. **38**(1): p. 66.
32. Sheffield, N.C., et al., *DNA methylation heterogeneity defines a disease spectrum in Ewing sarcoma.* Nat Med, 2017. **23**(3): p. 386-395.
33. Bachmaier, R., et al., *O-GlcNAcylation is involved in the transcriptional activity of EWS-FLI1 in Ewing's sarcoma.* Oncogene, 2009. **28**(9): p. 1280-4.
34. Nigdelioglu, R., et al., *Transforming Growth Factor (TGF)-beta Promotes de Novo Serine Synthesis for Collagen Production.* J Biol Chem, 2016. **291**(53): p. 27239-27251.
35. Selvarajah, B., et al., *mTORC1 amplifies the ATF4-dependent de novo serine-glycine pathway to supply glycine during TGF-beta1-induced collagen biosynthesis.* Sci Signal, 2019. **12**(582).
36. Marchetto, A., et al., *Oncogenic hijacking of a developmental transcription factor evokes vulnerability toward oxidative stress in Ewing sarcoma.* Nat Commun, 2020. **11**(1): p. 2423.
37. Dobin, A., et al., *STAR: ultrafast universal RNA-seq aligner.* Bioinformatics, 2013. **29**(1): p. 15-21.
38. Love, M.I., W. Huber, and S. Anders, *Moderated estimation of fold change and dispersion for RNA-seq data with DESeq2.* Genome Biol, 2014. **15**(12): p. 550.

Chapter 5 Conclusions and Future Directions

Ewing sarcoma is a highly aggressive pediatric bone and soft tissue tumor for which targeted therapies do not yet exist. Treatment for Ewing sarcoma is not tailored to the degree of disease progression at diagnosis, but rather both patients with localized and metastatic disease are treated with maximum doses of chemotherapy as the standard of care, followed by local control with surgery and/or radiation; a treatment regimen that has not improved in decades [1]. Importantly, the presence of metastasis at diagnosis is the best predictor of poor prognosis, and these patients as well as patience who relapse after initial treatment have a 5-year survival of less than 20% [1]. Furthermore, long term toxicities associated with treating children and adolescents with high-dose chemotherapy, such as cardiac problems, secondary malignancies, and infertility, are also a major consideration that warrant better treatment options for Ewing sarcoma patients. Therefore, there is a very critical unmet need to better understand the biology and underlying mechanisms governing Ewing sarcoma progression, with a focus on key regulators of metastasis in particular, in order to advance these findings to new targeted therapies.

We uncovered a previously unidentified role for the enigmatic and multifaceted protein menin as an oncogenic driver in Ewing sarcoma [2]. Menin has been best described to function as a central activator of gene expression through interaction with MLL in trithorax group (TrxG) complexes [3]. While EWS-FLI1, owing to its highly

disordered structure, has presented challenges in successfully therapeutically targeting the oncogenic transcription factor [1], preclinical and clinical assessment of small molecules targeting menin have been underway for several years for the treatment of MLLr leukemias [4-6]. Therefore, the advent of targeting menin in the context of Ewing sarcoma provided an attractive and feasible therapeutic opportunity warranting further evaluation. As a cancer characterized by epigenomic and transcriptional reprogramming, we hypothesized that targeting of menin, may repress oncogenic pathways that drive Ewing sarcoma cancer progression, such as activation of *HOXD* gene expression [2, 7]. Surprisingly, we found that the earliest and most significant effect of menin inhibition on the transcriptome represented downregulation of amino acid metabolic pathways, particularly of genes in the serine biosynthesis pathway (SSP). Work by other groups concurrently found that regulation of the SSP was at least in part EWS-FLI1 dependent [8, 9]. Thus, the work in this thesis began with the goal of dissecting the molecular mechanism(s) by which menin and EWS-FLI1 impact on modulation of the SSP, as well as identifying vulnerabilities that may be exposed by menin and/or EWS-FLI1 targeting.

In Chapter 2, through gain and loss of function studies, we found that activation of the SSP in Ewing sarcoma is regulated by the master transcriptional regulator, ATF4. Through further molecular and transcriptomic studies, we discovered that menin inhibition and EWS-FLI1 loss of function both led to dramatic reductions in ATF4 and an ATF4-regulated gene expression program. Importantly, we found a GGAA motif site at the *ATF4* gene promoter and evaluation of ChIP sequencing and ChIP-qPCR validation revealed FLI1 enrichment at this locus along with active H3K4me3 and H3K27Ac

marks, supporting a direct mechanism of transcriptional activation by EWS-FLI1 [10]. While menin inhibition similarly diminished ATF4 levels, our results showed that protein level changes in ATF4 coincided with and often preceded changes in *ATF4* transcript levels. This finding, combined with evaluation of global and ATF4 promoter-specific H3K4me3 levels upon menin inhibition indicate TrxG-independent mechanisms by which menin regulates ATF4 expression, which warrant further evaluation. Extending our findings to another cancer in which menin plays an oncogenic role, we identified downmodulation of an ATF4-regulated gene expression program in MLLr B-cell ALL cells upon treatment with the next generation and more potent menin inhibitor, MI-3454.

In Chapters 3 and 4, we functionally characterized two downstream targets of this EWS-FLI1-menin-ATF4 axis, ASNS and PHGDH, respectively. Our findings show that ASNS is an important regulator of the metastatic potential of Ewing sarcoma cells, and that loss of ASNS significantly rewires transcript level expression of EMT and ECM-associated pathways. While PHGDH has received extensive focus in Ewing sarcoma [8, 9, 11, 12], it is still unclear which precise function PHGDH plays in maintaining viability and tumorgenicity. Through unbiased transcriptomic analysis, our preliminary data reveal possible non-canonical functions for PHGDH and identified an antagonism of EWS-FLI1-regulated gene signatures.

Exploring potential synthetic lethal metabolic interactions with menin inhibition

Our finding of an EWS-FLI1-menin-ATF4 containing axis in Chapter 2 left us with a few unanswered questions. First, we hypothesized that targeting of this axis may expose a vulnerability to metabolic agents directed downstream at pathways under the

control of ATF4. To begin to address this, we focused on the ATF4 target, *ASNS*, given that current FDA-approved treatments exist using bacterial-derived L-asparaginase (ASNase) for pediatric patients with B-cell ALL. Treatment with MI-503 lead to marked

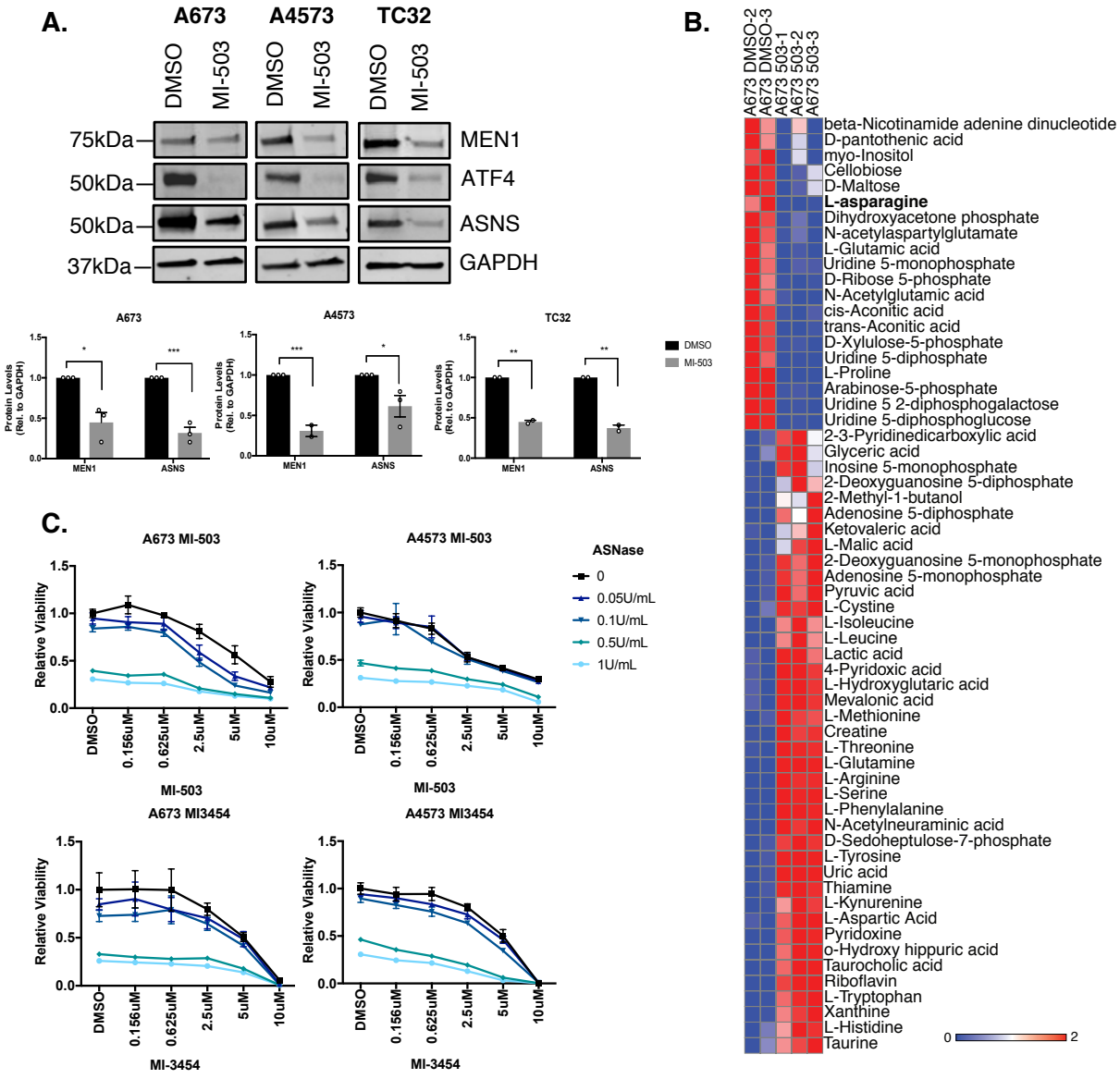

Figure 5-1 Combined menin inhibition and ASNase treatment is not synergistic in inhibiting the cell viability of Ewing sarcoma cells.

A. Representative western blot of MEN1, ATF4, and ASNS protein expression after 72 hours of treatment with 3μM MI-503 in three Ewing sarcoma cell lines (N=3). B. LC/MS metabolomics analysis of intracellular metabolites in A673 cells treated with 3μM MI-503 for 72 hours. C. Cell viability analysis of A673 and A4573 cells co-treated with increasing concentrations of MI-503 or MI-3454 and ASNase (N=1).

and significant downregulation in *ASNS* expression (**Figure 2-6**), and we showed that this reduction followed at the protein level as well (**Figure 5-1A**). Further, LC-MS metabolomics analysis demonstrated reduced asparagine levels upon 72-hour treatment of A673 cells with MI-503 (**Figure 5-1B**), in sum suggesting that the *de novo* synthesis of asparagine was impaired with menin inhibition. We therefore predicted that treatment with MI-503 or MI-3454 in combination with the extracellular asparagine-depleting enzyme, ASNase would act synergistically to inhibit the growth of Ewing sarcoma cells *in vitro* but found no apparent synergy upon treatment with both agents (**Figure 5-1C**). Therefore, co-treatment with ASNase and menin inhibitors did not show a promising combinatorial effect on inhibiting cell viability.

In a similar line of thinking as our ASNS studies, we showed that menin inhibition led to significant reductions in expression of *SLC7A11*, a component of the cystine-glutamate antiporter, system x_C-. As described in Chapter 4 (**Figure 4-3A**), system x_C- is responsible for the import of cystine, a precursor for both cysteine synthesis, as well as the major antioxidant, GSH. The depletion of cysteine with engineered human cyst(e)inase is currently being evaluated in preclinical cancer models for reducing cancer growth [13]. We therefore predicted that menin inhibition would expose a vulnerability to cysteine depletion and that exposure to menin inhibitors in combination with cyst(e)inase would show greater potency on reducing the growth of Ewing sarcoma cells *in vitro*. When A673 and A4573 cells were co-treated with 50nM cyst(e)inase and increasing concentrations of MI-503 or MI-3454, our results suggest that there may be a combinatorial effect, particularly in A673 cells (**Figure 5-2A**). However, A4573 cells showed greater sensitivity to cyst(e)inase treatment alone, and the response to the

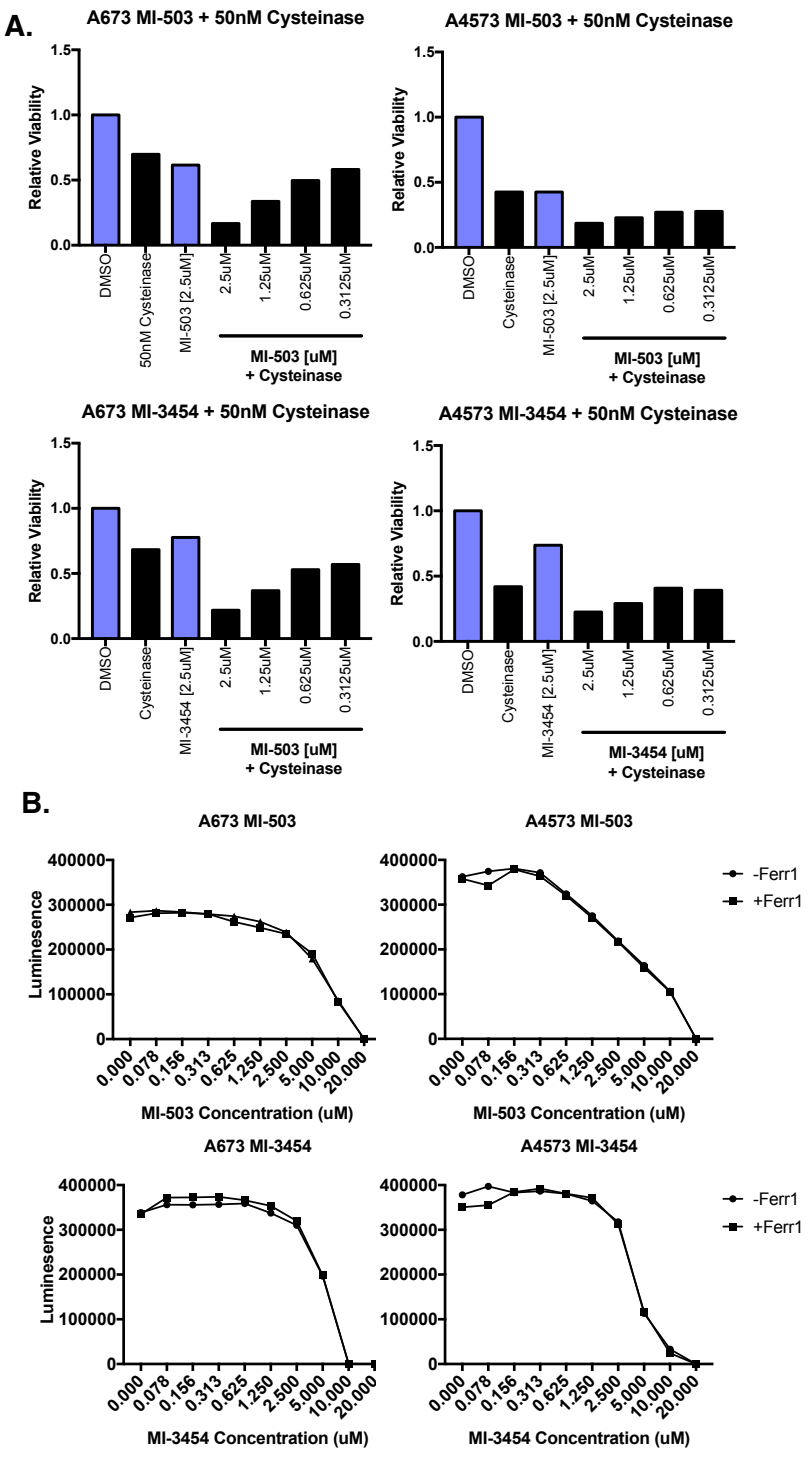

Figure 5-2 Menin inhibition does not appear to restrict growth through induction of ferroptosis

A. Cell viability analysis of 50nM cyste(e)inase in combination with increasing doses of MI-503 or MI-3454 in A673 and A4573 cells (N=1). B. Cell viability of A673 and A4573 cells treated with MI-503 and MI-3454 in the presence or absence of 1μM ferrostatin 1 (Ferr1) (N=1).

combination appeared to be dominated by the effects of cyst(e)inase (**Figure 5-2A**).

Recent studies in breast and ovarian cancer cell lines have concluded that menin inhibitors promote cell killing, at least in part, through the induction of ferroptosis [14]. This finding seemed translatable to our Ewing sarcoma studies based on our results that menin inhibition impairs expression of *SLC7A11*, presumably reducing GSH levels that protect against ferroptosis (**Figure**

4-3A). However, we were unsuccessful at reproducing the data from Kato *et al*. in our cell lines and were not able to rescue the effects of menin inhibition with ferroptosis inhibitors, ferrostatin-1 (**Figure 5-2B**) or N-acetylcysteine (data not shown). Therefore, this suggest that effects on cysteine pathways and GSH metabolism may not be the predominant pathways impacted upon pharmacologic menin inhibition, which is in line with results from our metabolomics data (**Figure 5-1B**). Further studies including extracellular cysteine depletion and targeting of *de novo* cysteine synthesis through the transsulfuration pathway in combination with menin inhibition are needed to further explore this vulnerability.

It is important to note that our combination experiments focused the evaluation of cell viability to test possible synergy between menin inhibitors and ASNase or cyst(e)inase. Therefore, these experiments do not fully rule out the possibility that this strategy may have success *in vivo.* For instance, we have not interrogated the effect of pharmacologic menin inhibition on cell migration and invasion, and it is possible that metastatic phenotypes can be reversed by dual targeting on menin and amino acid metabolic pathways. In support of this, recent data from our lab shows that genetic loss of menin leads to reduced metastatic colonization and growth in *in vivo* tail vein mouse models (data not shown). Further, ASNS is a downstream target of menin, and a regulator of metastasis (Chapter 3). Future experiments will focus on testing these hypotheses and take advantage of more relevant *in vivo* models, such as the PuMA model [15] and renal subcapsular model [16] to more thoroughly investigate whether menin inhibition exposes metabolic vulnerabilities that may exploited *in vivo*.

Our work has very clearly identified distinct effects of targeting menin by complementary approaches. We created menin knockout (KO) single-cell clones using CRISPR/Cas9 and found that KO of menin did not sensitize these cells to MI-503 (**Figure 5-3A**). Furthermore, ATF4 expression was retained in menin KO single cell clones, in contrast to the effects of pharmacologic menin inhibition (**Figure 5-3B**). Thus, the metabolic effect of acute menin loss with inhibitor-treated cells is not fully or faithfully recapitulated by genetic menin ablation. These findings are in line with the work from

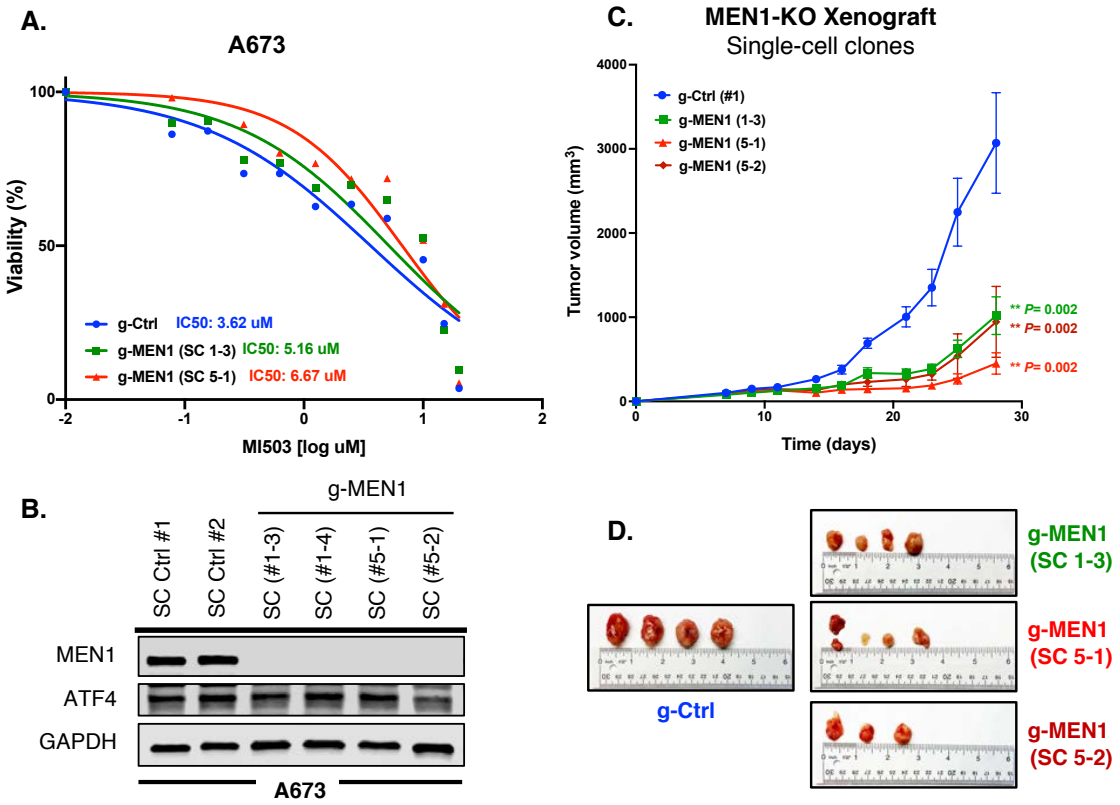

Figure 5-3 Menin KO cells show reduced growth *in vivo* but do not have increased sensitivity to MI-503 *in vitro*.

A. Dose response curve of menin KO single cell clones or control cells treated with MI-503 (N=1). B. Western blot analysis for MEN1 and ATF4 in menin KO single cell clones compared to control. C. Tumor volume of subcutaneous xenograft tumors from mice injected with control or menin KO cells. D. Photograph of tumors at endpoint from experiment in (C). Data were generated by Mohamed Ahmed and Nicolas Garcia.

other groups, which has identified discrepancies comparing genetic and pharmacologic menin inhibition [6, 17, 18]. These results are perhaps not surprising, given the extensive rewiring that must occur in the establishment of single cell clones, and the critical importance of a transcription factor such as ATF4 in maintaining cell viability in response to cell stress. However, Ewing sarcoma cells are highly sensitive to both genetic menin loss and pharmacologic menin inhibition with the MI- series of compounds *in vitro*, and menin KO inhibits tumor growth *in vivo* (**Figure 5-3C**). Importantly, preliminary transcriptomic data comparing the effects of MI-503 and the independently-developed and the more potent compound VTP-50469 in Ewing sarcoma cell lines has uncovered significant differences between these small molecules that both presumably target the menin:MLL interaction (**Figure 5-4A-B**)**.** We hypothesize that these differences and how the two inhibitors differentially disrupt menin-containing complexes might explain discrepancies, with *in vitro* and *in vivo* sensitivities to both agents in Ewing sarcoma models [2, 12, 19]. Our ongoing work will focus on mechanisms to degrade menin acutely, such as through PROTAC [20] chemistry, to more clearly investigate menin's function in metabolic regulation.

Given that menin resides within an intricate protein complex and does not, itself, have any functional domains, disruption of menin interferes with numerous potentially functional interactions. Our ongoing work is aimed at further exploring critical menin interacting partners in the context of Ewing sarcoma. Aside from its role in menin:MLL containing TrxG complexes, menin has also been shown to directly interact with MYC and promote transcriptional elongation at gene promoters, and menin and MYC were also recently found to interact in prostate cancer cells [21, 22]. Preliminary

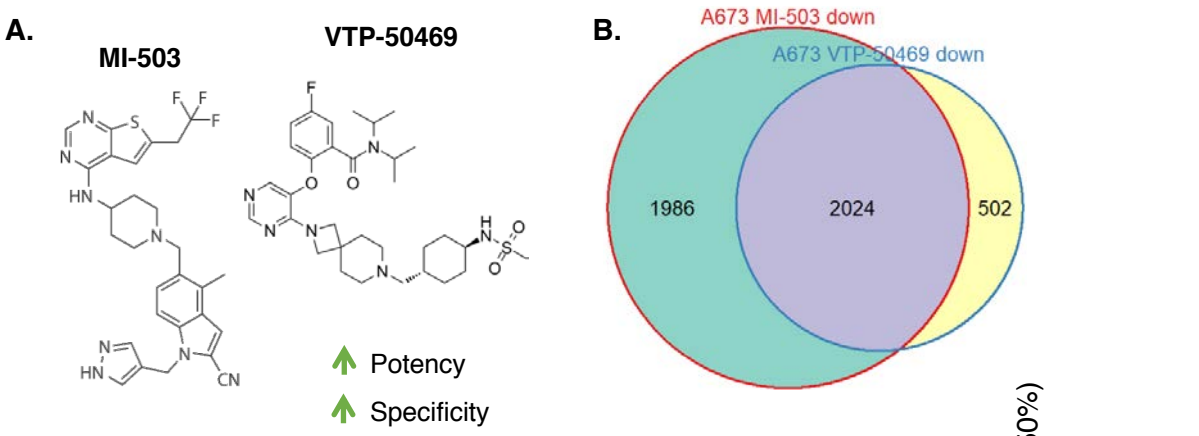

C.

Gene Set Name	# Genes in Gene Set (K)	# Genes in Overlap (k)	k/K	p-value	FDR q-value
HALLMARK_MYC_TARGETS_V1	**200**	**100**	**0.5**	**3.16E-75**	**1.58E-73**
HALLMARK_MYC_TARGETS_V2	**58**	**42**	**0.7241**	**4.43E-42**	**1.11E-40**
HALLMARK_G2M_CHECKPOINT	200	64	0.32	3.33E-34	5.55E-33
HALLMARK_MTORC1_SIGNALING	200	59	0.295	1.74E-29	2.17E-28
HALLMARK_E2F_TARGETS	200	58	0.29	1.42E-28	1.42E-27
HALLMARK_DNA_REPAIR	150	41	0.2733	1.44E-19	1.20E-18
HALLMARK_UNFOLDED_PROTEIN_RESPONSE	113	27	0.2389	7.20E-12	5.14E-11
HALLMARK_PI3K_AKT_MTOR_SIGNALING	105	25	0.2381	4.63E-11	2.89E-10
HALLMARK_OXIDATIVE_PHOSPHORYLATION	200	35	0.175	8.39E-11	4.66E-10
HALLMARK_GLYCOLYSIS	200	30	0.15	7.01E-08	3.51E-07

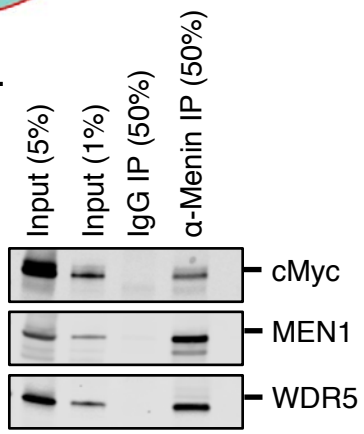

Figure 5-4 Menin directly interacts with MYC in Ewing sarcoma cells

A. Structure of menin:MLL inhibitors, MI-503 and VTP-50469. B. Overlap in significantly downregulated genes with 72 hours of treatment with MI-503 or VTP-50469. C. MSigDB analysis of Hallmark pathways for genes commonly downregulated in (B). D. Menin immunoprecipitation from nuclear extracts of A673 cells identifying an interaction with MYC and WDR5. Data were generated by Kate Braun.

transcriptomic data comparing the effects of MI-503 and the independently developed and more potent compound VTP-50469 in Ewing sarcoma cell lines (**Figure 5-4A**) revealed an overlap in 2,024 genes significantly downregulated by both inhibitors (**Figure 5-4B**). Interestingly, the top Hallmark pathways identified from genes in this overlap resided in the MYC targets gene set (**Figure 5-4C**). We further showed using co-immunoprecipitation studies from nuclear lysates that menin and MYC directly interact (**Figure 5-4D**). We are therefore testing the hypothesize that this menin:MYC interaction is important for mediating the oncogenic effects on menin in Ewing sarcoma

and exploring whether this trithorax-independent mechanism may explain the regulation of amino acid metabolism by menin (**Figure 5-6**). In support of this model, MYC was recently shown to interact with the menin interacting protein, WDR5, specifically at genes involved in protein synthesis [23, 24]. Furthermore, MYC has also been shown to activate ATF4, which acts as a rheostat to alleviate proteotoxicity and balance protein synthesis by co-occupying MYC target gene promoters [25]. Menin has also been shown to target mTORC1 activity [26]. Whether a menin-MYC-WDR5 complex exists in amino acid and protein translation regulation is something we are continuing to explore, and an exciting hypothesis given prior success in targeting the MYC:WDR5 interaction [23, 24].

Menin protein is highly stable and regulated by EWS-FLI1

In our EWS-FLI1 loss-of-function studies, we discovered that loss of EWS-FLI1 led to reproducible loss of menin protein expression, with no impact on menin transcript levels (**Figure 5-5A**), suggesting a mechanism independent of transcriptional regulation by the fusion. Furthermore, our findings show that the half-life of menin is much longer in Ewing sarcoma cell lines than other mesenchymal cell lines (data not shown). Our ongoing efforts are focused on better understanding the mechanisms by which EWS-FLI1 may function to maintain menin protein levels in Ewing sarcoma. Ubiquitination is the best characterized post-translational modification (PTM) of menin, although others, such as phosphorylation and SUMOylation have been described [27-33]. Pharmacologic inhibition of menin in Ewing sarcoma leads to loss of menin protein as early as 24 hours [2, 10], which has been described to be due to ubiquitin proteasomal

degradation in other cell types [30, 32, 34]. We are actively testing the hypothesis that EWS-FLI1 modulates menin ubiquitination through direct or indirect effects on ubiquitin ligases or deubiquitinating enzymes that act on menin (**Figure 5-6**). The effect of these PTMs on menin protein stability, localization, and function is not well understood. While menin is predominately thought to be a nuclear protein, it can also localize to the cytoplasm and can play a role in cell signaling [3, 35]. Our preliminary findings suggest that menin is found both in the nucleus as well as in the cytoplasm (**Figure 5-5B**), and we will continue to use immunoprecipitation and localization studies to better investigate its functions. Although menin is found at the transcription start site of many active genes, it regulates the level of H3K4me3 and transcriptional activation of a limited number of genes [17]. Therefore, ongoing CUT&RUN experiments for both menin and EWS-FLI1 will be used to determine potential cooperative mechanism in the nucleus that regulate gene expression. Interestingly, EWS-FLI1 directly interacts with the menin interacting

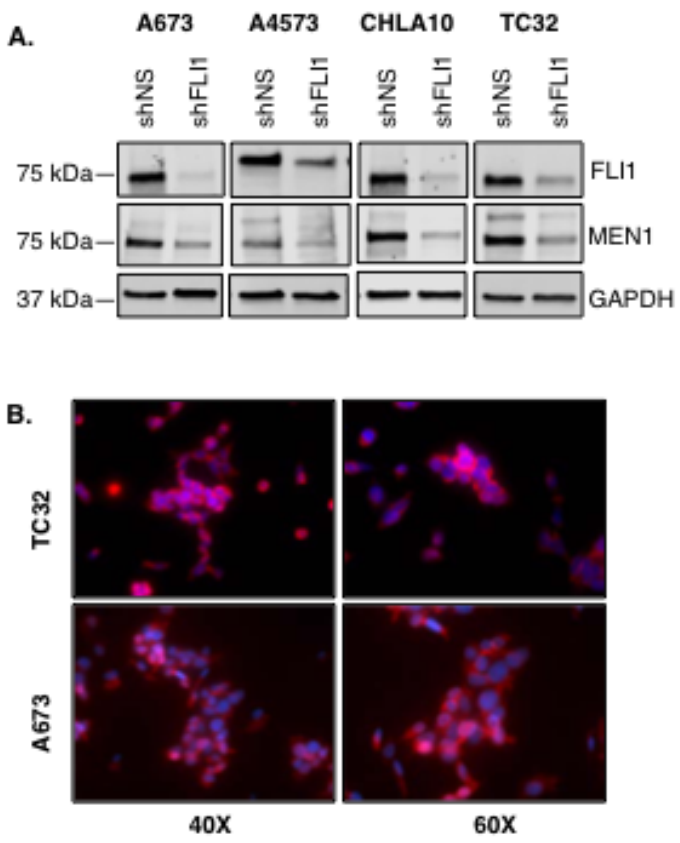

Figure 5-5 Menin protein is regulated by EWS-FLI1

A. Representative western blot for FLI1 (EWS-FLI1) and menin protein levels in four Ewing sarcoma cell lines 96 hours post shFLI1 knockdown (N=3). B Immunofluorescence imaging using anit-MEN1 (A300-105A) and DAPI counterstain (nucleus) (N=1).

protein, WDR5 at enhancers [36], and we have not ruled out the possibility that menin could be present in these complexes.

Insights into regulation of a metastatic cell state

This thesis identified a previously undiscovered role for ASNS activation in regulating metastasis in Ewing sarcoma (Chapter 3). As described in Chapter 3, To this date, ASNase has not been approved for use in the treatment of solid tumors, largely owing to dose-limiting toxicities [37]. However, numerous studies have identified ASNS as a biomarker that predict poor prognosis in solid tumors [38-43]. Only two studies have mechanistically characterized the role of ASNS in regulating metastasis in cancer [38, 40]. Work in breast cancer models has suggested that asparagine regulates metastatic progression by incorporating into asparagine-rich EMT factors, such as TWIST1 [38], and more recent work in colorectal cancer linked a SOX12-ASNS axis to increased proliferation and metastasis [40]. Paradoxically, we found through transcriptomic analysis that the pathways most significantly upregulated with ASNS inhibition involved EMT and ECM modifying pathways. Our continued work is focused on more deeply characterizing protein level changes in EMT-associated factors *in vitro* and *in vivo* to determine whether transcriptional upregulation could represent a compensatory mechanism. In support of this, asparagine has been shown to regulate mTORC1 and protein translation [44, 45]. Of note, mTORC1 has also been shown to translationally regulate ATF4 [46-48], and asparagine restriction activates this axis [49]. We are actively exploring whether asparagine controls translation of metastatic factors via mTORC1 in Ewing sarcoma (**Figure 5-6**). These studies may link back to our

hypothesized role for menin in regulating protein translation [23, 24], and its underexplored function targeting mTORC1 [26].

From a therapeutic standpoint, recent work has demonstrated that electron transport chain inhibition decreases asparagine and reduces cancer cell proliferation, providing a viable combination between mitochondrial inhibitors like metformin and ASNase [50]. Furthermore, asparagine has been shown to exchange for serine, a non-essential amino acid that we and others have been shown to be important for regulating tumorgenicity in Ewing sarcoma [8, 9, 11, 12]. If asparagine itself is indeed important for regulating the metastatic phenotype in Ewing sarcoma one could envision possible therapeutic combinations such as serine restriction, mitochondrial inhibition, etc. that could be evaluated in Ewing sarcoma.

EWS-FLI1 "Low" cell state

Our *in vivo* work assessing EWS-FLI1 loss on metastatic growth using A673 cells uncovered an interesting distinction between the behavior of EWS-FLI1-expressing and EWS-FLI1 "Low" cells. In Ewing sarcoma, work in zebrafish has uncovered a model of cell heterogeneity where EWS-FLI1 "Low "cells are thought to exhibit more mesenchymal features, more cell-matrix interactions, and more invasive properties; while EWS-FLI1 high cells have more cell-cell interactions and are more proliferative [51]. Using our tail vein mouse model, we find that infiltration of EWS-FLI1 knockdown cells is observed in the lung after 24 hours, while presumed to be lost in control cells. EWS-FLI1 knockdown cells also show an expected delay in metastatic colonization, however, when they do colonize, they occupy the lung instead of the liver—the primary

metastatic location for A673 cells. These findings raise interesting questions about the biology of Ewing sarcoma cells and the role of the tumor-initiating EWS-FLI1 oncogene in regulating cell state. We hypothesize that the increased cell-matrix interactions promoted by the EWS-FLI1 “Low” state may make Ewing sarcoma cells more specifically amenable to adhere to the lung, explaining the delay leaving the lung after initial infiltration and the favoring of the lung for colonization and engraftment. In contrast, control cells are able to colonize the liver early on and quickly proliferate, likely due to high levels of the oncogene. Why EWS-FLI1 “Low” cells more preferentially metastasize to the lung requires further exploration. Additional experiments are needed to measure how EWS-FLI1 and mesenchymal marker levels change at each metastatic location, and whether re-expression of EWS-FLI1 is needed after colonization in order to promote tumor growth.

TGF-β and Wnt signaling

TGF-β and Wnt signaling can regulate EMT [52], and our lab has showed that EMT and ECM factors are regulated by Wnt/ β-catenin signaling, which alter the TME and drive progression in subpopulations of Ewing sarcoma cells [53, 54]. Furthermore, Wnt/β-catenin-activated cells phenocopy the EWS-FLI1 “Low” highly migratory cell state characterized by a metastatic gene program [51, 54]. Importantly, menin has been shown to regulate EMT by interfering with TGF-β signaling [55, 56], and to modulate β-catenin signaling [57]. Of note, menin plays a known role in BMP-2, TGF-β dependent osteogenesis, by binding to SMAD1/5 and RUNX2 in MSCs [58, 59], while it can block differentiation of pre-osteoblasts by binding to JUN-D and SMAD3 [60]. EWS-FLI1

expression in MSCs can inhibit differentiation by binding to RUNX2 [61]. Therefore, whether the undifferentiated state of Ewing sarcoma is partly due to competition between menin and EWS-FLI1 for binding RUNX2 or other interaction partners is an attractive hypothesis that we are continuing to explore. Quite interestingly, RUNX2 can also directly interact with ATF4 and other “accessory factors” to regulate osteoblast-specific gene expression [62]. Therefore, it is intriguing to hypothesize that EWS-FLI1 expression disrupts protein interactions that drive osteogenesis and maintain normal bone homeostasis. Whether menin, ATF4, and ASNS are somehow linked in response to these signals within subpopulations of highly aggressive metastatic cells is a hypothesis that warrants further study.

Conclusions

In sum, this thesis began by exploring the function of the enigmatic epigenetic regulator, menin, and its unexpected role in regulation of amino acid metabolism [12]. Our molecular analyses identified a novel axis by which the EWS-FLI1 oncoprotein and menin converge on activation of the master transcriptional regulator ATF4 [10], which helps maintain homeostasis under stress [63] and has been shown to serve as a rheostat to control protein synthesis from genotoxic stress [25]. Our characterization of pathways downstream of this EWS-FLI1-menin-ATF4 axis identified ASNS as a vulnerability and key regulator of metastatic progression. Any therapy is unlikely to have major therapeutic success when used as a single agent. We propose that targeting of this complex network through combination strategies using metabolic therapies and small molecules that expose metabolic vulnerabilities may prove useful in the clinic.

While this approach would be particularly important for metastatic patients, the hope is that it would ultimately reduce or replace the highly cytotoxic chemotherapeutic regimen with agents with more favorable toxicity profiles as the standard of care for all patients.

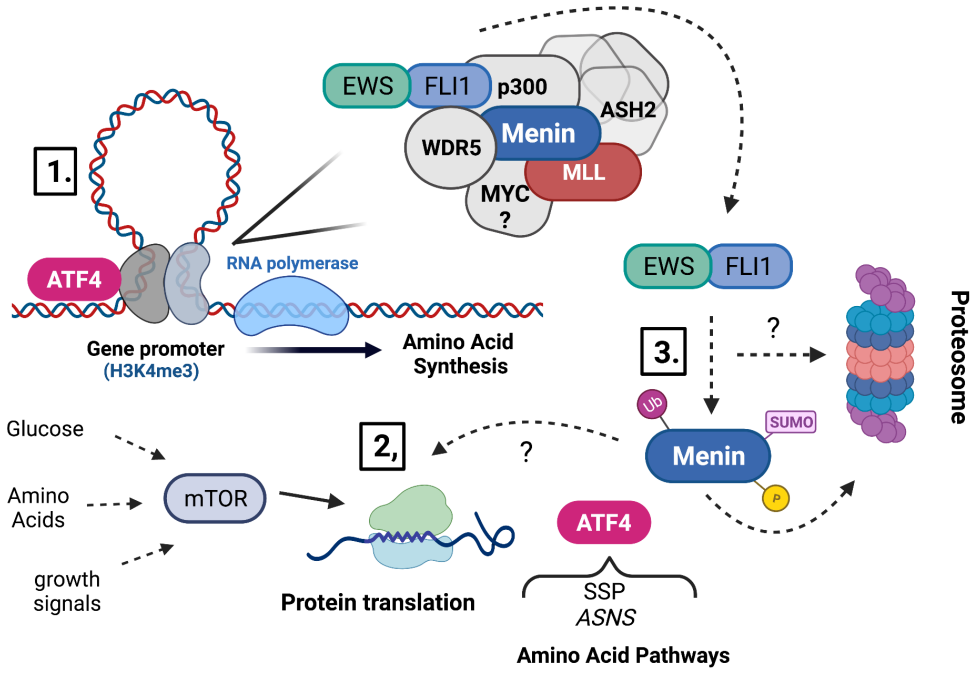

Figure 5-6 Thesis Working Model

The work from this thesis identified a convergence of EWS-FLI1 and menin on the regulation of ATF4. Ongoing work is focused on (1) understanding the function of menin as a gene-expression regulator in cooperating with EWS-FLI1 and/or MYC to modulate amino acid pathways (2) deciphering transcription independent mechanism by which menin may control the translation of ATF4, such as through control of mTORC1 and (3) explore how EWS-FLI1 supports the maintenance of high levels of menin in Ewing sarcoma. We hypothesize that control of amino acid pathways via ATF4 may feed into controlling protein homeostasis critical for promoting tumorgenicity and survival during metastasis.

References

1. Riggi, N., M.L. Suva, and I. Stamenkovic, *Ewing's Sarcoma.* N Engl J Med, 2021. **384**(2): p. 154-164.
2. Svoboda, L.K., et al., *Tumorigenicity of Ewing sarcoma is critically dependent on the trithorax proteins MLL1 and menin.* Oncotarget, 2017. **8**(1): p. 458-471.
3. Matkar, S., A. Thiel, and X. Hua, *Menin: a scaffold protein that controls gene expression and cell signaling.* Trends Biochem Sci, 2013. **38**(8): p. 394-402.
4. Borkin, D., et al., *Pharmacologic inhibition of the Menin-MLL interaction blocks progression of MLL leukemia in vivo.* Cancer Cell, 2015. **27**(4): p. 589-602.
5. Klossowski, S., et al., *Menin inhibitor MI-3454 induces remission in MLL1-rearranged and NPM1-mutated models of leukemia.* J Clin Invest, 2020. **130**(2): p. 981-997.
6. Krivtsov, A.V., et al., *A Menin-MLL Inhibitor Induces Specific Chromatin Changes and Eradicates Disease in Models of MLL-Rearranged Leukemia.* Cancer Cell, 2019. **36**(6): p. 660-673 e11.
7. Svoboda, L.K., et al., *Overexpression of HOX genes is prevalent in Ewing sarcoma and is associated with altered epigenetic regulation of developmental transcription programs.* Epigenetics, 2014. **9**(12): p. 1613-25.
8. Sen, N., et al., *EWS-FLI1 reprograms the metabolism of Ewing sarcoma cells via positive regulation of glutamine import and serine-glycine biosynthesis.* Mol Carcinog, 2018.
9. Tanner, J.M., et al., *EWS/FLI is a Master Regulator of Metabolic Reprogramming in Ewing Sarcoma.* Mol Cancer Res, 2017. **15**(11): p. 1517-1530.
10. Jimenez, J.A., et al., *EWS-FLI1 and Menin Converge to Regulate ATF4 Activity in Ewing Sarcoma.* Mol Cancer Res, 2021. **19**(7): p. 1182-1195.
11. Issaq, S.H., et al., *EWS-FLI1-regulated serine synthesis and exogenous serine are necessary for Ewing sarcoma cellular proliferation and tumor growth.* Mol Cancer Ther, 2020.
12. Svoboda, L.K., et al., *Menin regulates the serine biosynthetic pathway in Ewing sarcoma.* J Pathol, 2018. **245**(3): p. 324-336.
13. Cramer, S.L., et al., *Systemic depletion of L-cyst(e)ine with cyst(e)inase increases reactive oxygen species and suppresses tumor growth.* Nat Med, 2017. **23**(1): p. 120-127.
14. Kato, I., T. Kasukabe, and S. Kumakura, *MeninMLL inhibitors induce ferroptosis and enhance the antiproliferative activity of auranofin in several types of cancer cells.* Int J Oncol, 2020. **57**(4): p. 1057-1071.
15. Scopim-Ribeiro, R., et al., *NSG Mice Facilitate ex vivo Characterization of Ewing Sarcoma Lung Metastasis Using the PuMA Model.* Front Oncol, 2021. **11**: p. 645757.
16. RA, V.A.N.N., et al., *Tissue-directed Implantation Using Ultrasound Visualization for Development of Biologically Relevant Metastatic Tumor Xenografts.* In Vivo, 2017. **31**(5): p. 779-791.
17. Dreijerink, K.M.A., et al., *Enhancer-Mediated Oncogenic Function of the Menin Tumor Suppressor in Breast Cancer.* Cell Rep, 2017. **18**(10): p. 2359-2372.

18. Phillips, R.E., et al., *Target identification reveals lanosterol synthase as a vulnerability in glioma.* Proc Natl Acad Sci U S A, 2019. **116**(16): p. 7957-7962.
19. Kurmasheva, R.T., et al., *Evaluation of VTP-50469, a menin-MLL1 inhibitor, against Ewing sarcoma xenograft models by the pediatric preclinical testing consortium.* Pediatr Blood Cancer, 2020. **67**(7): p. e28284.
20. Bekes, M., D.R. Langley, and C.M. Crews, *PROTAC targeted protein degraders: the past is prologue.* Nat Rev Drug Discov, 2022.
21. Luo, Y., et al., *The scaffold protein menin is essential for activating the MYC locus and MYC-mediated androgen receptor transcription in androgen receptor-dependent prostate cancer cells.* Cancer Commun (Lond), 2021. **41**(12): p. 1427-1430.
22. Wu, G., et al., *Menin enhances c-Myc-mediated transcription to promote cancer progression.* Nat Commun, 2017. **8**: p. 15278.
23. Thomas, L.R., et al., *Interaction of the oncoprotein transcription factor MYC with its chromatin cofactor WDR5 is essential for tumor maintenance.* Proc Natl Acad Sci U S A, 2019. **116**(50): p. 25260-25268.
24. Thomas, L.R., et al., *Interaction with WDR5 promotes target gene recognition and tumorigenesis by MYC.* Mol Cell, 2015. **58**(3): p. 440-52.
25. Tameire, F., et al., *ATF4 couples MYC-dependent translational activity to bioenergetic demands during tumour progression.* Nat Cell Biol, 2019. **21**(7): p. 889-899.
26. Suzuki, J., et al., *The tumor suppressor menin prevents effector CD8 T-cell dysfunction by targeting mTORC1-dependent metabolic activation.* Nat Commun, 2018. **9**(1): p. 3296.
27. Feng, Z.J., et al., *SUMO modification of menin.* Am J Cancer Res, 2013. **3**(1): p. 96-106.
28. Francis, J., et al., *The menin tumor suppressor protein is phosphorylated in response to DNA damage.* PLoS One, 2011. **6**(1): p. e16119.
29. He, X., et al., *Menin localization in cell membrane compartment.* Cancer Biol Ther, 2016. **17**(1): p. 114-22.
30. Jiang, Z., S. Wan, and B. Xing, *Wild-type menin is rapidly degraded via the ubiquitin-proteasome pathway in a rat insulinoma cell line.* Biosci Rep, 2019. **39**(10).
31. Sundaresan, S., et al., *Gastrin Induces Nuclear Export and Proteasome Degradation of Menin in Enteric Glial Cells.* Gastroenterology, 2017. **153**(6): p. 1555-1567 e15.
32. Wu, Y., et al., *Disruption of the menin-MLL interaction triggers menin protein degradation via ubiquitin-proteasome pathway.* Am J Cancer Res, 2019. **9**(8): p. 1682-1694.
33. Yaguchi, H., et al., *Menin missense mutants associated with multiple endocrine neoplasia type 1 are rapidly degraded via the ubiquitin-proteasome pathway.* Mol Cell Biol, 2004. **24**(15): p. 6569-80.
34. Cherif, C., et al., *Menin inhibition suppresses castration-resistant prostate cancer and enhances chemosensitivity.* Oncogene, 2022. **41**(1): p. 125-137.
35. Guru, S.C., et al., *Menin, the product of the MEN1 gene, is a nuclear protein.* Proc Natl Acad Sci U S A, 1998. **95**(4): p. 1630-4.

36. Riggi, N., et al., *EWS-FLI1 utilizes divergent chromatin remodeling mechanisms to directly activate or repress enhancer elements in Ewing sarcoma.* Cancer Cell, 2014. **26**(5): p. 668-681.
37. Koprivnikar, J., J. McCloskey, and S. Faderl, *Safety, efficacy, and clinical utility of asparaginase in the treatment of adult patients with acute lymphoblastic leukemia.* Onco Targets Ther, 2017. **10**: p. 1413-1422.
38. Knott, S.R.V., et al., *Asparagine bioavailability governs metastasis in a model of breast cancer.* Nature, 2018. **554**(7692): p. 378-381.
39. Lin, H.H., et al., *Autophagic reliance promotes metabolic reprogramming in oncogenic KRAS-driven tumorigenesis.* Autophagy, 2018. **14**(9): p. 1481-1498.
40. Du, F., et al., *SOX12 promotes colorectal cancer cell proliferation and metastasis by regulating asparagine synthesis.* Cell Death Dis, 2019. **10**(3): p. 239.
41. Zhang, J., et al., *Asparagine plays a critical role in regulating cellular adaptation to glutamine depletion.* Mol Cell, 2014. **56**(2): p. 205-218.
42. Thomas, T.M., et al., *Elevated Asparagine Biosynthesis Drives Brain Tumor Stem Cell Metabolic Plasticity and Resistance to Oxidative Stress.* Mol Cancer Res, 2021. **19**(8): p. 1375-1388.
43. Apfel, V., et al., *Therapeutic Assessment of Targeting ASNS Combined with l-Asparaginase Treatment in Solid Tumors and Investigation of Resistance Mechanisms.* ACS Pharmacol Transl Sci, 2021. **4**(1): p. 327-337.
44. Krall, A.S., et al., *Asparagine promotes cancer cell proliferation through use as an amino acid exchange factor.* Nat Commun, 2016. **7**: p. 11457.
45. Meng, D., et al., *Glutamine and asparagine activate mTORC1 independently of Rag GTPases.* J Biol Chem, 2020. **295**(10): p. 2890-2899.
46. Ben-Sahra, I., et al., *mTORC1 induces purine synthesis through control of the mitochondrial tetrahydrofolate cycle.* Science, 2016. **351**(6274): p. 728-733.
47. Park, Y., et al., *mTORC1 Balances Cellular Amino Acid Supply with Demand for Protein Synthesis through Post-transcriptional Control of ATF4.* Cell Rep, 2017. **19**(6): p. 1083-1090.
48. Torrence, M.E., et al., *The mTORC1-mediated activation of ATF4 promotes protein and glutathione synthesis downstream of growth signals.* Elife, 2021. **10**.
49. Pathria, G., et al., *Translational reprogramming marks adaptation to asparagine restriction in cancer.* Nat Cell Biol, 2019. **21**(12): p. 1590-1603.
50. Krall, A.S., et al., *Asparagine couples mitochondrial respiration to ATF4 activity and tumor growth.* Cell Metab, 2021. **33**(5): p. 1013-1026 e6.
51. Franzetti, G.A., et al., *Cell-to-cell heterogeneity of EWSR1-FLI1 activity determines proliferation/migration choices in Ewing sarcoma cells.* Oncogene, 2017. **36**(25): p. 3505-3514.
52. Zhang, J., X.J. Tian, and J. Xing, *Signal Transduction Pathways of EMT Induced by TGF-beta, SHH, and WNT and Their Crosstalks.* J Clin Med, 2016. **5**(4).
53. Hawkins, A.G., et al., *Wnt/beta-catenin-activated Ewing sarcoma cells promote the angiogenic switch.* JCI Insight, 2020. **5**(13).
54. Pedersen, E.A., et al., *Activation of Wnt/beta-Catenin in Ewing Sarcoma Cells Antagonizes EWS/ETS Function and Promotes Phenotypic Transition to More Metastatic Cell States.* Cancer Res, 2016. **76**(17): p. 5040-53.

55. Cheng, P., et al., *Menin Coordinates C/EBPbeta-Mediated TGF-beta Signaling for Epithelial-Mesenchymal Transition and Growth Inhibition in Pancreatic Cancer.* Mol Ther Nucleic Acids, 2019. **18**: p. 155-165.
56. Qiu, H., et al., *MEN1 deficiency leads to neuroendocrine differentiation of lung cancer and disrupts the DNA damage response.* Nat Commun, 2020. **11**(1): p. 1009.
57. Luo, Y., et al., *MEN1 silencing aggravates tumorigenic potential of AR-independent prostate cancer cells through nuclear translocation and activation of JunD and beta-catenin.* J Exp Clin Cancer Res, 2021. **40**(1): p. 270.
58. Sowa, H., et al., *Menin is required for bone morphogenetic protein 2- and transforming growth factor beta-regulated osteoblastic differentiation through interaction with Smads and Runx2.* J Biol Chem, 2004. **279**(39): p. 40267-75.
59. Gorbacheva, A., et al., *The role of menin in bone pathology.* Endocr Connect, 2022.
60. Naito, J., et al., *Menin suppresses osteoblast differentiation by antagonizing the AP-1 factor, JunD.* J Biol Chem, 2005. **280**(6): p. 4785-91.
61. Li, X., et al., *The Ewing's sarcoma fusion protein, EWS-FLI, binds Runx2 and blocks osteoblast differentiation.* J Cell Biochem, 2010. **111**(4): p. 933-43.
62. Xiao, G., et al., *Cooperative interactions between activating transcription factor 4 and Runx2/Cbfa1 stimulate osteoblast-specific osteocalcin gene expression.* J Biol Chem, 2005. **280**(35): p. 30689-96.
63. Wortel, I.M.N., et al., *Surviving Stress: Modulation of ATF4-Mediated Stress Responses in Normal and Malignant Cells.* Trends Endocrinol Metab, 2017. **28**(11): p. 794-806.

Appendix I: Supplemental Figures

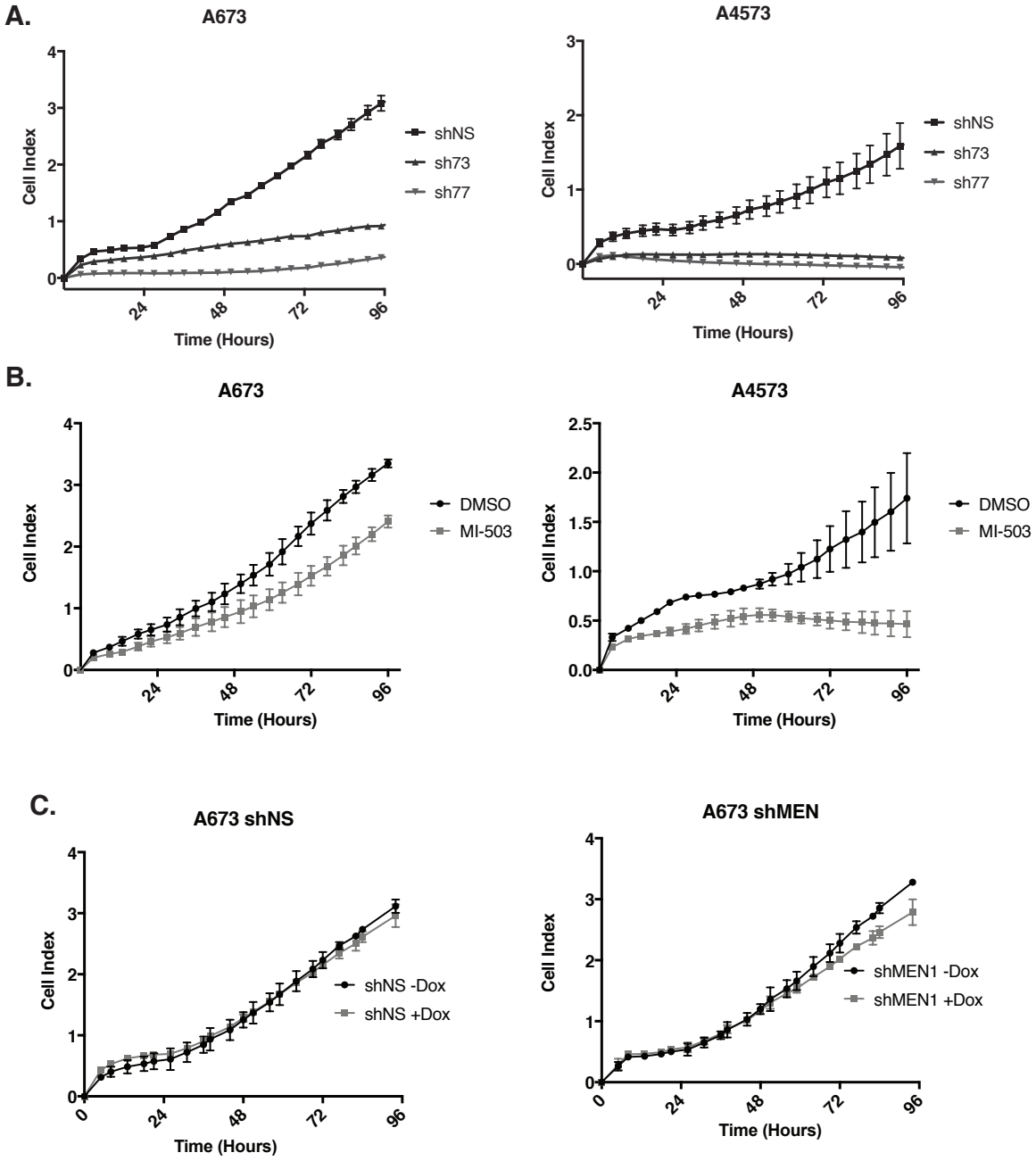

Supplementary Figure S2 1 Real-time cell proliferation analysis of shATF4, MI-503 treatment, and dox-inducible shMEN1 knockdown in Ewing sarcoma cells.

A, RTCA xCelligence proliferation assay of A673 and A4573 cells with shNS, or shATF4 (sh73, sh77) knockdown. Data represents the mean of technical quadruplicates. B, RTCA xCelligence proliferation assay of 3 μM MI-503-treated A673 and A4573 cells (N=2). C, RTCA xCelligence proliferation assay of dox-inducible shNS or shMEN1 A673 cells after 72 hours treatment with doxycycline (N=2). Data represent the mean of 2 independent biological replicates.

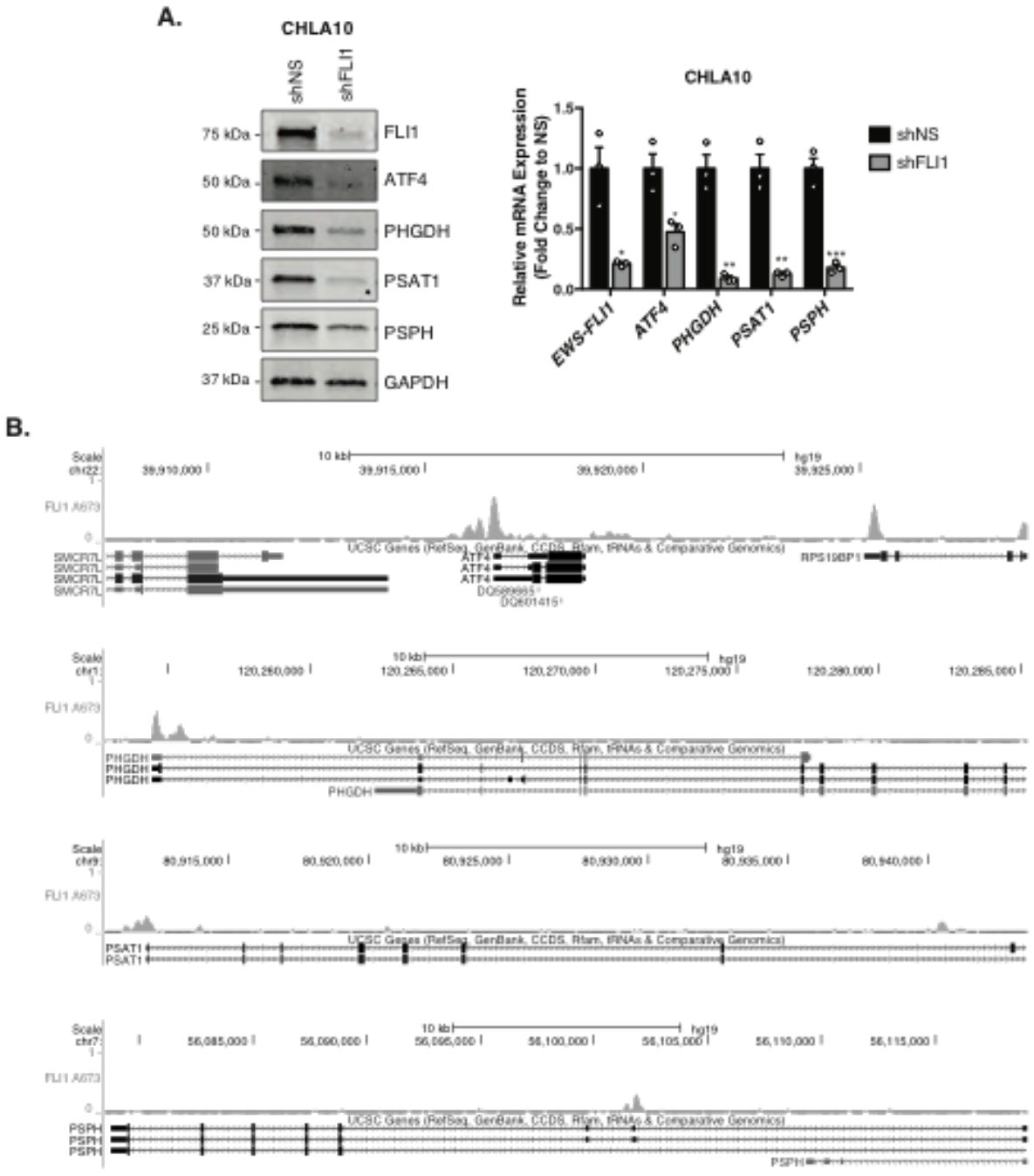

Supplementary Figure S2 2 Effect of shFLI1 knockdown in CHLA10 Ewing sarcoma cells and publicly available ChIP-seq of EWS-FLI1 at the *ATF4* and SSP gene promoters.

A, Representative western blot (30 µg) and qRT-PCR for FLI1 (EWS-FLI1), and SSP (PHGDH, PSAT1, and PSPH) protein and mRNA levels after 96 hours of EWS-FLI1 knockdown (N=3). B, Publicly Available ChIP-seq of EWS-FLI1 at the ATF4 and SSP Gene Promoters. UCSC Genome Browser screenshot of publicly available ChIP-seq tracks for FLI1 (EWS-FLI1) at the ATF4, PHGDH, PSAT1, and PSPH gene promoters in A673 Ewing sarcoma cells [37]. Error bars represent SEM from independent biological replicates. * p<0.05; ** p<0.01; *** p<0.001; Two-tailed t-test.

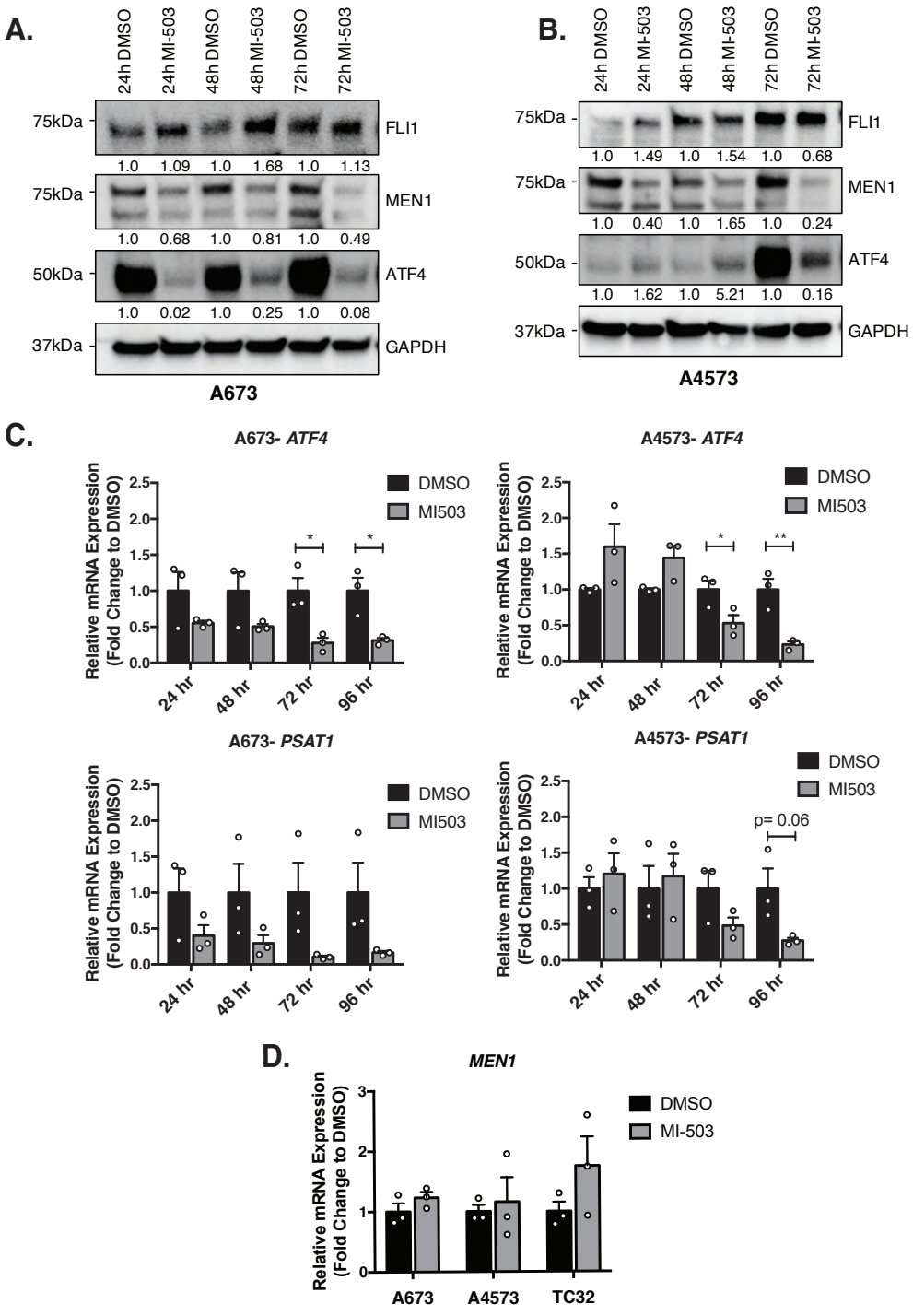

Supplementary Figure S2 3 Timecourse for the effect of MI-503 on ATF4 in Ewing sarcoma cell lines.

A, Representative western blot for FLI1 (EWS-FLI1), MEN1, and ATF4 protein after 24-72 hours of 3 μM MI-503 treatment in A673 and B, A4573 Ewing sarcoma cells (N=3). C, qRT-PCR for ATF4 and PSAT1 mRNA expression after 24-72 hours of 3 μM MI-503 treatment (N=3). D, qRT-PCR for MEN1 mRNA in three Ewing sarcoma cell lines after 96 hours of treatment with 3 μM MI-503 or DMSO control (N=3).

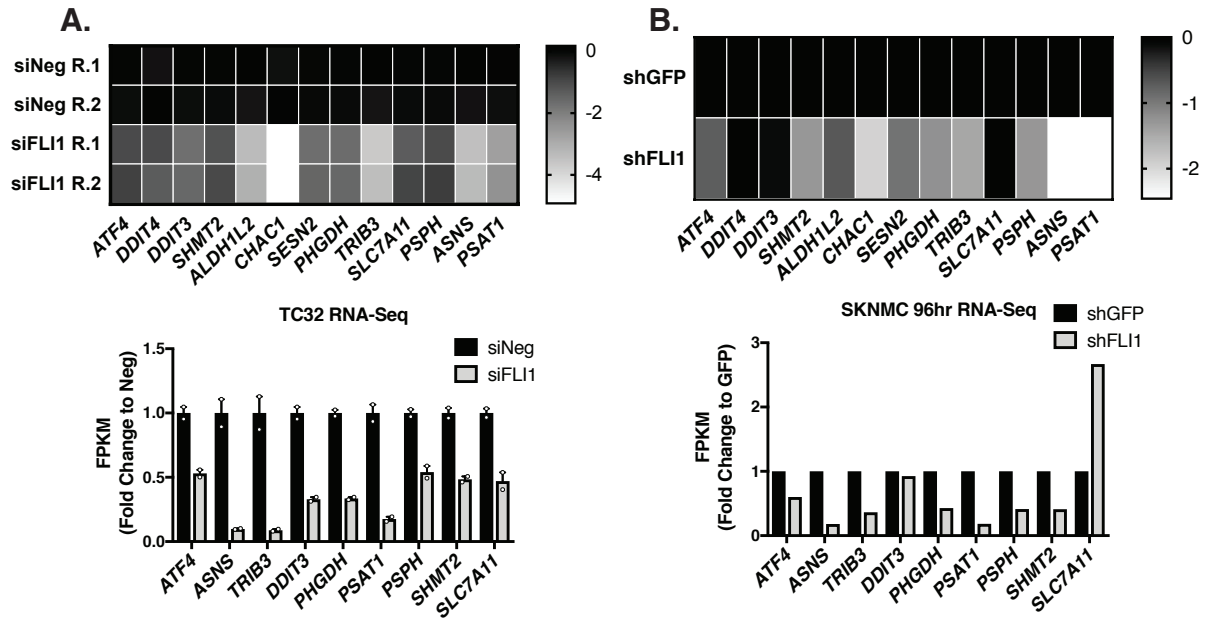

Supplementary Figure S2 4 Publicly available RNA-Seq data of EWS-FLI1 knockdown.

A, Heatmap of Log2FoldChange in expression and bar graph of changes in FPKM levels of selected ATF4 target genes from publicly available RNA-seq data of FLI1 (EWS-FLI1) knockdown in two biological replicates of TC32 cells [17]. B, Heatmap of Log2FoldChange in expression and bar graph of changes in FPKM levels of selected ATF4 target genes after 96 hours of FLI1 (EWS-FLI1) knockdown in SKNMC Ewing sarcoma cells [8].

Appendix II: Supplemental Materials and Methods

Supplementary Methods

shRNA Sequences	
shRNA Plasmid Sigma-Aldrich Oligo ID	**Hairpin Sequence**
pLKO.1 scramble – (SHC002) (shNS)	CCGGCAACAAGATGAAGAGCACCAACTCGAGTTG GTGCTCTTCATCTTGTTGTTTTT
pLKO.1 shATF4 – TRCN0000013573 (#73)	CCGGGCCTAGGTCTCTTAGATGATTCTCGAGAATC ATCTAAGAGACCTAGGCTTTTT
pLKO.1 shATF4 – TRCN0000013577 (#77)	CCGGGTTGGTCAGTCCCTCCAACAACTCGAGTTGT TGGAGGGACTGACCAACTTTTT
pLKO.1 shFLI1 – TRCN0000005322	CCGGCGTCATGTTCTGGTTTGAGAT-CTCGAG-ATCTCAAACCAGAACATGACGTTTTT
pLKO.1 shKMT2B – TRCN0000005959 (#59)	CCGGCCAGCACTATAAGTTCCGTTACTCGAGTAAC GGAACTTATAGTGCTGGTTTTT
pLKO.1 shKMT2B – TRCN0000005960 (#60)	CCGGCGCATGGATGACTTTGATGTACTCGAGTACA TCAAAGTCATCCATGCGTTTTT
pLKO.1 shPHGDH— TRCN0000233029	CCGGCAGGACTGTGAAGGCCTTATTCTCGAGAATA AGGCCTTCACAGTCCTGTTTTTG
pLKO.1 shPHGDH— TRCN0000028520	CCGGGCTTCGATGAAGGACGGCAAACTCGAGTTT GCCGTCCTTCATCGAAGCTTTTT
TRIPZ Inducible Lentiviral shRNA (Dharmacon)	Mature Antisense
Non-silencing shRNA Control Cat. ID: RHS4743	
shMEN1 Clone Id: V2THS_76534 Cat. ID: RHS5087-EG4221	TTGATACAGACTGTACTCG

Western Blot Antibodies			
Protein	**Antibody Name**	**Catalog #**	**Dilution**
anti-FLI1 (EWS-FLI1)	Anti-FLI1 antibody	Abcam ab15289	2 µg/mL
anti-ATF4	ATF-4 (D4B8) Rabbit mAb	Cell Signaling 11815	1:1000

anti-Menin	Menin Rabbit pAb	Bethyl Laboratories A300–105A	1:5000
anti-PHGDH	3PGDH (6B2) Mouse mAb	Santa Cruz Biotechnology sc100317	1:1000
anti-PSAT1	PSAT1 Rabbit pAb	Thermo Fisher PA5–22124	1:1000
anti-H3K4me3	H3K4me3 ChIP-Seq Grade Rabbit pAb	Diagenode C15410003-50	1:1000
anti-H3	Histone H3 Rabbit pAb	Cell Signaling 9715	1:1000
anti-p-eIF2a (Ser51)	Phospho-eIF2α (Ser51) (119A11) Rabbit mAb	Cell Signaling 3597	1:1000
anti-eIF2α	eIF2α Antibody, Rabbit pAb	Cell Signaling 9722	1:2000
anti-GAPDH	GAPDH (14C10) Rabbit mAb	Cell Signaling 2118	1:1000
anti-GAPDH	GAPDH (6C5) Mouse mAb	Thermo Fisher AM4300	1:20,000
Anti-Vinculin	Vinculin (E1E9V) Rabbit mAb	Cell Signaling 13901	1:5000

qRT-PCR Primer Sequences	
Primer	**Sequence (5' - 3')**
mATF4 F	ATGGCCGGCTATGGATGAT
mATF4 R	CGAAGTCAAACTCTTTCAGATCCATT
hATF4 F	GTTCTCCAGCGACAAGGCTA
hATF4 R	GCATCCAAGTCGAACTCCTT
hASNS F	GGAAGACAGCCCCGATTTACT
hASNS R	AGCACGAACTGTTGTAATGTCA
hPHGDH F	CTGCGGAAAGTGCTCATCAGT
hPHGDH R	TGGCAGAGCGAACAATAAGGC
hPSAT1 F	ACAGGAGCTTGGTCAGCTAAG
hPSAT1 R	CATGCACCGTCTCATTTGCG
hPSPH F	GAGGACGCGGTGTCAGAAAT
hPSPH R	GGTTGCTCTGCTATGAGTCTCT
hASNS F	GGAAGACAGCCCCGATTTACT
hASNS R	AGCACGAACTGTTGTAATGTCA
hTRIB3 F	AAGCGGTTGGAGTTGGATGAC
hTRIB3 R	CACGATCTGGAGCAGTAGGTG
hCHOP F *(DDIT3)*	GGAAACAGAGTGGTCATTCCC
hCHOP R *(DDIT3)*	CTGCTTGAGCCGTTCATTCTC
hSLC7A11 F	GCGTGGGCATGTCTCTGAC

hSLC7A11 R	GCTGGTAATGGACCAAAGACTTC
hSHMT2 F	GCCTCATTGACTACAACCAGCTG
hSHMT2 R	ATGTCTGCCAGCAGGTGTGCTT
EWS-FLI1 (ESPB1) F	CGACTAGTTATGATCAGAGCAGT
EWS-FLI1 (ESPB2) R	CCGTTGCTCTGTATTCTTACTGA
HPRT F	TGACACTGGCAAAACAATGCA
HPRT R	GGTCCTTTTCACCAGCAAGCT
18S F	GCAATTATTCCCCATGAACGA
18S R	GGCCTCACTAAACCATCCAAT
EEF1A1 F	CGTTACAACGGAAGTAAAATC
EEF1A1 R	CAGGATAATCACCTGAGC

Taqman Probes	
Probe	**Assay #**
EWSR1-F (EWS-FLI1)	Hs03024497_ft
MEN1	Hs00365720_m1
B2M	Hs00984230_m1
18s	Hs03003631_g1

ChIP-qPCR Primers	
Primer	**Sequence (5'-3')**
PHGDH Promoter F	CGTAAGGCAGCAAACACGTA
PHGDH Promoter R	CCAGCGATAAACCAAAGGTG
PSAT1 Promoter F	AGGAGCAACTGCTTCGACTC
PSAT1 Promoter R	CCTGCGCTAATTGGTTCGC
ATF4 ChIP Neg F	CCCCTCCCAACCTGAACTTC
ATF4 ChIP Neg R	CCTCTAGCCCTCTCTCCCTC
ATF4 Promoter (FLI1 binding site) F	GTCCTCGGCCTTCACAATAA
ATF4 Promoter (FLI1 binding site) R	GGAGTGATCTCCCAGACACG
EWS-FLI1 Neg F	ATGGTGATTCTCAGCCTCCA
EWS-FLI1 Neg R	TGCAGGATTTAAGGGAACCA
ATF4 Promoter (H3K4me3) F	CACTTGAGCCGGATGAAAAT
ATF4 Promoter (H3K4me3) R	AGTCTGCATGGCTCCTCCTA
H3K4me3 Neg F	CTCCCATGTAGCTGTGACCA
H3K4me3 Neg R	GGAGGCCAGGAGTTTGAAAT

Supplementary Materials:

Other Lentivirus Plasmids

pLenti CMV/TO Puro empty (w175-1) (addgene #17482)

pLenti CMV Puro- mATF4 (addgene #24874)

Viral Packaging Plasmids

pCD/NL-BH*DDD (addgene, #17531)

pMD2.G (addgene, #1225)